Progress in Organic and Macromolecular Compounds

Proceedings

International Conference Progress in Organic and Macromolecular Compounds
29th Edition
ICMPP – Petru Poni Institute of Macromolecular Chemistry
Iasi | Romania | October 4 - 6, 2023

ISSN 2810 – 2126 | ISSN – L 2810 – 2126

Edited by

Marcela MIHAI | *Editor-in-Chief*

Radu-Dan RUSU | *Editor*

Cover by

Catalin-Paul CONSTANTIN | Radu-Dan RUSU

Technical editing by

Radu-Dan RUSU | Catalin-Paul CONSTANTIN | Marius-Mihai ZAHARIA

Dear colleagues from Romania and abroad

It is our pleasure to invite you to attend at the 29th edition of the Progress in Organic and Macromolecular Compounds Conference, MACRO Iasi 2023, a traditional event organized by the Petru Poni Institute of Macromolecular Chemistry, between 4 and 6 October 2023, in Iasi.

The Conference addresses polymer and organic chemists and physicists from academia, research institutes and industry, being intended as a dynamic platform for the presentation and sharing of their research and ideas.

MACRO Iasi 2023 gives a broad overview of major topics in organic and polymer synthesis and physics, multifunctional polymeric architectures, engineering of polymeric materials and their applications.

Best wishes for a professionally rewarding conference!

Valeria HARABAGIU and Bogdan C. SIMIONESCU

Chairpersons of MACRO Iasi 2023

Chairpersons of MACRO Iasi 2023

Valeria HARABAGIU and Bogdan C. SIMIONESCU

Program Chair

Marcela MIHAI

International Scientific Board

- David HADDLETON (U Warwick, UK)
- Eric GUIBAL (CME, Ales, France)
- Dieter SCHLUTER (ETH Zurich, Switzerland)
- Andreas FERY (IPF, Dresden, Germany)
- Stergios PISPAS (NHRF, Athens, Greece)
- Patrick NAVARD (CEMEF, Sophia Antipolis, France)
- Svetlana BRATSKAYA (ICB FEBRAS, Vladivostok, Russia)
- Olya STOILOVA (IP-BAS, Sofia, Bulgaria)
- Tania BUDTOVA (CNRS, Sophia Antipolis, France)
- Raluca-Ioana STEFAN-VAN STADEN (INCEMC, Bucharest, Romania)
- Carmen TEODOSIU (TU, Iasi, Romania)
- Florica MANEA (UPT, Timisoara, Romania)
- Calin DELEANU (CCO, Bucharest, Romania)
- Anton AIRINEI (ICMPP, Iasi, Romania)
- Maria CAZACU (ICMPP, Iasi, Romania)
- Mariana PINTEALA (ICMPP, Iasi, Romania)
- Luminita MARIN (ICMPP, Iasi, Romania)
- Gheorghe FUNDUEANU-CONSTANTIN (ICMPP, Iasi, Romania)
- Mariana Dana DAMACEANU (ICMPP, Iasi, Romania)
- Mariana CRISTEA (ICMPP, Iasi, Romania)

Organizing Board

Program

- Marcela MIHAI
- Sergiu COSERI
- Radu Dan RUSU

Editorial

- Marius-Mihai ZAHARIA
- Catalin Paul CONSTANTIN
- Catalin BUZDUGAN

Executive

- Narcisa Laura MARANGOCI
- Mirela ZALTARIOV
- Florica DOROFTEI
- Ana-Lavinia VASILIU
- Elena-Daniela LOTOS
- Melinda Maria BAZARGHIDEANU
- Narcis PRICOB

CONTENT

INVITED LECTURES

LECTURES

ORAL COMMUNICATIONS

POSTER PRESENTATIONS

PROJECTS

SPONSORS

INVITED LECTURERS

Aatto Ilmari LAAKSONEN

PhD: Theoretical Chemistry, Stockholm University (SU), Arrhenius Laboratory 1981.
Docent (habilitation): Physical Chemistry SU 1984.
Post-doctoral fellow: Daresbury Laboratory UK, 1982, IBM Laboratory USA 1983-1985.
Sen. Lecturer: Physical Chemistry SU 1987-1999.
Full Professor: Physical Chemistry SU 2000-present.
Sabbaticals: Dalhousie University (Canada) 1993-94, 1995, JAERI (Japan) 2002, 2005.
Guest Professor: University of Cagliari (Italy), Nanyang Tech University (Singapore), Jilin University (China), University of Sao Paulo (Brazil), Nanjing Tech (China), Luleå University of Technology, Uppsala University Ångström Laboratory, Stellenbosch Institute of Advanced Study (South Africa).
ERA Chair: Petru Poni Institute of Macromolecular Chemistry.
Research interests: In silico modelling in materials science, biopharma and green chemical engineering..

Olya STOILOVA is professor of macromolecular chemistry at the Institute of Polymers, Bulgarian Academy of Sciences (IP-BAS). Since 2013 until 2021 she was elected as scientific secretary of Nanosciences, new materials and technologies Research division of the Bulgarian Academy of Sciences and was a member of the Governing council of the Academy. Her expertise covers design of hybrid materials based on natural and synthetic polymers (gels, films, nanoparticles, electrospun materials), development of polymeric materials with defined and desirable properties, and controlled structure for a wide range of applications – biomedicine, water purification, environmental protection, agriculture, etc. She is leading researcher in polyelectrolyte complexes, as well fabrication of fibrous polymeric materials by electrospinning, their characterization and possible applications. She has published more than 40 research papers with over of 950 citations, H-index 19. She is a co-author of one chapter in book and one interactive vocational training tools in the field of Food Industry. She is a project leader and participant of more than 25 national and international research projects and is the inventor of 1 utility model and 1 patent. Since 2021, she is heading the Polymeric Biomaterials Department at the IP-BAS, which is focusing on the development of novel biocompatible and biodegradable polymeric materials, polymer-inorganic hybrid nanoparticles and nanocomposites, and design of biomaterials for tailored applications.

Rénato FROIDEVAUX is full professor of biocatalysis at Lille University in France. He is heading the team « Biotransformation, biocatalysis and enzyme » in the BioEcoAgro Joint Cross-Border Research Unit. His research concerns enzymatic biocatalysis (homogeneous and heterogeneous) applied to hydrolysis of agro-food proteins for obtaining bioactive peptides, enzymatic biocatalysis applied to the valorization of lignin for obtaining biobased aromatics. More recently, he developed the concept of "hybrid catalysis" which consists of combining chemical catalysis and enzymatic biocatalysis for biomass valorization. This interdisciplinary concept involves the search for new enzymes, the search for compatible reaction conditions between (bio)catalysts and the development of different types of reactors (one-pot one step, two-pots one-step) and Multi Catalytic Hybrid Materials (also called MMCH) for heterogeneous (bio)catalysis. Author and co-author of more than 50 articles mostly in JCR, 3 book chapters and 3 patents. Total citations almost 800 (WoS), H Index 16. He is a project leader and participant of more

than 25 national and international research projects. He is responsible of an Industrial Chair called « Charles Viollette », financed by the European Metropole of Lille and the University of Lille. This chair brings together academic partners from Lille and Canada (INAF in Quebec) and industrial partners in the development of co-products from the agricultural and agro-food industries by biotechnological tools for the production of bioactive molecules for animal, human nutrition and plant health. He was a lecturer in enzyme biocatalysis from 2004 to 2009 in the Franco-Romanian Master's "Bioprocesses in the Agrifood field" between Al. I. Cuza University of Iasi and Lille University, then director of this master's until 2013. Currently, he works with the Technical University Gheorghe Asachi of Iasi (Dr. Alexandra BLAGA) for the implementation of a double master'degree in (bio)chemical engineering.

Alexander BISMARCK research group, the Polymer & Composite Engineering (PaCE) Group, is a

multi-disciplinary team with research interests in the manufacture and characterisation of fibre reinforced high performance (nano) composites, porous materials and hydrogels. The group focuses on the development of renewable materials, biomaterials for applications in tissue engineering, composite super-capacitors and emulsion templating for the synthesis of porous polymers (so called polymerisable High Internal Phase Emulsions (polyHIPEs)). Furthermore, the group is interested in the social dimensions of materials research. He is also affiliated member of The Composite Centre at Imperial College London and visiting professor of the Department of Chemical Engineering.

Daniel B. WERZ received a BS in chemistry at Heidelberg University, Germany, in 1997, a diploma

in 2000, and a Ph.D. in organic chemistry from Heidelberg University in 2003 with Rolf Gleiter. Following his doctoral studies, he was a Postdoctoral Fellow with Peter H. Seeberger at ETH Zurich, Switzerland. In December 2006 he joined Göttingen University as an Assistant Professor. In 2013 he took the position of an Associate Professor at the University of Braunschweig, in 2018 he was promoted at the same university to Full Professor. In 2022 he moved to the University of Freiburg. His main research interests include the development of novel efficient methods for the synthesis of hetero- and carbocyclic compounds (e.g. by cyclopropane chemistry, cascade reactions and Pd catalysis). In addition, he is interested in carbohydrates, glycolipids and fluorescent dyes. His awards include inter alia an Emmy Noether Fellowship of the German Research Foundation, a Heisenberg Fellowship, the “Dozentenstipendium” of the Fund of Chemical Industry, the ORCHEM Award, a JSPS Visiting Professorship in Japan, and an ERC Consolidator Grant. Since 2017 he has been Distinguished Visiting Professor at the IIT Bombay, in 2018 he has become Visiting Scholar at Tel Aviv University in Israel.

Anne LADEGAARD SKOV is a professor of polymer technology at DTU in Denmark and is

heading the Danish Polymer Centre. She is a world-leading expert in silicone elastomer synthesis, characterization, and utilization. Her main focus is on making artificial muscles via dielectric elastomers. She has published more than 160 publications and has been granted 13 patent families. Anne Ladegaard Skov is active in building bridges between research and industry and has taken a sabbatical leave in 2021 to focus on creating the company Glysious. She is furthermore cofounder of another 3 companies that are either spun out or still in the incubator environment. Anne Ladegaard Skov has received multiple prizes for her work, including the Elite Forsk award in 2022, granted by the Danish Ministry of Higher Education and Science, and the Grundfos Prize in 2022, regarded as one of the most prestigious prized in Denmark for technical research.

Piotr RYCHTER is researcher and university teacher at Jan Długosz University in Częstochowa, Faculty of Science and Technology, Department of Biochemistry, Biotechnology and Ecotoxicology. Position: associate professor. Research topic focuses on environmental and health aspects of biodegradable and biocompatible polymers including biodegradation, controlled release system of agrochemicals. Participated in several national and international scientific projects mostly related to environmental and health aspects of biodegradable and biocompatible polymers. Awarded four medals (three gold and one silver) for the inventions at national and international invention shows in Warsaw, Bangkok, Hong Kong. Participant of numerous international and national conferences. Participant of three research internships: Centre of Polymer and Carbon Materials Polish Academy of Sciences, Zabrze Poland, Institute of Polymers of Slovak and Bulgarian Academy of Sciences. Several delivered lectures within an Erasmus programme at various Universities in Europe like Cagliari University, University of Perugia, Joseph Fourier University in Grenoble, Centre of Polymer Systems, Thomas Bata University (Zlin - Czech Republic), Polymer Institute of Slovak Academy of Sciences. Author and co-author of more than 70 articles mostly in JCR. Total citations almost 700 (WoS), H Index 12. From 2021 head of Interdisciplinary Science and Research Centre at Jan Dlugosz University in Czestochowa.

MACRO Iași 2023

IN SILICO STUDIES OF NATURE'S HIERARCHICAL CREATIONS

Aatto Ilmari Laaksonen[1,2,3,4]
[1]*Department of Materials and Environmental Chemistry, Arrhenius Laboratory, Stockholm University, Stockholm, Sweden*
[2] *Centre of Advanced Research in Bionanoconjugates and Biopolymers, Petru Poni Institute of Macromolecular Chemistry, Romanian Academy, Iasi, Romania*
[3]*State Key Laboratory of Materials-Oriented and Chemical Engineering, Nanjing Tech University, Nanjing, P. R. China*
[4]*Department of Engineering Sciences and Mathematics, Division of Energy Science, Luleå University of Technology, Luleå, Sweden*
**aatto@mmk.su.se*

1. Introduction

Nature is the most brilliant engineer, creating many of its magnificent structures hierarchically. Nature also uses composite solutions by mixing soft and hard to make the matter strong and this way be able to dissipate energy, become mechanically resistant and prevent cracks. Most importantly, this also allows the structures to continue to grow successively when needed. Our bones and skin are typical examples, while all plants and trees manifest the idea perfectly. All the above structures start from molecules and from there starts even the underlying hierarchy.

In this talk we study hierarchical structures on molecular level. We apply an *in-house* multiscale modelling methodology based on hierarchical successive coarse-graining. We utilize *inverse problem solving* to compute the molecular models and corresponding interactions from results of detailed lower order systems of high resolution. This hierarchical coarse-graining and super coarse graining allow us to study successively larger and larger structures this way connecting long length scales. Examples are given of modelling genetic materials.

We demonstrate that *In silico* hierarchical multiscale modelling is an ideal tool to learn molecular architectures from Nature. The work is an example of activities in the current ERA Chair project "BioMat4CAST *In Silico* Laboratory for Complex and Smart Biomaterials" at Petru Poni Institute of Macromolecular Chemistry. BioMat4CAST has its goals set high to closely integrate advanced experimental studies and next generation of molecular modelling.

2. Inverse problem solving

Science uses systematic methods to explore unknowns, make predictions, and verify results. The most common approach is solving "forward problems" using mathematical models to understand and control phenomena. In some cases, these solutions can be "reversed" to solve "inverse problems," helping us trace back to the original cause of events.

Inverse problem-solving is not new; it's prevalent in fields like physics, engineering, and increasingly in chemistry due to growing data and advanced computing [1,2]. For example, by knowing certain key material properties allows scientists to work backward to find the molecules and synthesis methods needed.

3. Models and methods

We present a method that uses inverse problems to develop accurate computational models for studying interactions between particles. This method starts by taking data on how particles are distributed in space, either from computer simulations or real-world experiments. It then reverses this data to uniquely determine the forces acting between the particles [3].

To go into more detail, our method allows us to build a force-field that accounts for the effects of a surrounding fluid (solvent). It also offers a systematic approach for creating models that work at multiple scales, from the level of individual atoms all the way up to larger structures. This multi-scale approach is built through a step-by-step simplification process known as 'successive coarse-graining. We provide several examples to demonstrate that this method can be broadly applied to various situations [4,5].

4. Concluding remarks

Spatial multi-scale modelling by utilizing inverse problem solving through successive hierarchical coarse-graining is an ideal method to study structures created by Nature from cellulose and human skin to packing of genomes. Currently it requires well-posed systems to reverse the causality and extensive amounts of computing time for large macromolecular systems. Future developments in machine learning techniques [**6**] will make to a powerful bottom-up tool together with advanced top-down experimental techniques.

Acknowledgements

European Union's Horizon Europe research and innovation programme under grant agreement No 101086667, project BioMat4CAST.

References

[1]. Yaman F, Yakhno, VG, Potthast R. A Survey on inverse problems for applied sciences *Math. Probl. Eng.*, 976837, 1-19, 2013
[2]. Sanchez-Lengeling B, Aspuru-Guzik A. Inverse molecular design using machine learning: Generative models for matter engineering, *Science* 361, 360-365, 2018
[3]. Lyubartsev A, Laaksonen A. Inverse problems and hierarchical multiscale modelling of biological matter, In: Abadie MJM, Pinteala M, Rotaru A, editors. New Trends in Macromolecular and Supramolecular Chemistry for Biological Applications. Switzerland: Springer Nature; pp. 213-238, 2021
[4]. Lyubartsev A, Laaksonen A. Calculation of effective interaction potentials from radial distribution functions:A reverse Monte Carlo approach, *Phys. Rev. E*, 52, 3730-3737, 1995
[5]. Lyubartsev A, Mirzoev A, Chen LJ, Laaksonen A. Systematic coarse-graining of molecular models by the Newton inversion method. *Faraday Discuss.* 144, 43-56, 2010
[6]. Sanchez-Lengeling B, Aspuru-Guzik A. Inverse molecular design using machine learning: Generative models for matter engineering, *Science* 361, 360-365, 2018

ADVANCED ELECTROSPUN MATERIALS: FROM DESIGN TO PROSPECTIVE APPLICATIONS

Olya Stoilova*
Laboratory of Bioactive Polymers, Institute of Polymers,
Bulgarian Academy of Sciences, Sofia, Bulgaria
**stoilova@polymer.bas.bg*

1. Introduction

Electrospinning is an electrohydrodynamic process in which fibers with diameters in the nanometer range are created by electrostatic spinning from polymer solutions or melts. Nowadays, electrospinning has drawn a great attention as the only technique for simple, inexpensive and effective fabrication of new generation of polymeric materials (the so-called "mats"). In addition, electrospinning allows production of mats in different configurations and assemblies. Moreover, the prepared materials have unique properties like extremely high surface area, lightness and porosity.

Nevertheless, more studies are required to fabricate targeted electrospun materials with desired design, morphology and controllable properties relevant to prospective applications. The article give an overview on the most recent approaches and innovative methods for fabrication of versatile electrospun hybrid materials with targeted design, as well as on characterization of its morphology and properties. Special attention will be paid to variety of possible applications of the fabricated mats designed for photocatalytic water purification from organic pollutants, for tissue engineering as compatible with human mesenchymal stem cells scaffolds, for enzyme immobilization and for plant protection in agriculture.

2. Results and discussion

Several types of electrospun polymeric-inorganic materials based on biocompatible and biodegradable poly(3-hydroxybutyrate) (PHB) or cellulose acetate, nanoparticles from iron oxide (Fe_3O_4), titanium dioxide (TiO_2) or commercially available nanoclays (NCs), and chitosan oligosaccharides (COS) were prepared by combining electrospinning, electrospraying, coating and coaxial electrospinning [1-5]. In this manner targeted design of the fabricated hybrid polymer materials was achieved. The new materials exhibit magnetic and photocatalytic properties, and enhanced adsorption ability.

Electrospinning of a polymer and nanoparticles (NPs) or NCs mixtures resulted in the preparation of hybrid fibrous materials type "*in*". The simultaneous electrospinning of polymer and electrospraying of NPs dispersions led to fabrication of type "*on*" materials. The fixing of NPs onto polymer fibers took place during electrospraying, because COS were added directly to the NPs dispersion. Another approach for NPs fixing is by dip coating of electrospun fibers into NPs dispersion (type "*coat*"). The combined electrospinning of a polymer and NPs mixture and electrospraying of a NPs dispersion resulted in the fabrication of materials "*in-on*" type. Thus, combining the methods of electrospinning and electrospraying enable the preparation of hybrid materials with a purposefully modified surface pattern. In addition, simultaneous electrospraying of NPs dispersion and coaxial electrospinning allowed one-step fabrication of hybrid fibrous materials, composed of core–shell fibers, decorated with NPs (Figure 1).

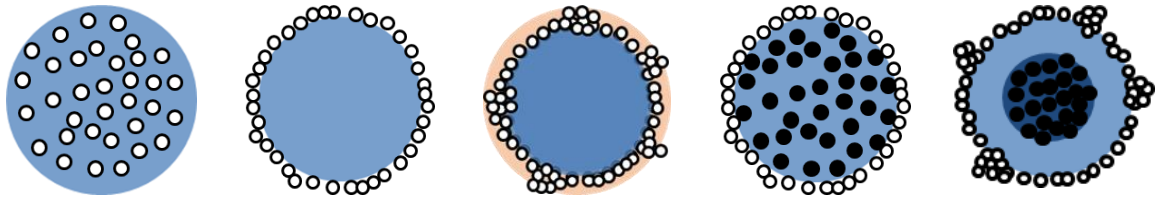

Figure 1. Types of the fabricated electrospun polymeric-inorganic materials.

It was shown that depending on the disposition of the nanoparticles – "*on*" the surface of the fibers, "*in*" the bulk of the fibers or "*on*" the surface and "*in*" the fibers, their photocatalytic activity can be successfully controlled and modulated. Thus, the proper combining of electrospinning and electrospraying enables the fabrication of hybrid materials of different design with purposefully selected properties for a variety of applications.

Surface morphology of the electrospun materials was observed by scanning electron microscopy (SEM). As seen, the fibrous PHB mats obtained by electrospinning are composed of uniform and defect-free fibers (Figure 2), while the electrospun materials type "*in*" – of cylindrical fibers with thicker parts along their length. This specific surface morphology is due to the Fe_3O_4 and TiO_2 NPs incorporated into the fibers, part of which probably aggregate during electrospinning. In contrast to them, hybrid fibrous materials type "*on*", prepared by simultaneous electrospraying and electrospinning, consist of fibers with rough and decorated with NPs surface (Figure 2).

It is notable that the TiO_2 nanoparticles are relatively uniformly distributed along the length of the fibers forming aggregates. A significant enrichment of the surface of the mats with NPs was achieved in the case of materials type "*coat*", prepared by dip coating. In the case of materials type "*in-on*", the formation of larger aggregates on the surface of the fibers is observed. This can be attributed to the presence of COS, as well as of the two types of NPs in the dispersion.

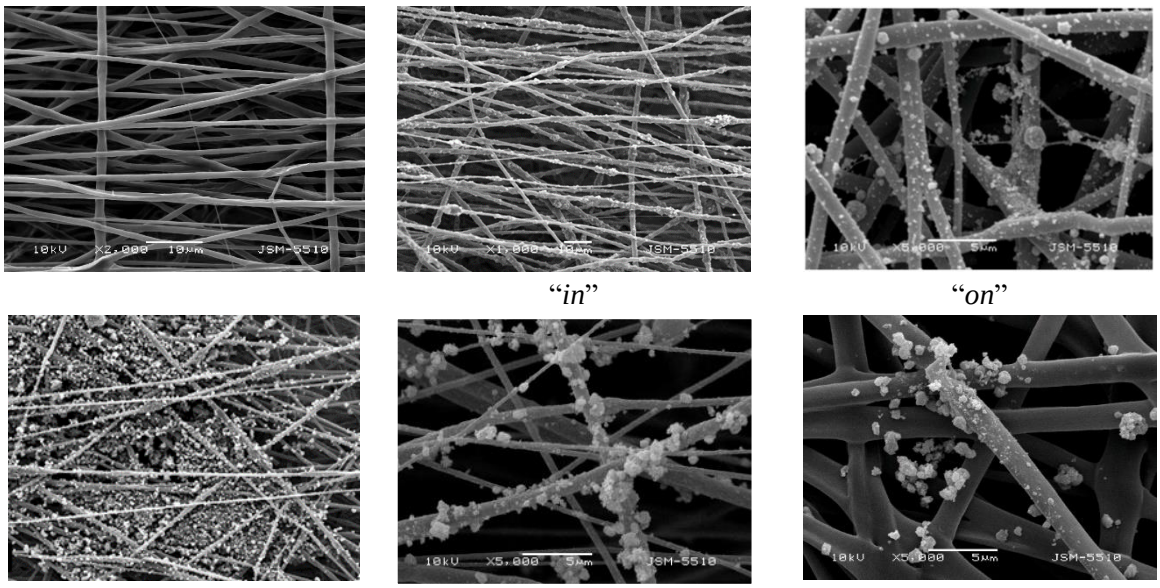

Figure 2. SEM micrographs of electrospun: PHB; TiO_2-*in*-PHB; TiO_2-*on*-PHB; TiO_2-*coat*-PHB; TiO_2-*on*-(Fe_3O_4-*in*-PHB); TiO_2-*on*-core (PVA/Fe_3O_4)/shell (PHB/PCL).

Novel hybrid fibrous materials having a surface purposefully decorated with TiO_2 nanoparticles display excellent stability and preserve almost completely their photocatalytic activity after threefold use under UV light irradiation in the presence of a model organic pollutant. Moreover, they exhibit high bactericidal activity against *E. coli* and complete inhibition of fungal growth of *P. chlamydospora*.

In addition, the fibrous scaffolds are compatible with human mesenchymal stem cells and provide a favorable environment for their development. Notably, the type of the nanoclay strongly influenced the adsorption ability of hybrid fibrous materials toward Cr(VI) ions and MB dye. The results indicated that the novel multifunctional hybrid fibrous materials are promising scaffolds for the regenerative medicine and tissue engineering, as well as for use in water and air purification from organic pollutants.

Acknowledgements

This work was supported by the European Regional Development Fund within the Operational Programme "Science and Education for Smart Growth 2014 - 2020" under the Project CoE "*National center of mechatronics and clean technologies*" BG05M2OP001-1.001-0008-C01. Some of the equipment included in INFRAMAT (Bulgarian Roadmap for Research Infrastructure) supported by Bulgarian Ministry of Education and Science was used in these studies.

References

[1]. Korina E, Stoilova O, Manolova N, Rashkov I. Multifunctional hybrid materials from poly(3-hydroxybutyrate), TiO_2 nanoparticles, and chitosan oligomers by combining electrospinning/electrospraying and impregnation, *Macromol. Biosci.*, 13, 707-716, 2013

[2]. Korina E, Stoilova O, Manolova N, Rashkov I. Poly(3-hydroxybutyrate)-based hybrid materials with photocatalytic and magnetic properties prepared by electrospinning and electrospraying, *J. Mater. Sci.*, 49, 2144-2153, 2014

[3]. Korina E, Stoilova O, Manolova N, Rashkov I. Polymer fibers with magnetic core decorated with titanium dioxide prospective for photocatalytic water treatment, *JESE*, 6(2), 2075-2084, 2018.

[4]. Spasova M, Stoilova O, Manolova N, Rashkov I, Naydenov M. Electrospun eco-friendly materials based on poly(3-hydroxybutyrate) and TiO_2 with antifungal activity prospective for Esca treatment, *Polymers*, 12, 1384-1395, 2020

[5]. Tsekova P, Stoilova O. Fabrication of electrospun cellulose acetate/nanoclay composites for pollutant removal, *Polymers*, 14, 5070, 2022

HYBRID CATALYSIS: A POWERFUL SYNERGY BETWEEN CHEMICAL AND BIOLOGICAL CATALYSIS

Rénato Froidevaux,[1]* Alexandra Gimbernat,[1] Antoine Lancien,[1] Pascal Dhulster,[1] Franck Dumeignil,[2] Damien Delcroix,[3] Nicolas Lopes Ferreira,[3] Egon Heuson,[2] Jean-Sébastien Girardon[2]

[1]UMRT BioEcoAgro 1158, Equipe Biotransformation/Enzymes et Biocatalyse, Univ. Lille, INRAE, Univ. Liège, UPJV, JUNIA, Univ. Artois, Univ. Littoral Côte d'Opale, ICV – Institut Charles Viollette, Lille, France

[2]Univ. Lille, CNRS, Centrale Lille, Univ. Artois, UMR 8181 - UCCS - Unité de Catalyse et Chimie du Solide, Lille, France

[3]IFP Energies Nouvelles, Solaize, France

**renato.froidevaux@univ-lille.fr*

1. Introduction

The use of biomass as a raw material is particularly attractive as a potentially competitive strategy to overcome the scarcity of fossil fuels and try to minimize the negative environmental impact associated with their use. Indeed, biomass is the main source of renewable carbon and usable to obtain chemical intermediates. Nevertheless, the transformation of highly functionalized molecules from biomass requires a renewal of the knowledge acquired during the implementation of existing petrochemical processes. Thus, the concept of bio-refinery is currently the focus of many international studies. The conversion of biomass in these new production units requires the design of new processes and the control of these new chemical transformations marking industrial renewal. The combination of biological catalysis and chemical catalysis, called "hybrid catalysis", is part of these new concepts that can meet the emerging challenges posed by the biomass valorization to produce platform molecules which could be used as substitute for synthesis of food-grades polymers, for cosmetic applications, etc [1].

In this context, I presented two examples developed between UMRtBioEcoAgro for enzyme biocatalysis and UCCS for heterogeneous catalysis: an innovative hybrid process two-pots one-step for obtaining 5-hydroxymethylfurfural (5-HMF) from D-glucose, and a one-pot one-step hybrid process which allows a direct conversion of 5-HMF into AMFC (5-aminomethyl-2-furancarboxylic acid), combining immobilized transaminase and heterogeneous catalyst.

2. Experimental

Concerning the first example, the compatibility issues related to the coupling of the D-glucose isomerization enzyme and the chemical dehydration catalyst have been solved by the implementation of a liquid membrane carrying the D-fructose. A hybrid catalysis process was then implemented in a specially designed innovative "H-reactor". This process made it possible to remove the lock related to the compatibility of the operating conditions and to exceed the yield limitation related to the thermodynamic equilibrium of the isomerization reaction, theoretically about 50%. Concerning the second example, the process includes an intermediate reaction product which is 5-aminomethyl-2-methylalcohol furfural (HMFA) obtained through the action of transaminase onto the aldehyde moiety of the HMF. The remaining alcohol function is then oxidized into carboxylic acid by the heterogeneous catalyst.

3. Results and discussion

The 5-HMF production ask for the glucose isomerization into fructose and the fructose dehydration to 5-HMF. This original catalysis coupling process allows to shift the thermodynamic equilibrium of the glucose enzymatic isomerization reaction, theoretically about 50%, by the integration of a simultaneous chemocatalytic fructose dehydration to 5-HMF (Figure 1) [1] in a hybrid catalysis process "two pots – one step" (Figure 2) [2,3].

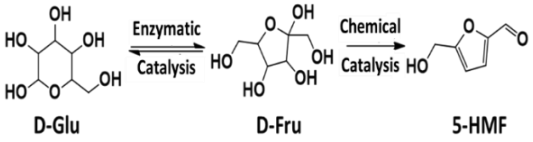

Figure 1. Reaction scheme of the hybrid catalysis process for the glucose transformation.

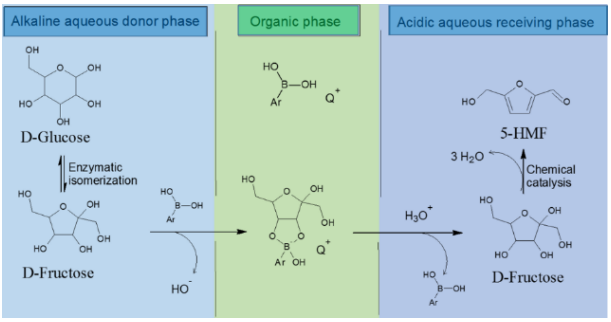

Figure 2. Hybrid catalysis concept developed.

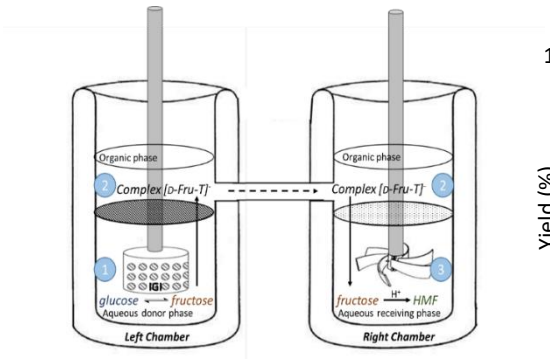

Figure 3. "H-reactor" for improvement of "2P-1S" hybrid catalysis and graphical representation of isomerization yield, extraction yield, extraction yield, dehydration yield and D-glucose conversion.

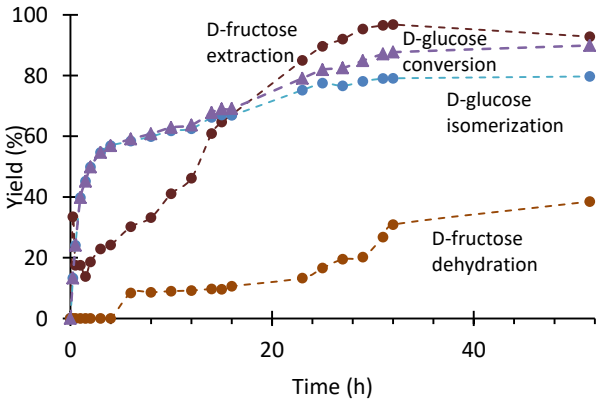

Figure 4. Graphical representation of isomerization yield, extraction yield, extraction yield, dehydration yield and D-glucose conversion.

A "H-reactor" was developed specifically for the implementation of hybrid catalysis for direct conversion of D-glucose to 5-HMF (Figure 3). This reactor is made up of two cylindrical chambers linked by a tubing connection whose length can be modified (all in glass and temperature controlled). The left chamber contains the aqueous donor phase in which the glucose isomerization occurs using an immobilized glucose isomerase introduced in an agitation basket (phase 1). The formed D-fructose is extracted from the aqueous donor phase by formation of a fructoboronate complex [D-Fru-DCPBA] to the organic phase (phase 2). The organic phase is circulating between the two chambers. The D-fructose is then released into the aqueous receiving phase (phase 3). In this aqueous phase the D-fructose dehydration reaction is realized [3]. The D-fructose extraction yield increases during the experiment to reach 96.8% after 32h (Figure 4). The isomerization yield increases to reach 79.1% after 32h. The 5-HMF yield increases to reach 30.9% after 32h. The calculation of the glucose conversion after 32h results in 87.7%. Isomerization and D-glucose conversion have not changed since 32h. The extraction yield of 96.8% after 32h demonstrates an efficient D-fructose transport in the reactor. The isomerization yield of 79.1% highlights an isomerization equilibrium shift of 29% due to the simultaneous D-fructose extraction from the

aqueous donor phase. The dehydration yield of 30.9% after 32h validates the feasibility of 5-HMF production by hybrid catalysis process in the H-reactor [4].

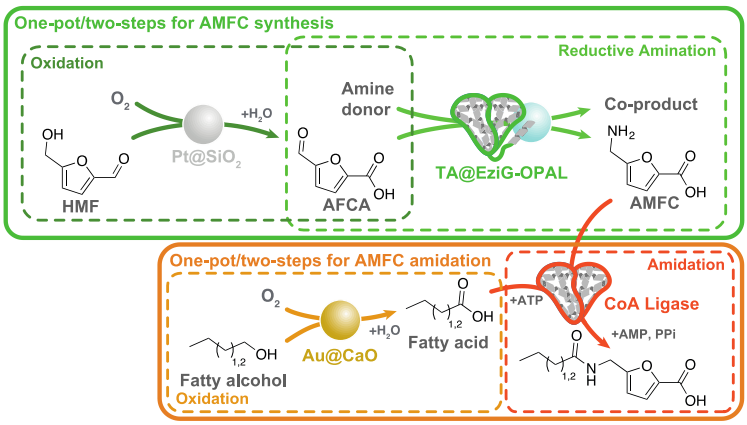

Figure 5. Hybrid catalytic processes for AMFC synthesis and amidation

Concerning the second example, we recently proposed the synthesis of AMFC directly from HMF using a hybrid one-pot/two-step process combining a platinum nanoparticle and a transaminase, both immobilized on silica beads (Figure 5) [5]. This process resulted in a 77% yield of the desired product, with 100% conversion of HMF and only one by-product, FDCA, another high value compound. A one-pot/one-step process is currently being developed using a newly discovered thermostable transaminase. In addition, this first hybrid step has since been complemented by a second step to obtain new amphiphilic molecules from AMFC, to target the production of innovative surfactants. The idea was to be able to graft aliphatic chains onto the amine function through the formation of an amide bond using sustainable catalysts and common alcohols. We therefore developed a second hybrid route, this time combining a gold nanoparticle immobilized on different supports to carry out the oxidation of the aliphatic alcohols into fatty acids, the latter then being coupled to the AMFC with the help of a CoA ligase, also thermostable. Here, 71% and 44% of amide formation could be obtained after 64h with butanol and pentanol as starting material respectively, in a one-pot/two-step process. Noteworthy, the limiting step remains the enzymatic one with 100% of alcohols to acids conversion. In addition to the overcoming of this bottleneck, a fully integrated one-pot/one-step process is also currently being developed.

References

[1]. Heuson E, Dumeignil F. The various levels of integration of chemo- and bio-catalysis towards hybrid catalysis. *Catal. Sci. Technol*. 10, 7082-7100, 2020

[2]. Gimbernat A, Guehl M, Capron M, Lopes Ferreira N, Froidevaux R, Girardon JS, Dhulster P, Delcroix D, Dumeignil F. Hybrid catalysis: an innovative concept for valorization of biosourced saccharides to value-added chemicals, *ChemCatChem* 9, 2080-2084, 2017

[3]. Dumeignil F, Guehl M, Gimbernat A, Capron M, Lopes Ferreira N, Froidevaux R, Girardon JS, Wojcieszak R, Dhulster P, Delcroix D. From sequential chemoenzymatic synthesis to integrated hybrid catalysis: taking the best of both worlds to open up the scope of possibilities for a sustainable future, *Catal.: Sci. Technol*. 8, 5708-5734, 2018

[4]. Gimbernat A, Guehl M, Lopes Ferreira N, Heuson E, Dhulster P, Capron M, Dumeignil F, Delcroix D, Girardon JS, Froidevaux R. From a sequential chemo-enzymatic approach to a continuous process for HMF production from glucose, *Catalysts* 8, 335-355, 2018

[5]. Lancien A, Wojcieszak R, Cuvelier E, Duban M, Dhulster P, Paul S, Dumeignil F, Froidevaux R, Heuson E. Hybrid conversion of 5-hydroxymethylfurfural to 5-aminomethyl-2-furancarboxylic acid: toward new bio-sourced polymers. *ChemCatChem*. 13, 247-259, 2021

FLUORESCENT DYES BY RATIONAL DESIGN AND SERENDIPITOUS DISCOVERIES

Daniel B. Werz*
Institute of Organic Chemistry, Albert-Ludwigs-Universität Freiburg, Freiburg, Germany
**daniel.werz@chemie.uni-freiburg.de*

Abstract

The rich chemistry of the BODIPY motif, together with its beneficial photophysical properties, has markedly boosted the popularity of this user-friendly fluorophore over the last few decades [1,2]. The diversity of easily incorporated fluorescence modulation modes has set the stage for a variety of sensorically active species.

The talk describes which physical-organic rationalization led to the development of the BOIMPY motif showing a significant red-shift with respect to the parent BODIPY [3,4]. In addition, a simple synthetic route to oligomerized ethano-linked BODIPYs (up to an octamer) is presented which can be further oxidized to huge completely conjugated systems [5,6]. Photophysical properties and biological properties are discussed by experimental and theoretical means [7].

It is shown that the suprastructure of the oligomeric dyes plays a significant role for their absorption and emission properties and that the conjugated systems are interesting NIR fluorophores.

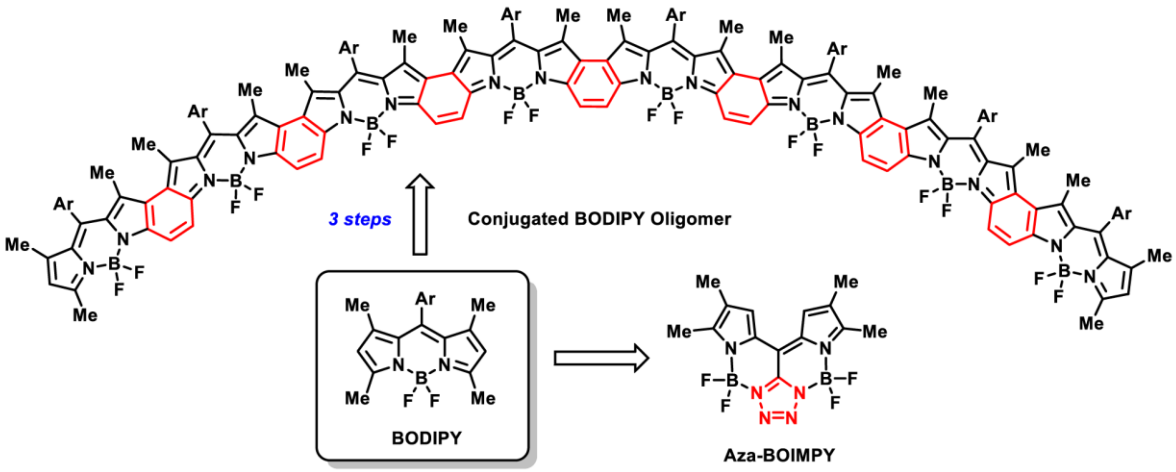

Scheme 1. BODIPY, (Aza-)BOIMPY and highly conjugated BODIPY oligomer.

References

[1]. Loudet A, Burgess K. BODIPY Dyes and their derivatives: Syntheses and spectroscopic properties, *Chem. Rev*. 107, 4891-4932, 2007
[2]. Ulrich G, Ziessel R, Harriman A. The chemistry of fluorescent BODIPY dyes: Versatility unsurpassed. *Angew. Chem. Int. Ed*. 47, 1184-1201, 2008
[3]. Patalag LJ, Jones PG, Werz DB. BOIMPYs: Rapid access to a family of red-emissive fluorophores and NIR dyes. *Angew. Chem. Int. Ed*. 55, 13340-13344, 2016

[4]. Patalag LJ, Jones PG, Werz DB. Aza-BOIMPYs: A tetrazole auxochrome for highly red-emissive dipyrromethene-based fluorophores. *Chem. Eur. J*. 23, 15903-15907, 2017
[5]. Patalag LJ, Phong Ho L, Jones PG, Werz DB. Ethylene-bridged oligo-BODIPYs: Access to intramolecular J-aggregates and superfluorophores. *J. Am. Chem. Soc*. 139, 15104-15113, 2017
[6]. Patra A, Patalag LJ, Jones PG, Werz DB. Extended Benzene-Fused Oligo-BODIPYs: In three steps to a series of large, arc-shaped, near-infrared dyes. *Angew. Chem. Int. Ed*. 60, 747-752, 2021
[7]. Patalag LJ, Ahadi S, Lashchuk O, Jones PG, Ebbinghaus D, Werz DB. GlycoBODIPYs: Sugars serving as a natural stock for water-soluble fluorescent probes of complex chiral morphology. *Angew. Chem. Int. Ed*. 60, 8766-8771, 2021

ARTIFICIAL MUSCLES FROM BUNDLES OF SILICONE-BASED DIELECTRIC ELASTOMER FIBERS

Anne Ladegaard Skov,* Zhaoqing Kang, Liyun Yu
Technical University of Denmark, Department of Chemical and Biochemical Engineering, Danish Polymer Center, Kgs. Lyngby, Denmark
**al@kt.dtu.dk*

1. Introduction

Silicone-based fibers are highly flexible and can respond to external stimuli and thereby mimic natural muscles. When integrated into soft robotic systems, these fibers can form muscle-like structures that can closely replicate the functions of biological muscles, thus making them one of the most promising materials for artificial muscles [1,2]. Moreover, their versatility allows for easy bundling, facilitating the design of actuator systems capable of generating substantial output forces. This opens exciting possibilities for advanced robotic systems and flexible devices requiring powerful actuation [3,4]. In this study, we utilized a spinning process and a photocurable thiol-ene-based silicone resin to fabricate silicone hollow fibers. These fibers were then employed to construct fiber actuators, using an ionic liquid as the inner electrode and an ionogel as the outer electrode. The resulting fiber actuators demonstrate significant linear strains.

2. Experimental

Mercaptopropyl PDMS (SMS-042, Mn = 6000-8000 g/mol) and vinyl-terminated PDMS (DMS-V31, Mn = 28000 g/mol) were purchased from Gelest. 1-ethyl-3-methylimidazolium bis(trifluoromethylsulfonyl)imide ([Emim][TFSI]), 2,2-dimethoxy-2-phenylacetophenone (DMPA), 2-ethyl-1-hexanol were purchased from Sigma-Aldrich. A thiol-ene PDMS formulation was selected as a spinning solution to prepare PDMS fibers, due to the high reaction conversion and rapid gelation. As seen in Figure 1, in this click reaction, thiol (R-SH) groups add to double bonds (C=C) to form an alkyl sulfide.

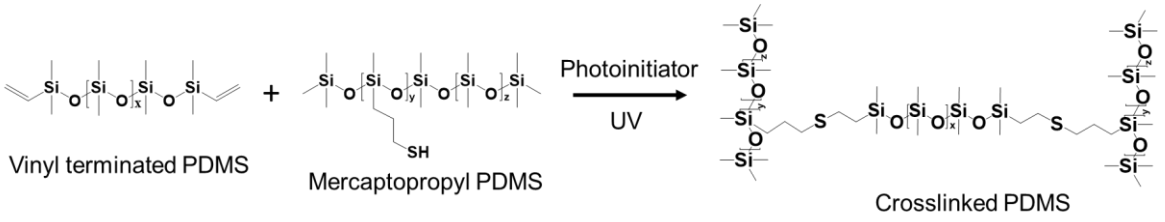

Figure 1. Thiol-ene click reaction to prepare PDMS fibers.

Figure 2a shows the preparation of PDMS fiber by the spinning method cured under UV-irradiation (λ = 365 nm, exposure energy = 300 mW/cm^2. Ionic liquid [Emim][TFSI] was injected and sealed in the hollow fiber as the inner electrode. After that, the PDMS fiber was coated with an ionogel with 75% [Emim][TFSI] as the outer electrode of the fiber actuator. As shown in Figure 2b, the ionogel is attached to the outside of the PDMS hollow fiber as the outer electrode with a uniform thickness of 6 μm.

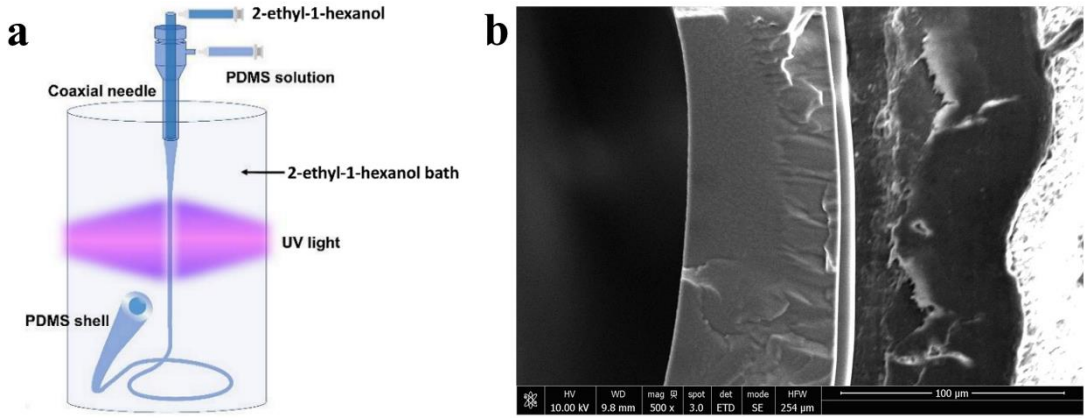

Figure 2. (a): Preparation of PDMS fiber by the coaxial spinning method;
(b): Cross-section of hollow fiber with ionogel outer electrode.

3. Results and discussion

Figure 3a shows that PDMS solid and hollow fibers present approx. 5 times higher tensile strength and strain at break compared to the film analog. In Figure 3b it is shown that the fiber actuator exhibits repeatable and stable linear actuation strain over 1000 cycles at different applied voltages. As shown in Table 1, the fiber actuator has a maximum axial strain of 9 % at 50 V/µm, which is approx. 4-fold higher than that of the planar actuator at the same electrical field.

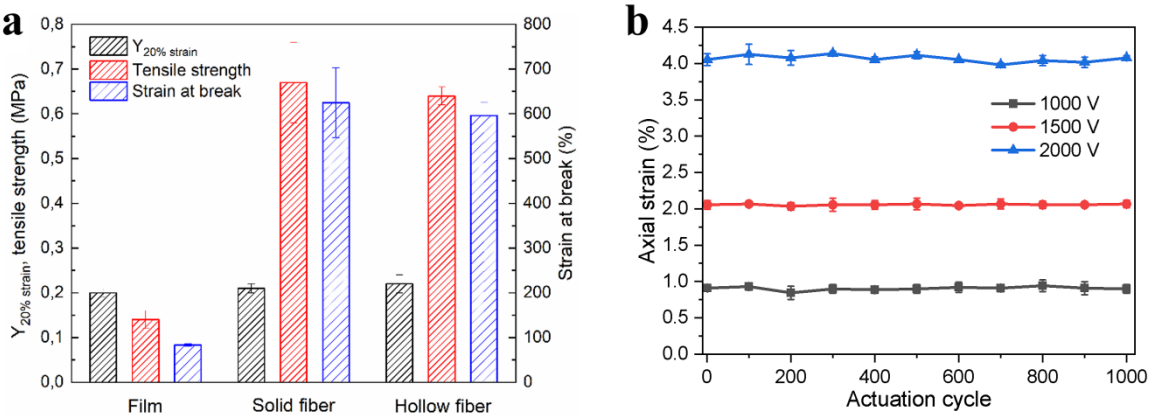

Figure 3. (a): Tensile properties of film, solid and hollow fibers;
(b): Cyclic actuation of fiber actuator at different voltages.

Table 1. Actuation strain of planar and fiber actuators.

Sample	Maximum strain (%)	Actuation strain @ 50 V/µm (%)
Planar actuator	4.5	2.3
Fiber actuator	9.0	9.0

We show the capability of bundling fiber actuators to increase the generated forces. For instance, by winding a long fiber into 22 actuation segments, a high weightlifting capacity of 14 g is achieved, accompanied by an actuation strain of approximately 3% (Figure 4a). Furthermore, when the actuation segments are set separately, the fibers still achieve a 2 mm actuation displacement (Figure 4b).

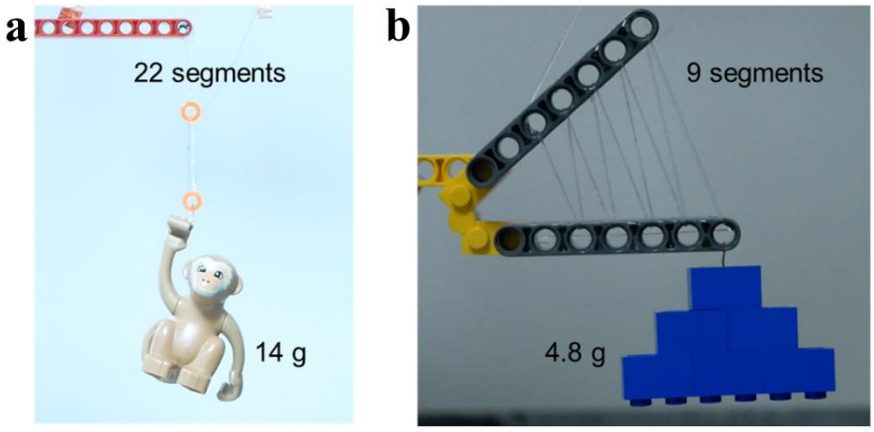

Figure 4. Lifting fiber actuation system. (a) Lifting a monkey; (b) Fibers combined with Lego bricks as a lifting device.

4. Conclusions

In this work, we developed a continuous wet spinning method to prepare silicone fibers using a photocurable thiol-ene reaction between sulfhydryl (R-SH) and alkene (C=C) groups. The dimensions of the fibers are adjusted by modifying the flow rate of the silicone layer and internal removable solvent during the spinning process. The developed and optimized silicone fiber has an external diameter of 463 μm and uniform wall thickness of 78 μm. The silicone fiber exhibits enhanced tensile properties, with a 596 % strain at break and 0.64 MPa tensile strength, compared to these of the planar film (86% strain at break and 0.14 MPa tensile strength). The fiber actuator is then assembled by injecting ionic liquid as the core electrode and dip-coating ionogel as the electrical outer sheath. The fiber actuator exhibits a large linear strain of 9 % and repeatable and stable linear actuation strain over 1000 cyclic actuation tests. Furthermore, the fiber actuator can be assembled into bundles by winding a long fiber into a bunch for increased forces. Large actuation displacement is achieved by increasing the length of the fiber actuator as well. Inspired by a human arm, a weight-lifting system with Lego models demonstrates the high potential of the fiber actuator as artificial muscles. The work presented herein provides a pathway for creating active soft matter with complex architectures to enable fast programmable actuation for multiple applications including artificial muscle.

Acknowledgements

This work is supported by the Department of Chemical and Biochemical Engineering, Technical University of Denmark, and the Institute of Process Engineering, Chinese Academy of Sciences.

References

[1]. Chortos A, Mao J, Mueller J, Hajiesmaili E, Lewis JA, Clarke DR. Printing reconfigurable bundles of dielectric elastomer fibers. *Adv. Funct. Mater.* 31, 2010643, 2021

[2]. Kang Z, Yu L, Nie Y, Skov A L. Crosslinking methodology for imidazole-grafted silicone elastomers allowing for dielectric elastomers operated at low electrical fields with high strains. *ACS Appl. Mater. Interfaces*. 14, 51384-51393, 2022

[3]. Smith M, Cacucciolo V, Shea H. Fiber pumps for wearable fluidic systems. *Science* 379, 1327-1332, 2023

[4]. Pelrine RE, Kornbluh RD, Joseph JP. Electrostriction of polymer dielectrics with compliant electrodes as a means of actuation. *Sens. Actuator A Phys.* 64, 77-85, 1998

ENVIRONMENTAL ASPECTS OF POLYMERS AND POLYMER WASTES

Piotr Rychter*
Faculty of Science and Technology, Jan Dlugosz University in Czestochowa, Czestochowa, Poland
**p.rychter@ujd.edu.pl*

1. Introduction

Nowadays, the western world has experienced a rapid increase in both production and consumption of plastics. Growing consumption of these microbial resist materials has further lead to increased amounts of solid wastes. Lack of degradability and the closing of landfill sites as well as growing water and land pollution problems have led to the led concern about plastics. The growing global environmental and social concern, high rate of depletion and the increasing cost of petroleum resources, as well as new environmental regulations have awakened the search for sustainable alternatives. Conventional plastics have successfully replaced many other products made of metal or glass over the years and have been used extensively in medical, domestic and industrial applications. Traditional, non-degradable polymers are utilized in almost every manufacturing industry in the world because of the favorable balance of mechanical, technological and cost factors. Synthetic polymers are present in everyday life. They are used in short-term applications in the form of disposable packaging, furniture, utensils or accessories, enhancing life quality and comfort. During the past decades a wide variety of synthetic polymers have been developed by industry to satisfy the increasing market demand. The widespread use of plastics and their slow rate of degradation, and consequently long life in the environment, results in a serious pollution problem especially in the leading industrialized countries.

A huge problem concerning the methods for the proper disposal of plastics exists for many years. The cost of collecting and processing waste plastics typically exceeds the value of the material. Plastic recycling is complicated and often uneconomical process. With this respect, it is expected that landfilling and harmful environmental impact of plastic wastes will be still crucial environmental problem of many countries all over the world over the next years. Therefore there is an urgent need to reuse polymers or at least try to substitute conventional polymers with biodegradable ones wherever it is possible. From few decades, biobased, biodegradable and biocompatible polymers are in the phase of intensive study due to their nontoxicity against environment and human body, therefore their use should be the challenge all over the world in face of worldwide plastic wastes contamination [1-5].

In this work, environmental application of few polymers both biodegradable and not, like for example poly(methylene-co-cyanoguanidine, selected polyethylenimines and hydrogels, PLA/PEG blends, starch based films will be presented.

2. Results and discussion

In the present study few groups of polymers were tested towards their usefulness for environmental and agricultural purposes. Starch based polymers modified with plasticizer urea, promoted the growth of plants growing when buried in soil (Figure 1a).

Poly(methylene-co-cyanoguanidine) (PMCG) buried in soil, released within 6 months, degradation products which were nutrients for plants (Table 1). Inconclusive results were obtained during phytotoxicity evaluation of selected polyethylenimines (PEIs) including poly(2-ethyl-2-oxazoline) (PEtOx) as an N-acyl-substituted PEI, linear polyethylenimine (LPEI) and branched polyethylenimine (BPEI). Blends of polylactide (PLA) with poly(ethylene glycol) (PEG) were very promising as the carrier of Matribuzin – soil applied herbicide (Figure 2).

Impact of hydrogels: poly(acrylamide-*co*-sodium 4-hydroxy-2-methylenebutanoate), borate-crosslinked poly(vinyl alcohol), poly(acrylamide), and poly(acrylamide-*co*-sodium acrylate) on water holding capacity of soil and plant growth demonstrated that bio-based superabsorbent, (prepared from renewable monomer Tulipalin A) promoted growth of plants in contrast to PVA based hydrogels (Figure 1b).

a) b)

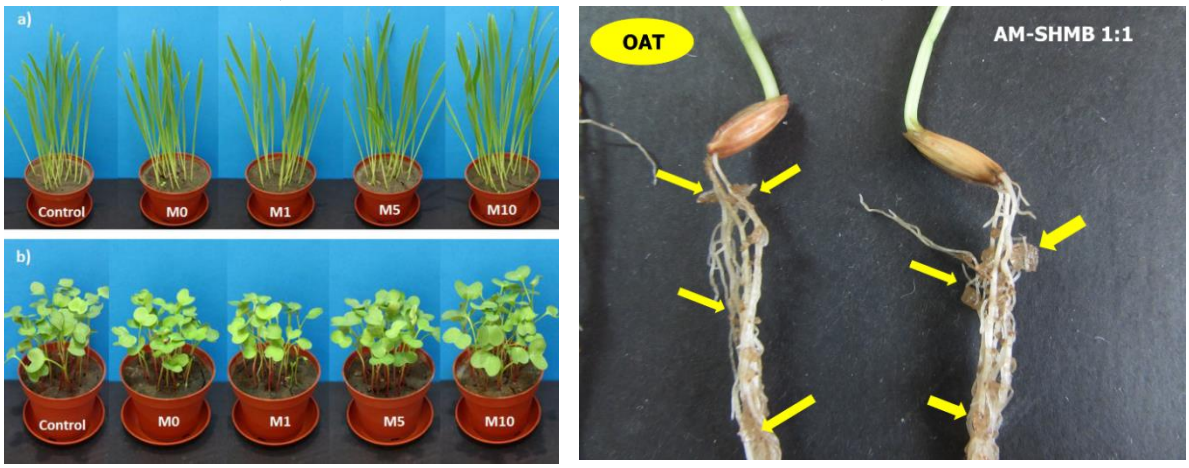

Figure 1. Photographs of a) plants growing 14 days in the presence of starch modified with growing concentration of plasticizer – urea; b) roots of oat with attached hydrogels during growth.

Table 1. Effect of PMCG on the shoot height and yield of radish sprouts (mean ± SD) determined after 14 days of growth in the soil containing different amounts of PMCG present in the soil for a different period. Negative values mean that examined parameter was higher (promoted growth) compared to the control plants.

PMCG (mg/kg of soil)	0	1 month	3 months	6 months
	SHOOT HEIGHT (% compared to control plants)			
20	-2.5±1.4	-10.2±0.2	-15.7±1.7	-9.8±3.3
100	-4.0±0.0	-16.4±0.5	-22.8±0.7	-12.3±1
500	-4.1±0.3	-16.6±0.1	-22.6±0.6	-21.5±1.5
1000	-4.7±0.5	-6.2±0.2	-8.3±0.7	-15.3±0.4
2000	5.7±2.5	6.0±2.1	16.4±4.5	17.5±5.5
	YIELD (% compared to control plants)			
20	2.9±1.6	-4.1±1.9	-9.2±1.5	-13.5±0.5
100	-18.8±0.2	-6.0±0.1	-21.2±0.4	-12.3±1
500	-14.2±0.2	-27.6±0.4	41.3±0.5	-44.0±0.3
1000	-25.3±0.9	-33.8±0.0	-53.3±0.4	-54.1±0.2
2000	18.4±1.0	17.7±1.8	23.0±2.4	12.0±2.5

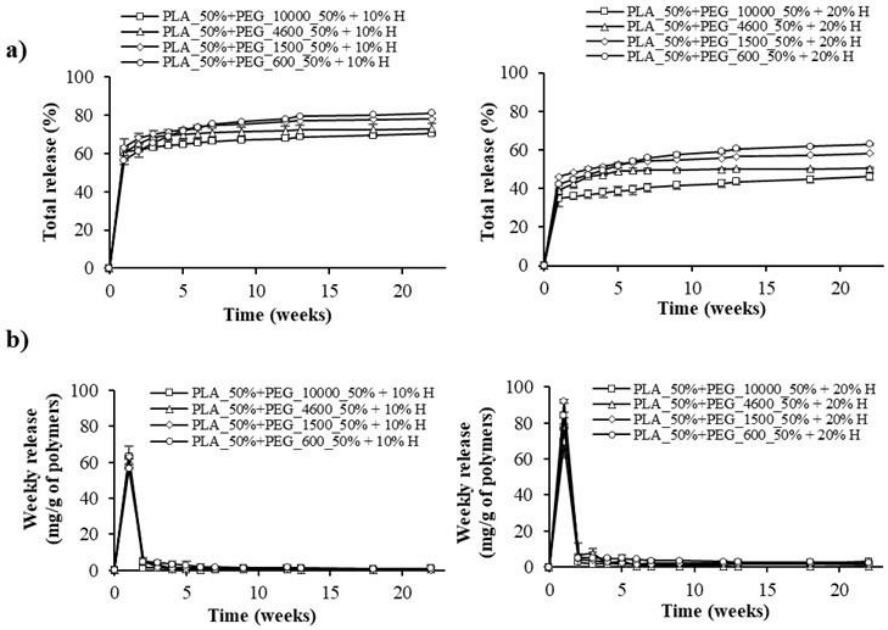

Figure 2. Curves of the release process of Metribuzin from PLA/PEG 50/50 blends loaded with 10% and 20% of herbicide (10%H and 20%H, respectively) during the time of study: (a) present percentage total release of Metribuzin and (b) weekly release of Metribuzin expressed as mg/g of polymer carrier (blend).

3. Conclusions

The following conclusion can be drawn from the work:

- Biodegradable polymers are very useful material for environmental/agricultural applications (play role not only polymeric carrier of active agent, but also may be useful fertilizer as they are)
- Some nonbiodegradable polymers may be reuse as fertilizer.
- Biobased hydrogels may be successfully used as an environmentally friendly water reservoir with soluble nutrients in arid and desert areas.

Acknowledgements

Research were financially supported by R&D subsidy of Faculty of Science and Technology of Jan Dlugosz University in Czestochowa.

References

[1]. Rychter P, Rogacz D, Lewicka K, Lacik I. Poly(methylene-*co*-cyanoguanidine) as an eco-friendly nitrogen fertilizer with prolonged activity. *J Polym Environ*. 27, 1317-1332, 2019

[2]. Rychter P, Christova D, Lewicka K, Rogacz D. Ecotoxicological impact of selected polyethylenimines toward their potential application as nitrogen fertilizers with prolonged activity. *Chemosphere*, 226, 800-808, 2019

[3]. Rychter P, Rogacz D, Lewicka K, Kollár J, Kawalec M, Mosnáček J, Ecotoxicological properties of Tulipalin A-based superabsorbents vs. conventional superabsorbent hydrogels, *Adv Polym Technol.* 2019, Article ID 2947152

[4]. Rychter P, Lewicka K, Rogacz D. Environmental usefulness of PLA/PEG blends for controlled release systems of soil-applied herbicides, *J Appl Polym Sci. 136*, 47856, 2019

[5]. Smola-Dmochowska A., Lewicka K, Macyk A, Rychter P, Pamuła E, Dobrzyński P. Biodegradable Polymers and Polymer Composites with Antibacterial Properties. *Int J Mol Sci.* 24, 7473, 2023


MACRO Iași 2023

THE MAGNETIC ANISOTROPY IN THE LANTHANIDE COORDINATION UNIT ASSEMBLIES

Marilena Ferbinteanu,[1]* Fanica Cimpoesu[2]
[1]*University of Bucharest, Faculty of Chemistry, Bucharest, Romania*
[2]*Institute of Physical Chemistry, Bucharest, Romania*
**marilena.cimpoesu@g.unibuc.ro*

1. Introduction

The lanthanide systems are a subject of enhanced interest and numerous studies with focus on their magnetic properties, which are promising for the building of nano-scale magnets. Due to the intrinsic magnetic anisotropy, complexes of certain lanthanide ions became interesting for special properties such as the single molecule magnet (SMM) phenomenon, as well rare-earth based single chain magnets (SCM) and single ion magnets (SIM) were reported. The variety of the SMM systems, from large d–f clusters, to d–f binuclears [1] demonstrates the rather large generality of the effect and the key role of the magnetic anisotropy on the lanthanide ions. We attempted the rationalization of such factors [2] defining our interest for systematic investigations in this area [3]. The complicate structure-properties relationships of lanthanides make their coordination chemistry a challenging open field that offers case studies serving to draw new magneto-structural correlations or thumb rules for the supramolecular assembling. To be distinguished from prototypic supramolecular chemistry, dealing with the packing of rather stable organic or d-type molecular units, the lanthanide complexes bring the issue of the relative floppiness of their own molecular structure. This is due to the fact that the bonding of the coordination complexes is practically of noncovalent, merely ionic, nature. Therefore, without the covalent type feature of directed bonds the positions of the ligands on the coordination sphere are more flexible, a feature favoring the versatility during the supramolecular and lattice packing. Hereby we discuss in details several study cases, trying to emphasize that the information drawn from the particular structure and properties can be used as a piece in the larger puzzle of lanthanide anisotropy paradigm. The compounds contain different lanthanide coordination units as neutral $[Er(NO_3)_3(H_2O)_4]$ (in **1**) or ionic as $[Er(NO_3)_4(H_2O)_2]^-$ (in **2**) and $[Er(NO_3)_5]^{2-}$ (in **3**), stabilized by d-cation complex units. In their relative simplicity, the neutral or ionic coordination units of lanthanide ions are structurally and magnetically interesting. The experimental investigation was completed with ab initio calculations done with state-of-the-art methods for the lanthanide units embedded in a sequence taken from the experimental structure.

2. Experimental

Synthesis: The synthesis and basic crystallographic data for the complexes $[Fe(bpca)_2][Er(NO_3)_3(H_2O)_4]\cdot NO_3\cdot H_2O$ (**1**) and $[Fe(bpca)_2][Er(NO_3)_4(H_2O)_2]$ (**2**), where bpca is bis(2-pyridilcarbonyl)amine, were described in previous papers, dedicated to their magnetic properties [4,5]. The synthesis of $[Zn(phen)_3][Er(NO_3)_5]$ (**3**) was done by coupling reaction between $[Zn(phen)_3](NO_3)_2$ and $Er(NO_3)_3\cdot 6H_2O$. The compound was characterized by single crystal X-ray diffraction method. *Ab initio calculations*: The CASSCF (Complete Active Space Self-Consistent Field) and spin orbit calculations were performed with the GAMESS program, using SBKJC effective core potential and basis set for Er(III) and 6-311G* basis set for the ligands. The bonding in the model Lu(III) complexes was analyzed by DFT calculations (Density

Functional Theory) with ADF (Amsterdam Density Functional) code, using gradient corrected Becke–Perdew functional and the TZP basis set.

3. Results and discussion

The network of compound **1** contains distinct d-complex cations and 1-D assembled $[Er(NO_3)_3(H_2O)_4]$ neutral units (Figure 1a). The non-coordinated nitrate ions play a role in the hydrogen bond bridging of neighbor lanthanide complex units. The supramolecular architecture association can be correlated with the orientation of computed dipole moments of each unit, considering their vectorial components (Figure 1b). Considering the Er…Er separation in the chain, around 7.7 Å, one may estimate, with dipolar formulas, energies in a 0.26 cm^{-1} range, suggesting that such effects can intervene in the intricate phenomena related with the magnetization relaxation. An interesting view to the magnetic anisotropy was added with the help of the ab initio calculations (Figure 1c).

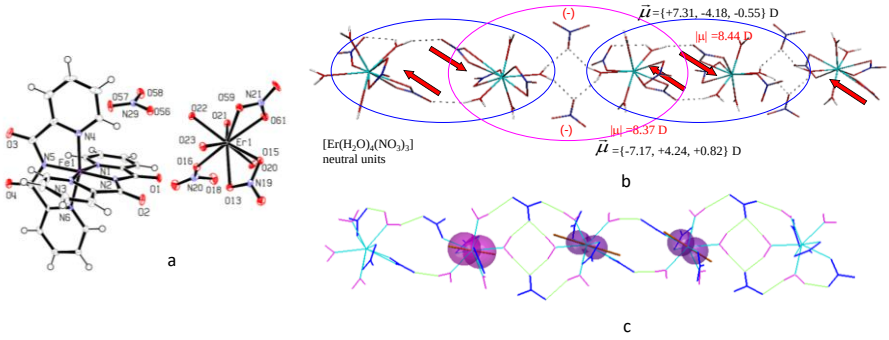

Figure 1. (a) The asymmetric unit of compound (**1**) with atom numbering scheme; (b) The electric dipolar ordering and hydrogen bonds for 1D assembled $[Er(NO_3)_3(H_2O)_4]$ units in (**1**); (c) The magnetization tensors for the ground states of the $[Er(NO_3)_3(H_2O)_4]$ units, obtained via CASSCF+SO ab initio calculations including subsequently the modeling of magnetic field effects.

The system (**2**) is a complex cation–complex anion type coordination compound, consisting of distinct d and f units (Figure 2a), interlinked by hydrogen bonds. Particularly, the f-type complex anions are associated in dimers (Figure 2b). The energy decomposition analyses based on DFT calculations offered supplementary insight into the coordination effects at the lanthanide ions and the hydrogen bond driven supramolecular association of the complex units. Special ab initio procedures and subsequent modeling afforded the computation of anisotropic magnetization tensors of the $[Er(NO_3)_4(H_2O)_2]^-$ f-type units (Figure 2c).

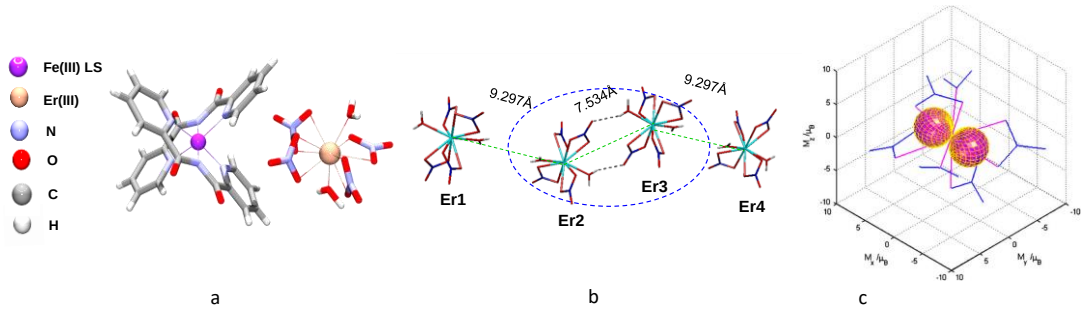

Figure 2. (a) The asymmetric unit of compound (**2**) with atom color scheme; (b) The hydrogen-bond-ed chain structure formed by $[Er(NO_3)_4(H_2O)_2]$ units in (**2**);(c) Magnetic anisotropy computed for Er(III) coordination unit (after CASSCF+SO calculations), represented as the momentum induced on the ion at external field.

Compound (**3**) is also a complex cation–complex anion type coordination compound with distinct d and f units (Figure 3a), without water molecules as ligand or in the network. The simple lanthanide pentanitrate are suitable for determining the Ligand Field parameters (Figure 3b) and mapping the SMM behavior trough the computation of anisotropic magnetization tensors (Figure 3c).

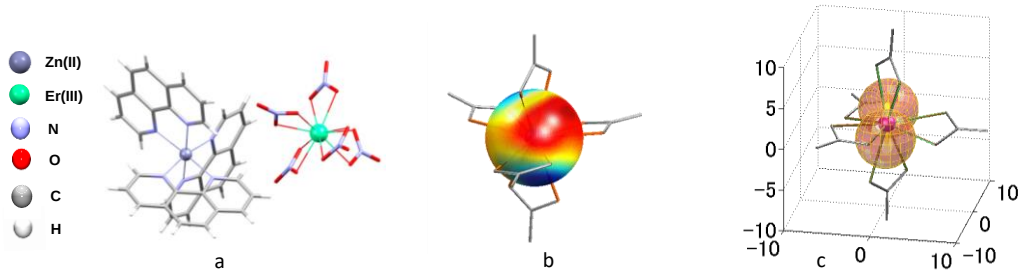

Figure 3. (a) The asymmetric unit of compound (**3**) with atom color scheme; (b) The Ligand Field potential map for J=15/2 Er(III) in (**3**);(c) Magnetic anisotropy as polar maps of the (dE/dB) field derivatives for the groundstates of the $[Er(NO_3)_5]^{2-}$ units in (**3**).

4. Conclusions

The stereochemistry and electronic structure of three lanthanide complex units with different number of coordinated aqua molecules are analyzed. The relative complexity of the different coordination and supramolecular association modes was decrypted with the help of properly designed post-computation analyses and numeric experiments. In this way, we advanced toward the understanding of the mechanisms acting in the supramolecular chemistry of coordination units, going beyond the usual qualitative description of crystal architectures and taxonomic account of long-range contacts. The work presented interdisciplinary, experimental and theoretical, insight into the bonding regime and magnetic properties of d–f system. The ab initio multi-configuration and spin orbit treatment of each lanthanide unit revealed the anisotropic magnetization tensor, in its relative orientation to the molecular frame.

Acknowledgements

This research was supported by National Romanian Office for Research, UEFISCDI, by the grant PN-III-P4-PCE-2021-1881, contract no. 123/2022.

References

[1]. Ferbinteanu M, Kajiwara T, Choi KY, Nojiri H, Nakamoto A, Kojima N, Cimpoesu F, Fujimura Y, Takaishi S, Yamashita M. A binuclear Fe(III)Dy(III) single molecule magnet. Quantum effects and models. *J. Am. Chem. Soc.* 128, 9008-9009, 2006

[2]. Paulovic J, Cimpoesu F, Ferbinteanu M, Hirao K. Mechanism of Ferromagnetic Coupling in Copper(II)-Gadolinium(III) Complexes. *J. Am. Chem. Soc.* 126, 3321-3331, 2004

[3]. Putz MV, Cimpoesu F, Ferbinteanu M. Structural Chemistry Principles, Methods, and Case Studies. Switzerland: Springer; 2018

[4]. Ferbinteanu M, Kajiwara T, Cimpoesu F, Katagiri K, Yamashita M. The magnetic anisotropy and assembling of the lanthanide coordination units in $[Fe(bpca)_2][Er(NO_3)_3(H_2O)_4]NO_3$. *Polyhedron* 26, 2069-2073, 2007

[5]. Ferbinteanu M, Cimpoesu F, Kajiwara T, Yamashita M. Magnetic anisotropy and molecular assembling in complex cation- complex anion type d-f coordination compounds. *Solid State Sci.* 11, 760-765, 2009

CROSS-LINKED POLYMER STRUCTURES: BENEFITS AND DRAWBACKS

Marc Jean Médard Abadie*
Institute Charles Gerhardt Montpellier ICGM, University of Montpellier, UMR 5253 CNRS-UM ENSCM, Pôle Chimie Balard Recherche, Campus CNRS, Montpellier, France
**marc.abadie@umontpellier.fr*

1. Introduction

The cross-linked polymeric structures [1], called as thermosets TSs or Duromers (high cross-linked) and Elastomers (low cross-linked), represent about 25% of the total polymers with a preponderance of use of thermoplastics TPs (≈ 75%) in the industry. This is mainly due to the intrinsic structure of thermosets that form a 3D network and therefore cannot be remolded unlike thermoplastics. It should be noted that the effects of cross-linking and crystallinity should be considered because they affect the solubility. Cross-linking and crystallinity are often visualized as 'similar' (in some sense) phenomena and are described with the same theories: crystalline regions are assumed to act as 'physical or giant cross-links'. However, thermosets have superior properties compared to thermoplastics *v.z.*, some general properties of TSs include: mechanical strength, thermal stability, chemical resistance, swelling behavior to cite some of them.

Semi-IPN or IPN (InterPenetrated Network) represent the ultimate super network as the mechanical properties are reinforced compared to simple cross-linked structure [2]. Recently a new class of polymers, called Vitrimers, possess dynamic covalent crosslinks [Covalent Adaptable Networks (CANs)] which imparts stability while being reprocessable [3]. We also have pseudo cross-linked systems where in situ physical gelation occurred via Hydrogen Bonding interactions or driven by hydrophobic interactions.

2. Fundamentals on 3D Structures

2a. A crosslinked system may be represented by Figure 1.

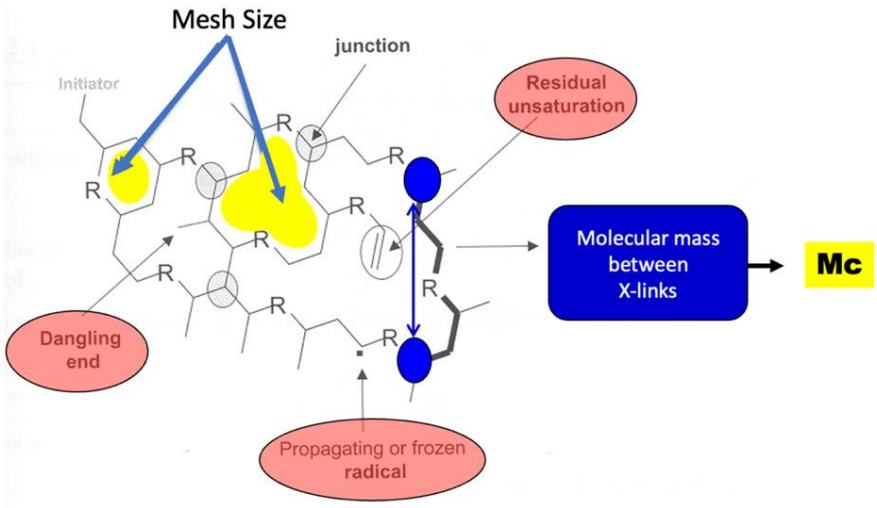

Figure 1. Representation of imperfect network.

Usually the 3D structures are inhomogeneous, contain cycles or loops, dangling ends and entanglements of molecular chains between crosslinks. We define ***Mc*** as the molecular mass between X-links that determines the network size called *Mesh size.*

We also define a 3D structure by considering the average functionality ***fav*** of the monomers involved in the cross-linking reactions *vz.* whether the chain polymerization or step polymerization mechanism is considered, Figure 2.

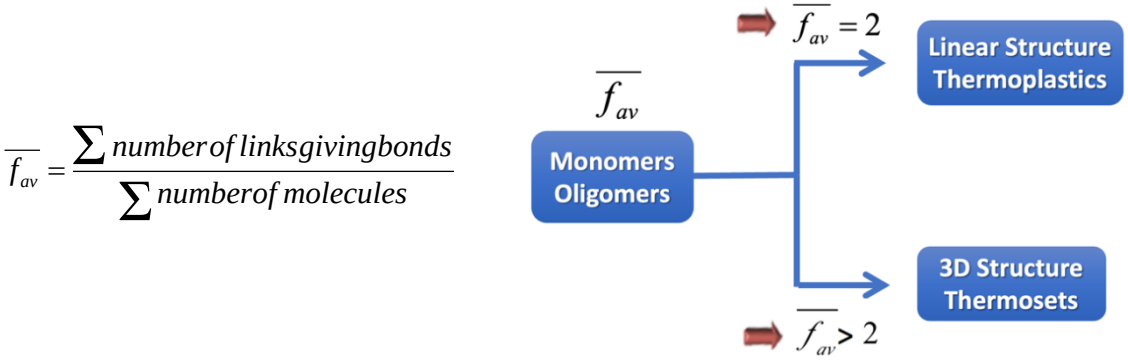

Figure 2. Average functionality number

2b. Relationship between ***Mc*** and degree of crosslinking ***Xc*** – Figure 3**.**

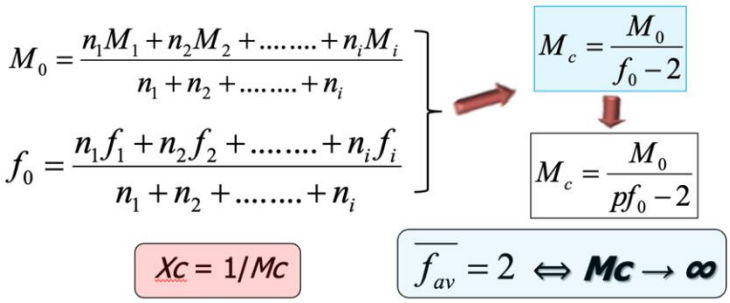

where :
- M_0 is the average molar mass,
- f_0 the average functionality of the mixture,
- ***Xc*** the degree of crosslinking,
- ***p*** the degree of conversion.

Figure 3. Degree of crossling ***X***c *vs.* ***Mc***.

2c. 3D curing *vs.* time. Cross-linked structures can only be created using multifunctional monomers or oligomers along with *fav* > 2. This physical transition is characterized by the determination of the gel time, beyond which no further processing is possible – Figure 4.

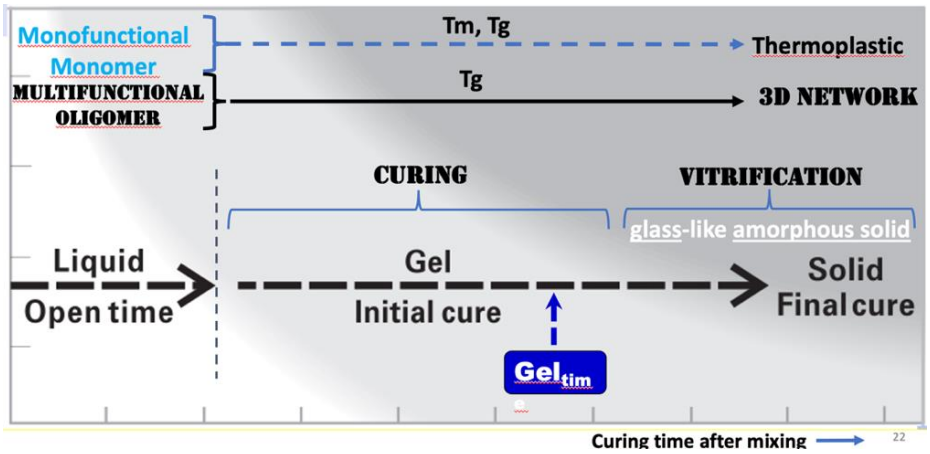

Figure 4. Curing time.

Different technics have been used to follow the kinetic of cross-linking reactions or the determination of the gel point (gel time) in the process of implementing 3D structures *e.g.*, viscosity or temperature *vs.* time, thermal mechanical analysis or rheological measurements.

3. Results and discussion

3a. Swelling control in hydrogels [4]. We have considered a mixture of two acrylates : hydroxy-ethyl methacrylate (HEMA) *fav* = 2 and di-methacrylated polyethylene glycol (PEGDMA) *fav* = 4. Results are described in Table 1.

Mass of PEG-DMA g (mol)	Mass of HEMA g (mol)	f_1	f_2	f_0	Mo (g/mol)	M_c (g/mol)	X_c (mol/g)
2.50 (1 mol)	0	4	0	4	330.37	165.19	$6.05\ 10^{-3}$
2.500 (1)	2.50 (1)	4	2	3	230.26	230.26	$4.34\ 10^{-3}$
0.500 (1)	4.50 (9)	4	2	2.20	150.16	750.81	$1.33\ 10^{-3}$
0.250 (1)	4.75 (19)	4	2	2.10	140.15	1 401.5	$0.71\ 10^{-3}$
0.125 (1)	4.875 (39)	4	2	2.05	126 .89	2 537.73	$0.39\ 10^{-3}$
0.050 (1)	4.95 (99)	4	2	2.02	132.14	6 607.12	$0.15\ 10^{-3}$
0	5.00 (100 mol)	0	2	2	130.14	∞	0

Table 1. Calculation of $\boldsymbol{X_C}$, $\boldsymbol{f1}$ and $\boldsymbol{f2}$ are the functionalities of PEGDMA and HEMA respectively, $\boldsymbol{f0}$ being the functionality of the system. $\boldsymbol{M_C}$ is the molar mass between crosslinks of PEGDMA and HEMA calculated from $\xi 2$. $\boldsymbol{X_C}$ is the degree of crosslinking of the system

It can be seen from the degree of crosslinking $\boldsymbol{Xc}$ in Table 1 that a decrease in the weight percentage of PEGDMA, results in a decrease of degree of crosslinking. Lowering the amount of PEGDMA system decreases the number of difunctional groups in the system, since PEGDMA acts as the only potential crosslinker in the reaction, less crosslinking occurs. Lower degree of crosslinking, $\boldsymbol{X_C}$ implies an increase in the 3D mesh size of the hydrogel, allowing for water to penetrate the crosslinked network.

3b. Gel time Control in Marine Composites Industry [5].

4. Conclusions

Rigorous control of a cross-linking reaction is not always possible. However, depending on the material, it is possible to correlate experimental physical quantities with theoretical calculations to optimize the desired properties.

References

[1]. Debdatta R. Chemistry and general applications of thermoset resins. In: Recent Advances and Applications of Thermoset Resins. 2nd ed. Amsterdam: Elsevier; pp. 1-172, 2022
[2]. Shreya C, Kajal G, Mohit K, Syed M, Sabu T. A detailed discussion on interpenetrating polymer network (IPN) based drug delivery system for the advancement of health care system. *J. Drug Delivery Sci. Technol*. 79, 104095, 2023
[3]. Zheng J, Png ZM, Ng SH, Tham GX, Ye E, Go SS, Loh XJ, Li Z. Vitrimers: Current research trends and their emerging applications. *Mater. Today* 51, 586-625, 2021
[4]. Hui LK, Lipik V, Abadie MJM, Biodegradable hydrogels by UV curing. In: to be published, Boca Raton: CRC Press; 2023
[5]. Abadie MJM. Fundamentals and challenges in curing process. In: Mukbaniani OV, Abadie MJM, Tatrishvili TN, editors. Chemical engineering of polymers. Production of functional and flexible materials. Waretown: Apple Academic Press; pp.215-230, 2017

POROUS SILICONES WITH TUNED SURFACE AND SENSING PROPERTIES

Carmen Racles,* Adrian Bele, Ana-Lavinia Vasiliu, Mihaela Dascalu, Maria Cazacu
Petru Poni Institute of Macromolecular Chemistry, Romanian Academy, Iasi, Romania
**raclesc@icmpp.ro*

1. Introduction

Polysiloxanes are considered the most important and commercial family of synthetic inorganic polymers [1], and silicone elastomers are outstanding materials with wide-span applications in medical field, construction, automotive, electronics, energy, engineering, aerospace and other domains. Creating pores in these materials is one way to expand their use, since silicone foams bring together the properties of silicone elastomers and those of foams, in materials with low density, heat and cold resistance, good electrical insulation, and biocompatibility [2]. The emulsion templating method, which relies on water droplets as porogen is one of the known approaches to create pores in silicone materials [3]. Other methods use gas porogens (e.g. CO_2) [2] or solid templates [4,5]. Various applications have been proposed for such materials, including sorbents [5], sensors [6], acoustic metamaterials [7], or cell-growth scaffolds [4].

We applied the emulsion template method, using amphiphilic siloxane oligomers as surfactants, to obtain porous silicones, by UV-initiated thiol-ene photoaddition [8], condensation and dehydrocoupling reactions, occurring within few minutes at room temperature. The as obtained materials were characterized in terms of morphology, surface properties and as capacitive pressure sensors. When emulsion template method was combined with dehydrocoupling or photoaddition cross-linking reaction and *in situ* chemical modification, silicone materials with tunable surface properties were obtained. The materials presented herein span from hydrophilic to highly hydrophobic with “lotus” or “petal” effect, as described in [9].

2. Experimental

The starting silicone reagents and surfactants have been prepared *in house*. The FT-IR spectroscopy (VERTEX 70, Bruker, Ettlingen, Germany) was used to monitor the reactions, SEM analyses (Quanta 200 from FEI Company or Verios G4 UC from Thermo Scientific) were performed for morphological characterization, tensiometry (Sigma 700 automated tensiometer from KSV) was used to characterize the initial emulsions and to measure the powder wetting behaviour. Mechanical measurements were made using an Instron 3365, two column universal mechanical testing machine, while the sensing behaviour was tested with LCR (Keysight U1733P).

3. Results and discussion

The general procedure for the preparation of porous silicones by thiol-ene photoaddition has been described in [8] and was based on mixing two emulsions stabilized with telechelic siloxane oligomers. Alternatively, the emulsion template was obtained using only one surfactant, and other cross-linking processes were applied. The polysiloxanes form the continuous phase in toluene, while water is the disperse phase. The pores are formed by cross-linking of the precursors (Scheme 1) in different conditions: UV-initiated thiol-ene photoaddition reaction of the vinyl-containing silicones (Vi-x), hydrolysis-condensation of OH-terminated polydimethylsiloxane (PDMS) with

tetraethoxysilane (TEOS), or dehydrocoupling reactions of poly(methylhydrogen)siloxane (PMHS) occurring between Si-H and Si-OH groups. After the solvents' evaporation, porous materials with different morphology and properties were obtained. The PMHS was chemically modified *in situ* with n-hexene or allyltrimethylsilane (ATMS), aiming to porous materials with increased hydrophobic behavior, while a Vi-50 siloxane copolymer was chemically modified *in situ* with mercaptoethanol (ME), to induce hydrophilic behavior.

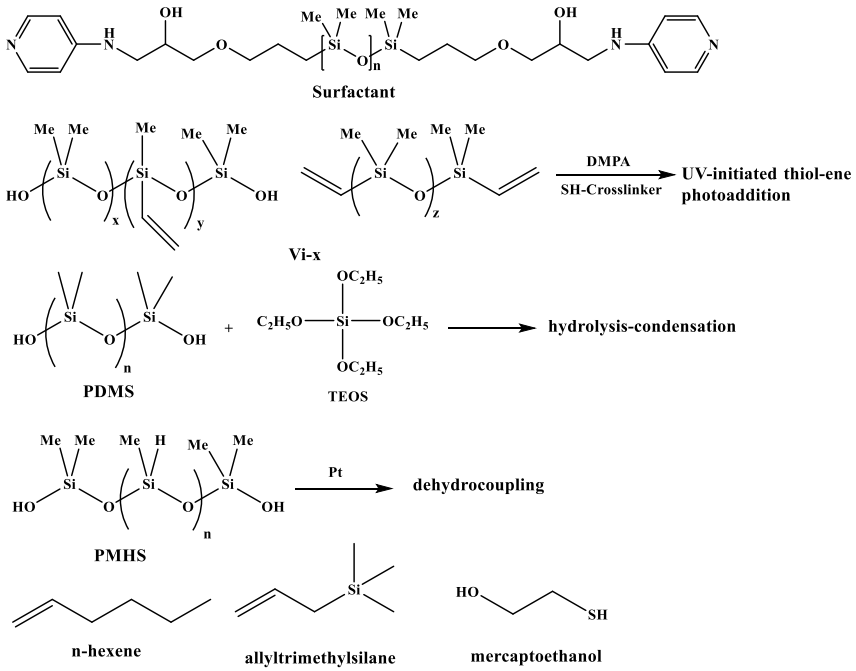

Scheme 1. Chemical structures of the starting reagents.

The mechanical properties of porous monoliths were measured in compression strain-stress tests and showed low Young's modulus, especially in the case of photoaddition samples. This was one premise for high sensitivity of capacitive pressure sensors, besides the high dielectric permittivity. Sensitivity values up to $8.7 \cdot 10^{-3}$ kPa^{-1} on 9-29 kPa were found, and sensing range between 2 and 300 kPa, spanning to ca. 2 MPa for a more robust, condensation-type material. A chart of capacitance change versus pressure is shown in Figure 1, with Y values indicated. The softest material was taken as the matrix of a composite with 5 wt.% MWCNT. The porous composite exhibited 70-fold increase in sensitivity (0.747 kPa^{-1} on 0 – 7.5 kPa sensing range), and a very high gauge factor of 89 (in the 25-50% compressive strain range). These porous silicones are promising for medical care sensor applications.

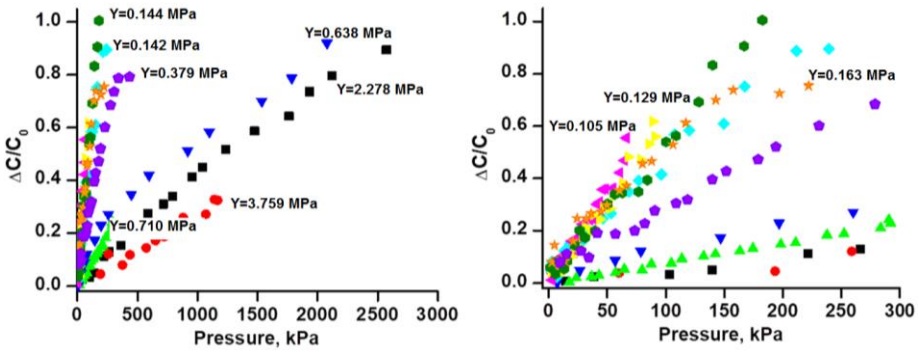

Figure 1. Capacitance change versus pressure and Young's modulus values for porous monoliths and reference materials.

The materials obtained as thick films in the photoaddition process exhibited good sorption capacity in toluene, THF and dichloromethane, with values close to 500% in certain cases [8]. The absorption capacity generally increased with the internal phase fraction (porosity). The static contact angle measurements showed interesting surface properties of the porous films, depending on porosity, with pseudo-hydrophilic or dual behaviour on the two surfaces (Janus-like membranes).

When porous materials were obtained as monoliths, their surface properties were tuned by their morphology (both evaluated as the "inner" surface or powder), and not only by their chemical structure, as envisaged. Lotus and petal effects were observed for materials with specific microstructure.

4. Conclusions

The preparation method is simple and low energy consuming, and the obtained porous materials are promising as sensors with wide sensing range, predictable based on their mechanical properties. The absorption of organic solvents can be further exploited in environmental applications. The wetting behaviour can be adjusted from synthesis, by its close correlation with the morphology. The method can be adapted to more sophisticated materials, especially composites, where the presence of nano-fillers or a second polymer (for example PEG nanoparticles dispersed in the aqueous phase) opens novel perspectives for high added value materials.

Acknowledgements

This work was partially supported by a grant of the Romanian Ministry of Research, Innovation and Digitization, CNCS/CCCDI–UEFISCDI: PN-III-P1-1_1-TE-2021-0156 (SilArtSkin).

References

[1]. González Calderón JA, Contreras López D, Pérez E, Vallejo Montesinos J. Polysiloxanes as polymer matrices in biomedical engineering: their interesting properties as the reason for the use in medical sciences. *Polym. Bull*. 77, 2749-2817, 2020
[2]. Yan H, Wang K, Zhao Y. Fabrication of silicone rubber foam with tailored porous structures by supercritical CO_2. *Macromol. Mater. Eng*. 302, 1600377, 2017
[3]. Abshirini M, Saha MC, Cummings L, Robison T. Synthesis and characterization of porous polydimethylsiloxane structures with adjustable porosity and pore morphology using emulsion templating technique. *Polym. Eng. Sci.* 61, 1-13, 2021
[4]. Si J, Cui Z, Xie P, Song L, Wang Q, Liu Q, Liu C. Characterization of 3D elastic porous polydimethylsiloxane (PDMS) cell scaffolds fabricated by VARTM and particle leaching. *J. Appl. Polym. Sci*. 133, 42909, 2016
[5]. Choi SJ, Kwon TH, Im H, Moon DI, Baek DJ, Seol ML, Duarte JP, Choi YK. A Polydimethylsiloxane (PDMS) sponge for the selective absorption of oil from water. *ACS Appl. Mater. Interfaces* 3, 4552-4556, 2011
[6]. Masihi S, Panahi M, Maddipatla D, Hanson A J, Bose A K, Hajian S, Palaniappan V, Narakathu BB, Bazuin BJ, Atashbar MZ. Highly Sensitive porous PDMS-based capacitive pressure sensors fabricated on fabric platform for wearable applications. *ACS Sens*. 6, 938-949, 2021
[7]. Zimny K, Merlin A, Ba A, Aristégui C, Brunet T, Mondain-Monval O. Soft porous silicon rubbers as key elements for the realization of acoustic metamaterials. *Langmuir* 31, 3215-3221, 2015
[8]. Racles C, Bele A, Vasiliu AL, Sacarescu L. Emulsion gels as precursors for porous silicones and all-polymer composites - A proof of concept based on siloxane stabilizers. *Gels 8*, 377, 2022
[9]. Feng L, Zhang Y, Xi J, Zhu Y, Wang N, Xia F, Jiang L. Petal Effect: A Superhydrophobic state with high adhesive force. *Langmuir* 24, 4114-4119, 2008

MALDI MASS SPECTROMETRY BASED ANALYTICAL APPROACH FOR THE ANALYSIS OF RING-OPENING OLIGOMERIZATION OF CYCLIC ESTERS IN THE PRESENCE OF CYCLODEXTRIN

Cristian Peptu,* Diana-Andreea Blaj, Mihaela Balan-Porcarasu, Valeria Harabagiu

Petru Poni Institute of Macromolecular Chemistry, Romanian Academy, Iasi, Romania
**cristian_peptu@yahoo.com*

1. Introduction

Cyclodextrin molecules represent a massive point of interest for the pharmaceutical industry for their capacity to encapsulate a wide range of molecules, starting from low molecular weight drug molecules to high molecular weight natural and synthetic polymers. Nevertheless, cyclodextrin polyol functionality recommends their use as building blocks in the synthesis of complex macromolecular architectures such as star polymers.

In this context, esterified cyclodextrins benefited from the formidable input of structural knowledge through mass spectrometry and NMR spectroscopy methods, allowing the understanding of the structural impact of reaction parameters on the structure of the obtained products, especially for the ring-opening oligomerization of cyclic esters.

The information that may be obtained consists of structural confirmation of the products through MS and MS/MS profiling, the identification of the possible secondary reactions such as transesterifications (interchain and backbiting), and system reactivity evaluation (kinetics) [1].

Witnessing the cyclodextrins (CDs) structural changes during derivatization poses a challenge due to the presence of numerous hydroxyl groups, resulting in multiple structural variations within a single product. This reduces the possibility of differentiating and identifying the formed products. Esterifying CDs through different techniques can yield derivatives with varying levels of substitution (SDs) and positional isomers possessing the same SD.

Additionally, the complexity of samples may rise when oligoester chains are linked to the CD molecule, as a result of the molecular mass distribution inherent in these oligomeric substituents.

These problems are tackled in the case of cyclodextrin modification through ring-opening oligomerization (ROO) of cyclic esters. The current presentation envisages the common mass spectrometry approaches such as MALDI MS and MS/MS with the close support of NMR spectroscopy to be employed for unraveling the fine details in the ROO initiated by the cyclodextrin derivatives.

3. Results and discussion

Ring-opening oligomerization of the cyclic esters, presented in Scheme 1, employs cyclodextrin as an initiator through the OH groups.

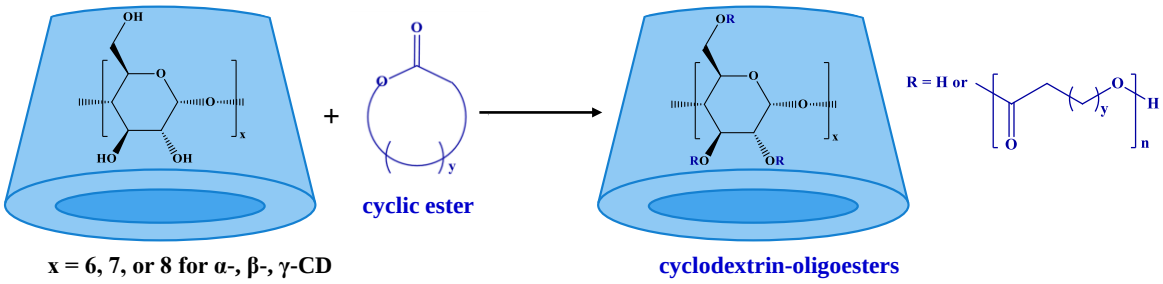

Scheme 1. The ring-opening oligomerization of cyclic esters initiated by cyclodextrins.

However, the role of cyclodextrin in these reactions has been under debate, considering their capacity to encapsulate cyclic esters molecules and hence to influence their ring-opening reaction. The pioneering work of Harada's group proposed a correlation between the size of the cyclodextrin cavity and the size of the cyclic ester to achieve the activation effect on the ROO reaction, in bulk conditions [2] and excess of cyclodextrins. Our synthesis approach employs ROO activation using amine organo-activators which, *a priori*, precludes cyclodextrin activation.

Although direct mass spectrometry characterization of the esterified cyclodextrins (ECD) through e.g. MALDI MS has become almost a routine analysis, quantitative analysis is difficult because mass spectra profiles do not reflect adequately the substitution degree, especially for macromolecular compounds with elevated dispersity index (Đ).

The analysis bias is connected with the mass discrimination problems of the common MALDI MS methods and may be corrected using chromatographic separations in tandem with MS [3] which fractionates the sample. However, low molecular weight compounds having low Đ, such as ECD, may be evaluated by MALDI MS using supplementary off-line NMR validation.

This approach has been first taken into consideration for the analysis of ROO of D,L-lactide (LA), in the presence of β-cyclodextrin [4]. The MS spectra collected throughout the reaction (Figure 1) reveal an increase in the *Mn* which was compared with the corresponding LA conversion measurements through NMR spectroscopy.

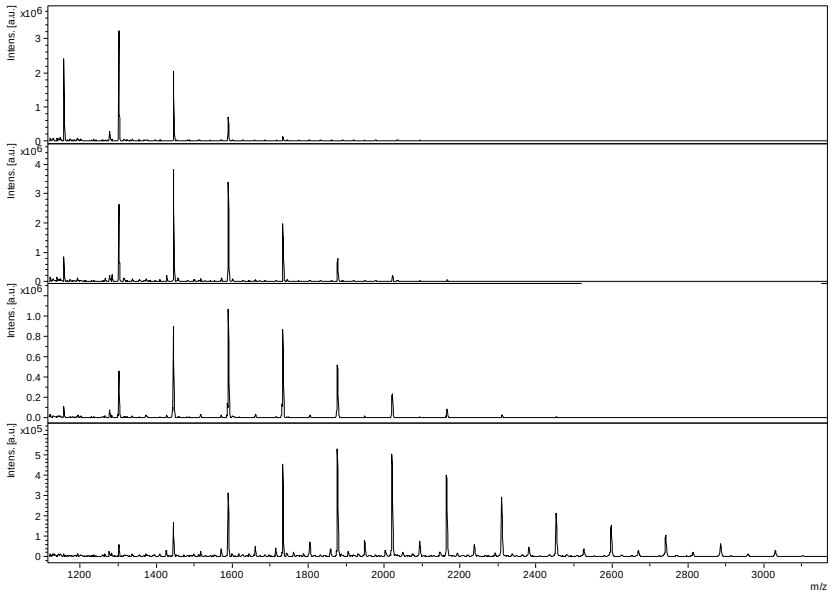

$$M_n = \frac{\sum_i^n A_i * m_i}{\sum_i^n A_i}$$

A_i – area of the MS peak m_i,
m_i – the mass associated to the MS species (for z=1 - the value of the m/z)

Figure 1. Quantitative MALDI MS analysis of the CDLA synthesis.

The agreement between NMR and MS was determined for two different MALDI MS matrices, namely α-cyano-4-hydroxycinnamic acid (CHCA) and 2,5-dihydroxybenzoic acid (DHB). A similar approach may be employed for the ROO of different cyclic esters, such as ε-caprolactone (CL) [5].

The monomer conversion determined through two complementary methods, MS and NMR revealed an excellent correlation degree for CHCA matrix, as may be observed from Figure 2, for both ROO of LA and CL. Thus, NMR confirmed that, for the considered sample, the MALDI MS may be used as a quantitative method for the evaluation of the ROO reaction system.

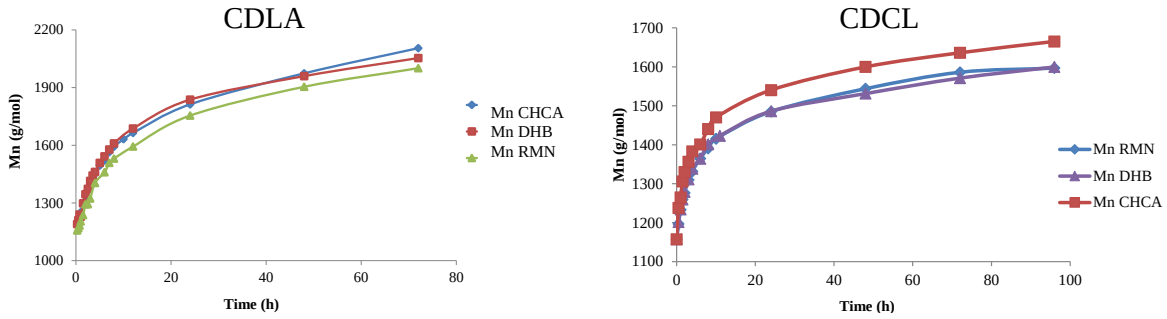

Figure 2. The plot of the monomer conversion measured through MALDI MS for CDLA and CDCL products [4,5].

Further experiments allowed us to employ this method for the comparison of different reaction parameters' effects on the ROO process such as amine organo-activators type, solvent, total concentration, cyclodextrin/cyclic ester molar ratio, and temperature.

These experiments will be further detailed in the presentation with emphasis on the advantages and limitations of the analytical approach.

References

[1]. Blaj DA, Kowalczuk M, Peptu C. Mass spectrometry of esterified cyclodextrins. *Molecules*, 28, 2001, 2023
[2]. Takashima Y, Osaki M, Harada A. Cyclodextrin-initiated polymerization of cyclic esters in bulk: Formation of polyester tethered cyclodextrins. *J. Am. Chem. Soc.* 126, 13588-13589, 2004
[3]. Peptu C, Balan-Porcarasu M, Siskova A, Skultety L, Mosnacek J. Cyclodextrins tethered with oligolactides-green synthesis and structural assessment. *Beilstein J. Org. Chem*., 13, 779-792, 2017
[4]. Blaj DA, Balan-Porcarasu M, Petre BA, Harabagiu V, Peptu C. MALDI mass spectrometry monitoring of cyclodextrin oligolactide derivatives synthesis. *Polymer*, 233, 124186, 2021
[5]. Peptu C, Blaj DA, Balan-Porcarasu M, Rydz J. Cyclodextrin-oligocaprolactone derivatives-synthesis and advanced structural characterization by MALDI mass spectrometry. *Polymers*, 14, 1436, 2022


MACRO Iași 2023

NOVEL PYRROL-2-ONE DERIVATIVES AS HUMAN CARBONIC ANHYDRASE ISOFORMS INHIBITORS

Cristina M. Al-Matarneh[1,2]*
[1]*Center of Advanced Research in Bionanoconjugates and Biopolymers, Petru Poni Institute of Macromolecular Chemistry, Romanian Academy, Iasi, Romania*
[2]*Research Institute of the University of Bucharest-ICUB, Bucharest, Romania*
**almatarneh.cristina@icmpp.ro*

1. Introduction

2,5(H)-pyrrol-2-one (DPO), a crucial component of many bioactive components or intermediates, is found in large quantities in pheromones, alkaloids, steroids, heme, chlorophyll, and other substances. DPO possesses a broad range of activities such as very potent antibacterial, FPR1 antagonists, cytotoxic and antitumor agents, tyrosinase inhibitors, antioxidant activity, carbonic anhydrase inhibitory or inhibitors of the annexin A2-S100A10 protein interaction [1].

Carbonic anhydrases (CAs) are ubiquitous metalloenzymes able to reversibly catalyze the hydration of CO_2 to H^+ and HCO_3^- [2]. Many biosynthetic processes, like as respiration, photosynthesis, pH regulation, and electrolyte secretion, are carried out by CA enzymes [3].

The principal sulfonamides, which coordinate the zinc ion with their terminal deprotonated nitrogen atom, are the traditional CA inhibitors (CAIs), which have been used in therapeutic settings for more than 70 years as diuretics and systemically active antiglaucoma medications [4]. This is due to their prospective structural characteristics, which have the potential to interact in diverse ways with a variety of biological targets.

Moreover, sulfonamides often have high pharmacological characteristics, including oral absorption and little side effects. They are also stable and simple to produce. By upsetting the anionic homeostasis of the cell, bis-sulfonamide, which consists of two groups of sulfonamide, may operate as apoptotic triggering agents in the treatment of cancer [5].

2. Experimental

Our aim was to synthesize hybrid molecules with pyrrol-2-one as a core and two active binding groups on its sides.

In order to obtain the proposed derivatives para-amino sulfonamide was reacted with aldehyde derivatives from the aromatic, aliphatic, or cyclic aldehyde class and pyruvic acid, in ethanol media in the presence of trifluoroacetic acid, in a catalytic amount. The library of newly synthesized compounds consists of 22 compounds with 1H-pyrrol-2(5H)-one structure and one 2-oxo-2,5-dihydrofuran derivative.

Among the synthesized compounds we integrated phenyl substituted compound (substituent varying for electron donating to electron withdrawing effect, from one to three substituents and different substitution positions), oxygen heterocycles (furan and piperonal) or aliphatic based substituents (one being phenyl attached to the main core through an aliphatic bridge).

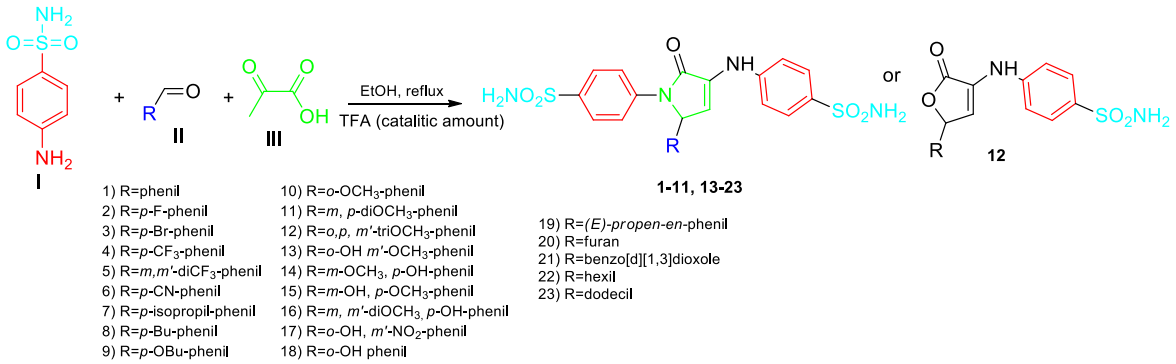

Scheme 1. Reaction pathway to compounds **1-23**.

3. Results and discussions

All the compounds were obtained in good yields (between 47 and 88%), the chemical structures were verified through NMR, IR and Maldi-MS techniques.

The compounds were tested in vitro against the physiologically most-relevant hCA isoforms such as hCAs I, II, IX and XII, by applying the stopped-flow technique and were compared with the standard sulfonamide inhibitor acetazolamide (AAZ). The results are resumed in Table 1.

Table 1. Inhibition data of human CA isoforms I, II, IX and XII with compounds **1-16** and **19-21** and AAZ by a stopped-flow CO_2 hydrase assay.

Cmp	hCA I	hCAII	hCA IX	hCA XII
1	52.7 ± 4.4	7.4 ± 0.5	26.1 ± 2.0	16.8 ±1.0
2	96.7 ± 6.3	23.3 ± 1.4	29.4 ± 2.8	93.9 ±9.3
3	293.5 ± 20.5	57.8 ± 4.4	18.4 ± 1.5	91.5 ±9.1
4	80.7 ± 6.7	9.1 ± 0.5	168.6 ± 16.7	38.0 ±2.2
5	12.3 ± 1.1	4.4 ± 0.3	39.7 ± 3.2	74.2 ±6.6
6	53.6 ± 4.3	9.4 ± 0.7	25.7 ± 1.7	74.5 ±6.5
7	237.5 ± 16.2	93.9 ± 8.5	23.9 ±1.8	61.9 ±4.9
8	870.9 ± 51.7	397.4 ± 23.7	30.6 ± 2.2	9.2 ±0.5
9	604.8 ± 54.4	333.6 ± 25.3	1.9 ± 0.2	6.7 ±0.3
10	51.1 ± 3.1	6.0 ± 0.4	10.8 ± 1.0	74.5 ±3.8
11	41.5 ± 3.3	9.2 ± 0.7	2.9 ± 0.2	65.9 ±4.6
12	357.5 ± 24.8	188.5 ± 16.6	1.8 ±0.1	36.5 ±2.0
13	45.5 ± 2.6	6.8 ± 0.4	3.4 ±0.2	47.0 ±3.8
14	3.9 ± 0.2	6.9 ± 0.6	3.2 ±0.3	17.1 ±1.6
15	34.9 ± 2.7	7.0 ± 0.5	2.4 ±0.2	63.9 ±5.2
16	36.9 ± 3.1	6.1 ± 0.3	3.7 ±0.3	20.1 ±1.6
19	416.4 ± 25.4	158.0 ± 11.6	211.3 ±13.2	8.5 ±0.8
20	46.9 ± 2.9	6.4 ± 0.5	25.8 ±2.3	5.9 ±0.6
21	95.5 ± 6.1	15.8 ± 1.2	150.4 ±9.5	8.1 ± 0.8
AAZ	250.0 ± 21.0	12.1 ± 1.0	25.8 ± 2.5	5.7 ±0.5

* Mean from 3 different assays, by a stopped flow technique (errors were in the range of ± 5-10 % of the reported values).

The cytosolic hCA I was inhibited by all series at concentrations ranging from low nanomolar (KI 3.9 nM for 14) to high nanomolar values (KI 870.9 nM for 8). The hydroxyl group was found to play an important role in the activity against this isoform; compound 14 was the most potent inhibitor with a KI of 3.9 nM. The second widely expressed cytosolic hCA II was better inhibited than hCA I, exhibiting similar features. Derivative 3 with a bromine atom was found to be less active than fluorine analogue 2 with KIs of 57.8 nM and 23,3 nM, respectively. The hydroxyl groups also played an important role in modulating activity, leading to low nanomolar inhibition as observed in compounds 14, 15.

All compounds in the series effectively inhibited the first tumor-associated hCA IX, with KIs ranging from low nanomolar (1.9 nM for 9) to medium nanomolar (211.2 nM for 19). Hydroxyl groups did not play a crucial role in the inhibition activity for this isoform, compound 12, which had three methoxyl moieties, showed a KI of 1.8 nM, making it the most potent inhibitor against hCA IX. The second tumor-associated hCA XII was highly inhibited by the series tested, with KIs in the low nanomolar range.

Docking studies were applied to explain the relationship between structural features and inhibition profiles of the most selective compounds 9 and 12 towards the tumor-associated isoforms hCA IX and XII. Given the stereocenter on one carbon in the five-ring central heterocycle, both (R)- and (S)-enantiomers of the selected compounds were investigated by docking to model the interactions they establish with the isoforms of the hCA.

4. Conclusions

A one-pot, three-component procedure was used to produce new dihydro-pyrrol-2-one compounds with two sulfonamide moieties, with trifluoroacetic acid acting as a strong catalyst. The resulting compounds were examined in comparison to four human carbonic anhydrase isoforms (hCA I, hCA II, hCA IX and hCA XII). The docking studies showed that the new pyrrol-2-one-sulfoamide hybrids act as zinc-binder in the carbonic anhydrase active site.

Acknowledgements

The support provided by the ICUB Fellowship for Young Researchers (Contract no. 26260/5.12.2022) is acknowledged.

References

[1]. Alp C, Ekinci D, Serdar M, Murat S. A novel and one-pot synthesis of new 1-tosyl pyrrol-2-one derivatives and analysis of Carbonic Anhydrase inhibitory potencies. *Bioorg. Med. Chem.* 18, 4468-4474, 2010

[2]. Clima L, Craciun F, Angeli A, Petreni A. Synthesis, computational studies and assessment of in vitro activity of squalene derivatives as Carbonic Anhydrase inhibitors. *ChemMedChem.*15, 2052-2057, 2020

[3]. Mishra CB, Kumari S, Angeli A, Bua S, Tiwari M, Supuran CT. Discovery of benzenesulfonamide derivatives as carbonic anhydrase inhibitors with effective anticonvulsant action: Design, synthesis, and pharmacological evaluation. *J. Med. Chem.* 61, 3151-3165, 2018

[4]. Angeli A, Kartsev V, Petrou A, Pinteala M, Brovarets V, Slyvchuk S, Pilyo S, Geronikaki A, Supuran CT. Chromene-containing aromatic sulfonamides with Carbonic Anhydrase inhibitory properties. *Int. J. Mol. Sci.* 22, 2021

[5]. Leechaisit R, Pingaew R, Prachayasittikul V. Bioorganic & medicinal chemistry synthesis, molecular docking, and QSAR study of bis-sulfonamide derivatives as potential Aromatase inhibitors. *Bioorg. Med. Chem.* 27, 115040, 2019

HYBRID NANOSTRUCTURES OF CHITOSAN AND POLY(*N*-ISOPROPYLACRYLAMIDE) WITH CARBOXYLATE END GROUP

Maria Karayianni,[1,2]* Elena-Daniela Lotos,[1] Ana-Lavinia Vasiliu,[1] Marcela Mihai,[1] Stergios Pispas[1,2]

[1]*Petru Poni Institute of Macromolecular Chemistry, Romanian Academy, Iasi, Romania*

[2]*Theoretical and Physical Chemistry Institute, National Hellenic Research Foundation, Athens, Greece*

**mkaragia@eie.gr*

1. Introduction

Over the years natural polymers like polysaccharides have attracted considerable scientific interest since they can serve as building blocks for the development of nanomaterials relevant to various biological applications. One such widely used polysaccharide is chitosan, which is derived from the deacetylation of chitin, the second most abundant biopolymer in nature found in marine crustaceans (i.e., shrimp, crab, lobster) and cuticles of insects [1,2]. Chitosan has a cellulose-like carbohydrate structure that renders it biocompatible, biodegradable, non-toxic and also provides unique antimicrobial and mucoadhesive properties [3]. Moreover, chitosan's overall properties can be further tuned through appropriate physical or chemical modification owing to the presence of the amino and hydroxyl active groups [4]. For instance, electrostatic interaction/binding with functional polymeric macromolecules bearing oppositely charged groups is possible, thus generating a new polymeric material with distinct physical properties.

2. Experimental

In this work, we investigate the electrostatic complexation of two chitosan samples, differing in molecular weight, and a poly(*N*-isopropylacrylamide) thermo-responsive homopolymer that bears a chargeable carboxylic end group, which enables the interaction with chitosan's amino groups. The molecular weight (MW) of the two chitosans were 162 kDa (Chit162K) and 1.46 kDa (ChitOligo), with corresponding degrees of deacetylation (DD) of approximately 88 and 90%, respectively. Dynamic and electrophoretic light scattering (DLS and ELS) techniques were employed in order to study the solution/dispersion properties, i.e., mass, size, size distribution and effective charge of the formed complexes as a function of the PNIPAM concentration, or equivalently the molar/charge ratio of the two components, as seen in Table 1.

Table 1. Characteristics of the complexes of the two Chit+PNIPAM systems.

Sample name	Chit conc. (mg/mL)	PNIPAM conc. (mg/mL)	mol PNIPAM/ mol Chit162K	mol PNIPAM/ mol ChitOligo	mol [+]/ mol [-]
Complex 4/1	0.4	0.1	2.1	0.02	370
Complex 4/2		0.2	4.2	0.04	185
Complex 4/4		0.4	8.3	0.08	92.5

Furthermore, the thermal response (up to 45 °C) as well as the effect of ionic strength on the preformed complexes was examined. Additionally, fluorescence spectroscopy measurements, utilizing pyrene as a probe, provided information regarding the hydrophobicity of the formed complexes, while STEM images further elucidated their morphology.

3. Results and discussion

As seen in Figure 1a the scattering intensity, which is proportional to the mass of the complexes, increases as the concentration of PNIPAM increases, thus proving the successful interaction/ complexation of the two chitosan samples with PNIPAM. Moreover, the mass of the complexes of the low MW chitosan is overall higher than the corresponding ones formed by the high MW sample, indicating a more compact structure probably due to less conformational constrains that allow for a higher degree of interaction with the PNIPAM homopolymer. The obtained zeta potential values (Figure 1b) show the reduced effective charge of the complexes in comparison to the corresponding chitosan samples (points at zero PNIPAM concentration), as expected due to the occurring charge neutralization. As a matter of fact, this effect is even more pronounced in the case of the ChitOligo+PNIPAM system again demonstrating the increased interaction between the two components. Regarding the size of the complexes, the corresponding size distributions (Figure 1c and d) reveal the presence of different populations of scattering species in solution in both cases, possibly corresponding to complexes comprising of different total number of chains. Still the ChitOligo+PNIPAM system exhibits overall significantly larger sizes of complexes.

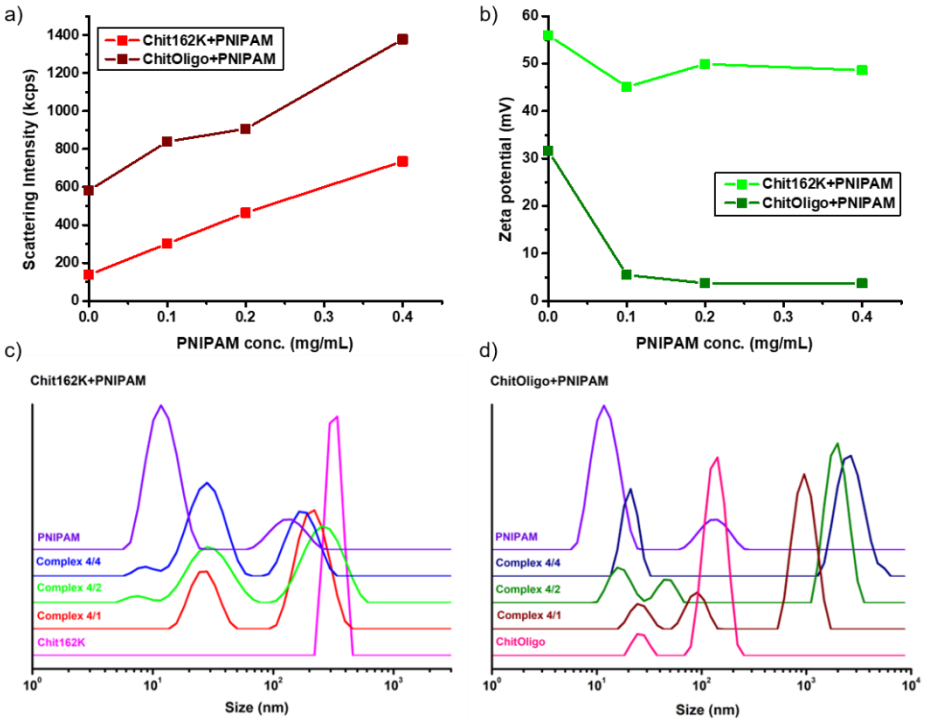

Figure 1. DLS and ELS results regarding: (a) the scattering intensity; (b) the zeta potential; (c) and (d) the size distributions, for the complexes of the two Chit+PNIPAM systems.

Additional information about the morphology of the complexes can be derived from the STEM images shown in Figure 2, where representative measurements of the Complex 4/4 of the two Chit+PNIPAM systems are presented. Both images suggest a homogenous globular dense structure for the complexes under study, with larger sizes observed in the case of low MW chitosan.

Finally, the thermal response of the formed complexes was examined by performing DLS measurements at different temperatures. The corresponding size distributions for the Complex 4/2 of the two systems (Figure 3) show that above 35 °C only one peak is discerned, suggesting the formation of compact structures owing to the increase of the hydrophobicity of the PNIPAM chains in the complexes. Nevertheless, this effect is reversible upon cooling.

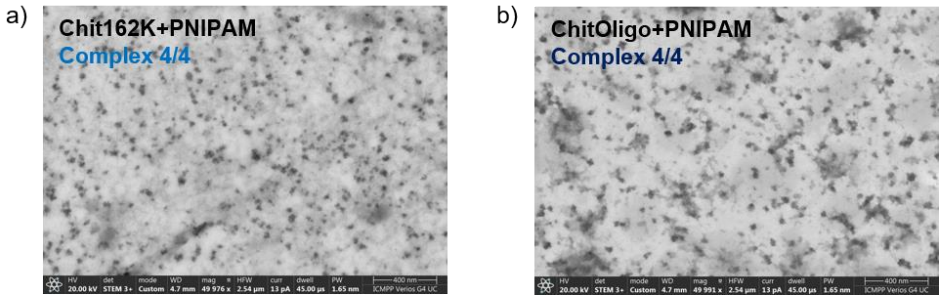

Figure 2. STEM images for the Complex 4/4 of the two systems: (a) Chit162K+PNIPAM; and (b) ChitOligo+PNIPAM.

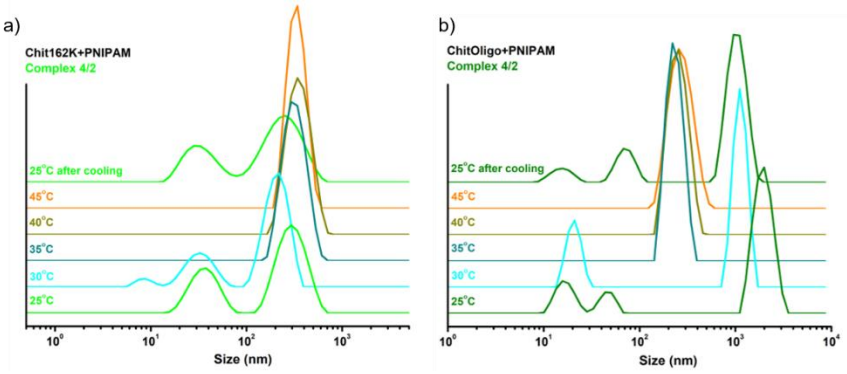

Figure 3. DLS size distributions at different temperatures for the Complex 4/2 of the two systems: (a) Chit162K+PNIPAM; and (b) ChitOligo+PNIPAM.

4. Conclusions

The successful electrostatic binding of a PNIPAM homopolymer bearing a carboxylate end group on two different chitosan biopolymers, of low and high molecular weight respectively, was established, leading to the formation of thermo-responsive hybrid nanostructures with characteristics relevant to the ratio of the two macromolecular components.

Acknowledgements

This work was financially supported by a grant of the Ministry of Research, Innovation and Digitization, project no. PNRR-III-C9-2022-I8-201, contract no. 760082/23.05.2023, within the National Recovery and Resilience Plan.

References

[1]. Karayianni M, Sentoukas T, Skandalis A, Pippa N, Pispas S. Chitosan-based nanoparticles for nucleic acid delivery: Technological aspects, applications, and future perspectives. *Pharmaceutics* 15, 1849, 2023

[2]. Desai N, Rana D, Salave S, Gupta R, Patel P, Karunakaran B, Sharma A, Giri J, Benival D, Kommineni N. Chitosan: A potential biopolymer in drug delivery and biomedical applications. *Pharmaceutics* 15, 1313, 2023

[3]. Abourehab MAS, Pramanik S, Abdelgawad MA, Abualsoud BM, Kadi A, Ansari MJ, Deepak A. Recent advances of chitosan formulations in biomedical applications. *Int. J. Mol. Sci.* 23, 10975, 2022

[4]. Fatullayeva S, Tagiyev D, Zeynalov N, Mammadova S, Aliyeva E. Recent advances of chitosan-based polymers in biomedical applications and environmental protection. *J Polym Res.* 29, 259, 2022

FLUORESCENT CARBON NANOPARTICLES SUSPENSION GENERATED BY PULSED LASER ABLATION IN ETHANOL

Bogdan-George Rusu,[1]* Cristian Ursu,[1] Daniela Ionita,[1] Victor Oancea,[1] Mihaela Olaru,[1] Gabriel Ababei,[2] Petru Nica[3]

[1]*Physics of Polymers and Polymeric Materials Laboratory, Petru Poni Institute of Macromolecular Chemistry, Romanian Academy, Iasi, Romania*

[2]*Materials Characterization Laboratory, National Institute of Research and Development for Technical Physics, Iasi, Romania*

[3]*Department of Physics, Gheorghe Asachi Technical University, Iasi, Romania*

**rusu.george@icmpp.ro*

1. Introduction

In recent years, the synthesis of graphene nanoparticle suspensions (GNPs) with high fluorescent stability as a new type of nontoxic functional material [1] has become a prominent focus due to their numerous potential applications (such as biomedical imaging, sensing, and photocatalysis) and the relatively simple synthesis routes. Among the various methods used in colloidal GNPs synthesis (such as liquid phase exfoliation, nanotube slicing and fullerene splitting [2], graphite oxide reduction, electrochemical synthesis, etc. [3]), Pulsed Laser Ablation in Liquid (PLAL) has emerged as the primary choice due to the wide range of experimental parameters available for tailoring their features (size distribution, shape, surface chemistry, etc.) and the lack of surfactants in the synthesis process.

PLAL is a green and straightforward method for the synthesis of a wide range of inorganic nanomaterials and composites. Typically, during the interaction of the laser beam with the target settled in liquid, at the focal point of the laser beam, the superficial layer of the subjected material surface is heated, melted, evaporated, and ionized to produce micro-bubbles. The bubbles expand until a particular pressure and temperature are reached, then collapse. Within the bubbles, the temperature reaches thousands of Kelvin with a pressure of several GPa, giving rise to some extreme conditions creating promises to produce novel materials. Being more affordable than vacuum technology, PLAL employs the suspension of generated NPs in a liquid medium instead of fuming in air [4].

This work focuses on the synthesis of fluorescent carbon nanoparticle (CNPs) suspensions in ethanol by using the PLAL technique. To enhance the properties of the obtained NPs, i.e., reduce their size and alter the surface chemistry, subsequent laser irradiation was performed. The applied synthesis procedure is fast, reliable and implies no use of surfactants or synthetic dyes.

2. Experimental

The experimental setup used for generating CNPs suspensions by the PLAL technique was presented in detail in our previous work [5]. The first harmonic (1064 nm, 10 ns pulse length) of a Nd:YAG laser (Brilliant, Quantel) with an energy of 30 mJ was focused on the surface of a pyrolytic graphite disk (1 mm in thickness and 2.54 cm in diameter) immersed to a depth of 5 mm by using a spherical lens of 5 cm focal length. The NP suspensions were generated by firing at 10 Hz a total number of pulses that varied between 3,000 and 18,000. The estimated laser fluence range was between 3.5 and 10.5 J/cm^2. The rotation of the graphite disk around its own axis was

performed, along with the linear translation of the focusing lens-deflection mirror assembly in the direction of the laser beam propagation, to ensure repeatability and an increased production rate. Afterwards, to reduce their size and alter the surface chemistry, UV laser irradiation of the obtained NP solutions was performed by using the third harmonic (355 nm) of Nd:YAG laser. A volume of 2.5 ml of CNPs solution was added to a quartz cuvette and subjected to the unfocused laser beam with an energy of 28 mJ, delivering at 10 Hz a total of 18,000 laser shots. Various analysis techniques, such as STEM, Raman, photoluminescence, TGA and FTIR, were applied to investigate the structural and chemical properties of the obtained NP solutions.

3. Results and discussion

In Figure 1, a STEM image of CNPs generated in ethanol for 18000 laser ablation pulses is presented. It can be easily seen that the obtained NPs suspension is constituted by a mixture of spheroid-like CNPs with a distribution size between 5 and 50 nm and larger graphene sheets with dimensions in the range of hundreds of nanometers. The structural analyses confirmed the presence of the two carbon allotropes in the nanoparticle suspensions, namely spheroid-type amorphous carbon particles and graphene sheets (see characteristic bands from Raman spectra, Figure 1b). FTIR spectra recorded for both pristine and laser-irradiated solutions revealed the presence of OH chemical groups at the surface of NPs, which makes it easy to be functionalized for various applications (Figure 1c).

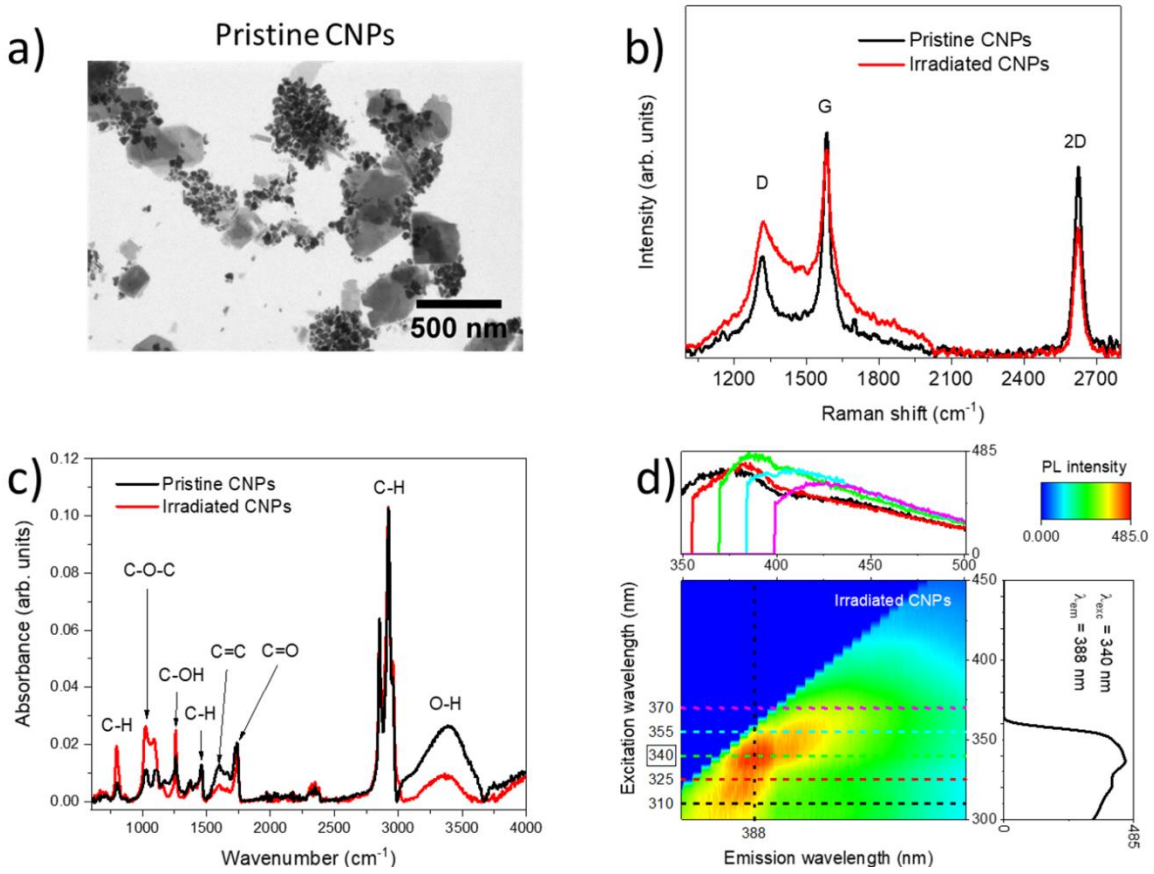

Figure 1. Optimized CNPs solution obtained for 18,000 laser shots for graphite ablation: a) STEM image of pristine CNPs; b) FTIR spectra of pristine and laser-irradiated solution; c) Raman spectra of CNPs before and after laser irradiation; and d) photoluminescence map of the laser-irradiated colloidal solution (laser-irradiated NPs solution were obtained by submitting the sample to 4,800 laser shots).

Subsequent laser irradiation was found to improve the photoluminescence of the CNPs suspensions. In Figure 1d, the excitation-emission map of the optimized sample obtained after UV laser irradiation with 4,800 laser shots is presented. The recorded excitation spectrum (black curve from the right-hand side) shows an emission maximum at 388 nm. Also, the emission spectra recorded for different excitation wavelengths (see curves from the top side of Figure 1d) exhibit a red shift of their maxima, demonstrating the presence in the obtained solution of carbon quantum dots induced by fragmentation during the laser irradiation process.

4. Conclusions

Stable CNPs suspensions with a mass concentration about 130 µg/ml were generated through pulsed laser ablation of pyrolytic graphite in ethanol without using any surfactant. The obtained CNPs suspension is constituted by a mixture of spheroid-like CNPs and graphene sheets with OH chemical groups bonded at the surface for both pristine and laser-irradiated solutions, which makes it easy to be functionalized for various applications. Subsequent laser irradiation was found to improve the photoluminescence of the CNPs suspensions and to promote the appearance of carbon quantum dots through a laser-induced fragmentation process.

References

[1]. Mei Q, Liu B, Han G, Liu R, Han MY, Zhang Z. Graphene oxide: From tunable structures to diverse luminescence behaviors. *Adv. Sci*. 6, 1900855, 2019
[2]. Alharbi TMD, Vimalanathan K, Lawrance WD, Raston CL. Controlled slicing of single walled carbon nanotubes under continuous flow, *Carbon*. 140, 428-432, 2018
[3]. Zangmeister CD. Preparation and Evaluation of Graphite Oxide Reduced at 220 °C. *Chem. Mater*. 22, 5625-5629, 2010
[4]. Al-Hamaoy A, Chikarakara E, Jawad H, Gupta K, Kumar D, Rao MSR, Krishnamurthy S, Morshed M, Fox E, Brougham D, He X, Vázquez M, Brabazon D. Liquid phase - pulsed laser ablation: A route to fabricate different carbon nanostructures. *Appl. Surf. Sci*. 302, 141-144, 2014
[5]. Lipsa FD, Ursu EL, Ursu C, Ulea E, Cazacu A. Evaluation of the antifungal activity of gold-chitosan and carbon nanoparticles on Fusarium oxysporum. *Agronomy*. 10, 1143, 2020

MODULATED DIFFERENTIAL SCANNING CALORIMETRY AS A TOOL FOR POLYMER CHARACTERIZATION

Daniela Ionita,[1]* Mariana Cristea,[1] Paul Lazar,[2] Constantin Gaina,[1] Bogdan C. Simionescu[1]
[1]*Petru Poni Institute of Macromolecular Chemistry, Romanian Academy, Iasi, Romania*
[2]*S.C. Laboratorium S.R.L., Targu Bujor, Romania*
**ionita.daniela@icmpp.ro*

1. Introduction

Thermal analysis is a key step in the polymer research; its right and proper use can solve a variety of problems in what concerns polymer applications and processing. The key issues in using thermal techniques are determining the appropriate experimental conditions to apply and how to successfully interpret the data. The present study attempted to apply conventional differential scanning calorimetry (DSC) and modulated differential scanning calorimetry technique (MDSC) in characterizing the structure of different polymers (PU, PET, PMMA, PLA) by studying the response of reversible or irreversible heat flow.

2. Experimental

Four commercial polymer samples with a weight of about 6 mg sealed in aluminum crucibles were analyzed with a Discovery DSC 250 (TA Instruments), under nitrogen flow (50 mL/min). The analyses were carried out using the same protocol. In the first step a standard DSC experiment was performed (first heating – cooling – second heating) at 20^{o}C/min from -100^{o}C up to 225^{o}C. Then a modulated conventional DSC experiment with a 3^{o}C/min heating rate, modulation amplitude 1^{o}C and modulation period of 60 s was performed.

3. Results and discussion

DSC is a basic thermal analysis technique used to measure the heat flow associated with physical and chemical changes evidenced by endothermic and exothermic processes. One of the main limitations of DSC is the analysis of complex transition which involves multiple processes which may overlap or the signal may be too low to be properly noticed. This can complicate the interpretation of the results and also reduce measurement accuracy and precision.

It is the case of PLA where the enthalpic relaxation is overlapped with the glass transition, while recrystallization occurs within its melting temperature range.

Moreover, conventional DSC does not allow these complex transitions to be properly analyzed since it measures only the sum of all thermal events in the sample. Hence, when multiple transitions occur in the same temperature range, results are often confusing and misinterpreted. So, the study of PET melting, separation of complex transition present in PU and identification of the glass transition of PMMA demand a more detailed study to increase the understanding of these processes.

Modulated DSC represents a powerful tool for the characterization of these types of polymers, since it provides more information than the conventional DSC [1-4]. A sinusoidal modulation (oscillation) is overlaid on the conventional linear heating or cooling ramp to yield a profile in which the average sample temperature changes sinusoidally rather than linearly. The deconvolution of the resultant heat flow provides not only the total heat flow obtained from conventional DSC,

but also separates the total heat flow into its heat capacity (reversing) and kinetic (non-reversing) components.

$$\frac{dH}{dT} = Cp\frac{dT}{dt} + f(t,T)$$

where: $\frac{dH}{dT}$ – total heat flow (mW or W/g);
Cp – heat capacity component of the total heat flow (J/°C);
$\frac{dT}{dt}$ – heating rate (°C/min);
$f(t,T)$ – kinetic component of the total heat flow.

The reversing signal provides information on the glass transition and some melting, while the non-reversing signal shows just the kinetic processes (enthalpic relaxation, cold crystallization, evaporation, decomposition, melting) (Figure 1, Table 1).

Table 1. Summary of modulated DSC results of PLA, PMMA, PU and PET samples

Sample	Reversing heat flow		Non-reversing heat flow	
	T_g, °C	T_1, °C	T_2, °C	T_3, °C
PLA	72	175	164	176
PMMA	121	-	74	121
PU	25	-	65	153
PET	86	242	250	-

PLA

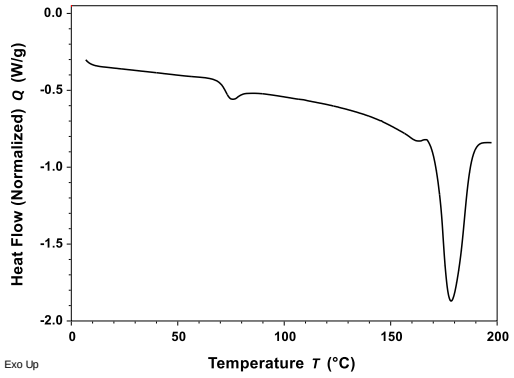

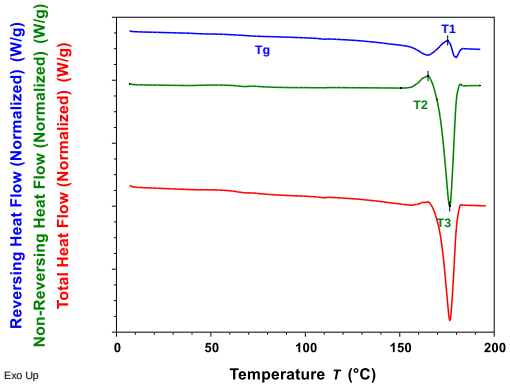

PMMA

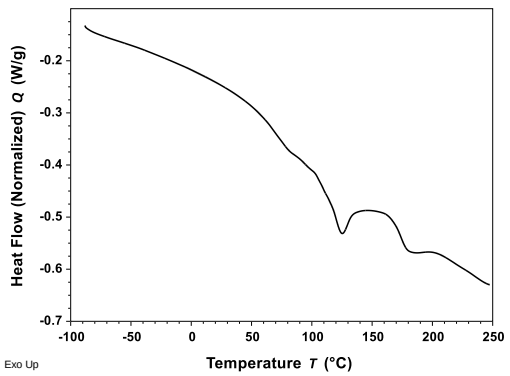

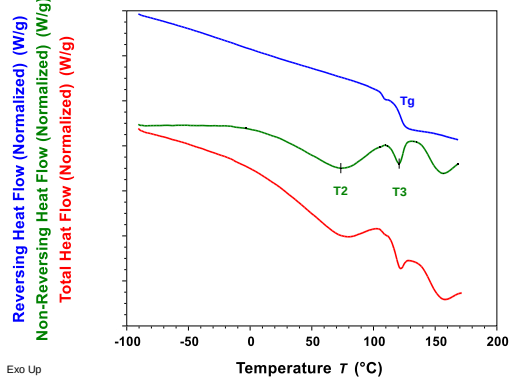

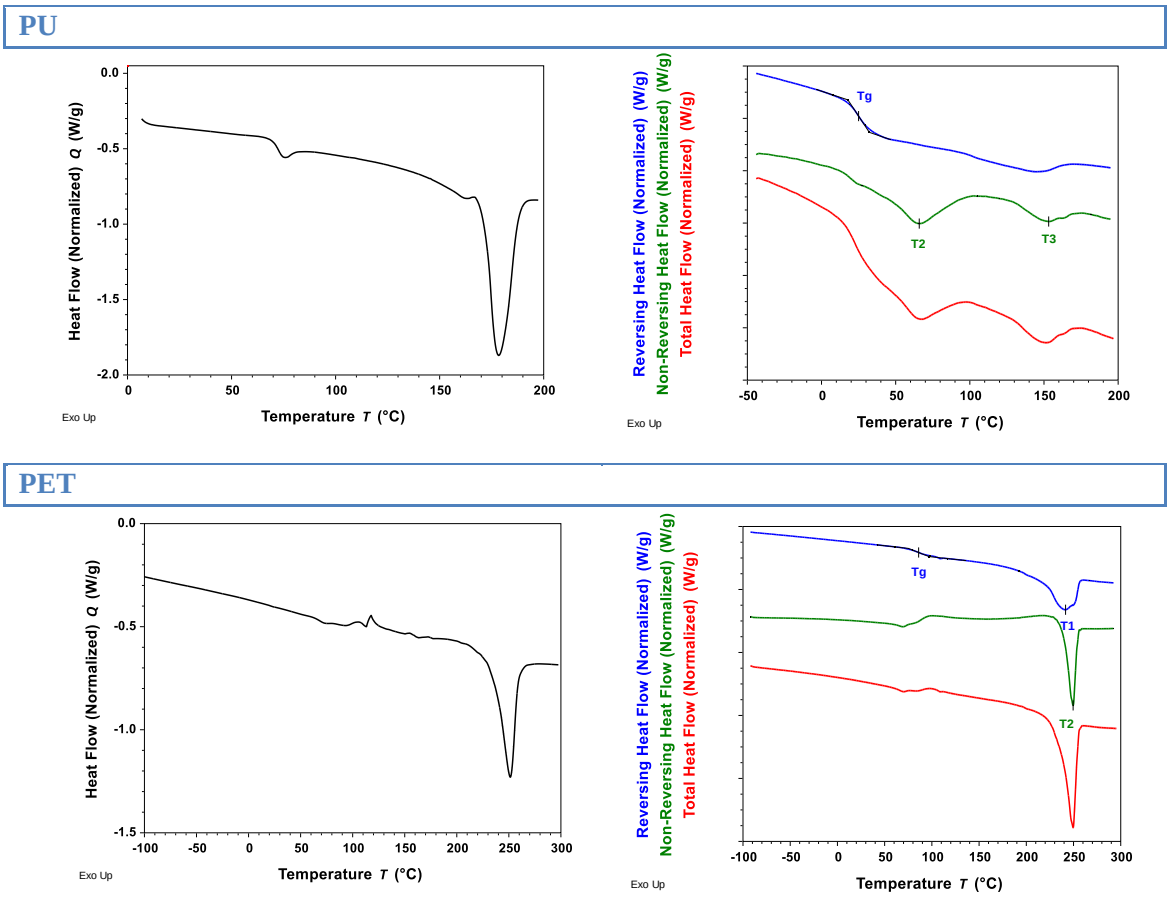

Figure 1. DSC (left side) and MDSC (right side) scans of PMMA, PU, PET, PLA.

The glass transition, crystallization and melting conducted by MDSC in different experimental conditions are explained through the analysis of the thermal response of various polymers by the optimization of modulation parameters (heating rate, modulation period, modulation amplitude).

4. Conclusions

MDSC offers a number of advantages over conventional DSC studies for studying semicrystalline polymers. It offers a more complete characterization of polymers and provides a deeper understanding of the transitions taking place with temperature. However, a special attention should be given to the experimental conditions.

References

[1]. Schick C. Temperature modulated differential scanning calorimetry (TMDSC) - basics and applications to polymers. In: Gallagher PK, editor. Handbook of thermal analysis and calorimetry, vol. 3. Amsterdam: Elsevier Science; pp. 713-810, 2002

[2]. Righetti MC. Crystallization of polymers investigated by temperature-modulated DSC. *Materials* 10, 442, 2017

[3]. Menczel JD. Use of MTDSC in the detection of weak glass transition: the hysteresis peak. *J. Therm. Anal. Calorim.* 148, 6047-6057, 2023

[4]. Scoppio A, Cavallo D, Müller A, Tranchida D. Temperature modulated DSC for composition analysis of recycled polyolefin blends. *Polym. Test.* 113, 107656, 2022

FUNCTIONALIZATION OF 5-BROMOSALICYLALDEHYDE AS MANNICH, SCHIFF-BASE, AND NITRONYL-NITROXIDE LIGANDS AND THEIR COMPLEXES

Stefan Dimitriu,[1,2]* Sergiu Shova,[3] Marius Andruh[1,2]
[1]*Costin D. Nenitescu Institute of Organic and Supramolecular Chemistry, Romanian Academy, Bucharest, Romania*
[2]*University of Bucharest, Faculty of Chemistry, Bucharest, Romania*
[3]*Petru Poni Institute of Macromolecular Chemistry, Romanian Academy, Iasi, Romania*
**stefan.dimitriu.02@gmail.com*

1. Introduction

5-bromosalicylaldehyde has a great potential of forming various ligands, due to the possibility of Mannich and Schiff functionalizations [1], as well as conversion of formyl groups into nitronyl-nitroxide free stable radical moieties [2] (Figure 1).

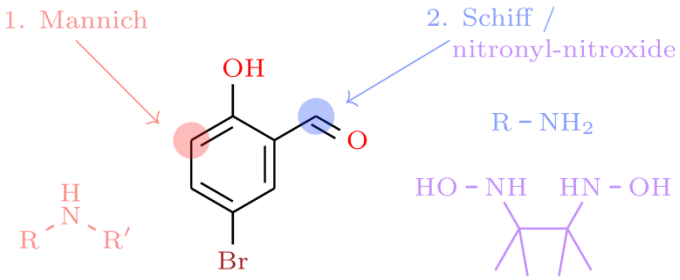

Figure 1. Functionalization of 5-bromosalicylaldehyde.

The resulting ligands present multiple compartments able to accommodate metal ions. This leads to various applications, including nuclearity control in coordination compounds synthesis [3] and magneto-structural correlations [4]. Particularly interesting are the nitronyl-nitroxide ligands (Figure 2), which contain an oxygen atom with an unpaired electron, resulting in paramagnetic properties.

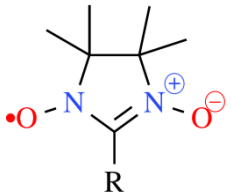

Figure 2. The nitronyl-nitroxide radical moiety.

2. Results and discussion

In this work, three Mannich reactions were conducted, starting from 5-bromosalicylaldehyde, resulting in simple, double, and triple condensation products (Figure 3). The amines employed were N-methylpiperazine, piperazine, and tris[2-(methylamino)ethyl]amine. The products have been characterized by NMR spectroscopy.

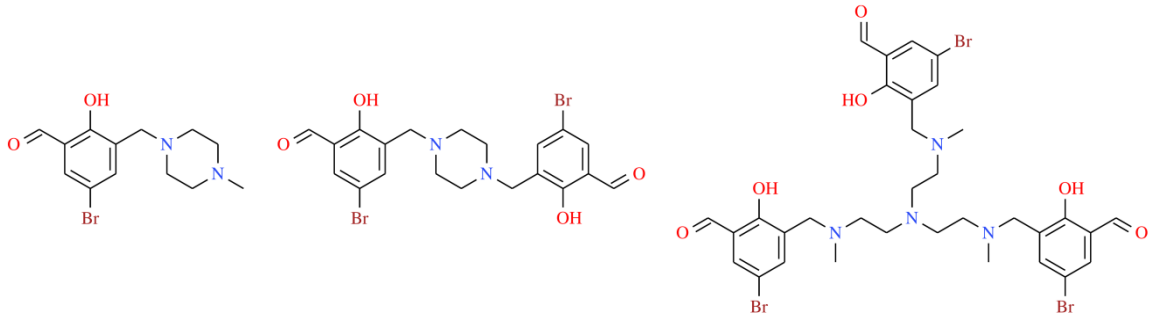

Figure 3. Mannich products starting from 5-bromosalicylaldehyde and: (left) N-methylpiperazine; (middle) piperazine; (right) tris[2-(methylamino)ethyl]amine.

Further, Schiff bases were synthesized, using amines bearing one, two, or three NH_2 groups, leading to compartmental ligands. Alternatively, the Mannich bases were also functionalized as nitronyl-nitroxide radicals, which have been characterized by mass spectrometry.

In the case of the tripodal Mannich base (obtained from tris[2-(methylamino)ethyl]amine), the number of nitronyl-nitroxide groups could be controlled from the reaction stoichiometry.

Complexes of Mannich (Figure 4), Schiff-bases (Figure 5), and nitronyl-nitroxide radicals (Figure 5) with Cu(II), Ni(II), and Mn(II) metal ions were obtained. Their structures were determined by single-crystal X-ray diffraction measurements.

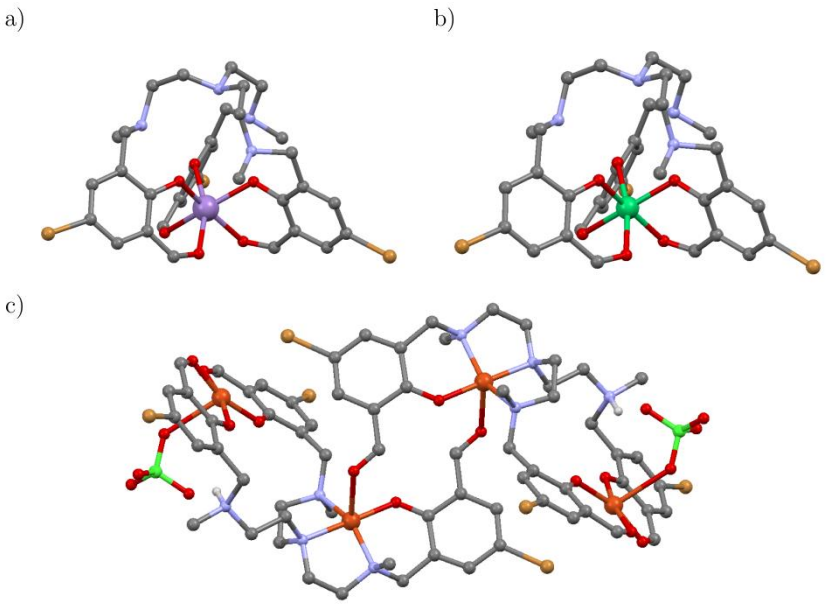

Figure 4. Coordination compounds of the tripodal Mannich base with: (a) Mn(II); (b) Ni(II); (c) Cu(II).

A Mannich-Schiff cage (Figure 5) was obtained starting from the Ni(II) complex of the tripodal Mannich base and tris(2-aminoethyl)amine. The metal ion prevented the formation of polymerization products, due to the template activity.

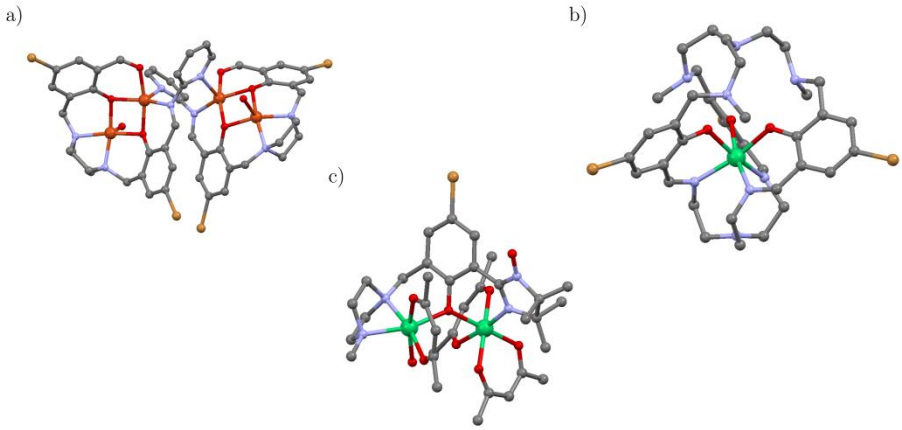

Figure 5. Coordination compounds of: (a) the Schiff-base synthesized from the double Mannich base and 2-aminopyridine with Cu(II); (b) a Mannich-Schiff cage synthesized from the triple Mannich base with Ni(II); (c) the imino-nitroxide radical derived from the simple Mannich base with Ni(II).

3. Conclusions

The primary Mannich functionalization of 5-bromosalicylaldehyde has the advantage of strong bonds between the building units of the target molecule, with respect to Schiff-bases. However, Schiff further functionalization brings more diversity to the ligands, while nitronyl-nitroxide functionalization brings paramagnetic properties. In the case of the tripodal Mannich base, the stereochemical preference of the metal ions plays an important role in the structure of the coordination compound, due to the versatility of the ligand, and metal ions can be used for template synthesis of Schiff-bases.

Acknowledgements

S.D. is grateful to Dr. Constantin Draghici, Conf. Dr. Augustin Madalan and Ph.D. students Andrei Patrascu, Cristian Spinu, and Mihai Raduca for their help.

References

[1]. Crane JD, Fenton DE, Latour JM, Smith AJ. Unsymmetric dicopper(II) complexes of dinucleating ligands bearing chemically distinct co-ordination environments. *J. Chem. Soc., Dalton Trans.*. 2979-2987, 1991

[2]. Ullman EF, Osiecki JH, Boocock DGB, Darcy R. Studies of stable free radicals. X. Nitronyl nitroxide monoradicals and biradicals as possible small molecule spin labels. *J. Am. Chem. Soc.* 94, 7049-7059, 1972

[3]. Andruh M. Oligonuclear complexes as tectons in crystal engineering: structural diversity and magnetic properties. *Chem. Commun*. 2565-2577, 2007

[4]. Oyarzabal I. et al. Magneto-thermal properties and slow magnetic relaxation in Mn(II)Ln(III) complexes: influence of magnetic coupling on the magneto-caloric effect. *Dalton Trans*. 51, 12954-12967, 2022

CHARACTERIZING THE INFLUENCE OF BASE SELECTION ON THE *IN VITRO* DISSOLUTION PROFILE OF CHRYSIN FROM SEMISOLID TOPICAL PREPARATIONS

Alexandra Bujor,[1] Eleonora Carbone,[2] Ilenia Quercia,[2] Mousa Sha'at,[1] Monica Iliuta Stamate,[1] Piera di Martino,[2] Lacramioara Ochiuz[1]*

[1]*Grigore T. Popa University of Medicine and Pharmacy, Faculty of Pharmacy, Iasi, Romania*
[2]*University of Camerino, School of Pharmacy, Camerino, Italy*
**lacramioara.ochiuz@umfiasi.ro*

1. Introduction

Experimental studies have demonstrated the potential of topically applied flavonoids to counteract specific clinical and histological alterations within the epidermis and dermis. These alterations arise due to the impact of UV radiation exposure and chronological aging. Flavonoids exert multiple effects on the skin such as: restoration of keratinocyte ultrastructural integrity, stimulation of collagen synthesis within the dermal layer, enhancement of vascularization, and normalization of hyperkeratinization [1]. Besides aging, flavonoids can bring multiple benefits in other various skin conditions such as eczema, acne, or psoriasis as they possess anti-inflammatory, antioxidant, antimicrobial and wound healing properties. However, their effectiveness can vary depending on factors such as the specific flavonoid compound, its concentration, the formulation used, and individual skin characteristics [2,3].

Chrysin, a flavonoid known as 5,7-dihydroxyflavone, is found in citrus fruits, passion flowers, honey, propolis and mushrooms and it has recently drawn scientists' attention for its pharmacological effects [4]. For example, the effectiveness of chrysin was assessed within an animal model with induced psoriasis-like symptoms. Histological analyses of chrysin-treated skin revealed a notable amelioration of inflammatory indicators, leading to a reduction in both the extent and severity of psoriasis. Under chrysin treatment, the activation of the NF-κB pathway in epidermal keratinocytes, a central player in inflammation, was notably attenuated [5]. Considering the extended therapeutic potential of flavonoids, in particular that of chrysin, we conducted *in vitro* release studies and we analyzed the factors that can influence the therapeutic efficacy of this compound when formulated in semisolid topical preparations.

2. Experimental

A spectrophotometric UV-VIS method was used for the quantitative determinations in this study, with a maximum absorbance measured at 315 nm for chrysin.

Three formulations (hydrogel, organogel and cream) containing chrysin (0.5% w/w) were developed based on Carbopol® 940 (1%), poloxamer (20%) and eucerin (5%) respectively.

Determination of chrysin solubility in different dissolution media: To identify a suitable receptor medium for *in vitro* dissolution test, the solubility of chrysin in different media was analyzed. Four media were tested, as follows: (i) 0.1M phosphate buffer (pH 7.4) and ethanol in a ratio of 4:1; (ii) 0.1M phosphate buffer (pH 7.4) and ethanol in a ratio of 3:2 (iii) 0.1M phosphate buffer (pH 7.4) plus 0.5% Tween 20; (iv) 0.1M phosphate buffer (pH 5.5) and ethanol in a ratio of 4:1. Ethanol was selected as the reference solvent, in which chrysin is freely soluble. For each selected solvent, a

0.05 mg/mL chrysin solution was prepared. The samples were kept at 37 °C with stirring for 12 hours. After filtering through syringe filters of 0.45 µm, the chrysin content was analyzed by UV-VIS method, and the solubility was expressed as the recovery percentage.

An in vitro dissolution test was conducted to analyze the release of chrysin from the three different topical formulations. The test was performed using enhancer cells with a diameter of 2.5 cm, using the SR 8 Plus Series device according to the following protocol: dissolution medium was a mixture of phosphate buffer pH 7.4:ethanol=3:2, in a volume of 100 mL; the sample mass was 0.6 g; we used nylon synthetic membrane with pore diameter Ø = 0.45µm; temperature was set at 37 °C ± 0.2 °C and rotation speed at 100 rpm. The synthetic membrane was placed in the dissolution medium for 24 hours, before performing the *in vitro* test, in order to optimally hydrate and dilate the pores. The membrane is employed to mimic the skin barrier and provide insights into how a formulation interacts with the skin's layers. The test was performed over an interval of 24 hours, every 2 hours we collected a volume of 1 mL sample, which was replaced with fresh medium; the concentration of chrysin was determined using the spectrophotometric method.

3. Results and discussion

Chrysin was used in concentrations between 0.001-0.06 mg/mL to obtain an absorbance lower than 1.2 units (Figure 1). The method showed linearity in this interval, with an R^2=0,9999. The UV-VIS spectra of chrysin is shown in Figure 1 (λ_{max}=315 nm). The excipients used for topical formulations did not interfere with λ_{max} of chrysin.

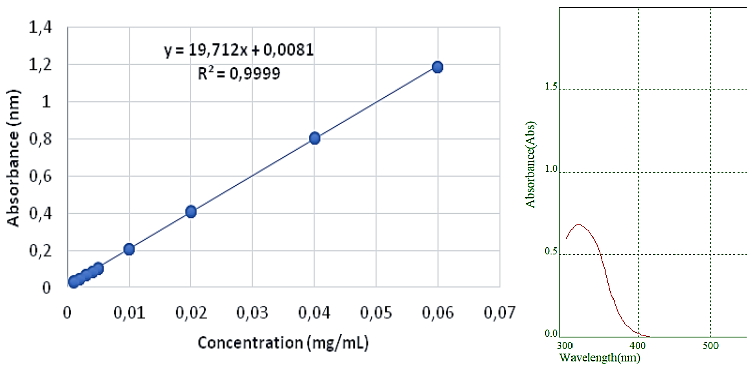

Figure 1. Chrysin UV VIS parameters method (linearity curve and UV-VIS spectra).

When testing the solubility in different media, we obtained for chrysin total recovery in ethanol and 95.64% recovery in phosphate buffer (PBS) pH 7.4: ethanol (EtOH) mixture (3:2) (Figure 2).

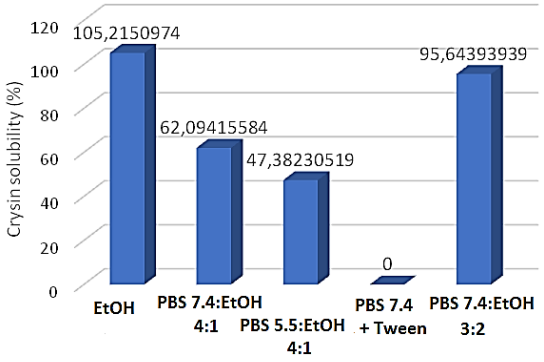

Figure 2. Graphical representation of chrysin solubility in different dissolution media – expressed as percentage of recovery (%) (PBS, *phosphate buffer*; EtOH, *ethanol*).

Chrysin is practically insoluble in phosphate buffer pH 7.4 mixed with 0.5% Tween 20; the surfactant was not able to achieve the micellar solubilization of chrysin. A lower pH of phosphate buffer was not suitable to achieve a higher solubilization of chrysin, as shown by the phosphate buffer pH 5.5: ethanol mixture (4:1) (Figure 2). When analyzing the equilibrium solubility expressed in µg/mL, we obtained the values 5.26, 3.10, 2.36 and 4.78 µg/mL in ethanol, PBS 7.4: EtOH (4:1), PBS 5.5: EtOH (4:1), PBS 7.4: Tween 20 (0,5%) and PBS 7.4: EtOH (3:2) respectively. Based on these results, in order to perform the release of chrysin in dissolution test, we selected the mixture PBS 7.4: EtOH (3:2) as a dissolution medium. The results of the *in vitro* dissolution test showed that the highest release (60.29%) of the total chrysin content is from the organogel formulation (Figure 3). Regarding the hydrogel type formulation with chrysin, after 24 h, it yielded to a release 48.78% of the total incorporated substance. The least efficient matrix for facilitating chrysin release was the eucerin based cream, with a released chrysin percentage below 20%. This can be justified by chrysin being blocked in the matrix forming certain chemical bonds with cream excipients. However, this type of formulation might be suitable for prolonged release of active substance over a period exceeding 24 h.

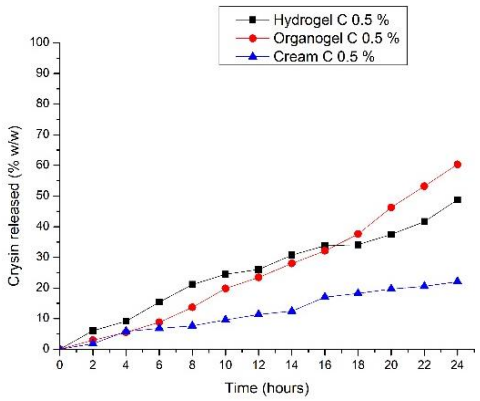

Figure 3. Dissolution test - *in vitro* chrysin release from three different formulations.

4. Conclusions

Flavonoids are an important group of natural compounds with multiple therapeutic valences. The studies conducted in this research aimed to analyze the influence of matrix formulation on the release of chrysin through a synthetic membrane. According to the obtained results, the organogel based on poloxamer is optimal for the release of chrysin over a period of 24 hours.

References

[1]. Menaa F, Menaa A, Treton J. Polyphenols against skin aging. In: Watson RR, Preedy VR, Zibadi S, editors. Polyphenols in human health and disease, vol. I, London: Academic Press; pp. 819-830, 2014

[2]. Čižmárová B, Hubková B, Tomečková V, Birková A. Flavonoids as promising natural compounds in the prevention and treatment of selected skin diseases. *Int. J. Mol. Sci.* 24(7), 6324, 2023

[3]. Bujor A, Ochiuz L, Sha'at M. Stoleriu I, Stamate MI, Simon VL, Miron A. Chemical, antioxidant and in vitro permeation and penetration studies of extracts obtained from Viburnum opulus and Crataegus pentagyna. *Farmacia* 68(4), 672-678, 2020

[4]. Islam MM, Nagaraja S, Hafsa NE, Meavanige G, Basheeruddin Asdaq SM, Anwer K. Polyphenol chrysin for management of skin disorders: Current status and future opportunities. *J. King Saud Univ., Sci.* 34, 102026, 2022

[5]. Li HJ, Wu NL, Pu CM, Hsiao CY, Chang DC, Hung CF. Chrysin alleviates imiquimod-induced psoriasis-like skin inflammation and reduces the release of CCL20 and antimicrobial peptides. *Sci. Rep.* 10(1), 2932, 2020

EXPLOITING THE POTENTIAL OF XANTHAN AND LIGNIN FOR THE ADSORPTION OF DEGRADED OIL

Narcis Anghel, Irina Apostol,* Mirela Fernanda Zaltariov, Iuliana Spiridon
Petru Poni Institute of Macromolecular Chemistry, Romanian Academy, Iasi, Romania
**apostol.irina@icmpp.ro*

1. Introduction

Oils are a concerning issue due to their impact on the water wildlife as well as damage to terrestrial environments. Industries such as chemical, petrochemical, or pharmaceutical are the mainly responsible for oily wastewater [1]. This is why, reducing the pollutants and their converting into economic value-added products became a global priority.

Argan oil is widely used in cosmetic or pharmacological industries. Elevated temperatures, along with exposure to air, light, or moisture, make it prone to numerous chemical reactions including oxidation, hydrolysis, and the breakdown of fatty acids. Consequently, the oil becomes degraded and develops toxicity as it generates harmful compounds such as peroxides, aldehydes, or ketones. For those reasons, numerous attempts have been made to design suitable and inexpensive materials/methods to retain the degraded oils from wastewaters [2].

The present study is focused on the preparation of new adsorptive materials based on xanthan (XG) and lignin esters. The adsorption of degraded argan oil (which was stored at high temperature and UV light for 24 months) onto the obtained materials was investigated.

2. Experimental

LignoBoost (LB) lignin was esterified with oleic and stearic acid through an enzymatic reaction, using lipase from *Candida cylindraceea* as catalyst. Further, LB and its esters (LBOL or LBST) were embedded into XG matrix under magnetic stirring. The adsorptive materials (XG, XG/LB, XG/LBOL and XG/LBST, respectively) were obtained by freeze-thawing cycles, followed by lyophilization. FTIR spectra of materials were recorded using a Vertex 70 FTIR spectrometer from Brüker, equipped with an ATR (Attenuated Total Reflectance) device (ZnSe crystal). The solid-state ^{13}C NMR spectra of lignin esters were obtained on a Bruker AvanceHD-400 MHz NMR spectrometer to evidence the structural differences between LB and LB esters.

Adsorption experiments of degraded argan oil have been performed. The equilibrium sorption capacity q_e (g/g), the amount of retained altered oil at a specific time interval q_t (g/g) and the altered oil removal efficiency R (%) were calculated. SEM images of materials, before and after oil adsorption were collected using a VEGA TESCAN microscope with a low-vacuum secondary electron detector at an acceleration voltage of 20 kV, at room temperature.

3. Results and discussion

FTIR and ^{13}C NMR spectra (Figure 1) confirmed the chemical modification of LB by the presence of characteristic peaks assigned to aliphatic carbon atoms. According to SEM images (Figure 2a), all the obtained materials presented interconnected pores.

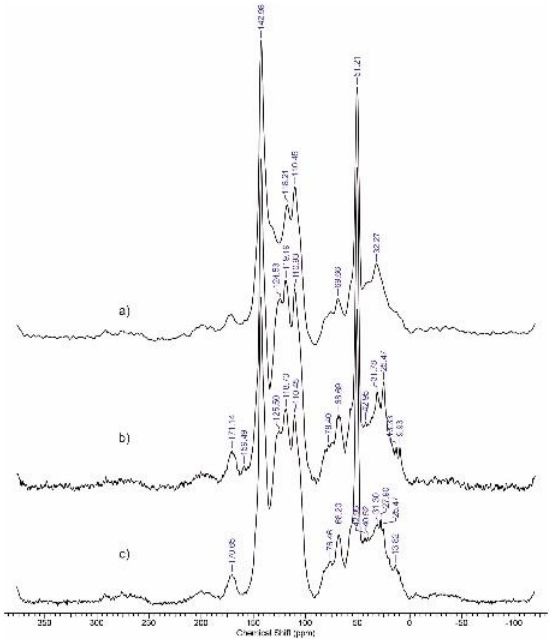

Figure 1. ^{13}C NMR spectra of lignin and its derivatives (a) LB; b) LBOA; c) LBST.

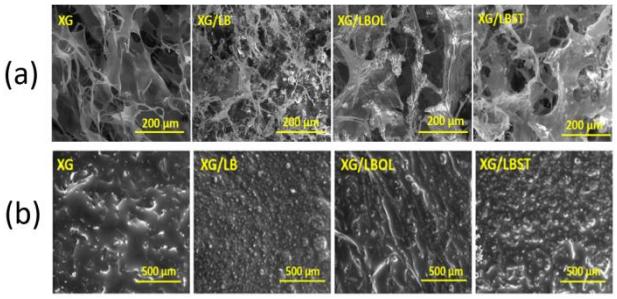

Figure 2. SEM micrographs of materials (a) before and (b) after degraded argan oil loading.

Before adsorption experiments, the density, acid value (AV), free fatty acids content (FFA), iodine value (IV) and (peroxide value) POV of degraded argan oil were evaluated (Table 1). Based on all the gathered data, it is evident that the material has undergone an alteration process, resulting in the breaking of several double bonds within the oil structure.

Table 1. Characteristics of analyzed oil samples.

Sample	Density, g/cm^3	Acid value (AV), mg KOH/g	Free fatty acids (FFA), wt%	Iodine value (IV), g I_2/100 g sample	Peroxide value (POV), meq/kg
Argan oil	0.81	1.03	0.51	9.62	0.98

After the oil sorption experiments it was revealed that over 60% of the total oil quantity was retained. XG, XG/LB and XG/LBST materials retained the highest amount of degraded argan oil (61.19, 55.15 and 53.02 g/g) (Table 2).

Table 2. Adsorption capacity values.

Material	[a] q_e ± SD (g/g)		
	Argan oil		
	1 g	2 g	3 g
XG	42.58 ± 0.96	54.40 ± 1.52	61.19 ± 3.43
XG/LB	42.62 ± 3.77	53.17 ± 1.73	55.14 ± 0.93
XG/LBOL	34.76 ± 2.06	42.08 ± 0.90	43.39 ±2.64
XG/LBST	37.46 ± 2.22	47.43 ± 1.91	53.02 ± 3.86

[a] Data are expressed in the mean ± standard deviation (n = 3)

SEM images of all the materials loaded with argan oil (Figure 2b) demonstrate that their pores are entirely filled with oil molecules.

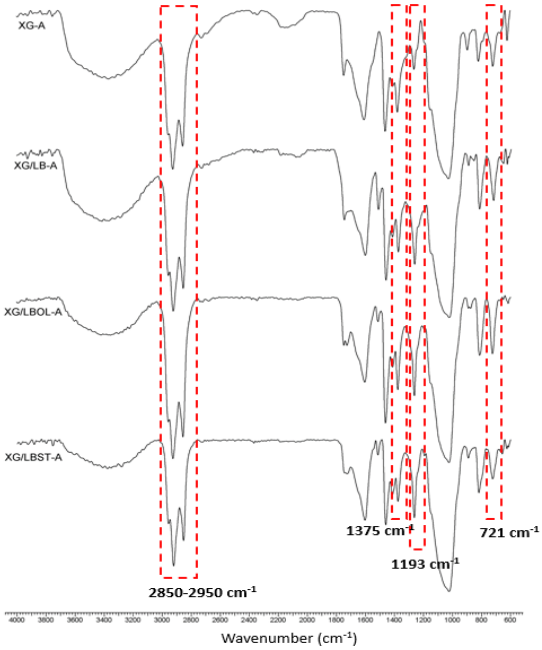

Figure 3. FTIR spectra of materials after degraded argan oil adsorption.

The adsorption kinetics was performed to investigate the oil adsorption mechanism. The experimental data correlate with the Pseudo-Second Order kinetic model (the correlation coefficient, R^2, ranges between 0.9814 and 1.0000). This model is suitable for expressing the kinetics of physisorption and mass transfer/diffusion processes [3] for crude oil adsorption.

FTIR spectra of the materials after the adsorption process (Figure 3) did not reveal the presence of new chemical bonds forming between oil molecules and the polysaccharide matrix, proving that the studied process is of a physical nature. The adsorption equilibrium of altered argan oil onto XG, XG/LB and XG/LBOL materials was best expressed by the Langmuir model (values of R^2 between 0.9894 and 1.0000).

These results indicate monolayer deposition of altered oil molecules onto the adsorbents surfaces. The adsorption equilibrium of argan oil onto XG/LBST was well described by the Henry isotherm model (R^2 value of 0.9997). This model typically describes adsorption at lower concentrations [4].

4. Conclusions

In this study, LB underwent an enzymatically catalyzed reaction to be esterified with oleic and stearic acid. Subsequently, materials based on XG and LB esters were obtained, and their adsorptive properties were investigated. Our results indicated that all the adsorbents could retain more than 50 g/g of degraded argan oil.

Kinetic studies showed a good correlation with the PSO model for all experimental data. FTIR spectra of materials loaded with oil suggested that the adsorption process is of a physical nature. Equilibrium data fitted well with Henry and Langmuir isotherm models.

This study introduces new possibilities for using lignin and its derivatives in wastewater treatment.

References

[1]. Mohammed F, Guillaume D, Warland J, Abdulwali N. Analytical methods to detect adulteration of argan oil: A critical review. *Microchem. J.* 168, 106501, 2021
[2]. Cheng Y, Xu P, Zeng W, Ling C, Zhao S, Liao K, Suna Y, Zhou A. Highly hydrophobic and ultralight graphene aerogel as high efficiency oil absorbent material. *J. Environ. Chem. Eng.* 5, 1957-1963, 2017
[3]. Guo Q, Amendola E, Lavorgna M, Li Z, Feng H, Wu Y, Fei G, Wang Z, Xia H. Robust and recyclable graphene/chitosan composite aerogel microspheres for adsorption of oil pollutants from water. *Carbohydr. Polym.* 290, 119416, 2022
[4]. Kalam S, Abu-Khamsin SA, Kamal MS, Patil S. Surfactant adsorption isotherms: a review. *ACS Omega*. 6, 32342-32348, 2021

WHEN A NITRONYL NITROXIDE LIGAND MEETS AMINES TO FORM SCHIFF BASES. LIGANDS DESIGN AND THEIR COMPLEXES

Mihai Raduca,[1,2]* David Hunger,[3] Sergiu Shova,[4] Marius Andruh[1,2]
[1]*Faculty of Chemistry, University of Bucharest, Bucharest, Romania*
[2]*Costin D. Nenitescu Institute of Organic and Supramolecular Chemistry, Romanian Academy, Bucharest, Romania*
[3]*Institute of Physical Chemistry, University of Stuttgart, Stuttgart, Germany*
[4]*Petru Poni Institute of Macromolecular Chemistry, Romanian Academy, Iasi, Romania*
**fiidemn@gmail.com*

1. Introduction

Nitronyl nitroxide compounds (NN) are stable, persistent organic radicals which can be used to obtain hybrid magnetic materials [1]. The design of the NN ligands with coordination sites aimed for specific metal ions is mostly in conjunction with the pursued properties. A common synthetic strategy to introduce more coordination fragments in the molecule is via Schiff reactions employing primary amines. The number of NNs containing a free formyl moiety is however limited to few examples [2], most of them being byproducts from the synthesis of a diradical. In this paper, we report a consistent protocol to convert just one out of two formyl groups into NN radical, and we show how combining two or more NNs via Schiff condensations could generate ligands and complexes with interesting topologies and properties.

2. Results and discussion

Novel nitronyl nitroxid ligands, HL^1 and HL^2, have been synthesized starting from 2-hydroxy-3-(hydroxymethyl)-5-methylbenzaldehyde (HL^a) and 2,6-diformyl-p-cresol (HL^b), respectively, following the synthetic protocol reported in the literature (Figure 1) [3]. Using the ligand HL^1, three 2p-4f binuclear complexes, $[Ln_2(L^1)_2(hfac)_4]$, where Ln = Gd, Tb, Dy and hfac = hexafloroacetylacetonate anion, have been obtained and characterized showing an antiferromagnetic interaction between the magnetic spins [4]. Moreover, 2,6-diformyl-*p*-cresol (HL^b) can be used to obtained the corresponding diradical (HL^3). Its synthesis and crystal structure are known and, more recently, a copper trinuclear complex has been reported [5]. In this work we show that the monoradical HL^2, i.e. 2-(2-hydroxy-3-formyl-5-methylphenyl)-4,4,5,5-tetramethyl-4,5-dihydro-1H-imidazolyl-1-oxyl 3-oxide, can be also systematically synthesized and further employed as a ligand. The ligand HL^2 was purified using column chromatography and recrystallization from diethyl ether yielding dark blue crystals characterized via X-ray diffraction on single crystal (Table 1) and EPR spectroscopy. A similar series of 2p-4f binuclear complexes, $[Ln_2(L^2)_2(hfac)_4]$, has been obtained and characterized. The overall antiferromagnetic coupling is also observed at low temperatures. X-ray diffraction studies on single crystal and on powder reveal that these compounds, $[Ln_2(L^2)_2(hfac)_4]$, present polymorphism as they are crystalizing both in a monoclinic (μ) and a triclinic (τ) crystal system.

Due to the fact that HL^2 has a free carbonyl group, Schiff bases with primary amine could be formed, enhancing the number of heteroatoms from the molecule available for coordination. Thus, several homo- and hetero-diradicals have been synthesized using 1,3-diaminopropane (H_2L^4), 2,2′-(ethylenedioxy)bis(ethylamine), 4-amino-TEMPO, 4,4'-oxydianiline. A tripodal triradical (H_3L^5)

has been synthesized using tris(2-aminoethyl)amine, and it was characterized via X-ray diffraction on single crystal (Figure 2b). The polydentate paramagnetic ligands have been reacted with different 3d and 4f hexafluoroacethylacetonato complexes giving rise to mono- and oligonuclear complexes with exciting properties (Figure 2a).

The dinuclear complex $[Yb_2(H_2L^4)(hfac)_4]$ crystalizes in two different triclinic systems exhibiting two colors: green and blue (Table 1). The two types of crystal can be mechanically separated and the X-ray powder diffraction on powder indicated the purity of the crystalline phase. The similar mononuclear complexes $[Ln(H_2L^4)(hfac)_3]$ were obtained and structurally characterized.

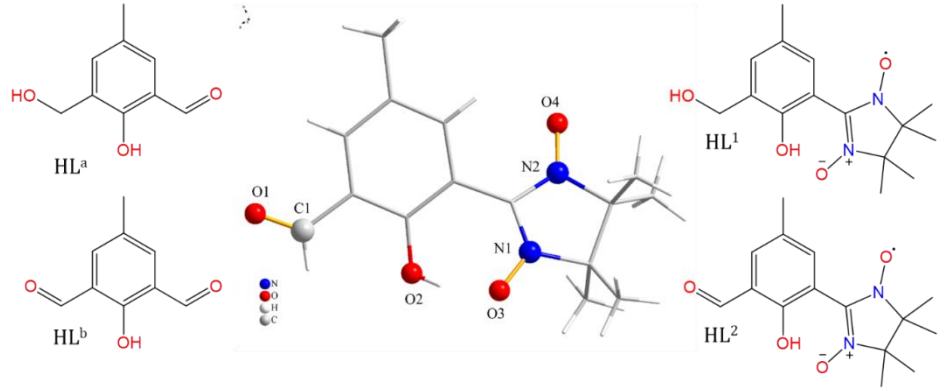

Figure 1. The structures of HL^a, HL^b, HL^1 and HL^2. Perspective views of the molecular structure of HL^2 determined by X-ray diffraction. The interatomic distance C1-O1 from the formyl group is 1.207 Å, in agreement with carbon double bonded to the oxygen. The interatomic distances corresponding to the heteroatoms from the radical moiety are N1···O3 = 1.301 and N2···O4 = 1.272 Å, respectively. The (O2-)H2···O3 distance for the intermolecular hydrogen interaction is 1.704 Å (O2···O3 = 2.503 Å) and the corresponding O2-H2···O3 angle is 164.2º.

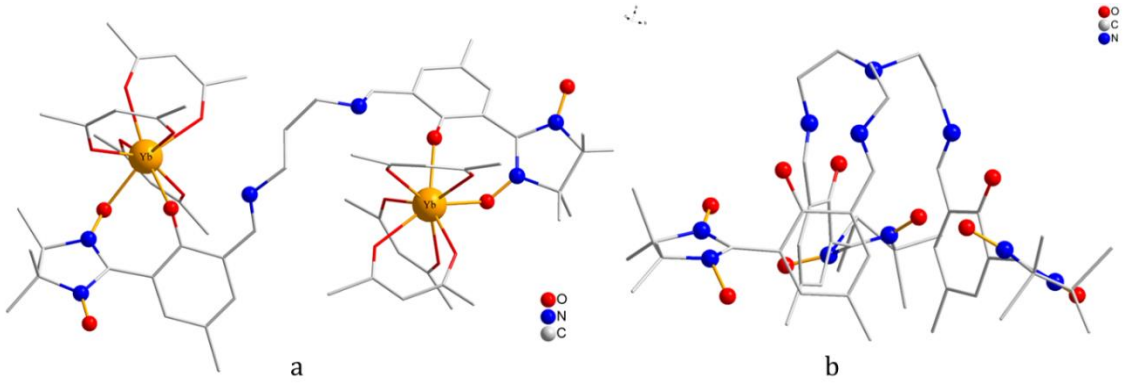

Figure 2. (a) Crystal structure of the dinuclear complex $[Yb_2(H_2L^4)(hfac)_4]$.
For clarity, fluorine and hydrogen atoms are not represented. (b) Crystal structure of the tripodal triradical ligand H_3L^5. Hydrogen atoms have been removed for clarity.

3. Conclusions

A novel nitronyl nitroxide ligand, HL^2, bearing a formyl moiety has been synthesized and characterized, i.e. 2-(2-hydroxy-3-formyl-5-methylphenyl)-4,4,5,5-tetramethyl-4,5-dihydro-1H-imidazolyl-1-oxyl 3-oxide. A series of di- and tri-radical ligands was obtained via Schiff reactions using several amines and, furthermore, mono- and oligonuclear complexes were synthesized and characterize using these multi-spin ligands.

Table 1. Crystal data and structure refinement for HL^2, τ-$[Yb_2(H_2L^4)(hfac)_6]$ and τ-$[Yb_2(H_2L^4)(hfac)_6]$.

Compound	**HL^2**	**τ-$[Yb_2(H_2L^4)(hfac)_6]$ blue**	**τ-$[Yb_2(H_2L^4)(hfac)_6]$ green**
Chemical formula	$C_{15}H_{19}N_2O_4$	$C_{63}H_{50}F_{36}N_6O_{18}Yb_2$	$C_{63}H_{50}F_{36}N_6O_{18}Yb_2$
M (g mol^{-1})	291.32	2209.17	2209.17
Temperature, (K)	293(2)	293(2)	293(2)
Wavelength, (Å)	0.71073	0.71073	0.71073
Crystal system	*Monoclinic*	*Triclinic*	*Triclinic*
Space group	*I2/α*	*P-1*	*P-1*
a (Å)	16.4769(11)	12.3096(5)	16.6951(5)
b (Å)	11.2095(5)	18.5103(9)	17.0745(7)
c (Å)	16.9351(10)	20.0019(8)	17.7303(8)
α (º)	90	101.265(4)	94.149(3)
β (º)	110.636(7)	103.606(4)	112.593(4)
γ (º)	90	100.169(4)	107.243(3)
V (Å^3)	2927.2(3)	4224.3(3)	4356.1(3)
Z	8	2	2
D_c (g cm^{-3})	1.322	1.737	1.684
μ (mm^{-1})	0.097	2.344	2.273
F(000)	1240	2156	2156
GOF	1.044	1.051	1.034
Final R_1, wR_2 [I>2σ(I)]	0.0413, 0.1098	0.0488, 0.1303	0.0516, 0.1306
R_1, wR_2 (all data)	0.0610, 0.1184	0.0780, 0.1449	0.0870, 0.1475
$\Delta\rho_{min}/\Delta\rho_{max}$ (e Å^{-3})	0.22, -0.18	1.24, -0.66	2.17, -1.91

Acknowledgements

MR is grateful to "Costin D. Nenitescu" Institute of Organic and Supramolecular Chemistry for founding this study.

References

[1]. Alberola A, Coronado E, Giménez-Saiz C, Gómez-García CJ, Romero F, Tarazón A. Hybrid magnetic materials based on nitroxide free radicals and extended oxalato-bridged bimetallic networks. Eur. J. Inorg. Chem. 2005, 389-400, 2005

[2]. Caneschi A, Gatteschi D, Sessoli R. Magnetic properties of a layered molecular material comprising manganese hexafluoroacetylacetonate and nitronyl nitroxide radicals. *Inorg. Chem*. 32, 4612-4616, 1993

[3]. Ullman EF, Call L, Osieki JH. Stable free radicals. VIII. New imino, amidino, and carbamoyl nitroxides. *J. Org. Chem*. 35, 3623-3631, 1970

[4]. Raduca M, Martins DOTA, Spinu CA, Hillebrand M, Tuna F, Ionita G, Madalan AM, Lecourt C, Sutter JP, Andruh M. A new nitronyl-nitroxide ligand for designing binuclear Ln III complexes: Syntheses, crystal structures, magnetic and EPR studies. *Eur. J. Inorg. Chem*. e202200128, 2022

[5]. Grenda S, Beau M, Luneau D. Synthesis, crystal structure and magnetic properties of a trinuclear copper(II) complex based on p-cresol-substituted bis(α-nitronyl nitroxide) biradical. *Molecules* 27, 3218, 2022

COMBINED ELECTRONIC ABSORPTION AND RAMAN SPECTRA OF SOME AZOBENZENE DERIVATIVES

Dragos Lucian Isac,[1]* Emilian Rosca,[1] Anton Airinei,[1] Elena Laura Ursu,[1] Razvan Puf,[1] Isabela Costinela Man,[2] Aatto Laaksonen[1]

[1] *Petru Poni Institute of Macromolecular Chemistry, Romanian Academy, Iasi, Romania*

[2] *Costin D. Nenitescu Institute of Organic and Supramolecular Chemistry, Romanian Academy, Bucharest, Romania*

**isac.dragos@icmpp.ro*

1. Introduction

Molecular photoswitches belong to a class of chemical compounds that undergoes different reactions when more than one photochromic entity is involved [1]. Based on this affirmation, these compounds can be used and play a central role in fundamental and applied research.

Azobenzene molecular system is a member of the molecular photoswitch family that can modify its internal coordinates such as bond length, valence, and dihedral angles during isomerization process [2,3]. The azobenzene chemical structure has two isomers: trans being more stable from a thermodynamic point of view in equilibrium energy state, and cis which is metastable. The conversion from trans to cis can be activated using UV light as an external source. While the cis isomer is metastable (as the reactant) it can reverse to the trans isomer, following two reaction pathways. The first reaction can occur in darkness being a slow process and the second reaction can be determined by visible light with a fast conversion. As can be seen, azobenzene derivatives can undergo an isomerization reaction in which the trans isomer plays the role of reactant, and cis represents the function of the reaction product. Since the reaction is reversible, the roles of the reactant and product of the reaction can undergo a reversal.

Thanking into account that we have more than one photochromic entity (trans and cis isomers), the azobenzene molecular system has advantages and opportunities to be employed in different applications such as nanomachines and smart materials [4], actuators [5,6], light-sensitive materials [7], energy storage [8] and self-assembling azopolymers and molecular machines [9].

The mechanism of isomerization reaction is still unclear and open for discussion. In order to understand the mechanism of this process which it is a mandatory for a chemist, a deep survey of electronic structure of the azobenzene compounds must be realized. In this case, a strong corroboration between experimental data and simulation is recommended.

Unless specified, the conversion from trans to cis and reverse usually happens by visiting the excited state process. In this case, it is more difficult to localize and propose a clear mechanism. But it is known that, the azobenzene has two well separated absorption bands, one in UV and other in visible region. By the UV irradiation of the trans isomers two type of excitation $\pi \rightarrow \pi^*$ ($S_0 \rightarrow S_2$) and $n \rightarrow \pi^*$ ($S_0 \rightarrow S_1$) appear. The $\pi \rightarrow \pi^*$ ($S_0 \rightarrow S_2$) transition is much higher in intensity by comparison with $n \rightarrow \pi^*$ ($S_0 \rightarrow S_1$) due to the symmetry-allowed dipole moment of excitation. The $n \rightarrow \pi^*$ ($S_0 \rightarrow S_1$) excitation has a small intensity because it is a forbidden transition by the electric dipole selection rules and orthogonality of molecular orbitals. During the irradiation process the absorbance of trans isomer, $\pi \rightarrow \pi^*$, decreases, while $n \rightarrow \pi^*$ transition intensity increases driving the formation of cis isomers.

On the other hand, the conversion from cis to trans occurs by the n → π* ($S_0 \rightarrow S_1$) excitation or does not visit this excited state, and a reaction intermediate appear. Introduction of some substituents on the azobenzene main core can make more difficult to understand the electronic structure as well as the reaction pathways. Also, the dynamics of isomerization reactions can be influenced by the polarity of solvents.

The main goal of this work was to investigate the electronic configuration and structural properties of some azobenzene derivatives (Figure 1). The electronic configurations have been described by UV-Vis absorption spectra, whereas structural characterization was made using the Raman scattering. Using UV-Vis spectra it can obtain the photophysical and photochemical properties of the azobenzene structure as well as the molecules' electronic state. The utilization of Raman spectroscopy can offer information about structural characteristics by interpreting the vibration spectra. However, when the incident laser used in Raman scattering matches an electronic transition wavelength both dual information about the nature of electronic excitation and structural properties can be obtained.

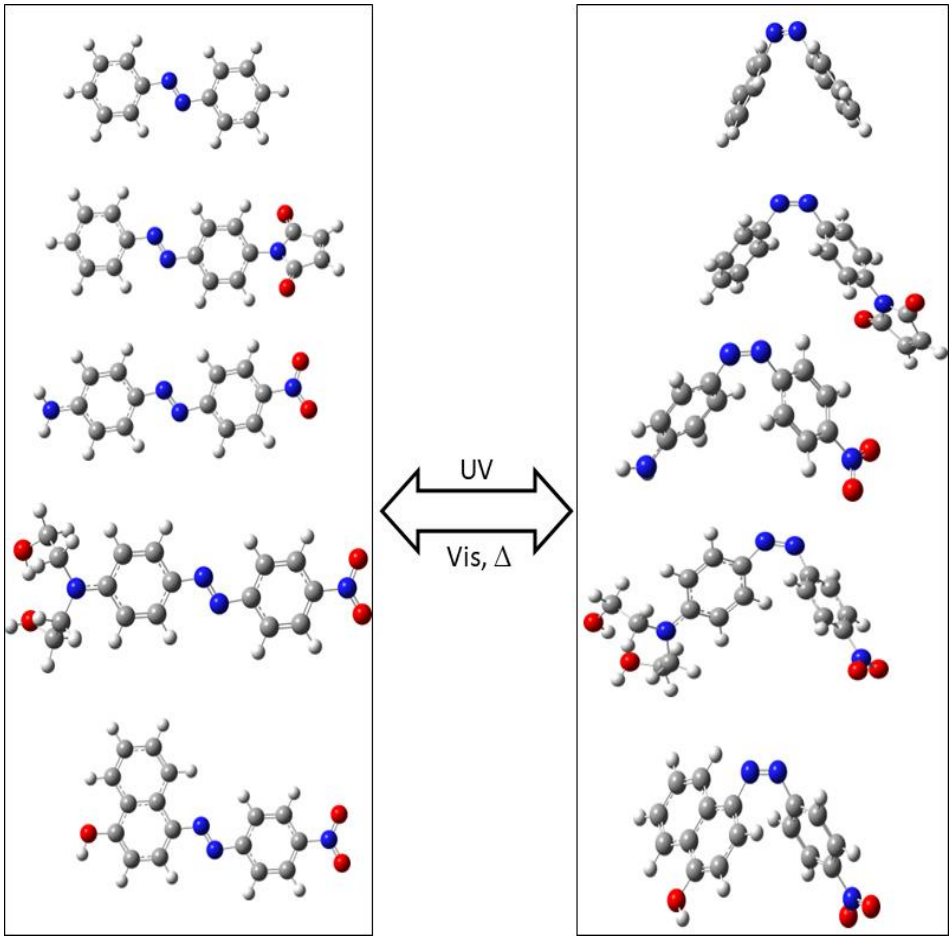

Figure 1. Representation of the azobenzene derivatives selected for investigation in their trans (left) and cis (right) conformations.

2. Results and discussion

When the incident laser utilized in Raman spectroscopy is closer to wavelength corresponding to an electronic transition of the compound under study, the signal Raman intensity can be enhanced. In our work, three lasers of different wavelengths have been used to obtain the Raman vibrations at

442, 633, and 785 nm. However, when the incident laser used at 442 nm can match the first electronic transition of azo derivatives that appears around 450 nm in UV-Vis spectra, the resonance Raman signal was lower in intensity as comparison to 633 and 785 nm excitation. To explain this situation, we employed some theoretical methods based on DFT and TD-DFT approaches.

Our results indicate the lower Raman signals appeared due to the presence of the $n \rightarrow \pi^*$ ($S_0 \rightarrow S_1$) transition of low intensity. The wB97XD/cc-pVT method predicts a good correlation between theory *vs.* experiment in the ground state of Raman signals When the excited states have been introduced in the calculation of resonance Raman, the CAM-B3LY/cc-pVTZ level of theory was in line with experimental data.

3. Conclusions

The present work represents a corroboration between theory and experiment. The mode of vibration and intensity of Raman signal measured by experimental determination was interpreted with a simulation modeling approach using DFT and TD-DFT levels of theory. Our theoretical results explained why the intensity of Raman signals was lower at the resonance. This effect appears because of the presence of the $n \rightarrow \pi^*$ excitation.

Acknowledgements

This work was supported by a grant of the Ministry of Research, Innovation and Digitization, CNCS - UEFISCDI, project number PN-III-P1-1.1-PD-2021-0060 (FingerprintAZO), within PNCDI III. This work also was supported by the research infrastructure developed through the European Social Fund for Regional Development, Competitiveness Operational Programme 2014–2020, Axis 1, Action: 1.1.3, Project “Infra SupraChem Lab-Center for Advanced Research in Supramolecular Chemistry” (Contract 339/390015/25.02.2021, cod MySMIS: 108983).

References

[1]. Fihey A, Perrier A, Browned WR, Jacquemin D. Multiphotochromic molecular systems. *Chem. Soc. Rev.* 44, 3719-3759, 2015
[2]. Isac DL, Airinei A, Homocianu M, Fifere N, Cojocaru C, Hulubei C. Photochromic properties of some azomaleimide derivatives and DFT quantum chemical study of thermal cis-trans isomerization pathways. *J. Photochem. Photobiol., A.* 390, 112300, 2020
[3]. Bandara HMD, Burdette SC. Photoisomerization in different classes of azobenzene. *Chem. Soc. Rev.* 41, 1809-1825, 2012
[4]. Lameijer LN, Budzak S, Simeth NA, Hansen MJ, Feringa BL, Jacquemin D, Szymanski W. General principles for the design of visible-light-responsive photoswitches: Tetra-ortho-Chloro-azobenzenes. *Angew. Chem.* 132, 21847-21854, 2020
[5]. Racles C, Ursu C, Dascalu M, Asanduleasa M, Tiron V, Bele A, Tugui C, Teodoroff-Onesim S. Multi-stimuli responsive free-standing films of DR1- grafted silicones. *Chem. Eng. J.* 401, 126087, 2020
[6]. Shang Y, Wang J, Ikeda T, Jiang L. Bio-inspired liquid crystal actuator materials. *J. Mater. Chem. C* 7, 3413-3428, 2019
[7]. Tochitsky I, Kienzler A, Isacoff E, Kramer H. Restoring vision to the blind with chemical photoswitches. *Chem. Rev.* 118, 10748-10773, 2018
[8]. Dong L, Chen Y, Zhai F, Tang J, Feng Y, Feng W. Azobenzene-based solar thermal energy storage enhanced by gold nanoparticles for rapid, optically-triggered heat release at room temperature. *J. Mater. Chem. A* 8, 18668-18676, 2020
[9]. Jerca FA, Jerca V, Hoogenboom R. Advances and opportunities in the exciting world of azobenzenes. *Nat. Rev. Chem.* 5, 51-69, 2022

S-BLOCK COORDINATION POLYMERS BUILT UP WITH SILICON-CONTAINING CARBOXYLATE LINKERS

Mirela-Fernanda Zaltariov,* Sergiu Shova, Maria Cazacu
Petru Poni Institute of Macromolecular Chemistry, Romanian Academy, Iasi, Romania
**zaltariov.mirela@icmpp.ro*

1. Introduction

Coordination polymers (CPs) are crystalline materials built up from the interconnection of organic linkers and metal nodes forming 1D chains, 2D layers or 3D networks. The linkers can have a variety of structures and different functionalities given rise to unprecedented structures [1] tailored for particular applications such as gas storage/separation, energy storage/ conversion, catalysis, chemical sensing, biomedical imaging and even the accommodation of switches and molecular machines [2-4]. The main features that recommend them in such applications are the high crystallinity and the large specific surface area, fine-tunable pore structures and the adjustable chemical functionalities. While the first row transition metal centers are often chosen for their predictive coordination behavior, CPs based on s-block metal centers are relatively less studied. However, the relatively high charge density and ionic nature of s-block metal ions promotes strong bonding interactions in particular with carboxylate ligands [5].

2. Experimental

Two silicon-containing carboxylate linkers: bis(carboxyphenyl)diphenyl silane (H_2L^1) and tris(carboxyphenyl)phenyl silane (H_3L^2) were used to prepare CPs by using Ba(II) and Ca(II) acetates, as metal ion sources, under solvothermal conditions. The products as colorless crystals were analyzed by single-crystal X-ray diffraction (SC-XRD) analysis (Figure 1) to determine their structures, these being also supported by the results of elemental and spectral analyses.

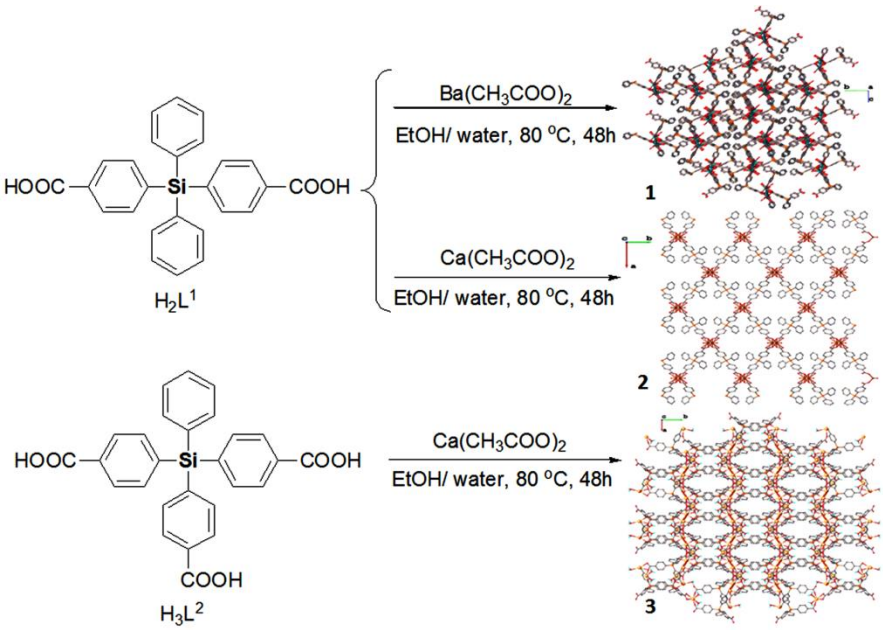

Figure 1. The synthetic pathways leading to Ba(II) and Ca(II) CPs and their crystal packing patterns.

3. Results and discussion

The formation of Ca(II) and Ba(II) CPs was studied primarily by IR spectroscopy that evidenced the disappearance of the characteristic bands assigned to the carboxylic groups at 1715 cm^{-1} (H_2L^1) and 1719 cm^{-1} (H_3L^2), and the appearance of the specific absorption bands attributed to the asymmetric and symmetric stretches of the carboxylate groups at 1537 and 1404 cm^{-1} (**1**), 1578 and 1396 cm^{-1} (**2**) and 1585 and 1395 cm^{-1} (**3**) (Figure 2).

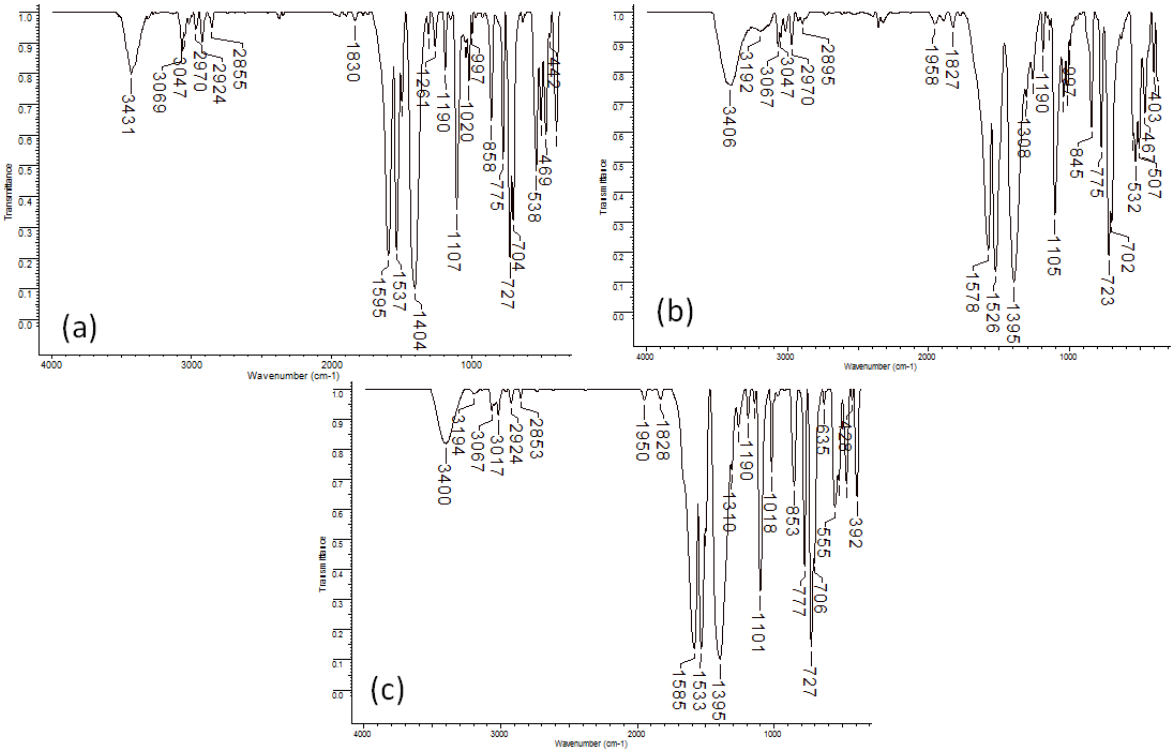

Figure 2. IR spectra of Ba-L^1 CPS (a), Ca-L^1 CPS (b) and Ca-L^2 CPS (c).

SC-XRD analysis revealed the formation of 2D dense structures in the case of H_2L^1 and 3D network in case of H_3L^2 (Figure 1), Ba(II) and Ca(II) centers being coordinated by multiple carboxylate groups in bidentate bridging and chelating coordination modes, with various coordination numbers (Figure 3).

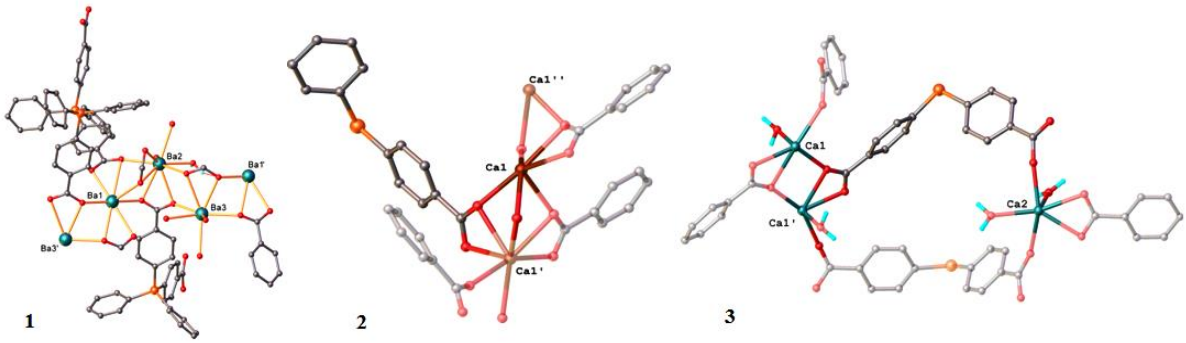

Figure 3. View of coordination environments of Ba(II)- and Ca(II)-based clusters for CPs **1** (Ba-L^1), **2** (Ca-L^1) and **3** (Ca-L^2).

The limitations in the development of s-block-based CPs are attributed to their instability in air and in aqueous media. The moisture stability of the compounds **1-3** was evaluated by dynamic water vapor sorption analysis (DVS), when no changes in masses and spectral patterns after desorption were evident (Figure 4a). The moderate values of the moisture sorption capacity, 11.65 % for **1**, 29.88 % for **2** and 15.43 % for **3**, are determined by the also moderate surface hydrophilicity and the free volume of the network, the latter being 11% for **1**, 25% for **2** and 31% for **3**. Ba(II) and Ca(II)-based CPS are stable up to 500 ^{o}C with first-weight loss of 5-7% at 49 ^{o}C and 133 ^{o}C corresponding to free solvent molecules in the structure (Figure 4b).

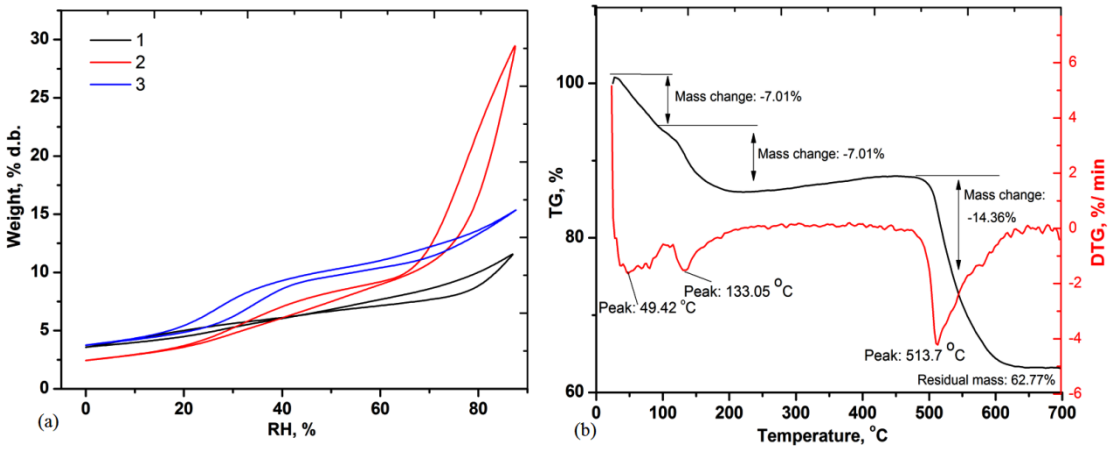

Figure 4. The sorption-desorption isotherms of CPS and the TG/ DTG curves for CPS **1.**

4. Conclusions

Ba(II) and Ca(II) CPs were built with carboxylate linkers having phenyl- and diphenyl silane units in their structure, under solvothermal conditions. These are the first alkaline earth metal -based CPs with silicon-containing carboxylate linkers. This work has shown that the nature of the ligands and the geometric needs of the s-block metals play a significant role in the packing pattern of CPs. The prepared CPs showed moisture and thermal stability, making them attractive platforms for applications in gas storage/separation and catalysis.

Acknowledgements

This work was supported by a grant from the Romanian Ministry of Research, Innovation, and Digitization, CNCS - UEFISCDI, project number PN-III-P4-ID-PCE-2020-2000, within PNCDI III, Contract 207/2021 (2D-PerMONSil).

References

[1]. Zhou HC, Long JR, Yaghi, OM. Introduction to metal-organic frameworks. *Chem. Rev.* 112, 673-674, 2012
[2]. Kirchon A, Day GS, Fang Y, Banerjee S, Ozdemir OK, Zhou HC. Suspension processing of microporous MOFs: A scalable route to high-quality adsorbents. *iScience* 5, 30-37, 2018
[3]. Zhao Y, Wang YJ, Wang N, Zheng P, Fu HR, Han ML, Ma LF, Wang LY. Tetraphenylethylene-decorated metal−organic frameworks as energy-transfer platform for the detection of nitro-antibiotics and white-light emission. *Inorg. Chem.* 58, 12700-12706, 2019
[4]. Martinez-Bulit P, Stirk AJ, Loeb SJ. Rotors, motors, and machines inside metal-organic frameworks. *Trends Chem*. 1, 588-600, 2019
[5]. Alnaqbi MA, Alzamly A, Ahmed SH, Bakiro M, Kegere J, Nguyen HL. Chemistry and applications of s-block metal–organic frameworks. *J. Mater. Chem. A*, 9, 3828-3854, 2021

MAGNETIC IONOTROPIC HYDROGELS FOR WATER POLLUTION MITIGATION

Andra-Cristina Enache,* Ionela Grecu, Petrisor Samoila, Corneliu Cojocaru, Valeria Harabagiu

Petru Poni Institute of Macromolecular Chemistry, Romanian Academy, Iasi, Romania
**humelnicu.andra@icmpp.ro*

1. Introduction

Water is a finite and essential resource for our survival, yet global climate change and human activities have negatively impacted the quality of drinking water in recent decades [1]. The synthetic dye-based industries are one of the most concerning sectors when it comes to water pollution [2]. Approximately one million tons of various organic dyes are manufactured each year, and their discharge into the environment threatens all living forms [3]. Methylene blue (MB) is a well-known heterocyclic cationic dye that is widely utilized in the pharmaceutical, medical, textile, and plastic sectors [3]. However, when ingested, MB is exceedingly toxic and poses a significant risk to human health (damaging the neurological and visual systems) [4]. Furthermore, MB's non-biodegradability and accumulating capability make it extremely hazardous to the environment and aquatic life [5]. Hence, this work reports a sustainable, cost-effective, and non-toxic carboxymethyl cellulose (CMC)-based sorbent (in the form of beads) for MB dye removal. The produced adsorbent adds value by i) preparing ionotropic hydrogels by cross-linking with iron cations; ii) enhancing adsorption using sodium dodecyl sulfate (SDS) for foaming and freeze-drying; iii) enabling effortless magnetic recovery of the spent sorbent by introducing manganese ferrite ($MnFe_2O_4$) into the polymer matrix.

2. Results and discussion

As detailed in Table 1, magnetic beads were prepared by modification of CMC with SDS and by introduction of manganese ferrite (CMC-Mn-S1, CMC-Mn-S2, and CMC-Mn-S3, respectively). These were further characterized by comparison with non-magnetic (CMC) and/or magnetic unmodified beads (CMC-Mn). Thus, the morphological, structural, elemental, and magnetic properties of the adsorbents were assessed using scanning electron microscopy (SEM), energy-dispersive X-ray analysis, Fourier-transform infrared spectroscopy (FTIR), and a vibrating-sample magnetometer (VSM). More details regarding the characterization and application of the produced CMC-based adsorbents may be found in our recently published work [6].

Table 1. Chemical composition and characteristics of CMC-based beads.

Beads Code	Beads Composition [1]				Beads Size [2]
	CMC (g)	$MnFe_2O_4$ (% *w*/*w*)	SDS (% *w*/*w*)	NaCl (% *w*/*w*)	(mm)
CMC	3	–	–	–	2.60 ± 0.28
CMC-Mn	3	10	–	–	2.23 ± 0.36
CMC-Mn-S1	3	10	0.2	4	1.76 ± 0.25
CMC-Mn-S2	3	10	0.4	4	2.09 ± 0.24
CMC-Mn-S3	3	10	0.8	4	1.97 ± 0.27

[1] All the beads were prepared by using a stock solution of 3% CMC, and a crosslinking bath of 0.1 M $Fe(NO_3)_3$.
[2] Average value (from 25 measurements) ± standard deviation.

In order to determine the adsorption of MB cationic dye from aqueous solutions onto the carboxymethyl cellulose-based beads (CMC, CMC-Mn, and CMC-Mn-S1-3), a batch adsorption screening assay was carried out. The preliminary results regarding the adsorption capacities (*q*, mg/g) and dye removal efficiency (*Y*, %) are highlighted in Figure 1. As expected, the addition of SDS surfactant during the gelling process of CMC led to increased adsorption capacities as compared with CMC and CMC-Mn beads. This may be attributed to the electrostatic repulsions of the $-O-SO_3^-$ groups from the SDS surfactant molecules and polyanionic CMC chains during the gelation process, which favor the formation of a more porous structure. After SDS removal, the electrostatic interactions between the carboxylic groups of CMC (present on the beads' surface and within their pores) and MB molecules are expected to be improved. CMC-Mn-S2 magnetic beads displayed the best adsorption performance, with the highest values of adsorption capacity (18.22 ± 0.23 mg/g) and color removal efficiency (72.38 ± 0.92%). In addition to these, CMC-Mn-S2 beads have been successfully applied as adsorbents for advanced experiments (adsorption kinetics and isotherms) due to their higher adsorption performance and relevant magnetization values [6].

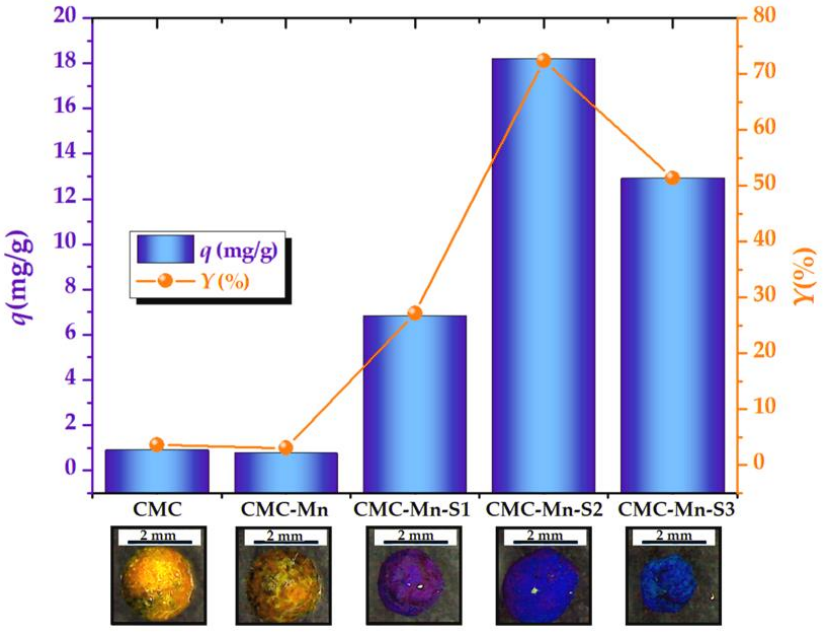

Figure 1. Batch adsorption assay (adsorption capacity—*q*, mg/g, and color removal efficiency—*Y*, %) for Methylene Blue (MB) removal from aqueous solutions at room temperature (sorbent dose of 2 g/L, contact time of 1 h, MB initial concentration of 50 mg/L); micrographs (by polarized light microscopy) of dried CMC-based beads after the adsorption process.

For an in-depth investigation of the adsorption rate of the adsorption process, the kinetic experimental data were analyzed using two kinetic models: Lagergren's pseudo-first-order model (PFO) and Ho's pseudo-second-order model (PSO). In addition, the adsorption process and the affinity of CMC-Mn-S2 beads toward MB molecules were investigated by using the Langmuir and Freundlich isotherm models. The Dubinin-Radushkevich (D-R) isotherm model was employed to determine the type of adsorption process by calculating the mean free energy of adsorption, E_S (kJ/mol). Likewise, the thermodynamic parameters such as Gibbs free energy (ΔG), enthalpy (ΔH), and entropy (ΔS) were assessed for the investigated adsorption process [6].

More than that, to demonstrate the suitability of CMC-Mn-S2 beads for cationic dye adsorption, other organic dyes were tested: crystal violet (CV) and brilliant green (BG), two additional cationic dyes frequently employed in pharmaceutical applications.

Desorption assays were performed in ethanol and acetone and the recovered adsorbent beads were subjected to further re-use tests. In addition, the molecular docking computations were performed to detail the intermolecular interactions between the cationic dye and the CMC-Mn-S2 adsorbent.

3. Conclusions

Sodium carboxymethyl cellulose (CMC) was used to produce stabilized ionotropic hydrogels in the form of beads by ionically cross-linking with iron cations. In order to facilitate the magnetic separation of sorbents from aqueous solutions, $MnFe_2O_4$ nanoparticles (synthesized by the sol-gel auto-combustion method) were introduced into the hydrogelated matrix. In addition, SDS surfactant was used as a porogen to increase the adsorption capacity and hydrodynamic stability of the CMC-based beads. Therefore, magnetic beads were prepared by modification of CMC with SDS surfactant (CMC-Mn-S1, CMC-Mn-S2, and CMC-Mn-S3, respectively), and characterized (morphologically, structurally, and magnetically) by comparison with non-magnetic (CMC) and magnetic unmodified beads (CMC-Mn). After evaluation of adsorption capacities, CMC-Mn-S2 was found to be the most promising material and was further subjected to in-depth examination. The adsorption kinetics was best described by the PFO model, and the maximum adsorption capacity was registered at lower temperatures (234 mg/g at 300 K). The isotherm data were best interpolated by the Langmuir isotherm model, suggesting a homogeneous monolayer adsorption mechanism. According to the thermodynamic parameters, it was found that the investigated adsorption processes occurred spontaneously ($\Delta G < 0$) and exothermically ($\Delta H = -34.57$ kJ/mol). After immersion in acetone, the spent sorbent was recovered (93% desorption efficiency) and successfully re-used for another adsorption test. In addition, molecular docking suggested that the interaction between MB dye and CMC was mainly based on electrostatic Coulomb forces ($\Delta E_{CL} = -33.25$ kcal/mol).

Due to the fact that CMC-based physical hydrogel formulations fulfill certain aspects, such as the use of natural, biocompatible, and non-toxic materials, reduced chemicals leakage, increased pollutant adsorption capacities, and ease of recovery, the investigated hydrogelated beads can be considered a promising sorbent for environmental applications.

Acknowledgements

This work was supported by a grant from the Ministry of Research, Innovation and Digitization, CNCS-UEFISCDI, project number PN-III-P1-1.1-TE-2021-0030, within PNCDI III.

References

[1]. Walker DB, Baumgartner DJ, Gerba CP, Fitzsimmons K. Surface Water Pollution. In: Brusseau ML, Pepper IL, Gerba CP, editors. Environmental and Pollution Science. London: Academic Press; pp. 261-292, 2019
[2]. El-Kousy SM, El-Shorbagy HG, Abd El-Ghaffar MA. Chitosan/montmorillonite composites for fast removal of methylene blue from aqueous solutions. *Mater. Chem. Phys*. 254, 123236, 2020
[3]. Sivakumar R, Lee NY. Adsorptive removal of organic pollutant methylene blue using polysaccharide-based composite hydrogels. *Chemosphere*. 286, 131890, 2022
[4]. Din MI, Khalid R, Najeeb J, Hussain Z. Fundamentals and photocatalysis of methylene blue dye using various nanocatalytic assemblies-A critical review. *J. Clean. Prod.* 298, 126567, 2021
[5]. Khan I, Saeed K, Zekker I, Zhang B, Hendi AH, Ahmad A, Ahmad S, Zada N, Ahmad H, Shah LA. Review on methylene blue: Its properties, uses, toxicity and photodegradation. *Water*. 14, 242, 2022
[6]. Enache AC, Grecu I, Samoila P, Cojocaru C, Harabagiu V. Magnetic ionotropic hydrogels based on carboxymethyl cellulose for aqueous pollution mitigation. *Gels*. 9, 358, 2023

COMPOSITE HYDROGELS BASED ON ALGINATES AND CALCIUM CARBONATE

Ana-Lavinia Vasiliu,* Elena-Daniela Lotos, Marius-Mihai Zaharia, Marcela Mihai
Petru Poni Institute of Macromolecular Chemistry, Romanian Academy, Iasi, Romania
**vasiliu.lavinia@icmpp.ro*

1. Introduction

Alginate is a biodegradable anionic polysaccharide with linear structure extracted from brown algae, consisting of (1–4)-α-L-guluronic acid blocks (GG) and (1–4)-β-D-mannuronic acid blocks (MM) [1]. Calcium alginate is the calcium salt of alginic acid, insoluble in water, while sodium alginate is the soluble form of alginic acid and is used in medical applications due to its properties of biocompatibility, biodegradability and non-cytotoxicity [2]. Zein, the amphiphilic protein extracted from corn, is capable of forming nanoparticles with different polysaccharides [3]. Calcium carbonate mineral has numerous biomedical applications, its' crystallization depending on a wide range of parameters [4]. As such, the present study investigates the *in situ* synthesis of composite hydrogels based on alginates and calcium carbonate.

2. Experimental

Two types of hydrogels were obtained. In the first case, commercial alginic acid calcium salt (ACa) and $CaCl_2$ were dispersed in 5 mL water and placed in a desiccator, having NH_4HCO_3 as a source of carbonate. The second type of hydrogels was obtained through a similar protocol, by dispersing ACa and $CaCl_2$ in 5 mL nonstoichiometric polyelectrolyte complexes (NPEC) solution. The NPECs were obtained by titration of alginic acid sodium salt (ANa) with a zein solution in 60% alcohol-water mixture (Z60), with a ratio between components of 1.2. The NPECs were characterized by dynamic and electrophoretic light scattering (DLS and ELS) and electron microscopy (SEM). In both experiments, after 5 days in the desiccator, the samples were freeze-dried and the resulting hydrogels were characterized by SEM and X-ray diffraction (XRD).

3. Results and discussion

The ANa was able to form nonstoichiometric complex nanoparticles with zein, by electrostatic interactions between the opposite charged components (the zeta potential, ZP, was 18.5 mV and -46.4 mV for Z60, and ANa, respectively, at pH =4). The SEM image in Figure 1 shows the size and shape of the Z60/ANa nanoparticles, while Table 1 summarizes the DLS and ELS information.

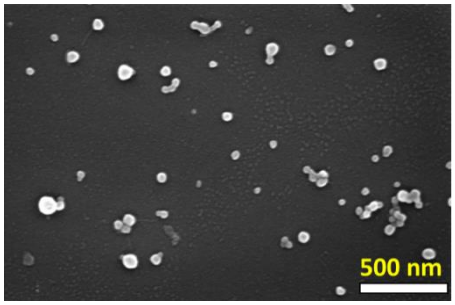

Figure 1. SEM image of Z60/ANa nanoparticles.

Table 1. DLS and ELS characterization.

Zeta Potential (mV)	Z60 (pH=4)	18.5
	ANa (pH=4)	-46.4
	Z60/ANa	-14.9
Size, Z-average (nm)	Z60	952
	Z60/ANa	102.4

The measurements showed that the obtained NPECs had about 100 nm, with a ZP of -14.9 mV, suggesting the orientation of alginate chains towards the exterior of the nanoparticles (the surface charge is negative although zein is in excess). As such, some carboxyl groups from the alginate could still be available on the surface of the NPECs, thus making possible further interactions.

The SEM image in Figure 1 shows that the NPECs have spherical shape and a lower diameter (average diameter ≈ 59 nm) than the one found by DLS investigations (Table 1). This phenomenon can be ascribed to the loss of water that occurred during the drying process on the silica wafers, since DLS measurements are conducted in solution, detecting the hydrodynamic radius, while SEM analysis is specific for dry state.

The *in situ* crystallization method allowed the formation of organized composite hydrogels based on commercial ACa dispersions, in the presence of $CaCl_2$ and CO_3^{2-} ions, regardless of the reaction medium (water or NPECs), the morphology of the hydrogels being presented in Figure 2.

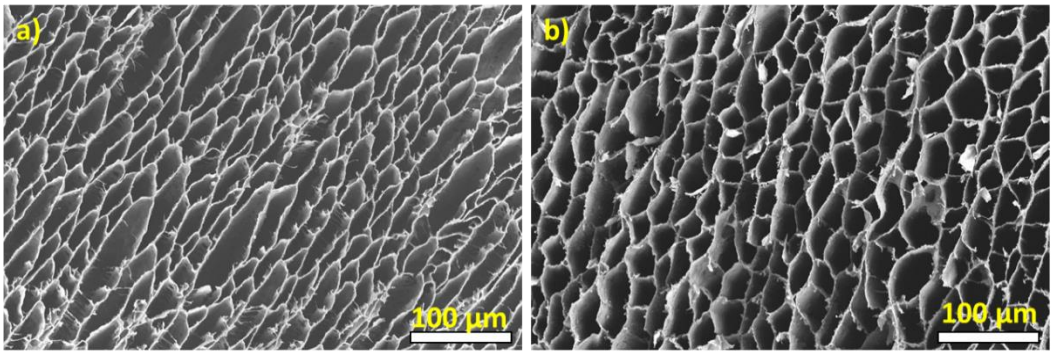

Figure 2. SEM images of the two types of hydrogels:
(a) ACa-$CaCO_3$; and (b) ACa-(Z60/ANa)-$CaCO_3$.

As can be seen in Figure 2, the ammonium diffusion method yielded homogeneous morphology, with well-defined pores in both types of hydrogels. In the case of ACa-$CaCO_3$ hydrogels, the average pore diameter (evaluated with ImageJ free software) was ~ 17 µm. By comparison, the presence of Z60/ANa nanoparticles in the reaction medium rendered larger pores, with an average pore diameter of ~ 24 µm. This behavior can be ascribed to the role of NPEC nanoparticles present in the ACa dispersion medium that acted as spacers in the crosslinking process. It is known that Ca^{2+} ions interact with the carboxylic groups of guluronic acids from different chains, creating "egg-box" structures [5]. As such, the availability of carboxylic groups on the surface of the NPECs may lead to an ionic crosslinking between the ACa dispersion and Z60/ANa nanoparticles.

The 5 days ammonium diffusion process was chosen based on our previous research [4], which indicated this specific time is ideal for the crystallization of $CaCO_3$ within the hydrogel matrix, without rendering excess of micronic crystals inside or on the surface of the material. However, the presence of calcium carbonate in the hydrogel matrix, as well as phase attribution, was highlighted by the XRD diffractograms presented in Figure 3.

The XRD diffractograms for both types of hydrogels are very similar, differing only in some of the peaks' intensity. The predominant polymorph in both cases is calcite, showing peaks at $2\theta = 23^o$, 29.5^o, 36^o, 39.3^o, 43.2^o, 48.5^o, 58.2^o. The presence of vaterite is clearly marked by the high intensity peak at $2\theta = 32.6^o$ and a lower intensity peak at 52.3^o.

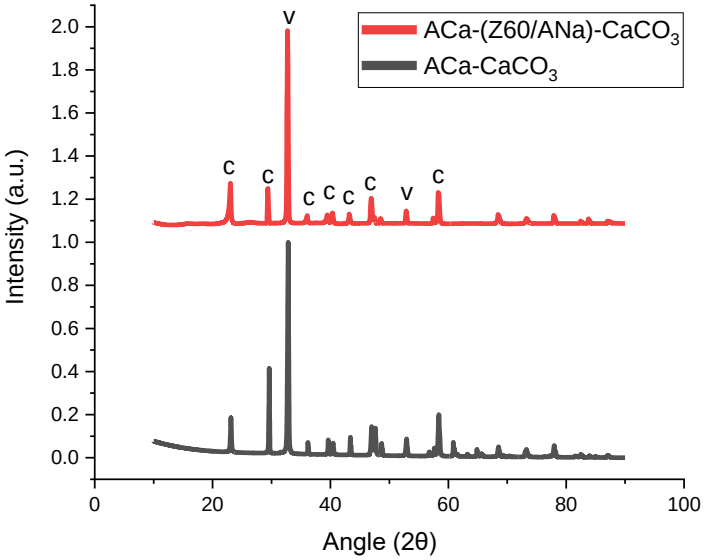

Figure 3. XRD diffractograms of both types of hydrogels.

Since vaterite is a less stable polymorph, it undergoes dissolution – recrystallization processes in time, at the end resulting calcite, the most stable polymorph of $CaCO_3$. Since the crystallization process in the present study took place over 5 days, most of the initial formed vaterite (if any) was transformed into calcite, through the Ostwald ripening mechanism.

4. Conclusions

The present study shows the synthesis and characterization of two composite hydrogels based on alginate and calcium carbonate, this being a proof of concept for creating low cost materials with highly organized three-dimensional structure. As a next step, the authors envision the incorporation of different drugs in the reaction medium, in order to obtain *in situ* multi-component composites.

Acknowledgements

This work was supported by the Ministry of Research, Innovation and Digitization, by project number PN-III-P4-ID-PCE-2020-1541, within PNCDI III - CCCDI-UEFISCDI, and by project number PNRR-III-C9-2022-I8-201, within the National Recovery and Resilience Plan.

References:

[1]. Wasupalli GK, Verma D. Polysaccharides as biomaterials. In: Thomas S, Balakrishnan P, Sreekala MS, editors. Fundamental Biomaterials: Polymers. Cambridge: Woodhead Publishing; pp. 37-70, 2018
[2]. Chaturvedi K, Ganguly K, More UA, Reddy KR, Dugge T, Naik B, Aminabhavi TM, Noolvi MN. Sodium alginate in drug delivery and biomedical areas. In: Hasnain MS, Nayak AK, editors. Natural polysaccharides in drug delivery and biomedical applications. London: Academic Press; pp. 59-100, 2019
[3]. Li M, Yu M. Development of a nanoparticle delivery system based on zein/polysaccharide complexes. *J. Food Sci.* 85(12), 4108-4117, 2020
[4]. Vasiliu AL, Dinu MV, Zaharia MM, Peptanariu D, Mihai M. In situ $CaCO_3$ mineralization controlled by carbonate source within chitosan-based cryogels. *Mater. Chem. Phys*. 272, 125025, 2021
[5]. Sellimi S, Younes I, Ayed HB, Maalej H, Montero V, Rinaudo M, Dahia M, Mechichi T, Hajji M, Nasri M. Structural, physicochemical and antioxidant properties of sodium alginate isolated from a Tunisian brown seaweed. *Int. J. Biol. Macromol*. 72, 1358-1367, 2015

INCREASING THE CHEMICAL FUNCTIONALITY OF BIOPOLYMERS USING BENZYL AMINES DERIVATIVES, THE CASE OF PULLULAN

Ioana-Sabina Trifan,* Sergiu Coseri
Petru Poni Institute of Macromolecular Chemistry, Romanian Academy, Iasi, Romania
**trifan.sabina@icmpp.ro*

1. Introduction

Due to its outstanding traits, including biocompatibility, biodegradability, and inherent antibacterial and antifungal activity, pullulan is one of the most researched polysaccharides in recent years. It is also one of the few polysaccharides with exceptional water solubility. Pullulan is also an attractive biopolymer due to its ability to be tuned into thin film layers and due to the multitude of hydroxyl groups in its structure that can be easily modified, especially by oxidation reactions with various selective types of oxidizing agents. The primary motivation for carrying out this kind of reaction is the possibility of obtaining novel derivatives with superior features that are not discussed in the scientific literature by using the oxidized derivatives of pullulan as intermediary molecules for subsequent reactions [1].

There are currently two primary protocols used to selectively oxidize polysaccharides, one of which uses sodium periodate and the other the stable radical TEMPO in the presence of sodium hypochlorite and sodium bromide. In the case of $NaIO_4$-oxidation, only the secondary hydroxyl groups are triggered and converted to aldehyde groups, while the bonds between the carbon atoms in the 2nd and 3rd positions are destroyed. Pullulan oxidation with the TEMPO radical/NaBr/NaClO system leads to the formation of an acid type-derivative as the primary alcohol groups are turned into carboxyl groups [1].

2. Experimental

Pullulan (M_w ~ 1.5 × 10^5 g/mol, TCI Europe), TEMPO radical ((2,2,6,6-tetramethyl-piperidin-1-yl)oxyl radical), sodium bromide (NaBr), sodium hypochlorite (NaClO), sodium periodate ($NaIO_4$), 4-aminoacetophenone, 4-aminobenzonitrile (4-ABN), *N*-hydroxysuccineimide (NHS), 1-ethyl-3-(3-dimethylaminopropyl)carboiimide (EDC), distilled water and dimethyl sulfoxide (DMSO) were received from Sigma-Aldrich Chemical Company and used as received, without further purification.

For each oxidation reaction performed, commercial pullulan was solubilized in distilled water under vigurous stirring. After a homogenous mixture was formed, the oxidation agent was added and the pH was adjusted (4 for $NaIO_4$ and 10 for TEMPO radical). In the case of $NaIO_4$-oxidation, the reaction was carried out in dark conditions. Both oxidation reactions were stopped after 6 hours and the mixtures were poured in acetone to induce precipitation which was also favored by the addition of a few amounts of NaCl. The precipitates were kept in the fridge for 24 hours before being purified by dialysis for a week and lyophilized. The reactions led to the formation of a dialdehyde derivative of pullulan (DAP) and carboxylated pullulan (6-CP) as a white products.

Each pullulan derivative was coupled with both amine compounds. The pullulan derivatives were dissolved in distilled water under intensive stirring, while the coupling compounds were separately dissolved in an appropiate solvent – distilled water heated at the temperature of 80 degrees (4-

AAph) or DMSO (4-ABN). A previous activation with EDC and NHS was necessary in the case of 6-CP as the carboxylated derivative is less reactive than the dialdehyde pullulan. Four novel derivatives of pullulan were obtained as white products after all mixtures were precipitated in acetone for a week and then lyophilized.

All the prepared samples, along with the commercial pullulan, were investigated by means of FTIR spectral analysis. NMR analyze is still a work in progress. The potassium bromide pellet method was used for the FTIR analyze, the transmittance spectra being recorded in the range of 4000-400 cm^{-1} by Shimadzu IRAffinity-1S spectrophotometer at the resolution of 4 cm^{-1} and after 32 scans.

3. Results and discussion

This work describes and investigates the synthesis and chemical structure characterizations of two oxidized pullulan derivatives obtained *via* oxidation with $NaIO_4$ and TEMPO radical [2], as well as their involvement in the synthesis of four novel derivatives by coupling processes with aromatic amines containing other groups which may play a key role in spreading their use in different scientific fields (Figure 1).

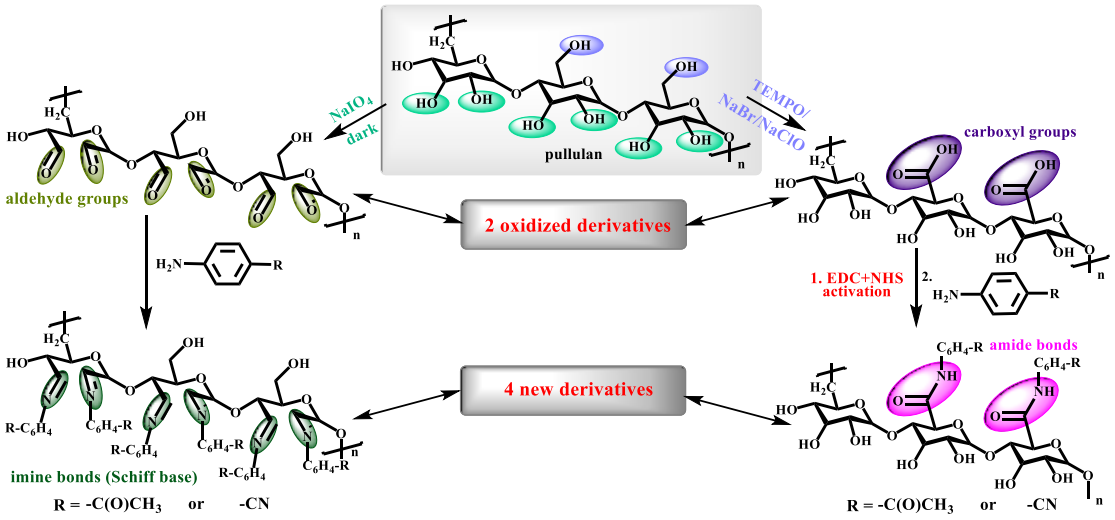

Figure 1. Scheme illustrating the obtaining of pullulan derivatives based on oxidation reactions with different selective agents and coupling reactions with amine compounds

Aromatic amines containing also other functional groups – 4-aminoacetophenone (4-AAPh) and 4-aminobenzonitrile (4-ABN) (Figure 2) – were chosen to be used in coupling reactions as it is well known that amines are able to react both with aldehydes and carboxyl acids and form Schiff bases (imine bonds) or amides (Figure 1). The ketone group attached to the benzene is a promising group to participate in photochemical reactions due to the fact that it is attached to a π-conjugated system and can homolytic cleavage and form reactive species as free radicals under light irradiation and the addition of a photoinitiator.

Therefore, the photopolymerization reaction may lead to the formation of photocrosslinked networks with possible applications in different fields. Regarding the second amine compound, the nitrile group can be used as a ligand to develop pullulan derivatives based-coordinative organogels by reacting with solutions of metals capable of coordinating. [3]

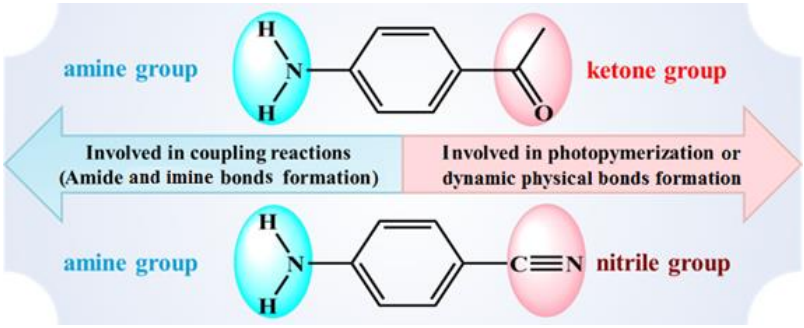

Figure 2. The chosen compounds to be grafted on the pullulan backbone emphasizing the newly introduced functional groups

The FTIR spectrum of pullulan highlights absorption bands for O-H stretching vibration at 3447 cm^{-1} which corresponds to the hydroxyl groups and at 2925 cm^{-1} which is characteristic of C-H stretching from the ethylene attached to the primary hydroxyl groups. [4] As expected, in the spectrum of DAP, it was hard to identify bands for the aldehyde groups, nor for the hypothetical hemiacetal groups due to their low absorption capacity. Regarding the spectrum of 6-CP, the main proofs that the reaction was successfully performed are the bands at 1712 cm^{-1}, 1607 cm^{-1} and 1417 cm^{-1} that correspond to the vibration of bonds in carboxyl groups, as well as the reduced band at 2925 cm^{-1} indicating the groups' conversion.

The spectra of synthesized coupled derivatives present bands at 2249 cm^{-1} characteristic of nitrile groups (for DAP_{CN} and 6-CP_{CN} samples) and a diminution of the bands appearing at 2925 cm^{-1} and 1740 cm^{-1} for the pullulan derivatives coupled with 4-AAPH (DAP_{OCH3} and 6-CP_{OCH3}).

4. Conclusions

Further on, the aim of the research is to evaluate other properties of these novel pullulan derivatives such as the wettability, mechanical properties, and thermal stability, as well as finding suitable applications based on their properties and the pending sequences. Considering the advantages that pullulan and its derivatives give in macromolecular chemistry research, it is obviously necessary to allocate importance to deeply understanding the properties and the applications that these compounds can be used in.

Acknowledgements

This work was supported by a grant of Executive Agency for Higher Education, Research and Innovation Funding, UEFISCDI, project code PN-III-P4-PCE-2021-0933, acronym "PHYCOMAT", within PNCDI III.

References

[1]. Biliuta G., Coseri S. Cellulose: A ubiquitous platform for ecofriendly metal nanoparticles preparation. *Coord Chem Rev.*, 383, 155-173, 2019
[2]. Baron RI, Duceac IA, Morariu S, Bostanaru-Iliescu AC, Coseri S. Hemostatic cryogels based on oxidized pullulan/dopamine with potential use as wound dressings. *Gels*, 8, 726, 2022
[3]. Orelma H, Vuoriluoto M., Johansson LS, Campbell JM, Filpponen I, Biesalski, M., Rojas OJ. Preparation of photoreactive nanocellulosic materials via benzophenone grafting. *RSC Adv.*, 6, 85100, 2016
[4]. Spatareanu A, Bercea M, Budtova T, Harabagiu V, Sacarescu L, Coseri S. Synthesis, characterization and solution behaviour of oxidized pullulan. *Carbohydr Polym.*, 111, 63-71, 2014

A COMBINED APPROACH FOR THE DEPOSITION HIGH QUALITY AND POROUS ZnO FILMS WITH APPLICATION IN PHOTOCATALYSIS

Cristian Ursu,[1]* Bogdan-George Rusu,[1] Andrei Dascalu,[1]
Mihaela Olaru,[1] Victor Oancea,[1] Petru Nica[2]
[1]*Physics of Polymers and Polymeric Materials Laboratory,*
Petru Poni Institute of Macromolecular Chemistry, Romanian Academy, Iasi, Romania
[2]*Department of Physics, Gheorghe Asachi Technical University, Iasi, Romania*
**cristian.ursu@icmpp.ro*

1. Introduction

Due to rapid population expansion and the acceleration of industrialization, environmental conservation and remediation are humanity's greatest concerns in the 21st century. The dumping annually hundreds millions of tons of industrial waste (such as heavy metals, extremely hazardous organic compounds like phenols, pesticides, fertilizers, and detergents, and synthetic dyes) into fresh water supplies has major consequences for human health and the environment. Heterogeneous photocatalysis is one of the most intriguing and possibly efficient solutions to the water crisis [1]. While much of the research aims to discover new photocatalytically active semiconductor-based materials, a more recent tendency is to focus on understanding the photocatalysis mechanism in order to increase its efficiency [2]. Despite the tremendous research conducted in the field, developed nano-photocatalysts do not yet have photo-conversion efficiencies suitable for practical applications [3]. Besides the well-known issues related to the large optical band gaps and rapid recombination of photogenerated charge carriers, a low photo-conversion efficiency is also due to the limited interfacial properties between catalyst and reagents.

Supported catalysis is a recent trend rewarded with the title of "green chemistry" [4]. Hierarchical macro-/mesoporous semiconductor films with well-defined pore size and architectures were designed through a variety of methods: hydrothermal, spray pyrolysis, self-assembly surfactant template, free-template methods [5], etc. However, the catalyst films are still showing a lower photocatalytic performance than those obtained in powder form because of their low surface area. Moreover, applying these techniques is rather complex, requires post-synthesis tricky procedures for template removal, and/or implies the use of chemicals potentially harmful for environment.

The current study addresses the issue of the development of catalyst films with a large surface area to improve both the contact between catalyst and reagents and the photoactivating efficiency. A cost-effective material with high technological potential, such as ZnO, and a combined approach of pulsed laser deposition (PLD) and laser annealing (LA) were used to fabricate ZnO porous films with appropriate intrinsic properties (related to structure and optics) and interface with reagents. By varying different experimental parameters, such as oxygen total deposition pressure, or combining the effects of oxygen deposition pressure and substrate temperature, highly porous ZnO thin films were obtained. LA, a powerful tool commonly applied to selectively heat a deposited film to achieve high temperatures for recrystallization, was used in situ in conjunction with PLD to efficiently nanostructure the growing film. The obtained porous films may serve as a basis for designing more complex photocatalysts with a high surface specific area, such as p-n heterojunctions.

2. Experimental

By varying different experimental parameters, such as the oxygen deposition pressure and substrate temperature, or by combining the effects of deposition pressure and temperature, ZnO porous films were produced by PLD. KrF excimer laser ablation (248 nm wavelength, 20 ns pulse length; Coherent) of a Zn metallic target (99.99% purity; Kurt Lesker) was performed (for 10,000 pulses) in an oxygen gas environment at 12 Pa and 120 Pa (Table 1). The glass substrate placed on axis at 5 cm from the target was heated resistively (up to 500 ^{o}C) or by laser annealing (LA). The LA was performed in situ using a XeCl excimer laser (308 nm wavelength, 20 ns pulse length; Coherent) for a laser fluence of 50 mJ/cm^2. To assess the influence of the experimental growing conditions on the film properties (morphology, structural quality, and optical transmittance), typical investigation methods, such as SEM, XRD, and UV-Vis, were applied.

Table 1. Experimental conditions used for ZnO film deposition and determined parameters.

Sample	Pressure (Pa)	Temperature (°C)	c (Å)	Crystallite size (nm)	Thickness (nm)
1#	12	RT	5.2305	25.4	350
2#	120	RT	-	-	2800
3#	120	500	5.1908	27.6	237
4#*	120	RT	5.2120	19.9	85

* UV laser annealing at 50 mJ/cm^2 applied during the ZnO film growth.

3. Results and discussion

ZnO films with a high surface specific area were deposited in a wide range of growing conditions. In Figure 1, the SEM-recorded morphologies are presented along with their determined cross-sections for the obtained ZnO films. The effect of deposition pressure increases is obvious when comparing the SEM images recorded for samples deposited at oxygen pressures of 12 Pa and 120 Pa, respectively. At low deposition pressure, the film appearance is compact, with a columnar growing structure that results in a film thickness of 350 nm (Table 1). With increasing deposition pressure to 120 Pa, a confinement effect of the working gas affects the deposited film quality. Due to the kinetic energy losses of the plasma particles, a low-adherent film with a fluffy granular morphology was grown. Hence, the laser ablation of the Zn metallic target at high deposition pressure yields the growth of a low-density film with a thickness of about 2800 nm.

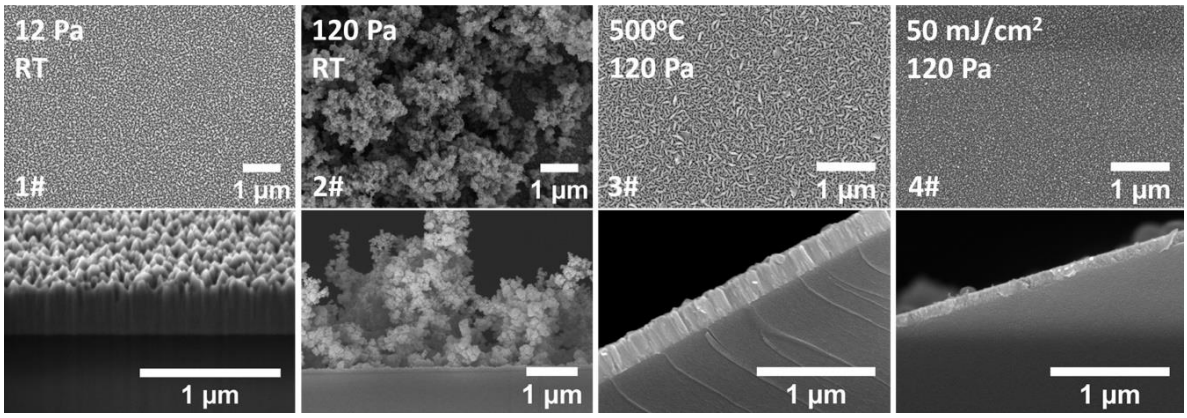

Figure 1. SEM topography and cross-sections of the PLD ZnO films: the effects of deposition pressure (12 Pa and 120 Pa), substrate temperature (RT and 500 ^{o}C), and UV laser annealing (for a laser fluence of 50 mJ/cm^2) applied during the film growth.

The deposition pressure increase also affects the optical properties and crystalline quality of the deposited film. The optical transmittance dramatically drops due to a more pronounced scattering of light when going toward the UV region, while the film becomes completely amorphous (Figure 2). When the substrate temperature was increased to 500 ^{o}C, both optical and structural properties improved, while the SEM results indicated the formation of a ZnP film with a high surface specific area. The particles that led to film growth enhanced their mobility on the substrate, so that a highly (002)-oriented wurtzite phase and an optically transparent ZnO film formed. To assess the influence of the UV laser annealing on the film properties, the XeCl laser irradiation was applied in situ under identical experimental conditions to sample 2#. Thus, the laser annealing applied for a laser fluence of 50 mJ/cm^2 during RT deposition of ZnO film has considerably improved the crystalline quality and optical transmittance (Figure 2). Moreover, the film thickness has dramatically decreased to 85 nm, probably due to the ablation effect of the laser used for annealing.

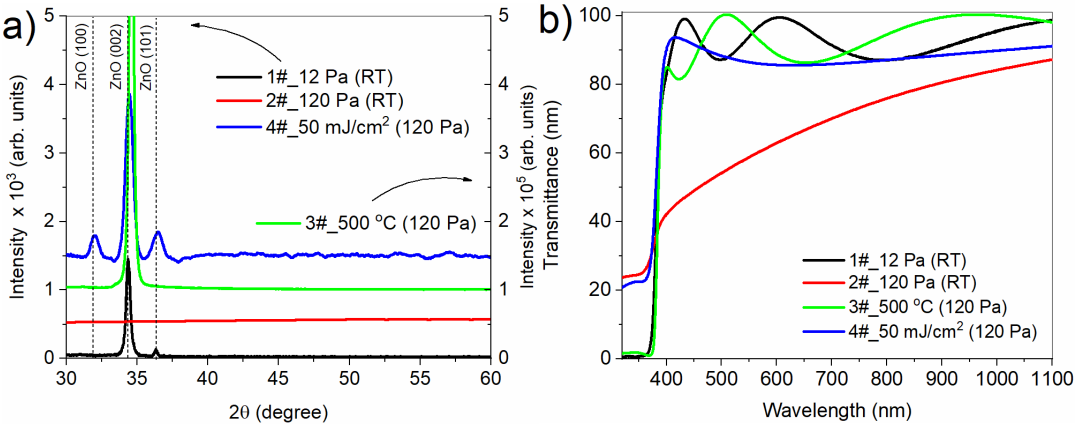

Figure 2. Effects of deposition pressure, substrate temperature, and UV laser annealing applied during the ZnO film growth on: a) crystalline quality and b) optical properties.

4. Conclusions

ZnO films with porous morphologies were successfully obtained by PLD for different experimental conditions. It was found that both O_2 deposition pressure and substrate temperature affect the film morphology and quality, while in situ UV laser annealing has a lesser effect on the investigated parameters. The presented results prove that the obtained ZnO films exhibit an increase in surface specific area, which could play a key role in improving the heterogeneous decomposition of organic pollutants. The obtained porous films might potentially be used as basis for the design of efficient photocatalysts with a large specific surface area, such as p-n heterojunctions.

References

[1]. Liu C, Kong D, Hsu PC, Yuan H, Lee HW, Liu Y, Wang H, Wang S, Yan K, Lin D, Maraccini PA, Parker KM, Boehm AB, Cui Y. Rapid water disinfection using vertically aligned MoS_2 nanofilms and visible light. *Nat Nanotechnol*. 11, 1098-1104, 2016

[2]. Pirhashemi M, Habibi-Yangjeh A, Rahim Pouran S. Review on the criteria anticipated for the fabrication of highly efficient ZnO-based visible-light-driven photocatalysts. *J Ind Eng Chem*. 62, 1-25, 2018

[3]. Shen CC, Zhu Q, Zhao ZW, Wen T, Wang X, Xu AW. Plasmon enhanced visible light photocatalytic activity of ternary $Ag_2Mo_2O_7$ @AgBr-Ag rod-like heterostructures. *J Mater Chem A*. 3, 14661, 2015

[4]. Nunes D, Pimentel A, Branquinho R, Fortunato E, Martins R. Metal Oxide-Based Photocatalytic Paper: A Green Alternative for Environmental Remediation. *Catalysts*. 11, 504, 2021

[5]. Yu JG, Su YR, Cheng B. Template-Free Fabrication and Enhanced Photocatalytic Activity of Hierarchical Macro-/Mesoporous Titania. *Adv Funct Mater*. 17, 1984-1990, 2007

CHITOSAN CROSSLINKING WITH A VANILLIN ISOMER TOWARD SELF-HEALING HYDROGELS WITH ANTIFUNGAL ACTIVITY

Manuela-Maria Iftime,* Irina Rosca, Andreea-Isabela Sandu, Luminita Marin
Petru Poni Institute of Macromolecular Chemistry, Romanian Academy, Iasi, Romania
**ciobanum@icmpp.ro*

1. Introduction

Due to increasing pathogen resistance to antibiotics, causing severe infections and wound challenges, there's a global need for advanced wound dressings. These dressings should be cost-effective, easy to make, sterile, non-toxic, and biodegradable, with excellent fluid absorption and antimicrobial properties. Various dressing materials have been developed from synthetic or natural polymers like membranes, films, fibers, patches, sponges, and hydrogels. However, limitations persist such as high costs, weak strength, difficult removal, and inadequate moisture for healing [1]. Chitosan-based hydrogels possess these attributes, ideal for wound care. Unlike traditional dressings, they're easy to remove, degrade naturally, and maintain moisture, aiding healing. However, they can dry and have weak mechanical stability when swollen [2]. In order to improve its properties, chitosan can be crosslinked with natural monoaldehydes, improving stability and swelling [3-4].

This study presents the synthesis and characterization of new chitosan hydrogels with antimicrobial properties *via* crosslinking using 5-methoxysalicylaldehyde, an isomer of vanillin [5]. The objective was to obtain biocompatible hydrogels for wound healing and bacterial prevention, with pH-sensitivity, self-healing, and antimicrobial traits properties.

2. Experimental

Materials: Low molecular weight chitosan (198 kDa and DA = 82%), 5-methoxysalicylaldehyde (98%), ethanol (99.8%), glacial acetic acid (99%) and lysozyme (40 000 units/mg protein) were purchased from Aldrich Co. (USA) and used as received. Acetate buffer solution (pH = 5.5), phosphate buffer (PBS) (pH = 7.4 and 8.5), bidistilled and ultrapure water were obtained in our laboratory.

Synthesis: A series of six hydrogels with different crosslinking degrees were prepared by acid condensation reaction of chitosan with 5-methoxysalicylaldehyde, adjusting a procedure described for other chitosan/aldehyde systems [3,5].

Equipment and methods: The hydrogels have been characterized by structural and supramolecular points of view by ^{1}H NMR spectroscopy (Bruker Advance DRX 400 MHz Spectrometer), Fourier transformed infrared spectroscopy (ATR-FTIR Bruker Vertex 70 Ettlingen Spectrometer), Wide angle X-ray diffraction (Rigaku Miniflex 600 diffractometer), Polarized light microscopy (Zeiss Axio Imager.A2m, camera Axiocam 208 cc, Carl Zeiss AG) and Scanning Electron Microscope (Scanning Electron Microscope SEM EDAX – Quanta 200, 20KeV). Their thermal stability was investigated by thermogravimetric analysis (TGA) (Discovery TGA 5500). Swelling studies, hydrolytic stability, *in vitro* enzymatic biodegradation and release profile of aldehyde were investigated in similar conditions mimicking the *in vivo* environment (PBS, pH = 7.4 at 37^{o}C). The *in vitro* release kinetics of aldehyde was evaluated using UV-visible spectroscopy, by recording the

characteristic absorption band at 258.87 nm, and fitting its absorbance on a predetermined calibration curve. The cytotoxicity of hydrogels was assessed by MTS assay using the CellTiter 96® AQueous One Solution Cell Proliferation Assay (Promega, Madison, WI USA). Also, the *antimicrobial activity* of the hydrogels was determined by disk diffusion assay against three bacterial strains, two yeast strains and three fungal strains.

3. Results and discussion

A series of six hydrogels was synthesized by varying the molar ratio between chitosan's amine units and 5-methoxysalicylaldehyde (Figure 1). To confirm that hydrogel formation was due to the occurrence of imine units and their self-organization into crosslinking clusters within chitosan chains, the hydrogels were extensive investigated from structural and supramolecular point of view, using FTIR, ^{1}H NMR, SEM, POM, and TGA techniques. In view of the evaluation of their potential for the targeted application, the hydrogels were tested to establish their ability to adsorb liquids and biodegrade in media mimicking the physiologic environment, their antimicrobial efficacy, and *in vitro* biocompatibility.

Figure 1. Synthesis of chitosan-based hydrogel.

The ^{1}H NMR spectra of the hydrogels revealed the formation of imine linkages, evidenced by the single band at 8.39 ppm corresponding to the imine proton [3,4]. They also indicated a notably high imination yield compared to other hydrogel systems, with the aldehyde proton completely disappearing after 7 days.

The FTIR spectra of the xerogels displayed modifications compared to the precursor materials (chitosan and 5-methoxysalicylaldehyde), confirming the formation of imine linkages by appearance of the characteristic absorption band around 1639 cm^{-1} [3,5].

Thermal curves of the xerogels revealed an important increase of the thermal stability compared with their precursors, in accordance with the formation of a dense network obtained by imination and formation of the ordered clusters (T_{10} corresponding to 10% weight loss progressively increased from 110°C for chitosan to 273°C for the hydrogel with the highest imination degree).

Furthermore, the 3D supramolecular arrangement of imine units into clusters was revealed using Wide Angle X-ray Diffraction and Optical Polarized Microscopy, which displayed the characteristic reflection at lower angle corresponding to the inter-layer d-spacing, and strong birefringence with banded textures, respectively. In parallel, SEM imaging showed a porous morphology, in close correlation with the crosslinking density, i.e. the pore diameter increased as the crosslinking degree decreased (Figure 2a).

All hydrogels showed self-healing ability, rapidly reshaping the hydrogel after cutting. Moreover, they easily passed through a needle without damaging the hydrogel state, indicating thixotropic behavior and injectability (Figure 2b).

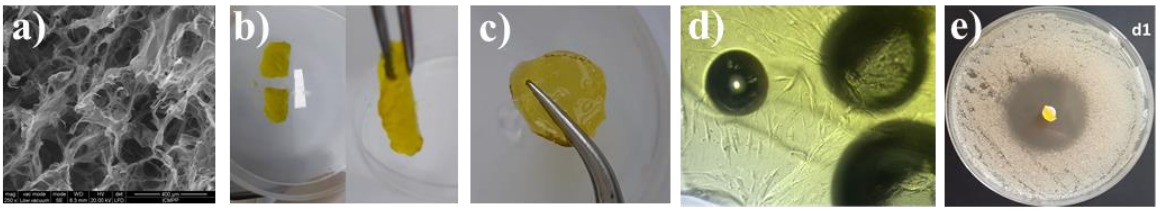

Figure 2. Representative images reveling some properties of the obtained chitosan hydrogels.

The hydrogels showed great capacity to adsorb liquids, reaching a swelling degree up to 26% in media of alkaline pH, characteristic to the wounds' exudate, and 54% in media of pH characteristic to normal dermis (pH = 5.5) (Figure 2c). In media containing lysozyme, an enzyme characteristic to the body fluids, and wound exudate, the hydrogels exhibited gradual weight loss reaching 35% after 21 days.

Among the studied hydrogels, those with an optimal crosslinking degree corresponding to a medium ratio of chitosan glucosamine and aldehyde of 1.5/1, 2/1 and 3/1 demonstrated non-cytotoxic effects on Normal Human Dermal Fibroblasts in the MTS test (Figure 2d), while having strong antifungal activity against *Candida Albicans* confirmed by disk diffusion assays (Figure 2e).

4. Conclusions

New hydrogels of natural origin, showing strong biocompatibility and effective antifungal properties, were prepared by a simple and easy method from chitosan and a vanillin isomer. The hydrogels exhibited porous morphology, facilitating significant swelling in various biological fluids (such as physiological and infected tissue pH), suggesting effective oxygen permeation and exudate drainage. Moreover, they were biodegradable and demonstrated self-healing properties, making them easily adaptable for application on skin lesions.

Acknowledgements

The research leading to these results has received funding from the Romanian National Authority for Scientific Research, MEN-UEFISCDI grant, project number RO-NO-2019-0540, (no. 14/2020).

References

[1]. Zhao X, Wu H, Guo B, Dong R, Qiu Y, Ma PX. Antibacterial anti-oxidant electroactive injectable hydrogel as self-healing wound dressing with hemostasis and adhesiveness for cutaneous wound healing. *Biomaterials*. 122, 34-37, 2017

[2]. Liang Y, He J, Guo B. Functional hydrogels as wound dressing to enhance wound healing, *ACS Nano*. 15, 12687-12722, 2021

[3]. Iftime MM, Morariu S, Marin L. Salicyl-imine-chitosan hydrogels: supramolecular architecturing as a crosslinking method toward multifunctional hydrogels. *Carbohydr Polym*. 165, 39-50, 2017

[4]. Marin L, Ailincai D, Morariu S, Tartau-Mititelu L. Development of biocompatible glycodynameric hydrogels joining two natural motifs by dynamic constitutional chemistry. *Carbohydr. Polym*. 170, 60-71, 2017

[5]. Iftime MM, Rosca I, Sandu AI, Marin L. Chitosan crosslinking with a vanillin isomer toward self-healing hydrogels with antifungal activity. *Int J Biol Macromol.* 205, 574-586, 2022

COMBINING ELECTROACTIVE AROMATIC MOIETIES AND VARIOUS CONTROLLED POLYMERIZATION METHODS TO ENDOW LINEAR AND FLEXIBLE POLYMERS WITH ADVANCED FUNCTIONS BY END-GROUP FUNCTIONALIZATION STRATEGY

Anca-Dana Bendrea,[1]* Demet Göen Colak,[2] Luminita Cianga,[1] Ioan Cianga[1]
[1]*Centre of Advanced Research in Bionanoconjugates and Biopolymers,*
Petru Poni Institute of Macromolecular Chemistry, Romanian Academy, Iasi, Romania
[2]*Istanbul Technical University, Faculty of Science and Letters,*
Department of Chemistry, Istanbul, Turkey
**anca.bendrea@icmpp.ro*

1. Introduction

The today modern society demands for innovative materials with elaborate properties for the contemporary advanced applications implying subtle responses. Polymeric materials, the appearance of which definitely shaped the technological evolution and marked the 20th century as the "polymer century" [1], can be the alternative of choice. The emergence of intrinsically conducting, conjugated polymers (CPs) in the field of polymer chemistry is a notable example in this sense [2]. Developing new functions in already existing conventional, flexible polymers by end-group functionalization using controlled polymerization methods [3] is one of the most plausible methodology for new advanced polymeric materials. Depending on the attached end groups, the new obtained materials not only are endowed with properties they never had [4] but, if they are polymerizable, the obtained macromonomers work as precursors of polymers with complex architecture and functions [5]. The development of CPs field was significantly impacted by the innovative idea of electroactive macromonomers, synthesized by placing an aromatic electrochemically polymerizable moiety as a final functional group to different types of flexible chains. They allowed the obtainment of grafted CPs of *rod-g-coil* type having high flexibility in properties tuning [6-9].

The aim of this report is to show, based on the experimental results, that due to the particular structure and of the multiple functionalities embedded by design, these electroactive macromonomers are interesting functional materials in their-self.

2. Results and discussion

The three electroactive macromonomers considered in this comparative study were synthesized by the so called "initiator methods" in only one step. In all cases commercially available functional low molecular weight compounds were used for reaction initiation. As the CPs resulted from the polymerization of the three compounds were intended to be used as biomedical materials, ε-caprolactone, lactide and 2-methyl-2oxazoline were chosen as the starting monomers. Thus, EDOT-functionalized oligo-ε-caprolactone (**EDOT-PCL**), and thiophene-ended oligo-(D,L-lactide) (**Th-PDLLA**) were obtained by in bulk controlled ring-opening polymerization (ROP) [7, 9], while thiophene end-functionalized oligo(2-methyl-2 oxazoline) (**Th-OMeOx**) was synthesized in solution, by controlled cationic ROP (CROP) [8]. As can be seen in Figure 1, the structure of presented compounds were engineered by the same design criteria, containing an aromatic, strong planar-interactive and polymerizable moiety at the α-chain end of a flexible oligomeric chain that

were obtained of well-defined length and with low polydispersity. At the opposite end all macromonomers expose a hydroxyl group that not only can be used for the subsequent modification but can be involved in intermolecular hydrogen bonds. While **Th-OMeOx** can be considered a typical-like amphiphile, due to hydrophilicity of oligo(2-methyl-2-oxazoline), **EDOT-PCL** and **Th-PDLLA** were designed exclusively from hydrophobic domains and denoted as "hydrophobic amphihile" [7,9].

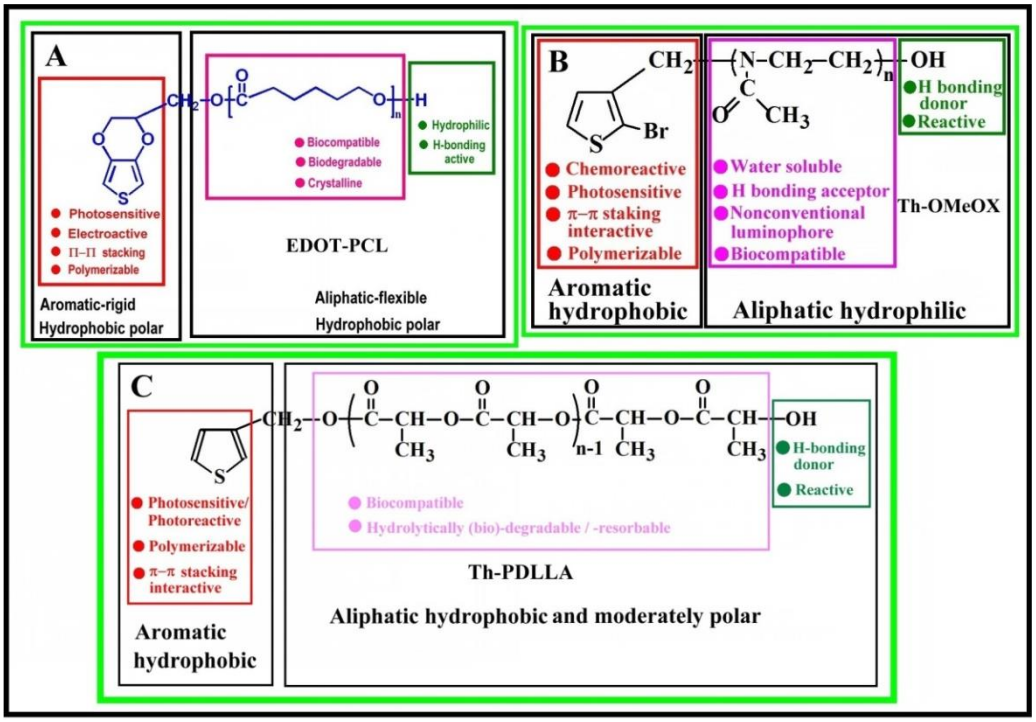

Figure 1. Structural formula and details on the design criteria of reported electroactive macromonomers as end-functionalized flexible oligomers: (A) EDOT-functionalized oligo-e-caprolactone (**EDOT-PCL**); (B) Th-end functionalized oligo(2-methyl-2-oxazoline) (**Th-OMeOx**); (C) Th-end functionalized oligo-(D,L-lactide) (**Th-PDLLA**).

However, all three compounds are characterized by anisotropy in shape and mismatch in rigidity between the constitutive parts, in a similar manner as the "shape amphiphile" [7]. These structures, even if not follow the block-copolymers rules, they self-assembly due to the subtle effects of the bulky terminal groups. The three macromonomers' self-assembling in solvents of different selectivity and polarity and also in thin films obtained from their dispersions were demonstrated by applying the specific investigation methods (DLS, NMR, UV-vis, fluorescence and AFM) [7-9], while in bulk microphase separation was evidenced by DSC measurements [6-9]. The behavior in thin film differentiated **EDOT-PCL** from the other two macromonomers. According to AFM results, an unexpected transformation of micelle-type nanostructures into hexagonally-shaped 2D lamellar single crystals, through breakout crystallization, took place by simple acetonitrile evaporation during the formation of the film on the mica support at room temperature [7].

Thus, due to the semicrystalline character of oligo-e-caprolactone, the self-assembling of **EDOT-PCL** is driving by both the microphase separation and crystallization. On the other hand, **Th-OMeOx** showed concentration-dependent fluorescence intensity in water and also wavelength excitation-dependent wavelength emission in both water and organic solvents. Tacking in account that thiophene is not fluorescent, this particular behavior of **Th-OMeOx** was associated with the clusteroluminescence phenomenon as a result of aggregation and through space interactions of

electron-rich groups in nonconjugated, non-aromatic oligo(2-methyl-2-oxazoline) [8]. Such a non-canonical photoluminescence was revealed also for Th-PDLLA for which the self-assembling and block-like character was also proved [9].

3. Conclusions

The three presented compounds, due to their multi-level amphiphilc character encoded in their structures, behave as "block-molecules". As a result, the applied investigations demonstrated that they naturally self-assembly in solution and in thin films. The self-assembling phenomenon is responsible for the appearance of the unexpected properties such as the clusteroluminescence in various solvents of **Th-OMeOX** and **Th-PDLLA** or the 2D lamellar single crystals, in thin film on mica, from ACN dispersion of **EDOT-PCL**.

The main conclusion of the present study is that, beside of being building blocks for the construction of CPs with complex architecture, the presented compounds behave as valuable functional materials in their-self. This confirms once again the strength and versatility of end-functionalization as an alternative way to synthesize materials with complex behavior and with added-value potential based on the existing conventional polymers.

Acknowledgements

This work was supported by the research infrastructure developed through the European Social Fund for Regional Development, Competitiveness Operational Programme 2014–2020, Axis 1, Action: 1.1.3, Project "Infra SupraChem Lab-Center for Advanced Research in Supramolecular Chemistry" (Contract 339/390015/25.02.2021, cod MySMIS: 108983).

References

[1]. Percec V, Xiao Q. From organic chemistry to chemical biology *via* macromolecules with Herman Staudinger. *Giant*, 4, 100036, 2020
[2]. Chakraborty B, Luscombe CK. Cross-Dehydrogenative Coupling Polymerization via C-H activation for the synthesis of conjugated polymers. *Angew. Chem. Int. Ed.*, 62, e202301247, 2023
[3]. Zhou D, Zhu LW, Wu BH, Xu ZK, Wan LS. End-functionalized polymers by controlled/living radical polymerizations: Synthesis and applications. *Polym. Chem*., 13, 300–358, 2022
[4]. Kim J, Jung HY, Park MJ. End-group chemistry and junction chemistry in polymer science: Past, present, and future. *Macromolecules*, 53, 746–763, 2020
[5]. Polymeropoulos G, Zapsas G, Ntetsikas K, Bilalis P, Gnanou Y, Hadjichristidis N. 50th Anniversary perspective: Polymers with complex architectures. *Macromolecules*, 50, 1253-1290, 2017
[6]. Molina BG, Bendrea AD, Lanzalaco S, Franco L, Cianga L, del Valle LJ, Puiggali J, Turon P, Armelin E, Cianga I, Aleman C. Smart design for a flexible, functionalized an electroresponsive hybrid platform based on poly(3,4-ethylenedioxythiophene) derivatives to improve cell viability. *J. Mater. Chem. B*, 8, 8864-8877, 2020
[7]. Bendrea AD, Cianga L, Ailiesei GL, Ursu EL, Colak DG, Cianga I. 3,4-Ethylenedioxythiophene (EDOT) end-group functionalized poly-e-caprolactone (PCL): Self-assembly in organic solvents and its coincidentally observed peculiar behavior in thin film and protonated media. *Polymers*, 13, 2720, 2021
[8]. Bendrea AD, Cianga L, Ailiesei GL, Colak DG, Popescu I, Cianga I. Thiophene α-chain-end-functionalized oligo(2-methyl-2-oxazoline) as precursor amphiphilic macromonomer for grafted conjugated oligomers/polymers and as a multifunctional material with relevant properties for biomedical applications. *Int. J. Mol. Sci*., 23, 7495, 2022
[9]. Bendrea AD, Cianga L, Colak DG, Constantinescu C, Cianga I. Thiophene end-functionalized oligo-(D,L-latide) as a new electroactive macromonomer for the „hairy-rod" type conjugated polymer synthesis, *Polymers*, 15, 1094, 2023

NONSTOICHIOMETRIC POLYELECTROLYTE COMPLEX NANOPARTICLES BASED ON ZEIN AND POLYSACCHARIDES

Elena-Daniela Lotos,* Ana-Lavinia Vasiliu, Marcela Mihai, Bogdan C. Simionescu
Petru Poni Institute of Macromolecular Chemistry, Romanian Academy, Iasi, Romania
**daniela.lotos@icmpp.ro*

1. Introduction

Due to their variety in the source of origin, low immunogenicity and low toxicity, biomaterials of natural origin have been extensively investigated for medical uses [1]. Zein (Z) is a natural macromolecule from corn, insoluble in water due to the high content of hydrophobic amino acids [2]. The instability of zein nanoparticles in aqueous solution and the poor solubility of zein are two drawbacks to the synthesis of zein nanoparticles. Stabilizers, such as polysaccharides (PZ), are typically incorporated into Z nanoparticles as a general strategy to increase their stability [3].

Polyelectrolyte complexes (PECs) are formed by interpolymer ionic condensation that occurs when oppositely charged polyelectrolyte solutions are mixed in water without the use of organic solvents, chemical cross-linkers, or surfactants. Controlling the assembly conditions of PECs can result in nanoparticles, macro-hydrogels or films [4].

This study follows the synthesis and characterization of nonstoichiometric polyelectrolyte complex (NPEC) nanoparticles based on zein and polysaccharides and their further interactions with drugs, for subsequent applications as antibacterial nanostructures.

2. Experimental

In order to obtain NPEC nanoparticles we used two polysaccharides as polyanions (sodium alginate (ALG) and chondroitin sulfate A (CSA)) and Z as the polycation. The samples were prepared at pH = 4 at different charge molar ratios (0.8 and 1.6). The NPECs formation has been realized by titration of polysaccharide solutions with zein solutions (two different alcohol concentrations were used for Z solutions: 60 and 70% denoted as Z60 and Z70, respectively).

The obtained nanoparticles were characterized by dynamic light scattering (DLS), zeta potential (ZP) and scanning electron microscopy (SEM). The ability of NPEC nanoparticles to entrap medicines was also examined in interaction with ciprofloxacin (CF): CF solution was added drop by drop to the freshly prepared complexes Z70/CSA 0.8 and Z70/ALG 0.8, under magnetic stirring. The antibacterial activity of NPEC/CF nanoparticles deposited on a non-woven cellulosic material (NWM) was evaluated against *E. coli* and *S. aureus*.

3. Results and discussion

In Table 1 are presented the NPEC nanoparticles' mean size, polydispersity index (PDI) and zeta potential values. We can observe that for both polymer ratios the particles with Z60 are slightly larger in size than those with Z70. This is probably a consequence of the higher water content in Z60 which favors zein aggregation. The values for the ZP are all negative, irrespective of the polysaccharide component and the charge molar ratio between polymers. This suggests that even when the polycation was in excess, the polysaccharide entrapped the zein and the ZP values are related to the surface available anionic groups.

Also, the PDI values below 0.2 found for most samples indicate that the particles are nearly monodisperse. Samples Z70/CSA 0.8 and Z70/ALG 0.8 were selected for further interaction with ciprofloxacin as a model drug.

Table 1. Mean particle size, polydispersity index and zeta potential of the obtained NPECs.

Sample	Z-average (nm)	PDI	Zeta potential (mV)
Z60/ALG 0.8	95.7	0.138	-19.6
Z70/ALG 0.8	85.3	0.325	-18.8
Z60/CSA 0.8	86.6	0.181	-19.4
Z70/CSA 0.8	123.9	0.274	-20.5
Z60/ALG 1.6	314.8	0.325	-9.9
Z70/ALG 1.6	122.4	0.053	-13.1
Z60/CSA 1.6	168.9	0.042	-15.1
Z70/CSA 1.6	101.8	0.166	-15.3

Figure 1 summarizes the characteristics of the NPECs after CF loading, by showing the morphology, ZP, PDI and average size of Z70/CSA 0.8 with CF, as being representative for the selected samples.

a)

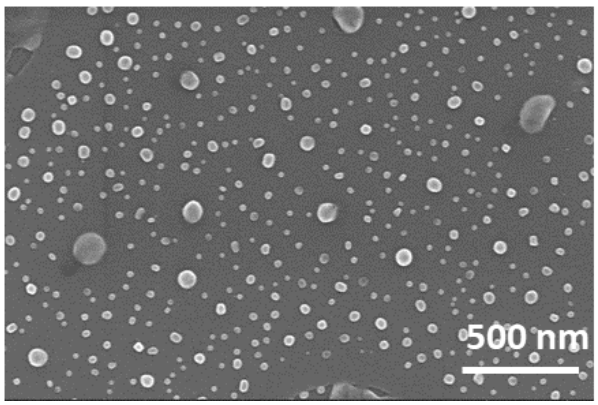

b)

Z-average	112 nm
PDI	0.2
ZP	-24 mV

Figure 1. (a) SEM image of Z70/CSA 0.8 + 15 mL CF; (b) Mean particle size, polydispersity index and zeta potential of Z70/CSA 0.8 + 15 mL CF.

The morphology of the nanoparticles with CF (Figure 1a) is similar to the bare NPECs (not shown here), spherical-shaped particles with an average diameter of 90 nm being present on the silicon wafer surface. The average diameter resulted from the analysis of SEM images (using ImageJ software) is slightly smaller than the one resulted from DLS measurements (Figure 1b) due to the fact that in dispersion the particles are in swollen state.

In Figure 1b are displayed the average size, PDI and ZP of particles after the interaction with the antibiotic. The ZP values are similar to the ones for the corresponding nanoparticles without ciprofloxacin (around -20 mV), suggesting the incorporation of the cationic drug inside the NPECs. Furthermore, the particle size and PDI values slightly decreased after drug loading, suggesting that CF improves the nanoparticles' physical properties by reducing the aggregation tendency.

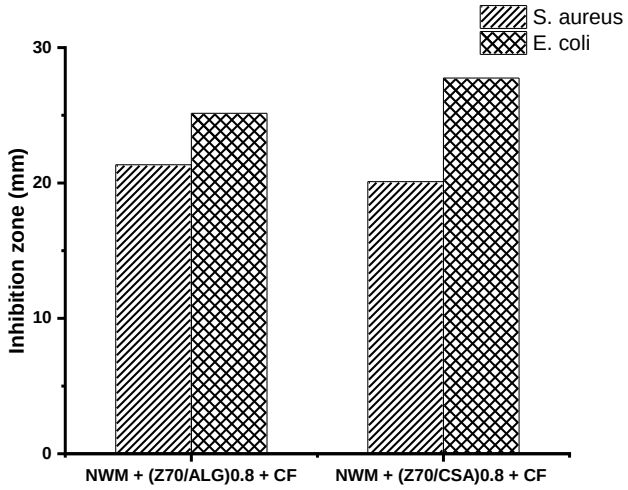

Figure 2. Antibacterial activity of the tested samples against the references strains (mm).

The antibacterial activity of the complexes with ciprofloxacin was evaluated by depositing the NPECs on NWM, and is presented in Figure 2. NPECs with CSA and ciprofloxacin showed up to 27 mm of inhibition zone against *E. coli*. Ciprofloxacin is well-known for its great efficacy against Gram-negative bacteria and its medium efficacy against Gram-positive bacteria. According to the current antibacterial test, independent of the polysaccharides used (CSA or ALG), the NPECs/CF have a larger inhibitory area for *E. coli* than for *S. aureus*.

4. Conclusions

In the current investigation, nonstoichiometric polyelectrolyte complexes comprising zein and two different types of polysaccharides – chondroitin sulfate A and sodium alginate – were synthesized and characterized. Samples Z70/CSA 0.8 and Z70/ALG 0.8 were chosen to interact with ciprofloxacin. Their antibacterial activity against *S. aureus* and *E. coli* was evaluated and the results showed a high level of antibacterial activity against both bacterial strains.

Acknowledgements

This work was supported by the Ministry of Research, Innovation and Digitization, by project number PN-III-P4-ID-PCE-2020-1541, within PNCDI III - CCCDI-UEFISCDI, and by project number PNRR-III-C9-2022-I8-201, within the National Recovery and Resilience Plan.

References

[1]. Ide W, Farrag Y. Natural polymeric materials as a vehicle for antibiotics. In: Kokkarachedu V, Kanikireddy V, Sadiku R, editors. Antibiotic Materials in Healthcare. London: Academic Press;pp. 51-64, 2020

[2]. Yuan Y, Ma M, Xu Y, Wang D. Surface coating of zein nanoparticles to improve the application of bioactive compounds: A review. *Trends Food Sci Technol* 120, 1-15, 2022

[3]. Ye W, Zhang G, Liu X, Ren Q, Huang F, Yan Y. Fabrication of polysaccharide-stabilized zein nanoparticles by flash nanoprecipitation for doxorubicin sustained release. *J. Drug Deliv. Sci. Technol.* 70, 103183, 2022

[4]. Wu D, Zhu L, Li Y, Zhang X, Xu S, Yang G, Delair T. Chitosan-based colloidal polyelectrolyte complexes for drug delivery: A review. *Carbohydr. Polym.* 238, 116126, 2020

PHARMACOKINETICS OF A MAGNESIUM SUPPLEMENT MONITORED BY NMR METABOLOMICS

Mara-Anastasia Isvoranu,[1,2]* Catalin Duduianu,[2,3] Calin Deleanu,[2,4] Alina Nicolescu [4]
[1]*IMC Krems University of Applied Sciences, Krems, Austria*
[2] *Costin D. Nenitescu Institute of Organic and Supramolecular Chemistry, Romanian Academy, Bucharest, Romania*
[3]*National University of Science and Technology Politehnica Bucharest, Faculty of Chemical Engineering and Biotechnologies, Bucharest, Romania*
[4]*Petru Poni Institute of Macromolecular Chemistry, Romanian Academy, Iasi, Romania*
**aisvoranu@yahoo.ro*

1. Introduction

Magnesium is a mineral important for the good health of the organism as it contributes to keeping the heart rhythm and blood pressure in normal ranges as well as maintaining the bones strong. In addition to this, magnesium deficiency was correlated with higher inflammatory markers. There are also some drugs, particularly those used in treating acid reflux, known for lowering the magnesium level in organism.

Recommended dietary magnesium doses for adults range between 300-450 mg/day. These doses may be easily filled up from natural foods including vegetables with leaves (e.g. spinach), nuts, beans, and whole-grain cereals [1]. However, there are currently several magnesium products available as food supplements or over-the-counter pharmaceuticals. These products include either magnesium alone as metallic ion, or in combination with other ions like calcium and zinc. Human use magnesium is conditioned either as inorganic salt (e.g. oxide, chloride, hydroxide, carbonate) or organic salts (e.g. citrate, orotate, lactate, aspartate) the organic ligands presumably enhancing the body absorption.

NMR became an indispensable tool in structure elucidation of pure compounds and until late 1980's this remained the most important type of application. Once the high field NMR spectrometers entered the chemical community, the method started to be used also for complex mixture analysis, entering in fields like medicine or food sciences. Today we see a rather balanced use of the NMR spectroscopy between the structure elucidation of pure compounds and analysis of complex mixtures.

When it comes to applications of NMR to complex systems, like biological ones, one should carefully balance between the excitement of the "potential" of the technique and claims of "ultimate diagnosis tool capabilities". Thus, one should be always aware which techniques and protocols are valuable to medical research and which ones can be extended to clinical practice.

2. Experimental

NMR spectra have been recorded on a Bruker Avance Neo 600 operating at 600.13 MHz for ^{1}H nuclei equipped with an inverse detection 5 mm probe. Samples have been recorded with 10% D_2O in 5 mm Wilmad 507 NMR tubes. NMR spectra have been recorded with the NOESY presaturation pulse sequence for suppression of the water signal. The chemical shifts are reported as δ values (ppm) and referenced to internal sodium trimethylpropionate-d4 (TSP).

3. Results and discussion

The present study describes preliminary pharmacokinetic results on follow-up of an organic magnesium medicine by NMR metabolomics. NMR metabolomics is an emerging field allowing simultaneous identification and quantitation of several metabolites in biological fluids. We have previously applied this technique for both pharmacokinetic studies [2] and medical diagnosis [3,4].

Among the biological fluids, urine is by far the most analyzed through ^{1}H-NMR Spectroscopy. This is mainly because this biological fluid has several advantages like: high metabolite content, accessibility, and little sample preparation requirements (without extractions or derivative preparations). In addition, the urinary metabolites are excreted in variable amounts, depending on the variations in hole-body homeostatic control, thus from urine analysis a time-dependent metabolite pattern can be obtained.

The "typical" ^{1}H-NMR spectrum of a urine sample is very crowded, most of the peaks corresponding to "normal" urinary metabolites being overlapped, as exemplified in Figure 1.

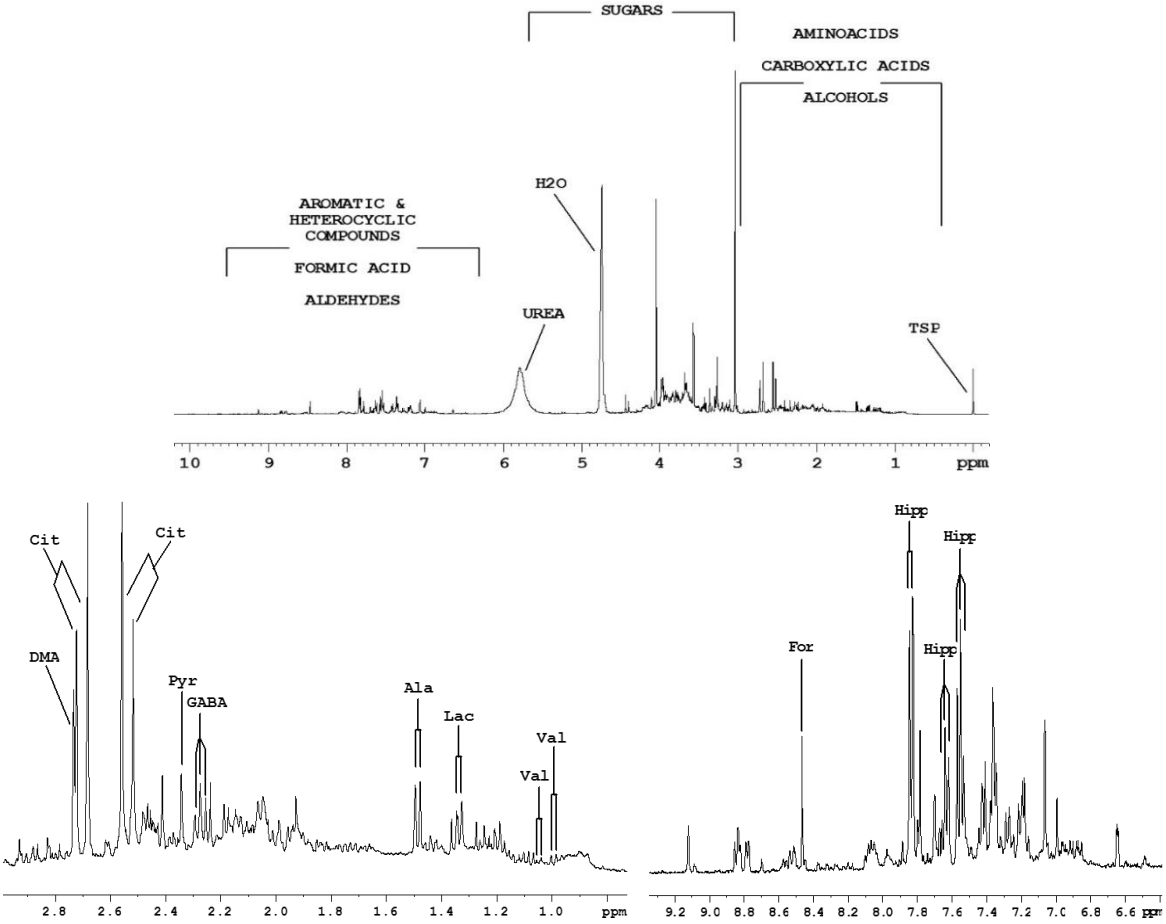

Figure 1. A typical spectrum of urine sample with delimitation of the main three spectral intervals (first row); some examples of signals assignments to corresponding metabolites in aliphatic region (second row, left) and aromatic region (second row, right). Abbreviations: Cit – citrate, DMA – dimethylamine, Pyr – pyruvate, GABA – gamma aminobutyrate, Ala – alanine, Lac – lactate, Val – valine, For – formiate, Hipp – hippurate.

Two doses of a magnesium supplement have been ingested by a volunteer and the body clearance of the organic ligand was followed in the urine by NMR spectroscopy, as exemplified in Figure 2.

First dose was 2/3 and the second dose was a full daily recommended quantity of the medicine in a single ingestion. Between experiments two months have been allowed in order to leave enough time for the body to recover from any medicine metabolomics effects.

Our findings show a total clearance of the organic ligand in 26 and 35 hours after a single dose of 2/3 and a full dose respectively of daily recommended quantity of the medicine.

High doses of magnesium and its organic ligands from supplements can interact with some medicines, including some types of antibiotics, and in some cases even with diagnosis of some disease. The ingestion of the magnesium-based medicine/supplement that we investigated, may lead to false positive diagnosis of some diseases.

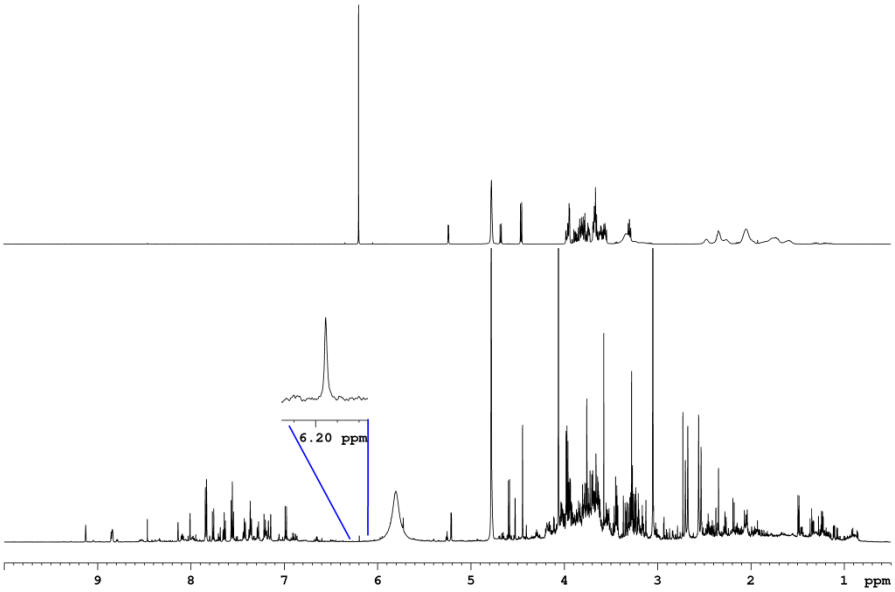

Figure 2. ^{1}H-NMR spectra of urine sample showing the presence of the organic ligand (bottom) and one tablet of magnesium supplement solubilized in water, showing signals from the organic ligand and other additives (top).

4. Conclusions

We have proven that NMR metabolomics can successfully monitor the organic ligand clearance in urine even after the ingestion of a single dose of 2/3 of daily recommended quantity of the medicine.

References

[1]. Rude RK. Magnesium, In: Ross AC, Caballero B, Cousins RJ, Tucker KL, Ziegler TR, editors. Modern Nutrition in Health and Disease. 11th ed. Baltimore: Lippincott Williams & Wilkins; pp. 159-175, 2012

[2]. Nicolescu A, Simionescu N, Ursu L, Deleanu C, Simionescu BC. The effect of therapeutic doses of paracetamol and aspirin on the NMR profile of urine at 400 MHz. *Rev. Roum. Chim*. 57 (7-8), 653-658, 2012

[3]. Vulturar R, Chis A, Baizat M, Cozma A, Suharoschi R, Nicolescu A, Deleanu C. A severe neonatal argininosuccinic aciduria case investigated by ^{1}H NMR spectroscopy. *Rev. Chim*. 71 (3), 210-218, 2020.

[4]. Nicolescu A, Blanita D, Boiciuc C, Hlistun V, Cristea M, Rotaru D, Pinzari L, Oglinda A, Stamati A, Tarcomnicu I, Tutulan-Cunita A, Stambouli D, Gladun S, Revenco N, Usurelu N, Deleanu C. Monitoring methylmalonic aciduria by NMR urinomics. *Molecules* 25 (22), 5312, 2020

MACRO Iași 2023

DESIGN AND SYNTHESIS OF PARTICLES BASED ON CHITOSAN GRAFTED POLY(ETHYLENEGLYCOL) METHYLETHER ACRYLATE AS CARRIERS FOR ANTIBIOTICS

Catalina Anisoara Peptu,[1]* Corina-Lenuta Logigan,[1] Christelle Delaite,[2] Crina-Elena Tiron,[3] Marcel Popa,[1,5,6] Cristian Peptu[4]

[1] *Department of Natural and Synthetic Polymers, Cristofor Simionescu Faculty of Chemical Engineering and Environmental Protection, Gheorghe Asachi Technical University of Iasi, Romania*

[2]*Laboratory of Photochemistry and Macromolecular Engineering, Institute J.B. Donnet, University of Haute Alsace, Mulhouse, France*

[3]*Regional Institute of Oncology, Iasi, Romania*

[4] *Petru Poni Institute of Macromolecular Chemistry, Romanian Academy, Iasi, Romania*

[5]*Faculty of Medical Dentistry, Apollonia University of Iasi, Romania*

[6]*Academy of Romanian Scientists, Bucharest, Romania*

**catipeptu@yahoo.co.uk*

1. Introduction

Among all natural polysaccharides, the most used as a support material for polymeric nanoparticles is chitosan (CS). Chitosan is a natural polysaccharide known for its excellent properties, including biocompatibility, biodegradability, non-toxicity, mucoadhesion, and the presence of highly reactive amine moieties. CS may be chemically modified to achieve specific goals such as enhancing solubility, mucoadhesion, and stability, thus expanding its potential applications in drug delivery [1]. Nanotechnology is used to design micro and nanoparticles (MPs, NPs) which are suitable as drug delivery support for various biomedical applications due to their unique properties. CS limited water solubility in neutral and basic pH media can be a challenge and limits its processability. In this work, CS is modified with poly (ethylene glycol) methyl ether acrylate (PEGA) to improve its properties for drug delivery applications.

2. Experimental

Micro and nanoparticles based on modified CS are prepared using a double crosslinking technique (ionic and covalent) in a water/oil emulsion. The prepared MPs/NPs were characterized structurally and morphologically using various techniques such as infrared spectroscopy, scanning electron microscopy, light scattering granulometry, and Zeta potential analysis. The water uptake capacity of MPs/NPs was studied under acidic and neutral pH conditions, revealing a pH-dependent behavior. The ability of MPs/NPs to serve as drug delivery systems was tested by encapsulating two separate antibiotics, Levofloxacin (LEV) and Ciprofloxacin (CIP), and excellent drug encapsulation and release capacity was observed. MPs/NPs were found to be biocompatible with cells and blood (cyto- and hemocompatible), indicating their potential suitability for biomedical drug delivery applications.

Materials

Chitosan (CS); Poly (ethylene glycol) methyl ether acrylate (PEGA); Glutaraldehyde (GA); Sodium sulphate (Na_2SO_4); levofloxacin (LEV); ciprofloxacin (CIP); Tween 80; Span 80; were purchased from Sigma-Aldrich, Saint Louis, MO, USA;

Methods

Chemically modified CS with PEGA via Michael addition reaction was performed according to a protocol reported by Han et al. [2]. To prepare micro/nanoparticles (MPs/NPs) based on the modified CS, a double crosslinking reaction is employed, which includes both ionic and covalent crosslinking, and is carried out in a water/oil emulsion. The advantage being the use of a lower amount of covalent crosslinker, which leads to a decrease in NPs toxicity [3].

3. Results and discussion

The work presented herein is focused on the use of PEGA to chemically modify CS for the improvement of its solubility in water and diminish its pH-dependent water swelling character by adding hydrophilic segments to CS linear chain. CS-PEGA structural characterization was performed via ^{1}H NMR (Figure 1) and FTIR (Figure 2), both demonstrating the formation of the new CS derivative.

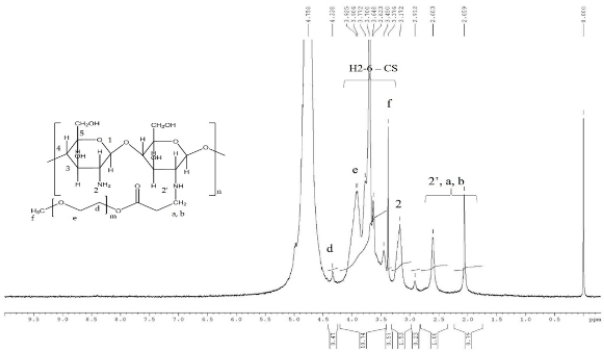

Figure 1. RMN spectra of CS-PEGA.

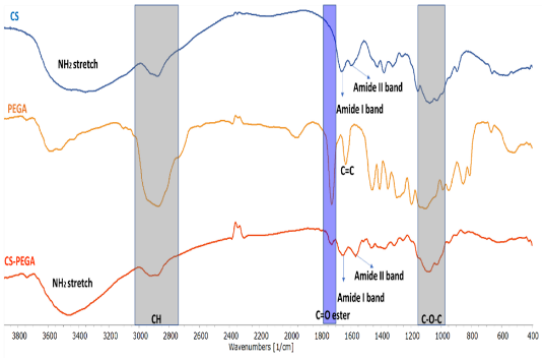

Figure 2. FTIR spectra of CS, PEGA, and CS-PEGA.

Further micro/nanoparticles-based modified CS were prepared through sequential ionic and covalent crosslinking. The studied process parameters are polymer concentration, stirring speed, and quantity of ionic crosslinker (Na_2SO_4) (Table 1).

Table 1. MPs/NPs – Experimental program preparation, size and zeta potential measurements

Sample Code	Polymer Solution Conc, %	Molar Ratio NH_2/ Na_2SO_4	Speed, Rpm	Water Phase, ml	The Organic Phase, mL	Surfactants Conc, %	Ionic/ Covalent Crosslinking Time, min	Average Diameter (LD), µm	Potential Zeta (mV)
P1	0.5	1:4	5000	50	200	2	60	2.7	11.4 ± 0.2
P2	0.5	1:4	9000	50	200	2	60	1.6	10.2 ± 0.3
P3	0.5	1:4	12000	50	200	2	60	0.78	12.9 ± 0.6
P4	0.5	1:4	15000	50	200	2	60	0.157	9.2 ± 0.3
P5	0.35	1:4	15000	50	200	2	60	0.092	11.8 ± 0.6
P6	0.5	1:5	15000	50	200	2	60	0.45	10 ± 0.4
P7	0.75	1:4	15000	50	200	2	60	0.6	12.8 ± 0.3

The MPs/NPs were structurally and morphologically characterized. Particles with variable size dependent on the crosslinking parameters were prepared. SEM images showed that MPs/NPs present a spherical shape, are homogeneous, separated, and average diameter depending on specific

preparation conditions from 2700 to 92 nm (Figure 3). Swelling properties were studied in acidic and neutral pH conditions, showing that pH-dependent behavior was maintained after grafting and double crosslinking. Moreover, the applicability of the prepared materials was further tested for drug loading and in vitro delivery of LEV or CIP, showing excellent capacity. MPs/NPs were found to be cyto- and hemocompatible demonstrating their potential for effective use as a controlled release system for different biomedical applications.

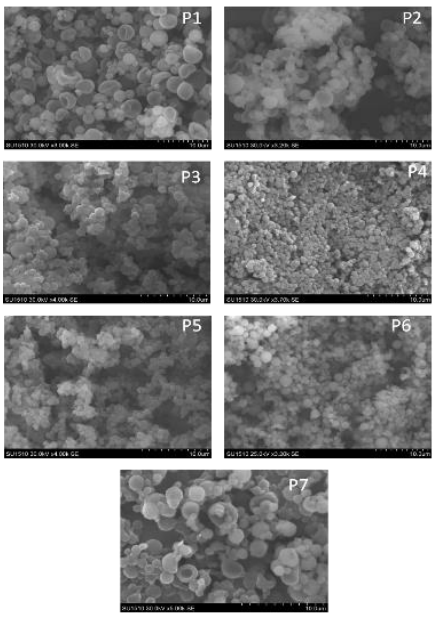

Figure 3. Micrographs SEM of MPs/NPs (magnification graphical bar length P1-P7:10 μm).

4. Conclusions

This work demonstrates the suitability of new CS derivative for the preparation of nanoparticulate systems through double emulsion crosslinking. The substitution degree of CS with PEG-acrylate was determined via NMR and was 20 %. Particles with variable size dependent on the crosslinking parameters were prepared via double crosslinking method. MPs/NPs showed a higher water retention capacity for the acidic media, compared to basic media. MPs/NPs drug release kinetics analysis demonstrated that the drug transport/release mechanism is predominantly diffusional. MPs/NPs hemocompatibility analysis revealed their hemocompatibility. Also, cytocompatibility studies demonstrated that NPs do not affect cell viability, thus confirming their low cytotoxicity.

Acknowledgements

This work was supported by a grant from the Ministry of Research, Innovation and Digitization, CNCS-UEFISCDI, project number PN-III-P4-PCE-2021-1365, within PNCDI III, (contract number PCE 115/2022).

References

[1]. Mohammed MA, Syeda JTM, Wasan KM, Wasan EK. An overview of chitosan nanoparticles and its application in non-parenteral drug delivery. *Pharmaceutics*. 9, 53, 2017
[2]. Han J, Zhang J, Yin R, Ma G, Yang D, Nie J. Electrospinning of methoxy poly(ethylene glycol)-grafted chitosan and poly(ethylene oxide) blend aqueous solution. *Carbohydr. Polym.*, 83, 270-276, 2011
[3]. Logigan CL, Delaite C, Tiron CE, Peptu C, Popa M, Peptu CA. Chitosan grafted poly (ethylene glycol) methyl ether acrylate particulate hydrogels for drug delivery applications. *Gels*. 8, 494, 2022

EXPLORING THE REMARKABLE PROPERTIES OF WATER SOLUBLE CHITOSANS

Larisa-Maria Petrila,[1]* Marius-Mihai Zaharia,[1] Florin Bucatariu,[1]
Marcela Mihai,[1] Stergios Pispas[1,2]
[1]*Petru Poni Institute of Macromolecular Chemistry, Romanian Academy, Iasi, Romania*
[2]*Theoretical and Physical Chemistry Institute,*
National Hellenic Research Foundation, Athens, Greece
**larisa.petrila@icmpp.ro*

1. Introduction

In the realm of biopolymers, chitosan has emerged as one of the most interesting compounds for both the scientific community and industrial sector. Derived from chitin, a natural polysaccharide abundantly found in the exoskeletons of crustaceans and the cell walls of fungi, chitosan has gained attention for its diverse applications in various areas, ranging from agriculture to the biomedical field and environmental protection [1,2]. While initially depicted as a waste product, chitosan has evolved into one of the most studied polysaccharides, demonstrating the scientific research's ability to unlock the latent potential of biomaterials from natural resources [3]. Its unique characteristics such as biocompatibility, biodegradability, and antimicrobial activity have positioned it as a valuable asset in the pursuit for sustainable solutions to emerging challenges. The plethora of applications chitosan finds in different fields is strongly related to its structural and functional properties. Chitosan is considered a robust and poorly soluble biopolymer, but its large number of functional groups makes it a potential candidate for biomedical applications such as drug and protein/gene delivery or active compound/chitosan polyelectrolyte complexes [4].

Herein, by delving into the molecular structure of two commercially available water soluble chitosan samples with different molar masses, we aim to better understand the characteristics of this polysaccharide in terms of structural and functional properties.

2. Experimental

The two samples of chitosan with low molar mass ($Chit_{oligo,}$ M_w = 1460 g/mol) and high molar mass chitosan ($Chi_{162K,}$ M_w= 162000 g/mol) were acquired from Shandong AK Biotech Co LTD. The FTIR-ATR spectra were collected using an Tracer-100 FTIR spectrometer (Shimadzu Corporation, Japan) equipped with a GladeATR module (PIKE Technologies, USA), in the 400-4000 cm^{-1} spectral region, with a resolution of 4 cm^{-1}. The WXRD studies were carried out on the Rigaku Miniflex 600 diffractometer (Rigaku, Tokyo, Japan) at 40 kV tube voltage and 15 mA emission current with Cu-Kα radiation at λ= 1.5406 Å wavelength. The samples were scanned using a paired two theta/theta scan type in the range 2θ = 2-90º with 0.01º step at 2º min^{-1} scanning speed. SmartLab II v.4 software was used for background removal, smoothing, and WPPF refinement, while the powder patterns were established using the Crystallography Open Database (COD). Based on FTIR-ATR and WXRD, the deacetylation degree (DD) of each chitosan sample was calculated, according to models proposed in the literature [5]. The properties of chitosans in solution and their inherent charge behavior were studied employing potentiometric and polyelectrolyte titrations, using the PCD 03 particle charge detector (Mütek GmbH, Germany). For potentiometric titration, the effect of the pH on the chitosan's streaming potential (mV) was

studied. The molecular charge density (meq/g) and the percent of functional groups that were initially hindered were calculated based on polyelectrolyte titrations with PESNa (10^{-3} M).

3. Results and discussion

The structural characterization of chitosan was performed based on the ATR-FTIR spectra (Figure 1a) and X-Ray diffractograms (Figure 1b).

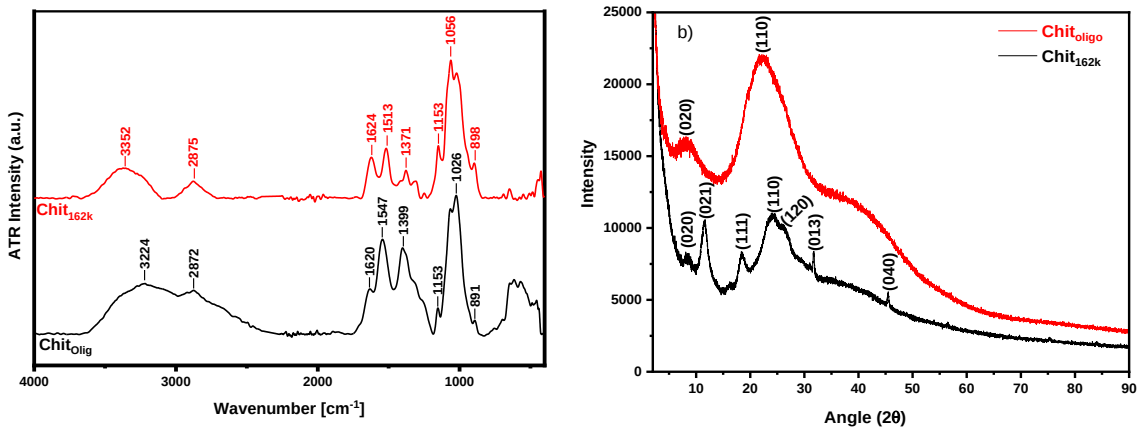

Figure 1. (a) ATR-FTIR spectra and (b) X-ray diffractograms of $Chit_{oligo}$ and $Chit_{162K}$.

The main bands had maxima at 1026-1056 cm^{-1}, characteristic to C–O stretching vibration, while the asymmetric stretching of C–O–C bridge appeared at 1153 cm^{-1} and ring vibration of carbohydrate at 891-898 cm^{-1}. The presence of the C=O stretching of the Amide I band, bending vibrations of the N–H (N-acetylated residues, Amide II band), and C–H bending were associated with the absorption peaks at 1620-1624 cm^{-1}, 1513-1547 cm^{-1}, and 1371-1399 cm^{-1}. The spectra registered for both chitosan samples present the same main bands, demonstrating the fact that there are no chemical structure differences between them. Further information about the chemical structure of chitosan was obtained from XRD (Figure 1b). The diffractogram of $Chit_{oligo}$ evidences the presence of two peaks at $2\theta \sim 8.2^{o}$ (020) and 22.1^{o} (110) which are characteristic to the crystal-I and crystal-II chitosan structures (COD-1951228), respectively, and both of these peaks demonstrate a high degree of crystallinity. In the X-ray diffractogram of $Chit_{162k}$, crystalline reflections of 020, 021, 111, 110 and a shoulder at 120, 013, and 040 were observed, corresponding to 2θ of 8.5°, 11.5°, 18.4°, 24.3°, 26.6°, 30.9°, and 45.5°, respectively.

The degree of deacetylation (DD) is an important property of chitosan which dictates its further use, as samples with high deacetylation degrees are more soluble and exhibit stronger polycation properties [3]. The DD can be determined by FTIR, using absorbance ratios of amide-I (1655 cm^{-1}) and hydroxyl group (3450 cm^{-1}). Based on the model proposed by Yasmeen et al. [5], we determined a DD of 87.92% for $Chit_{162K}$ and 90.72% for $Chit_{oligo}$, values which confirm the high solubility of chitosan. Similar results were obtained based on XRD calculations, were the DD obtained was 88.3% for $Chit_{162K}$ and 90.1% for $Chit_{oligo}$. The DD values obtained are consistent with the experimentally observed solubility of the two chitosan samples and suggest significant potential for utilization of these chitosan samples in studies and applications in aqueous media.

In order to better understand the behavior of the chitosan samples in solution, the potentiometric titration method was employed. As observed from Figure 2, both chitosan samples present a weak polyelectrolyte behavior, their streaming potential values being strongly influenced by variations of pH. The isoelectric point of $Chit_{oligo}$ is situated at pH ~ 7.5, almost one pH unit lower than in the

case of $Chit_{162K}$, which suggests that the low molar mass chitosan sample has a larger number of functional groups which be protonated in aqueous media. This behavior was also confirmed by the polyelectrolyte titrations (results not shown here), which evidenced that in aqueous solution $Chit_{oligo}$ has 97.4% of its functional amine groups fully charged, while $Chit_{162K}$ has only 66.4%.

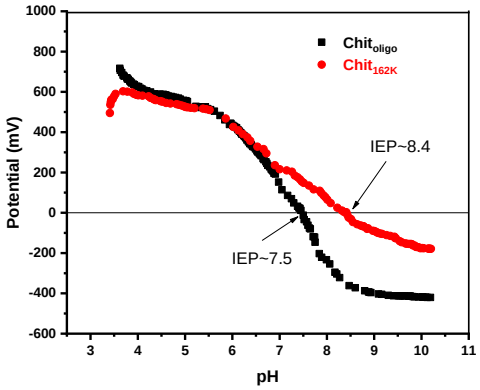

Figure 2. The variation of the potential as a function of pH for $Chit_{oligo}$ and $Chit_{162K.}$

These results suggest that the bulkier structure of longer chain $Chit_{162K}$ is shielding more of the underlying functional groups. Nevertheless, by carefully choosing the environmental conditions, the hindered functional groups can be successfully involved in the formation of new interactions, as observed by titrating the Chi_{162K} solution after protonation in strong acidic media.

4. Conclusions

Based on the structural characterization and the solution behavior studies, we demonstrate the polyelectrolyte behavior and confirmed the water solubility of these two particular chitosan samples, a property usually not expected for chitosan. The properties suggest potential application for these chitosan samples in forming interactions with various compounds such as natural and synthetic polymers, proteins, nucleic acids or other bioactive substances as the high number of functional groups are able to form different physical bonds.

Acknowledgements

This work was supported by the Ministry of Research, Innovation and Digitization, by project number PN-III-P4-ID-PCE-2020-1541, within PNCDI III - CCCDI-UEFISCDI, and by project number PNRR-III-C9-2022-I8-201, within the National Recovery and Resilience Plan.

References

[1]. Rinaudo M. Chitin and chitosan: Properties and applications. *Prog. Polym. Sci.*, 31, 603-632, 2006
[2]. Karayianni M, Sentoukas T, Skandalis A, Pippa N, Pispas S. Chitosan-based nanoparticles for nucleic acid delivery: Technological aspects, applications, and future perspectives. *Pharmaceutics*, 15, 1849, 2023
[3]. Harugade A, Sherje AP, Pethe A. Chitosan: A review on properties, biological activities and recent progress in biomedical applications. *React. Funct. Polym.* 191, 2023
[4]. Wani S, Ali M, Mehdi S, Masoodi MH, Zargar MI, Shakeel F. A review on chitosan and alginate-based microcapsules: Mechanism and applications in drug delivery systems. *Int. J. Biol. Macromol.* 248, 125875, 2023
[5]. Yasmeen S, Kabiraz M, Saha B, Qadir MD, Gafur MD, Masum S. Chromium (VI)) ions removal from tannery effluent using chitosan-microcrystalline cellulose composite as adsorbent. *Int. Res. J. Pure Appl. Chem.* 10, 1-14, 2016

INSIGHTS OF COLD PLASMA-INDUCED CHANGES IN STARCH PROPERTIES THROUGH MULTIVARIATE DATA ANALYSIS

Monica R. Nemtanu,[1]* Mirela Brasoveanu,[1] Catalin M. Ticos[1,2]
[1]*National Institute for Laser, Plasma and Radiation Physics, Electron Accelerators Laboratory, Bucharest-Magurele, Romania*
[2]*Horia Hulubei National Institute for R&D in Physics and Nuclear Engineering, Bucharest-Magurele, Romania*
**monica.nemtanu@inflpr.ro*

1. Introduction

Starch is a versatile and abundant biopolymer, finding extensive utility in the food and non-food sectors. As a naturally occurring carbohydrate, starch is composed of glucose units organized in linear (amylose) and branched (amylopectin) structures. This macromolecular architecture gives rise to its distinct functional properties, which are of interest for both research and technological applications. However, starch is often modified to enhance its functionality and extend its utilization [1]. Recent advances have highlighted the potential of low-temperature plasma, often known as cold plasma, as a promising tool for inducing transformative alterations in starch properties. The effects of cold plasma on starch have been observed to trigger multifaceted modifications, influencing properties such as pasting, rheology, gelatinization, crystallinity, granule morphology, and molecular weight [2]. These alterations primarily arise from either crosslinking or degradation, two competitive processes occurring on the polymer surface and its surrounding regions during plasma treatment and influenced by specific experimental conditions [3]. It is noteworthy to mention that these changes present complex interrelationships that demand a comprehensive investigative approach.

Multivariate analysis techniques find extensive application in diverse scientific domains, particularly those characterized by complex structures and numerous variables. These techniques can reveal insights and information, enhancing the process of decision-making and aiming for optimal solutions.

This study aimed to establish correlations between sample quantity and some physicochemical properties of starch exposed to cold plasma. Multivariate statistical analysis was employed to differentiate the concurrent processes of degradation and crosslinking. This approach can reveal the complex relationships between the initial sample characteristics and the subsequent changes resulting from plasma treatment.

2. Experimental

Native corn starch (powder; moisture content: ≤15%) was subjected to radio-frequency (RF) plasma, varying sample loading [3]. The samples were labelled as N for native starch and P, 1.5P, 2P (treated samples) based on loading (starch quantity per holder surface area). Physicochemical properties such as moisture content (m_c%), pH at 25±1 ^{0}C for 1% (w/v) gelatinized starch, granule solubility (s%) in water at 65 ^{0}C, paste clarity (light transmittance at 650 nm – T%) at 25±1 ^{0}C for 1% (w/v) gelatinized starch, apparent viscosity (η_a) at shear rate $\dot{\gamma}$ =100 s^{-1} and 25±1 ^{0}C of 5% (w/v) gelatinized starch, and relative crystallinity (RC%) of both control and modified starch samples were determined in triplicate. Further, multivariate analysis techniques such as factorial

analysis (FA) through the principal component method and hierarchical cluster analysis (HCA) using Ward's method were used.

3. Results and discussion

The behavior of the investigated physicochemical properties changed upon the exposure of starch to plasma, with distinct patterns depending on the sample loading.

To establish the correlation between the 7 dependent variables (moisture content, pH, solubility, viscosity, paste clarity, and relative crystallinity) and the independent variable (sample loading) and to reduce the variables, experimental data underwent FA in which the factors were extracted by the Principal Component method from the correlation matrix (Table 1) through varimax orthogonal rotation. In terms of correlations with sample loading, the moisture content (m_c%) and paste clarity (*T%*) showed good negative correlations, the pH had a moderate negative correlation, and the apparent viscosity (η_a) exhibited a moderate positive correlation. At the same time, the relative crystallinity (RC%) showed only a weak negative correlation, and solubility (*s%*) had no significant correlation with sample loading. Instead, pH showed strong positive correlations with both m_c% and RC%. The apparent viscosity moderately correlated negatively with *s%* and *T%*, while positively correlated with RC%.

Table 1. Correlation matrix (Pearson = *r*) of variables.

Variable	Sample loading	m_c%	pH	*s%*	*T%*	η_a	RC%
Sample loading	**1.000**	-0.850	-0.620	-0.295	-0.803	0.556	-0.323
m_c%	-0.850	**1.000**	0.931	-0.031	0.577	-0.052	0.745
pH	-0.620	0.931	**1.000**	-0.224	0.353	0.264	0.910
s%	-0.295	-0.031	-0.224	**1.000**	0.591	-0.689	-0.288
T%	-0.803	0.577	0.353	0.591	**1.000**	-0.634	0.135
η_a	0.556	-0.052	0.264	-0.689	-0.634	**1.000**	0.542
RC%	-0.323	0.745	0.910	-0.288	0.135	0.542	**1.000**

* Correlation coefficient, r = 0.90 – 1.00 (strong), r = 0.70 – 0.89 (good), r = 0.50 – 0.69 (moderate), r = 0.30 – 0.49 (weak), and r < 0.29 (negligible) [3].

Applying *Kaiser's criterion* for factor reduction (eigenvalue > 1), the FA grouped variables into two principal factors, explaining ~90% of the cumulative variance: Factor 1 (F1) with 51.3% and Factor 2 (F2) with 38.5% (Figure 1). Significant loading values characterized important variables within each factor. In F1, sample loading had a positive loading, while m_c%, pH, and RC% exhibited negative loadings. F2 included *s%* and *T%* with positive loadings and η_a with a negative loading. Hence, F1 displayed major correlations with the *initial sample characteristics* (sample loading and moisture content), whereas F2 showed an association with the *functional properties*, particularly the apparent viscosity. Sample and variable distributions in the F1-F2 plane, showing correlations and sample differentiation, are presented in Figure 1a. Plasma-modified samples occupied distinct quadrants from native starch. P samples, susceptible to degradation, moved significantly to the right side of F1. Similarly, 1.5P and 2P samples, prone to crosslinking, shifted right with F1>0 and F2<0. This visual distinction demonstrates the modified samples' divergence from the control sample (native starch) and each other. The FA outcome highlighted that the initial sample characteristics play a role in both the nature and magnitude of the modifications, as evidenced by the discernible physicochemical differences between the degraded P samples and the crosslinked 1.5P and 2P samples.

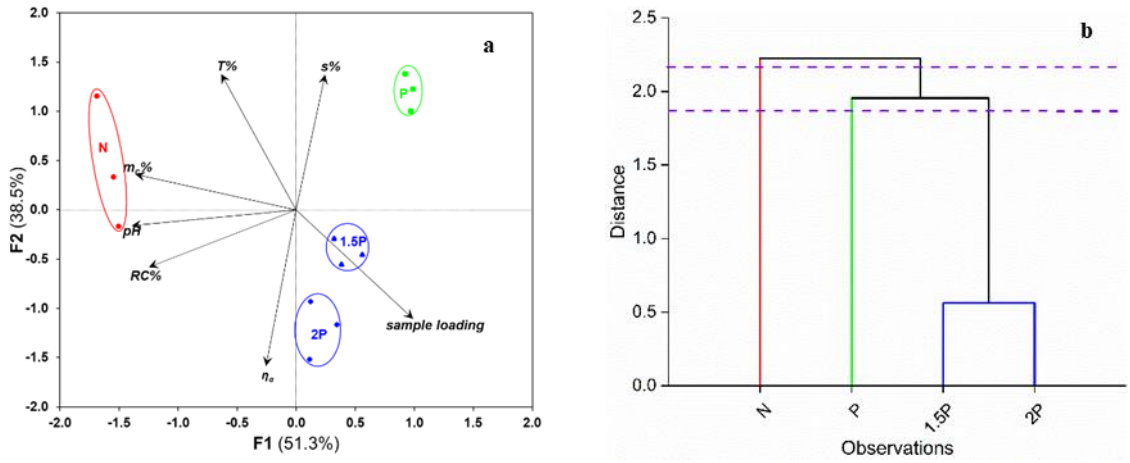

Figure 1. (a) Factor plot for factors F1 and F2; (b) Dendrogram obtained from AHC.

The examination further revealed the patterns of sample clustering based on the specific modification of the investigated starch properties (Figure 2b). For a good cophenetic correlation of 0.885, at a cut-off of 2.168, the samples could be distinctly classified into two sub-clusters: unmodified starch and plasma-modified starches. Further segmenting at 1.863 resulted in three clusters: cluster 1 of unmodified samples (native starch), cluster 2 including degraded samples (P) with the lowest sample loading, and cluster 3 consisting of crosslinked samples (1.5P and 2P).

4. Conclusions

RF plasma treatment induced sample loading-dependent changes in native starch properties (e.g., moisture content, pH, clarity, solubility, viscosity, and crystallinity), with opposing directions involving degradation and crosslinking. These reactions can occur concurrently under the same conditions, with the magnitude influenced mainly by the sample loading. FA showed that variables align along two principal factors (F1 and F2), explaining ~90% of variance. Plasma-modified samples occupied distinct right-side quadrants in the factorial space (F1>0), indicating significant alterations due to initial sample characteristics. Modified starches shifted similarly, but crosslinked ones had negative F2 values, underlining distinct modification pathways concerning functional properties. Clustering categorized samples by the type of modification (degradation or crosslinking) based on initial sample characteristics. This approach offers insights for experimental designs and expands the understanding of plasma treatment applications in studies on starch-based materials.

Acknowledgements

This work was supported by a grant of the Romanian Ministry of Research, Innovation and Digitalization, CNCS - UEFISCDI, project number PN-III-P4-PCE-2021-1778, within PNCDI III.

References

[1]. Chen S, Qin L, Chen T, Yu Q, Chen Y, Xiao W, Ji X, Xie J. Modification of starch by polysaccharides in pasting, rheology, texture and in vitro digestion: A review. *Int J Biol Macromol* 207, 81-89, 2022
[2]. Okyere AY, Rajendran S, Annor GA. Cold plasma technologies: Their effect on starch properties and industrial scale-up for starch modification. *Curr Res Food Sci* 5, 451-463, 2022
[3]. Brasoveanu M, Nemtanu MR, Ticos D. Influence of the sample loading on the contribution of competitive effects for granular starch exposed to radio-frequency plasma. *Innov Food Sci Emerg Technol.* 72, 102740, 2021

OXIDATION PROCESS OF WATER-SOLUBLE POLYSACCHARIDE IN THE *N*-HYDROXYPHTHALIMIDE-MEDIATIATED SYSTEM

Gabriela Biliuta,* Raluca-Ioana Baron, Sergiu Coseri
Petru Poni Institute of Macromolecular Chemistry, Romanian Academy, Iasi, Romania
**biliuta.gabriela@icmpp.ro*

1. Introduction

In recent years, several catalysts have been developed for the selective catalytic oxidation of polysaccharides. Among them, *N*-hydroxyphthalimide (NHPI) has attracted much attention due to its high selectivity and superior performance. NHPI demonstrated its exceptional catalytic power by promoting the oxidation of a wide range of organic compounds with dioxygen in the presence of a cocatalyst capable of abstracting a hydrogen atom by homolytic cleavage of the >N-O-H bond to form the active species, the phthalimide-*N*-oxy radical (PINO) [1-3].

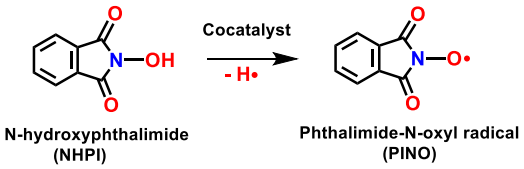

Figure 1. General scheme of the PINO radical generation from its hydroxyl precursor (NHPI).

Taking into account the great potential of this radical, we have proposed for the first time the use in the field of polysaccharide oxidation [1-3]. Therefore, we developed several cellulose oxidation protocols in the presence of NHPI/cocatalyst (metallic or nonmetallic)/NaBr/NaOCl. In this paper, we suggest a protocol for starch oxidation using NHPI in a metal-free system, this system being previously tested on cellulose but not on soluble polysaccharides that permit a homogenous medium. The generation of the active radical species PINO is made possible by the presence of NaOCl and NaBr as the actual oxidizing agents. As a water-soluble polysaccharide, we choose starch, a polymeric carbohydrate composed of linear amylose and highly branched amylopectin. As researchers strive for global sustainability and greener chemical processes, starch is one of the renewable materials of increasing interest. Modification of starch offers the opportunity to produce a wide range of chemicals. Fossil fuels are becoming increasingly expensive due to dwindling reserves and political conflicts. For example, more than 5 million metric tons of oxidized starch are currently used in the paper industry, mainly because of its good binding properties [4].

2. Experimental

Materials and reagents: NHPI, sodium bromide, 9% (wt) sodium hypochlorite and other chemicals and solvents were of pure grade (Sigma Aldrich), and used without further purification. Potato starch (PS), humidity content <10%, ash <0.5% and wheat starch (WS), humidity content <15%, ash <0.5%, was purchased from Fluka.

PINO-mediated oxidation of starch: Potato starch (1 g) was added to 200 mL deionized water/acetonitrile solution (5:1 vol) containing NHPI (0.5 mM/g starch) and sodium bromide (8 mM/g starch) using a magnetic stirrer. The pH was adjusted to 10 and then an 8% NaClO solution (10 mM/g starch for SO-10 and 25 mM/g starch for SO-25) was added to the mixture and kept at

room temperature for 5 h under vigorous stirring. The pH was carefully monitored and kept at pH = 10 during the reaction by using a 0.5 M NaOH solution (to compensate for the decrease in pH due to the formation of carboxyl groups).

Characterization: Infrared absorption spectra of starch and oxidized starch samples were recorded using a Bruker Vertex 70 spectrometer at a scan range from 4000 to 650 cm^{-1}, at a resolution of 2 cm^{-1} and 32 scans. The NMR spectra were obtained on a Bruker Avance DRX 400 MHz Spectrometer, equipped with a 5 mm QNP direct detection probe and z-gradients. ESEM photographs were taken on samples fixed with colloidal silver on copper supports. The samples were first sputter coated with a thin gold layer (EMITECH K 550×). The resulting coated surface was then examined using an Environmental Scanning 200 instrument.

3. Results and discussion

In this study, water soluble starch was oxidized by controlling the amount of NHPI, NaBr and reaction time and varying the amount of the NaClO (8%). The PINO free radical, derived from its hydroxyl parent, NHPI, is the key species capable of initiating the oxidation process. In our approach, the introduction of sodium hypochlorite in combination with sodium bromide plays a double role: (i) it ensures the conversion of NHPI to PINO, similar to systems with metal salts, and (ii) further oxidation of the PINO radical to the nitrosonium cation, the actual oxidant of the reaction. At this point, the oxidation of the starch will occur selectively at C6, converting the primary hydroxyl groups to carboxyl groups (Figure 2).

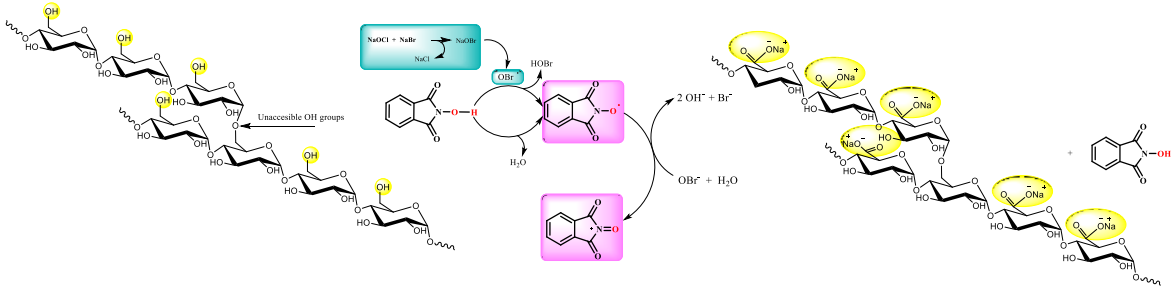

Figure 2. General scheme of PINO-mediated oxidation of starch.

Figure 3a shows the FTIR spectra of native and oxidized starch. The main differences are the appearance of the new double sharp peaks at 1609 cm^{-1} and 1419 cm^{-1} in the FTIR spectra of the oxidized samples, indicating the presence of the asymmetric and symmetric stretching vibrations of the $-COO^-$ groups, as a result of the primary oxidation of the OH groups. In addition, the bell-shaped peak centered at 3420 cm^{-1} in oxidized samples, assigned to the OH groups in starch, is still present in the oxidized samples, indicating that the secondary alcohol groups are not affected by the PINO-mediated oxidation. On the contrary, the peak located at 2930 cm^{-1} in native starch (shifted to 2937 cm^{-1} in oxidized starch), assigned to the $-CH_2$ stretching, and becomes much smaller after oxidation because of the conversion of the $-CH_2OH$ groups into $-COO^-$ groups. The C-O-C skeletal vibrations at 1152 cm^{-1} present in native starch are still present in the oxidized samples, confirming the preservation of the polymer structure of the oxidized products, so that the depolymerization processes were negligible. Figure 3b shows the ^{13}C NMR spectra of the native starch and the oxidised sample. The original sample shows a typical spectrum of starch with peaks from C6 at 63 ppm, C1 at 102 ppm and those from C2, C3, C4 and C5 between 72-79 ppm. After PINO oxidation, the almost complete disappearance of the peak at 63 ppm is clearly visible, and a new and strong peak is detected at 178 ppm, due to the newly formed -COOH group.

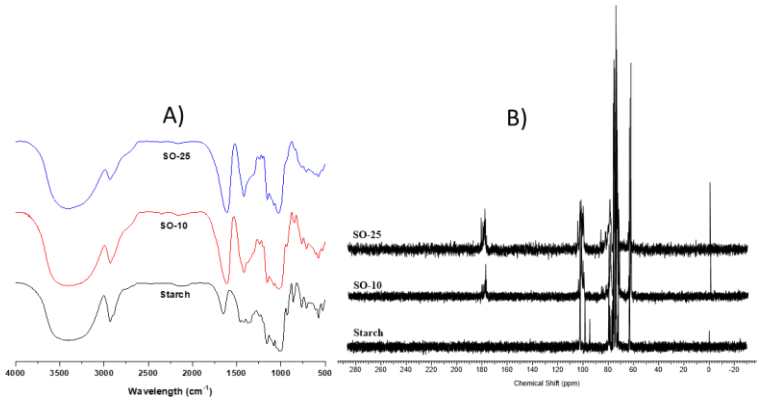

Figure 3. (a) FTIR spectra of the native starch and its PINO-oxidized correspondents; (b) NMR spectra of the native starch and its PINO-oxidized correspondents.

The morphology of the starch granules was studied both before and after oxidation using the SEM technique. The SEM picture of the native potato starch shows a quite large distribution of particle size, 5–50 μm, being smooth and revealing no defects, Figure 4. The SEM images of oxidized materials indicate that oxidized starch retains its granular structure. As oxidation of starch progresses, surface defects appear, suggesting that the oxidation process starts on the granule surface. The oxidized material with high substitution degrees along with defects on the surface contains some pores, suggesting that oxidation progresses from a given surface site to form a pore.

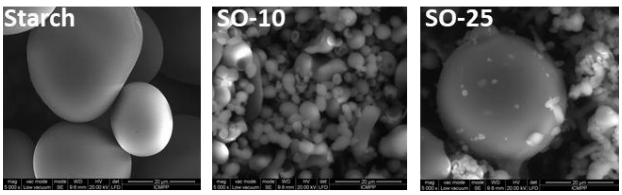

Figure 4. SEM microphotographs of starch before and after PINO-mediated oxidation

4. Conclusions

The starch oxidation method that we propose for the first time can be used successfully when it is desired to obtain a selectively oxidized assortment at the primary OH groups in the starch structure by choosing the reaction conditions (oxidant concentration, time, temperature) and being able to manipulate the content of carboxylic groups formed.

Acknowledgements

This work was supported by grants of the Ministry of Research, Innovation and Digitization, CNCS/CCCDI-UEFISCDI, project number PN-III-P1-1.1.-TE-2021-0597, within PNCDI III.

References

[1]. Coseri S. Phthalimide-N-oxyl (PINO) radical, a powerful catalytic agent: its generation and versatility towards various organic substrates. *Catal Rev*. 51, 218-292, 2009
[2]. Coseri S. A new and efficient heterogeneous system for the phthalimide *N*-oxyl (PINO) radical generation. *Eur J Org Chem*. 2007, 1725-1729, 2007
[3]. Coseri S. N-Hydroxyphthalimide (NHPI)/lead tetraacetate reactions with cyclic and acyclic alkenes. *J. Phys. Org. Chem*, 22, 397-402, 2009
[4]. Tomasik P, Schilling CH. Chemical modification of starch. *Adv. Carbohydr. Chem. Biochem*. 59, 175-403, 2004

PHYSICOCHEMICAL INVESTIGATION OF PLASMA-TREATED POLYMER SOLUTIONS FOR CANCER TREATMENT

Camelia Miron,[1]* Luminita Marin,[2] Valeria Harabagiu,[3] Adrian Fifere,[4] Mariana Pinteala,[4] Du Lyin,[1] Taishi Yamakawa,[1] Takashi Kondo,[1] Hiroki Kondo,[1] Shinya Toyokuni,[1,5] Masaaki Mizuno,[6] Hiromasa Tanaka,[1] Masaru Hori[1]

[1]Center for Low-temperature Plasma Sciences, Nagoya University, Nagoya, Japan
[2]Polycondensation and Thermostable Polymers Department,
Petru Poni Institute of Macromolecular Chemistry, Romanian Academy, Iasi, Romania
[3]Inorganic Polymers Department,
Petru Poni Institute of Macromolecular Chemistry, Romanian Academy, Iasi, Romania
[4]Centre of Advanced Research in Bionanoconjugates and Biopolymers Department,
Petru Poni Institute of Macromolecular Chemistry, Romanian Academy, Iasi, Romania
[5]Department of Pathology and Biological Responses, Nagoya University,
Graduate School of Medicine, Nagoya, Japan
[6]Center for Advanced Medicine and Clinical Research, Nagoya University Hospital,
Nagoya, Japan
**camelia@plasma.engg.nagoya-uac.jp*

1. Introduction

Chitosan, a polycationic biopolymer derived from natural chitin, has been considered a promising material for medical applications (such as drug delivery systems with antitumor activity), as it possesses unique properties such as biocompatibility, biodegradability, nontoxicity, mucoadhesion, and rich bioactivity including antioxidant, antimicrobial and antitumor properties [1-2]. Despite its unique physicochemical and biological properties, chitosan has not been extensively utilized in the clinic due to its poor mechanical properties and low solubility in water caused by the strong hydrogen bond network.

In this study, we present a method for structural modification of water-insoluble low-molecular-weight chitosan (190 kDa) by plasma discharges and generation of chitooligosaccharides (COS) with a selective cytotoxic effect on cancer cells. Solutions of chitosan 0.5% diluted in glacial acetic acid (1%) were irradiated by plasma formed in argon and a mixture of argon with nitrogen. The antitumor effect of cold atmospheric plasma-treated chitosan solution on breast cancer cell lines (MCF-7) and its selectivity in killing these cells, compared to non-tumorigenic epithelial cell lines (MCF-10A) was investigated.

2. Experimental

Plasma was ignited between stainless steel electrodes using a pulse power supply set at a peak-to-peak voltage of 9 kVp–p (Fuji Co., Ltd., Aichi, Japan). The repetition frequency was set to 9 kHz. Argon gas (99.998%) with a flow rate of 10 slm was used for purging the chamber (0.11 m^3) for 5 min. After purging, the argon gas was also mixed with nitrogen gas and delivered to the plasma chamber at different flow rates (Ar 1 slm, Ar/N_2 0.9/0.1). A quartz dish was used to irradiate for 5 minutes 8 mL of chitosan 0.5% diluted in acetic acid 1%. The plasma irradiated samples were investigated by LC-MS/MS, HPLC-ECD, and ESR, while the effect on the normal (MCF-10A) and cancer cells (MCF7) was tested by MTS assay.

3. Results and discussion

Cell viability was tested on the non-tumorigenic epithelial cell line (MCF-10A) and breast cancer cell line (MCF-7) by MTS assay. The plasma-treated chitosan solutions were prepared by irradiation of the chitosan solution (0.5%) with the non-thermal plasma (ignited in pure Ar, Ar/N_2 0.9/0.1 gas) for 5 min (Figure 1). The treated solutions were up to 16 times diluted in medium DMEM (-). The control sample was incubated with the DMEM (-) culture medium. The MTS assay results showed that both types of cells were entirely killed when incubated with plasma-treated solution diluted up to 16-fold for Ar plasma (Figure 1a). The 32-fold dilution showed selectivity, the normal cells were unharmed, while the cancer cells were killed (MCF-7 cell viability of 10.89 ± 2).

When nitrogen was added to the gas mixture, the normal cells were viable even at the 4-fold diluted sample, while the cancer cells were mostly killed (Figure 1b). The MCF-10A cells viability was 101.08 ± 9.5% and 104.76 ± 6.4% for the 8-fold and 16-fold diluted Ar/N_2 plasma irradiated solutions, while the MCF-7 cells were almost entirely killed, the highest viability being measured for the 16-fold sample (58.79 ± 8.3%).

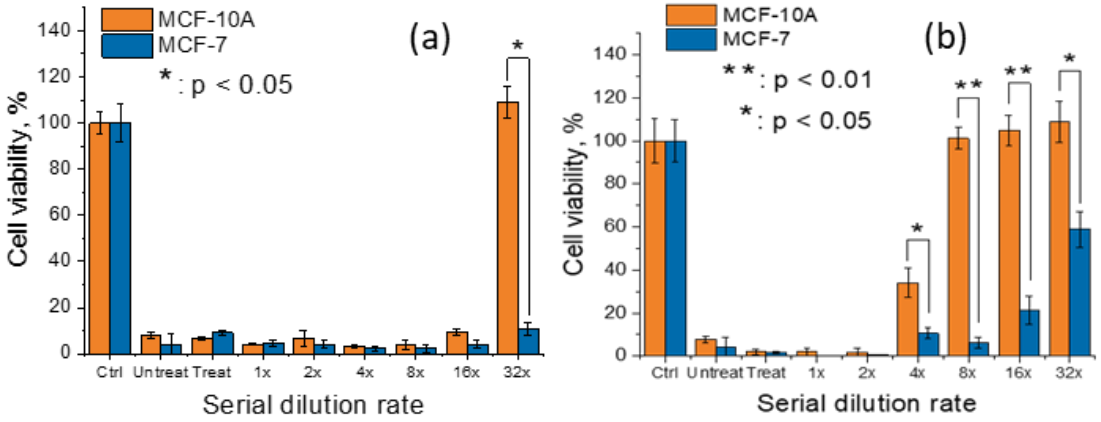

Figure 1. Cell viability tests of MCF-10A and MCF-7 cell lines conducted after incubation in untreated chitosan 0.5% (Untreat) and plasma-treated chitosan 0.5% (Treat) of **(a)** Ar and **(b)** Ar/N_2 samples, as well as in serially diluted chitosan solutions (1-fold to 32-fold diluted plasma treated samples in DMEM (-)).

The IDA TOF-MS ion scan mode for the control and plasma-treated solutions is shown in Figure 2a. After plasma irradiation, several compounds were generated, the most obvious in the mass spectra being chitosan oligosaccharides, such as chitobiose ($[C_{12}H_{24}N_2O_9\text{-}H]^-$, m/z 339.32, and $[C_{16}H_{28}N_2O_{11}\text{-}H]^-$, m/z 423.17), chitotriose ($[C_{18}H_{35}N_3O_{13}\text{-}H]^-$, m/z 500.209), chitotetraose ($[C_{24}H_{46}N_4O_{17}\text{-}H]^-$, m/z 661.27). This shows that chitosan was depolymerized in the plasma. The pH value of the control chitosan sample (3.63) has not changed much for the Ar (3.69), ArN_2 (3.72) plasma-treated samples. On the other hand, hydrogen peroxide (H_2O_2) was generated in Ar (1802.8 µM), Ar/N_2 (633.6 µM) in quite high concentrations. It is well known that H_2O_2 is inducing chitosan degradation by increasing the OH• radicals in the system, resulting in the formation of glucosamine and chitooligosaccharides [3]. Reactive oxygen species (ROS) are also generated in plasma [4]. OH•, O_2·-, and $^1O_2$ played important roles in chitosan depolymerization by attacking the amorphous structure of chitosan, resulting in the breakage of the intra- and intermolecular hydrogen bonds and β-(1,4) glycosidic bonds. Chitooligosaccharides (COS) effect on the MCF-10A and MCF-7 cells was also investigated by MTS assay (Figure 2). The initial concentration of

COS prepared was 50 mg/mL and it was up to 64-fold (0.78 mg/mL) diluted in DMEM (-). No selectivity could be observed for the concentrations in the range of 0.78 mg/mL to 12.5 mg/mL. A good killing effect on cancer cells was observed for the 25 mg/mL sample (viability of 17.49 ± 5.97), while the normal cells were almost unaffected (86.17 ± 10.37). The 50 mg/mL sample has also shown selectivity, but the viability was reduced to less than half for the MCF-10A cells (40.81 ± 7.97).

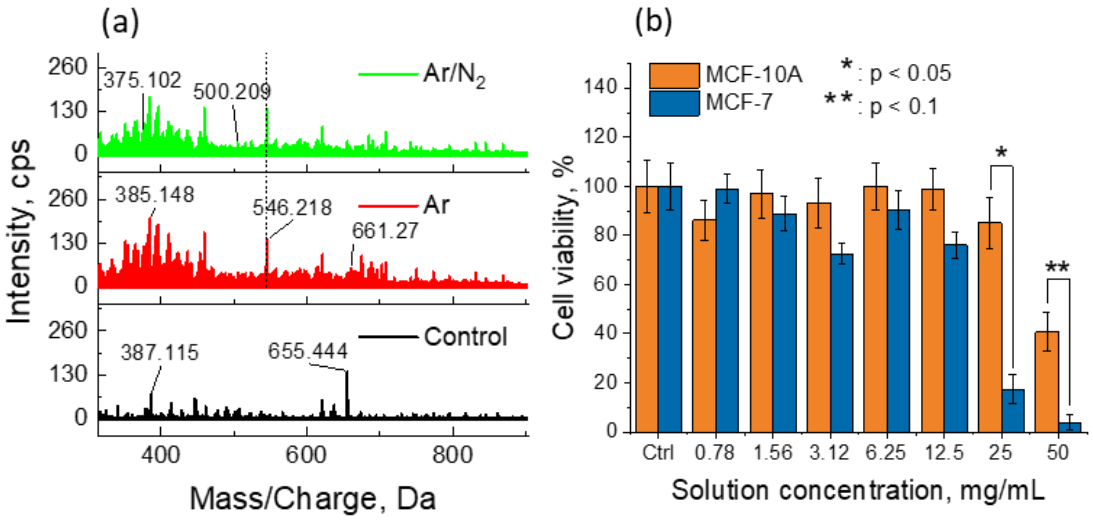

Figure 2. Mass spectra of control and plasma-treated chitosan and MTS assay of untreated chitooligosaccharides identified in the mass spectra of both treated samples. (a) LC-MS of untreated chitosan (control) and Ar, Ar/N_2 plasma-treated chitosan. (b) Cell viability tests of MCF-10A and MCF-7 cell lines were conducted after incubation in untreated chitooligosaccharides 50 mg/mL diluted in DMEM (-) up to 0.78 mg/mL.

4. Conclusions

It may be concluded that a variety of chemically active species are generated in chitosan solutions irradiated by Ar and Ar/N_2 plasmas, such as glucose and chitosan oligosaccharides. These compounds selectively killed the MCF-7 cancer cells, leaving the normal cells unharmed, depending on the concentration. The adjustment of the plasma parameters may give the possibility of engineering liquids that induce the desired effect on cells.

Acknowledgments

This study was supported by JSPS-KAKENHI nos. 19H05462, 17H02805, 20H00142, 21H04451.

References

[1]. Shiwei N, G RW, Jianrong W, Junzi W, Xuejing Z, Hong Z, Shude L, Li-Min Z. A novel chitosan-based nanomedicine for multi-drug resistant breast cancer therapy. *Chem. Eng. J.* 369, 134-149, 2019
[2]. Olaru AM, Marin L, Morariu S, Pricop G, Pinteala M, Tartau-Mititelu L. Biocompatible chitosan based hydrogels for potential application in local tumour therapy. *Carbohydr. Polym.* 179, 59-70, 2018
[3]. Wang D, Song R, Yue Liu, Ren J, Zhang Y, Wang T, Qu G. Simultaneous production of low molecular weight chitosan and reducing sugar via high molecular chitosan depolymerization by surface discharge plasma. *J. Cleaner Prod.* 316, 128295, 2021
[4]. Miron C, IshikawaK, Kashiwagura S, Suda Y, Tanaka H, Nakamura K, Kajiyama H, Toyokuni S, Mizuno M, Hori M. Cancer-specific cytotoxicity of Ringer's acetate solution irradiated by cold atmospheric pressure plasma. *Free Radical Res.* 57, 91-104, 2023

VISCOSITY AND FLOCCULATION PROPERTIES OF SOME CATIONIC PULLULAN DERIVATIVES

Maria-Magdalena Nafureanu,* Marieta Constantin, Luminita Ghimici
Petru Poni Institute of Macromolecular Chemistry, Romanian Academy, Iasi, Romania
**nafureanu.magda@icmpp.ro*

1. Introduction

Increasing interest for ionic polysaccharide derivatives investigation is based on their friendly behavior with environment and living organisms due to their non-toxicity, low price, biodegradability, etc. The content of ionic groups and salts concentrations have a great impact on the chain conformation which, at its turn, plays an important role for their performances in various practical applications, including the flocculation process.

In this context, the viscometric and flocculation behavior of some cationic pullulan derivatives with pendant quaternary ammonium salt groups, trimethylammonium propyl carbamate chloride ($TMAP_x$-P) was followed in water and salt solutions. The viscometric data have been interpreted in terms of the Wolf and Fedors models. The fungicide particles Bordeaux Mixture – *BM*, Dithane M45 – *Dt*, Melody Compact 49 WG – *MC* were chosen as contaminants in order to test the polymer ability to remove them from model suspensions.

2. Experimental

Materials

Cationic pullulan derivatives with different content of pendant quaternary ammonium groups (*$TMAP_x$-P*) prepared by chemical modification of Pullulan (Mw = 200 kg·mol^{-1}) (Figure 1).

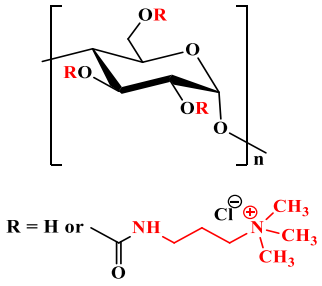

Figure 1. Chemical structure of the *$TMAP_x$-P* sample

Fungicides: Bordeaux mixture MIF type (IQV, Spain) (*BM*) – 20% copper as copper sulfate, Dithane M45 (Dow Agro Sciences) (*Dt*) – mancozeb as active ingredient, Melody Compact 49 WG (Bayer) (*MC*) – copper oxychloride and iprovalicarb, as active ingredients. *Salts:* NaCl, Na_2SO_4 (Sigma-Aldrich Chemie Gmbh, Steinheim, Germany), NaBr, $NaNO_3$ (Acros Organics, Geel, Germany), NaI (abcr GmbH, Karlsruhe, Germany) and Na_3PO_4 (Chempur Jana Lortza, Poland).

Methods

Viscometric measurements of the polysaccharide derivative solutions were performed at 25 °C by using an Ubbelohde suspended level viscometer (SCHOTT Geräte). Solutions of known polymer

concentrations (c_p = 0.5 g·dL^{-1}), were prepared either in pure Millipore-Q water or salt solutions of different concentrations, c_s = 4·10^{-5}M÷1M).

The flocculation tests were carried out at room temperature, in a Cole Parmer stirrer/hotplate with 9 places. The suspension of fungicides particles were placed into 100 mL beakers (50 mL each). Different volumes of TMAP$_x$-P solution were added to fungicide suspension under vigorous stirring (500 rpm) which was kept for another 3 min. Then the stirring speed was reduced to about 200 rpm for 15 min after which the suspension was left to settle.

The separation efficiency data, in terms of optimum dose ($dose_{op}$) or removal efficiency (%), and those regarding the possible mechanism of particle separation were collected by means of UV-Vis spectroscopy, zeta potential and particle aggregates size measurements.

3. Results and discussion

The viscosity measurements reveal a tipical polyelectrolyte behavior for TMAP$_x$-P in water and salt solutions with c_s = 4·10^{-5} and 1·10^{-3} M. Therefore, in order to find out the intrinsic viscosity ([η]), the Wolf and Fedors methods were used. The intrinsic viscosity decreased with ionic group content and salt concentration as shown in Table 1.

Table 1. Intrinsic viscosity ([η]) obtained by Wolf and Fedors methods for TMAPA$_x$-P in water and salt solutions

Polymer in water	$[\eta]_w$ (dL·g^{-1})[1]	$[\eta]_F$ (dL·g^{-1})[1]
TMAP$_{0.2}$-P	24.63	21.72
TMAP$_{0.4}$-P	28.51	28.40
TMAP$_{0.7}$-P	33.36	32.27

TMAP$_{0.4}$-P in NaCl c_s (mol·L^{-1})	$[\eta]_w$ (dL·g^{-1})[1]	$[\eta]_F$ (dL·g^{-1})[1]
4·10^{-5}	23.32	24.67
1·10^{-3}	8.68	8.88
1·10^{-2}	2.54	2.19
1·10^{-1}	0.92	1.13
1	0.61	0.59

[1] Intrinsic viscosity determined by Wolf [1] and Fedors [2] method.

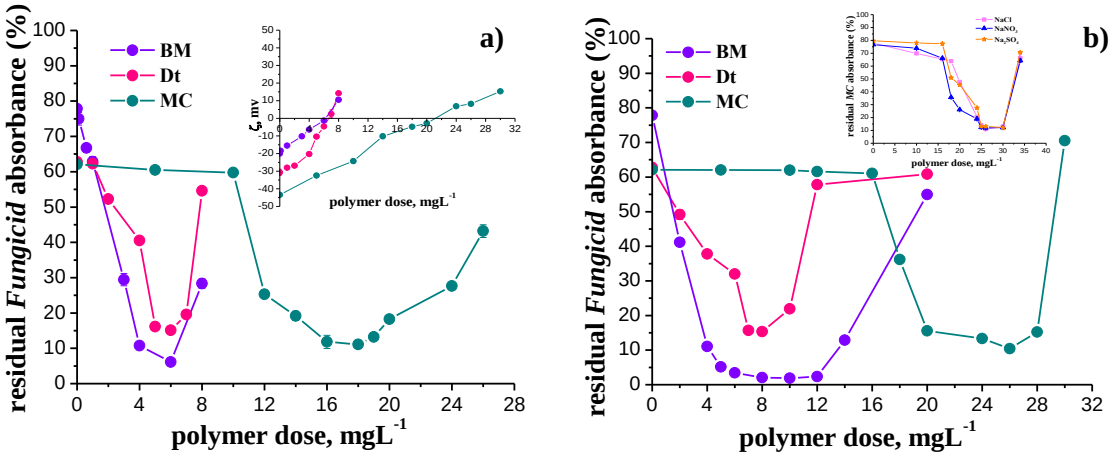

Figure 2. Dependence of residual absorbance (%) of fungicide dispersions on polymer dose: (a) TMAP$_{0.7}$-P, the insert: zeta potential (ζ); (b) TMAP$_{0.4}$-P, the insert: in the presence of salts

Zeta potential measurements indicated that the charge neutralization was the main mechanism involved in the fungicide separation process (ζ values close to zero recorded at $dose_{op}$).

The UV-Vis spectroscopy data presented in Figure 2 (a, b) emphasized a significant decreased of residual fungicide absorbance (%) with the polymer dose until the next minima values were obtained 15% for *Dt*, 6% for *BM* and 11% for *MC*. The $dose_{op}$ values were lower for the highest charged sample ($TMAP_{0.7}$-P). The addition of salts had a minor impact on the flocculation efficiency of $TMAP_{0.4}$-P; the residual fungicide content decreased in the order: *BM* > *MC* > *Dt*, for both polymer samples.

4. Conclusions

The viscometric behavior of the pullulan derivatives have been well described by Wolf and Fedors model.

All the fungicide particles have been successfully removed at $dose_{op}$ values between 6 $mg \cdot L^{-1}$ and 26 $mg \cdot l^{-1}$ (removal efficacy: *Dt* = 85%, *BM* = 94%; *MC* = 89%) where the aggregate sizes (D50) were 10.22 μm - 27.06 μm.

Acknowledgements

This work was supported by Ministry of Research, Innovation and Digitization, CNCS/CCCDI – UEFISCDI, project number PN-III-P4-ID-PCE-2020-0296, within PNCDI III.

References

[1]. Wolf BA. Polyelectrolytes revisited: Reliable determination of intrinsic viscosities. *Macromol Rapid Commun.* 28(2),164-170, 2007

[2]. Fedors RF. An equation suitable for describing the viscosity of dilute to moderately concentrated polymer solutions. *Polymer* 20(2), 225-228, 1979

EFFECT OF PREPARATIVE METHODS ON THE CHARACTHERISTICS OF ZnO NANOPARTICLES

Viorica Elena Podasca,* Andreea Laura Chibac-Scutaru, Violeta Melinte
Polyaddition and Photochemistry Department,
Petru Poni Institute of Macromolecular Chemistry, Romanian Academy, Iasi, Romania
**podasca.viorica@icmpp.ro*

1. Introduction

Environmental pollution is one of today's top problems since the discharge of organic hazardous pollutants in the surrounding environment have a detrimental effect on both public health and the ecosystem. Literature data report numerous photocatalyst from metal-oxide semiconductors category (TiO_2, ZnO, CeO_2) appreciated for their low cost and easy availability. However, the main drawback of these NPs is their large band gap (above 3.2 eV) which has resulted in inefficient solar energy use, which is why recent studies are focused on shifting their absorption beyond the UV region to benefit from visible light.

ZnO nanomaterials displayed outstanding chemical and physical characteristics, including chemical and thermal stability, nontoxicity, and cost efficiency, corroborated with a wide diversity of preparative methods (chemical precipitation, solvothermal, hydrothermal, sol-gel, microemulsion or green methods) and numerous application areas (UV-blocking agents, antibacterial and antifungal materials, chemical sensors, photocatalysts). The use of inorganic nanoparticles as photocatalysts is frequently accompanied by various drawbacks, especially their aggregation, which reduced the surface area and indirectly the photocatalytic ability, besides their difficult and expensive recovery and reuse operations.

Immobilizing photocatalysts on a variety of substrates, such as glass, carbonaceous substances, zeolites, ceramics, cellulosic materials, or polymers, is an effective technique to overcome these issues [1]. Given the great qualities such as high processability, film forming abilities, architectural diversity, and low cost, polymeric materials were extensively employed as templates to integrate inorganic nanoparticles. However, for an improved compatibility between phases, inorganic nanoparticles must be chemically modified with versatile organic molecules, often of trialkoxysilane type, to create covalent siloxane bonds on the surface of the nanoparticles [2].

Based on the aforementioned information, this study presents the design and preparation of a series of ZnO NPs. The effect of synthesis parameters on the dimensions and morphology of ZnO NPs will be studied in this work, together with their methodical characterization for the assessment of their structural, morphological and optical characteristics. Further, the as-prepared nanoparticles will be surface modified with silane derivatives for subsequent integration in polymeric supports, with the goal of avoiding nanoparticles agglomeration, translating photocatalytic activity towards visible light, and facilitating catalyst reusability/recovery after photocatalytic cycles.

3. Results and discussion

This study reports the preparation of 3 ZnO samples using various preparative conditions, according to the data from Table 1. The initial evaluation of the prepared samples, to confirm the proposed structures, was carried out using FTIR spectroscopy and X-ray diffraction (Figure 1).

Table 1. The experimental parameters used in the preparation of zinc oxide nanoparticles.

Sample	Precursors	Temperature (°C)	Time (h)
ZnO-1	$Zn(NO_3)_2$ x 6 H_2O	90	4
ZnO-2	$Zn(CH_3COO)_2$ x 2 H_2O	90	5
ZnO-3	$Zn(CH_3COO)_2$ x 2 H_2O	25	5

The analysis of the FTIR spectra (Figure 1a) showed the presence of absorption bands characteristic of the Zn-O bond in the region 600-400 cm^{-1} for the ZnO samples. The crystalline structure of ZnO NPs was evaluated by X-ray diffraction (XRD), the recorded diffractograms being illustrated in Figure 1b. The displayed spectra show sharp peaks, indicating a high degree of crystallinity, the main diffraction peaks appearing at 2θ angles of 31.9°; 34.5°; 36.4°; 47.7°; 56.7°, 63.0°; 66.5°; 68.1° and 69.2° are attributed to the crystal planes (100), (002), (101), (102), (110), (103), (200), (112) and (201) of the structure hexagonal wurtzite ZnO (JCPDS no. 5-0664).

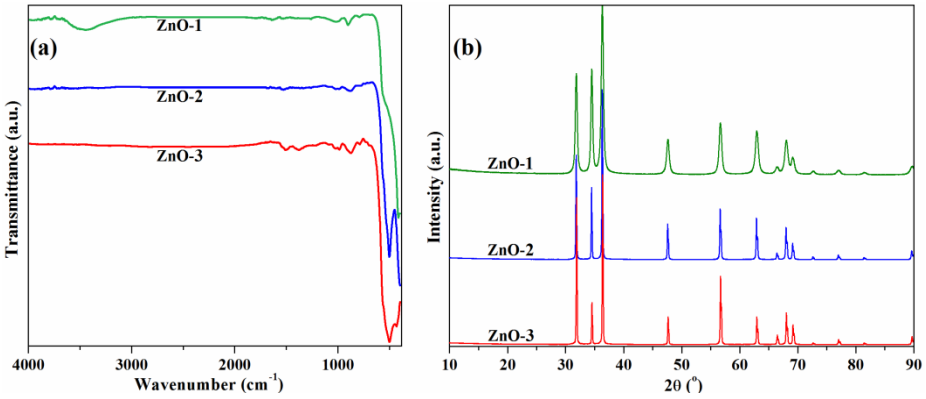

Figure 1. FTIR (a) and XRD (b) spectra for the synthesized zinc oxide nanoparticles.

The functionalization of ZnO nanoparticles with silane-type units and iodide ions was proposed as a convenient method of linking the inorganic units to various polymeric chains, aiming in this way for a better dispersion of the nanoparticles in the organic matrix and preventing their migration during photocatalytic activity testing (Figure 2).

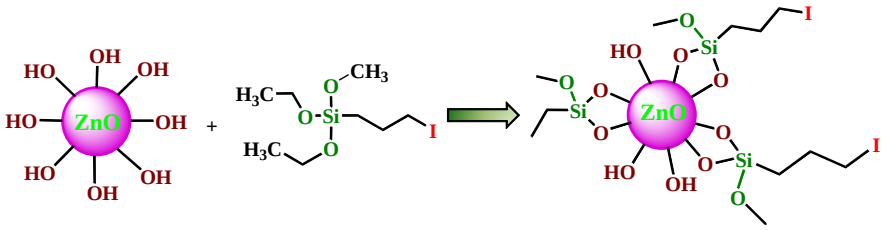

Figure 2. Functionalization of ZnO NPs with 3-iodopropyl trimethoxysilane.

The success of functionalization was easily evaluated by ATR-FTIR spectroscopy (Figure 3a). In addition to the presence of the absorption band characteristic to the Zn-O bond centered at 500 cm^{-1}, in the spectrum of the ZnO-2_I sample there are also bands at 3444 cm^{-1} and 1620 cm^{-1} given by the entrapped molecular water that appeared after the condensation process and which is embedded on the surface of the nanoparticles and the bands at 2928 and 2842 cm^{-1}, characteristic to the C-H bonds in the structure of the silane derivative, as well as the bands at 1208, 1064 and 808 cm^{-1} attributed to the asymmetric and symmetric vibrations of the Si-O-Si and Zn bonds -O-Si formed after functionalization.

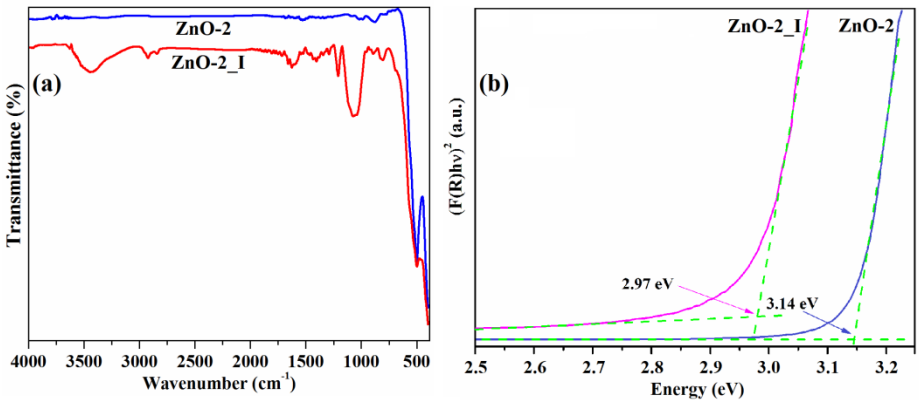

Figure 3. FTIR (a) and Kubelka-Munk diagrams (b) for the pristine and functionalized ZnO nanoparticles.

The band gap energy (E_g), an important parameter in the evaluation of the photocatalytic activity under different types of light was determined according to the Kubelka-Munk equation [3]:

$$(h\upsilon\ F(R))^2 = A\ (h\upsilon - E_g)$$

where $F(R) = (1 - R)^2 / 2R$, h is Plank's constant, υ is the frequency of light, A is the absorption coefficient and E_g is the bandgap energy. From the graphs illustrated in Figure 3b, it can be observed that the E_g value of the initial ZnO nanoparticles is 3.14 eV, and through functionalization with a silane-type derivative, the E_g value decreases to 2.97 eV, a reduction that can be attributed to the formation of metal-metal bonds of Si atoms with ZnO.

4. Conclusions

The presented research study describes a preparation of a series of ZnO nanoparticles, synthesized using various preparative conditions, their characterization being carried out by specific analytical methods (FTIR spectroscopy, X-ray diffraction) to confirm the structure and purity of the achieved samples. It should be pointed out that the estimation of the band gap energy values by means of Kubelka-Munk equation shows that they vary for ZnO NPs between 3.14 and 3.21 eV, and after functionalization with a silane-type derivative, the Eg value decreases to 2.97 eV, suggesting a possible photoexcitation of these ZnO NPs by photons from the visible domain.

Acknowledgements

This work was supported by a grant of the Ministry of Research, Innovation and Digitization, CNCS - UEFISCDI, project number PN-III-P4-PCE-2021-0933, within PNCDI III.

References

[1]. Srikanth B, Goutham R, Badri Narayan R, Ramprasath A, Gopinath KP, Sankaranarayanan AR. Recent advancements in supporting materials for immobilised photocatalytic applications in waste water treatment. *J. Environ. Manage*. 200, 60-78, 2017

[2]. Melinte V, Chibac-Scutaru AL, Culica ME, Coseri S. Mineralization versus photoreduction of 4-nitrophenol under the influence of surface functionalized CeO_2 nanoparticles, hosted by versatile cellulose supports. *Appl. Surf. Sci*. 565, 150494, 2021

[3]. Kubelka P. New contributions to the optics of intensely light-scattering materials Part II: nonhomogeneous layers. *J. Opt. Soc. Am.* 44, 330, 1954

FIXED- BED COLUMN STUDY FOR PB(II) REMOVAL FROM AQUEOUS SOLUTION USING SILICA COMPOSITE MICROPARTICLES

Ramona Ciobanu,[1]* Daniela Fighir,[1] Carmen Paduraru,[1] Florin Bucatariu,[1,2] Oana Plavan,[1] Andreea Gherghel,[1] Marcela Mihai,[1,2] Carmen Teodosiu[1]

[1]*Department of Environmental Engineering and Management, Cristofor Simionescu Faculty of Chemical Engineering and Environmental Protection, Gheorghe Asachi Technical University of Iasi, Romania*

[2]*Petru Poni Institute of Macromolecular Chemistry, Romanian Academy, Iasi, Romania*

**ramona.ciobanu@student.tuiasi.ro*

1. Introduction

The concern related to water contamination with heavy metal ions resulting from human activities increased in the recent years. These contaminants possess characteristics like persistency, toxicity, stability, low biodegradability, and bioaccumulative behavior, making them priority pollutants with significant implications for human health and water/wastewater treatment technologies [1]. According to Water Framework Directive chemicals are categorized into two primary lists of priority substances. The initial list, known as the “Black List”, encompasses hazardous priority substances recognized for their persistence, high toxicity, or potential for bioaccumulation. The second list, referred to as the “Grey List”, compiles priority substances that pose a notable environmental risk.

Heavy metal ions such as lead, nickel, cadmium etc., are often found in wastewater thus are one of the main subjects of many adsorption studies [2]. Moreover, they are associated with serious diseases, for example lead was found to be responsible for renal disturbances, hepatitis, encephalopathy, anemia, lung failure, bone lesions, and has been linked with certain human cancers [3]. The World Health Organization (WHO) recommends a maximum allowable lead concentration in drinking water of 0.01 mg/L [4]. Further, due to harmful impact of lead ions, governments have implemented environmental regulations concerning wastewater quality, compelling industries to eliminate these metals from their effluents prior to discharge. In this context, many researchers have been developed and used numerous water and wastewater treatment technologies such as membrane processes, ion exchange, coagulation and flocculation processes, oxidation processes and adsorption.

Adsorption is a widely used method in wastewater treatment due to its cost-effectiveness, efficiency, and ease of operation. Another strong advantage is the availability of a wide range of adsorbents. In this sense, activated carbon, zeolites, polymers, clays, biosorbents and nanoadsorbents, have been explored for the removal of priority pollutants. For example, a natural clay material was used as an adsorbent for Pb(II) removal from aqueous solutions, achieved adsorption capacity of 28.61 mg/g. A biosorption study of Pb(II) onto a brown macroalgae Fucus vesiculosus exhibited a maximum sorption capacity of 516.3 mg/g. Meanwhile, composite sorbents have gained popularity for their ability to combine the advantages of different materials, offering enhanced removal capabilities. Another research examined nanoparticles of hyperbranched polyethyleneimine/silica (PEI/Si) synthesized through a water-based sol-gel approach towards heavy metal ions. Exhibited a Langmuir sorption capacity for Pb(II) of 833.3 mg/g. Alternatively, polyethyleneimine-grafted graphene oxide (PEI/GO) proved effective Pb(II) removal in fixed-bed experiments. In terms of Freundlich isotherm model the maximum adsorption capacity achieved

64.94 mg/g. A bifunctionalized magnetic mesoporous silica (NZVI-SH-HMS) material was successfully used to remove Pb(II) from wastewater. The theoretical maximum adsorption capacity of NZVI-SH-HMS was 487.8 mg Pb(II)/g. Supplementary to batch studies, column adsorption experiments provide relevant insights into dynamic adsorption processes to large-scale wastewater treatment. Few studies have explored the continuous flow mode operation for lead removal. Notably, a mixture of magnetic graphene oxide (MGO) and sand proved effective results for Pb(II) removal in fixed-bed experiments with an adsorption capacity of 0.189 mmol/g. While, a fixed-bed column packed with activated bentonite displayed significant loading capacity of 21.359 mg/g for Pb(II) removal. In this research, the main objective was to remove lead ions Pb(II) from aqueous solutions using a novel composite sorbent with silica core and polyelectrolyte coacervate shell in fixed-bed column. Furthermore, the breakthrough behavior inside the column was investigated under pH variation.

2. Experimental

Adsorption experiments were carried out in an OMNIFIT column where ~0.7 g (10% organic fraction) of the composite IS/$(PEI\text{-}PAA)_c$ was added (Figure 1). The sorbent was obtained by direct deposition (one-pot approach) of polyethylenimine (PEI) and polyacrylic acid (PAA) interpolyelectrolyte coacervate $(PEI/PAA)_c$ onto silica inorganic substrate (IS). Then, the composite was cross-linked with glutaraldehyde (GA), at molar ratios r = [CHO] : $[NH_2]$ = 0.1. During the experiment, a peristaltic pump ensures a constant flow (2 mL/min) for the processing of 600 mL Pb(II) ion solutions (with initial concentrations of Pb(II) = 41.4 mg/L) inside the column. The heavy metal ions sorbed amount at equilibrium (q_e, mmol/g) was determined by using:

$$q_e = (C_0 - C_t)\cdot V/m \qquad (1)$$

where C_0 and C_t are the influent and effluent concentrations at a certain time of Pb(II) ions solution (mmol/L); V = volume of collected fraction (mL); m = amount of IS/$(PEI/PAA)_c$ – $r_{0.1}$ (mg).

The exhausted column was regenerated with 20 mL of HNO_3 solution (1 M) for Pb(II) ions extraction from composite, followed by 20 mL of NaOH (1 M) washing to composite activation. Between these stages, the composite was washed in column with deionized water (Adrona Crystal E, Grade I). The composite material was tested at both pH conditions to acid condition at pH=4 and alkaline condition at pH=10, respectively for a better understanding of the adsorption potential.

3. Results and discussion

Under dynamic conditions, a breakthrough curve is required to evaluate and to understand the sorption process and the composite microparticles limitation to load metal ions. The breakthrough curve is plotted as effluent concentration at a certain time (C_t) towards the effluent volume (Figure 2) and experimental parameters of the breakthrough curves are presented in Table 1. The breakthrough curve obtained for Pb(II) sorption onto IS/$(PEI/PAA)_c$ regenerated composite has a characteristic “S” shape and is dependent on the influent concentration. At a lower pH, the breakthrough point occurs slightly later. This behavior can be explained by the fact that the active sorption sites are more rapidly covered by the Pb(II). An increase of pH is associated with a higher amount of metal ions for the same quantity of sorbent and as result a smaller volume of synthetic aqueous solution was obtained before the sorbent became saturated. An increase of the Pb(II) sorption capacity was observed at higher pH value, since at pH=10 all amino groups of polycation chains are in a protonated form, while carboxylic groups of PAA and silanol groups of silica are negatively charged over a wide range of pH (pH >3.0) and favors the interaction with cations.

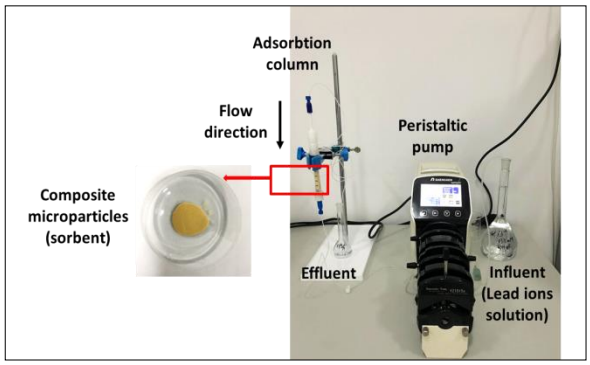

Figure 1. Dynamic adsorption of Pb(II) ions solution onto IS/(PEI/PAA)$_c$ composite microparticles

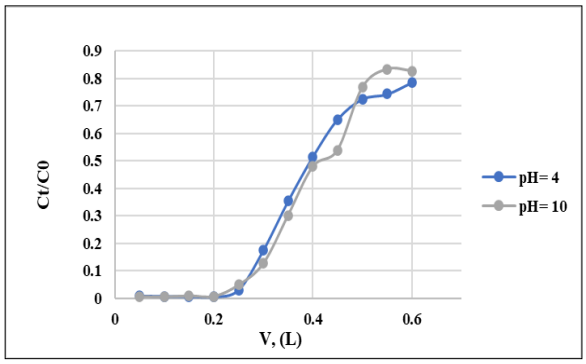

Figure 2. Breakthrough curves for sorption of Pb(II) onto IS/(PEI/PAA)c composite microparticles at different pH values

Table 1 Experimental parameters of the breakthrough curves for Pb(II) sorption

pH	C_0, mg/L	V_b (mL)	t_b (min)	q_b (mg/g)	V_s (mL)	t_s (min)	q_s (mg/g)
4	41.4	300	150	143.81	500	250	60.07
10	41.4	300	150	143.87	600	300	76.95

C_0 – influent concentration (mg/L); V_b – breakthrough volume (mL); t_b – breakthrough time (min); q_b – breakthrough sorbent capacity (mg/g); V_s – saturation volume (mL); t_s – saturation time (min); q_s – saturation sorbent capacity (mg/g).

4. Conclusions

The presented adsorption process was effective for the removal of lead ions from aqueous solutions. The results of the continuous studies using a fixed-bed containing silica composite microparticles showed the maximum adsorption capacity for Pb(II) of 218.73 mg/g at pH=4 and of 220. 82 mg/g at pH=10, respectively.

Acknowledgements

This work was supported by a grant of the Ministry of Research, Innovation and Digitization, CNCS/CCCDI–UEFISCDI, project number PN-III-P4-ID-PCE-2020-1199, within PNCDI III, contract PCE 56/2021, “Innovative and sustainable solutions for priority and emerging pollutants removal through advanced wastewater treatment processes” (SUSTINWATER).

References

[1]. Ahmed SF, Kumar PS, Rozbu MR, Chowdhury AT, Nuzhat S, Rafa N, Mahlia TMI, Ong HC, Mofijur M. Heavy metal toxicity, sources, and remediation techniques for contaminated water and soil. *Environ. Technol. Innov.* 25, 102114, 2022

[2]. Hargreaves AJ, Constantino C, Fotro G Cartmell E, Campo P. Fate and removal of metals in municipal wastewater treatment: a review. *Environ. Technol. Rev.* 7, 1-18, 2018

[3]. Boskabady M, Marefati N, Farkhondeh T, Shakeri F, Farshbaf A, Boskabady MH. The effect of environmental lead exposure on human health and the contribution of inflammatory mechanisms, a review. *Environ. Int.*, 120, 404-420, 2018

[4]. Lead in Drinking-water. Background document for development of WHO Guidelines for Drinking-water Quality. 2003.

HIGH PERFORMANCE AMORPHOUS POLYMER COMPOSITES

Diana-Ioana Bratilescu,[1]* Alexander Bismarck[1,2]
[1]*Polymer & Composite Engineering (PaCE) Group, Institute of Materials Chemistry & Research, Faculty of Chemistry, Vienna, Austria*
[2]*Department of Chemical Engineering, Imperial College of London, London, United Kingdom.*
**diana-ioana.bratilescu@univie.ac.at*

1. Introduction

Nowadays, carbon fiber-reinforced polymer composites represent one of the most advanced type of materials available. They are known for their exceptional mechanical properties and lightweight structure [1]. These properties lead to multiple applications in different sectors like the automotive, aerospace, construction, or sporting goods industry. Particularly for the aerospace industry, it is very important that the composite materials utilized do not only poses mechanical properties but are also heat resistant [2]. To that end, many high-performance thermoplastics such as poly(ether ether ketone) (PEEK), poly(ether sulphone) (PES), poly(phenylene sulphide) (PPS) have been explored as potential candidates [2,3]. Polyetherimide (PEI) represents a suitable choice to be a matrix for such composite materials exhibiting a high glass transition temperature of 217 ºC at relatively low cost compared to other high performance polymers such as PEEK or PES [3]. PEI possesses superior mechanical properties at temperatures up to 200 °C. Producing high T_g polymer composites is challenging [2]. Here, we present a simple method to produce carbon fiber-reinforced PEI tapes and laminates with 66 wt% carbon fibres using our purpose-build composite production line. The interface, microsection and mechanical properties of the resulting material are characterised.

2. Experimental

To produce carbon fiber-reinforced PEI composites, carbon fibers (Hexcel, HexTow® AS4D, 12 k) were first spread with an air-assisted fiber tow spreading unit (Izumi International Inc, US) to increase spacing between filaments. The width of the carbon fibers tow increased from 5 - 7 mm to 18 – 22 mm. The spread fibers were impregnated with the polymer by using the fibre impregnation line depicted in 1. Carbon fibres were placed into a continuous stirred aqueous resin impregnation bath containing 4.5 wt.% PEI and 0.45 wt.% surfactant (Cremophore A25 – Sigma Aldrich). The wet impregnated tow was passed through two infrared-ovens operated at 380 °C in which water was removed and the polymer melted. The impregnated tape, also called prepreg, was guided to a set of 3 cartridges operated at 260 °C with the purpose of smoothing the surface and removing the surplus polymer. Finally, the prepreg was collected on a winder. The impregnated tape containing 66 wt.% carbon fibers was cut and hot-pressed at 380 °C and 2 t for 60 minutes in a 12.5 x 2 x 0.22 cm mold.

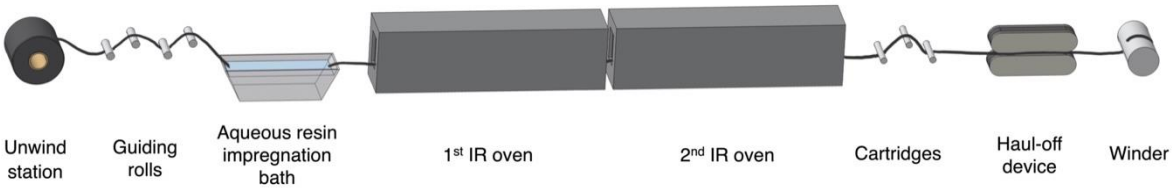

Figure 1. Schematic of powder impregnation composite production line.

Interfacial Characterization

The debonding behavior and interfacial properties were characterized by single fiber pull-out tests. A single carbon fibre taped onto a washer was embedded between 30 and 50 μm into molten PEI enclosed inside the cavity of a M3-type screw. After cooling down, the free-end of the carbon fibre was glued to a needle connected to a piezo-translator, while the screw containing the resin with the partially embedded fibre was screwed into a piezo-force meter. The force applied to the matrix-fibre interface was measured at a constant displacement rate of 1 μm/s with a 0.1 mN load cell. The applied force was measured as a function of the displacement, *S*. Multiple specimens were tested. Next, the maximum loads required to fully debond the fibre, F_{max}, were plotted against the embedded areas of the carbon fibre in the matrix, A_e, and the data was fitted to a linear curve. The apparent interfacial shear strength, τ, was obtained from the slope of that curve.

Composite Characterization

The density and void content of 2 x 1.2 x 0.22 cm the composite samples were determined using pycnometry (AccuPyc II 1350, Micrometrics Aachen, Germany) under helium. ASTM D2734-94 (Method A) was used as standard for the determination of the void content. The weight was determined using an analytical balance (Sartorius Cubis™ Series, model MSA225P, Göttingen, Germany).

The microsections of prepreg tape and unidirectional composites were analyzed under an optical microscope (DM2700M Leica with a DFC450 C Leica). Previous to that samples were embedded in EpoxiCure2 resin (Buehler, Düsseldorf, Germany) and cured for 24 hours. The samples were then grinded with varying grit size (Si P120, P320, P600, P1200 and P2500) and polished with diamond dispersions (9, 6 and 1 μm) on a Grinder Polisher Buehler machine.

The interlaminar shear properties of the CFR-PEI composites were tested through short beam shear tests following the ASTM D2344 standard. Prepregs of 2 x 1.2 x 0.22 cm were hot-pressed (Model 4126 Manual, Hydraulic Press, Carver, USA) in a metal mold. The tests were performed with a 10 kN load cell on a Instron machine (model 4502, Buckinghamshire, UK) with a span-to-thickness ratio of 5. Specimens were loaded at 1mm/min until failure. The short beam shear strength, F^{SBS}, was calculated using the following equation:

$$F^{SBS} = 0.75 \times \frac{P_m}{b \times d} \quad (1)$$

where P_m is the maximum load observed during testing, b is the measured specimen width and d is the measured specimen thickness. Five specimens were tested from each sample.

3. Results and discussion

Manufacturing of carbon fibre reinforced polyetherimide prepregs on the powder impregnation line depicted in Figure 1, imposed some difficulties regarding the sample manufacturing, namely resin uptake. This is shown in Figure 2. It can be clearly seen, that at first, the uptake of PEI was higher than the desired 66 wt% carbon fibres, which were achieved depending on the run between the 8th and 17th meter pulled. These irregularities can arise from the inhomogeneity of the resin bath, more precisely the choice or concentration of surfactant and affect the reproducibility of the experiments.

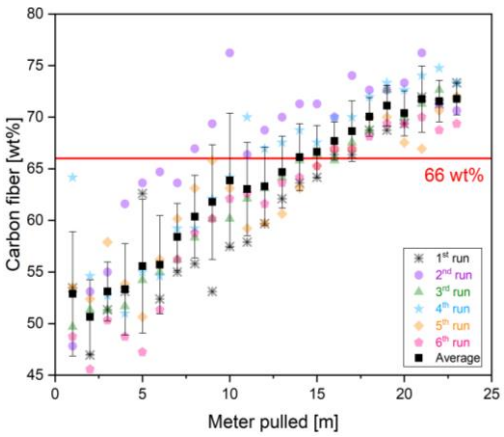

Figure 2. Uptake of PEI resin of the carbon fibres by each meter pulled during 6 consecutive runs and their average and standard deviation.

As illustrated in Figure 3, the optical microscopy images of the manufactured prepregs and laminates showed that carbon fibres were impregnated with polyetherimide, and the polymer was homogenously distributed. The voids that can be seen on the prepreg occurred most likely during the sample preparation for microscopy, which involves grinding and polishing. The single fibre pull-out tests and the short beam shear strength showed similar values of 43 ± 0.6 MPa and 44 ± 10.1 MPa, respectively.

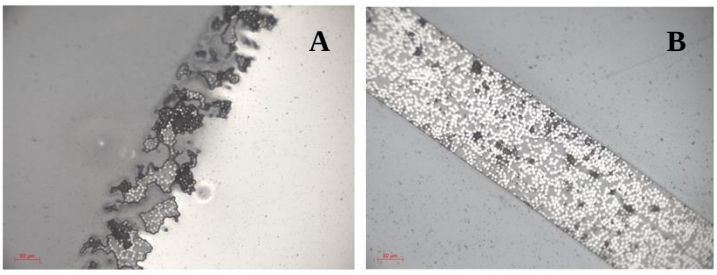

Figure 3. Microsections of A: prepreg, and B: laminate.

4. Conclusions

Carbon fibres-reinforced polyetherimide composites were successfully prepared using our powder impregnation line. The short beam shear of the composites was 44 ± 10.1 MPa. Future work will comprise upscaling on an industrial fibre processing line and investigate if PEI is a suitable matrix for nacre-like coated carbon fibres.

Acknowledgements

The authors kindly acknowledge University of Vienna for funding and SABIC for the PEI resin.

References

[1]. Åström BT. Manufacturing of Polymer Composites. 1st ed. Routledge; 1997
[2]. Gabrion X, Placet V, Trivaudey F, Boubakar L. About the thermomechanical behaviour of a carbon fibre reinforced high-temperature thermoplastic composite. *Composites, Part B*, 95, 386-394, 2016
[3]. Iredale RJ, Ward C, Hamerton I. Modern advances in bismaleimide resin technology: A 21st century perspective on the chemistry of addition polyimides. *Prog. Polym. Sci.*, 69, 1-21, 2017

SYNTHESIS, STRUCTURES AND ELECTROCHEMICAL INVESTIGATION OF IRON(II) COORDINATION COMPOUNDS WITH SEMICARBAZIDE DERIVATIVES LIGANDS

Gheorghe Ghiletchi,[1]* Tatiana Palamarciuc,[2] Oleg Palamarciuc,[2,3] Iuliana Besleaga,[3] Peter Rapta,[4] Sergiu Shova,[5] Vladimir Arion[3]

[1]*University of Vienna, Institute of Inorganic Chemistry, Vienna, Austria*
[2]*Moldova State University, Faculty of Physics and Engineering, Chisinau, Republic of Moldova*
[2]*Moldova State University, Faculty of Chemistry and Chemical Technologies, Chisinau, Republic of Moldova*
[3]*Institute of Physical Chemistry and Chemical Physics, Faculty of Chemical and Food Technology, Slovak University of Technology in Bratislava, Bratislava, Slovak Republic*
[4]*Institute of Physical Chemistry and Chemical Physics, Slovak University of Technology in Bratislava, Slovak Republic*
[5]*Inorganic Polymers Department, Petru Poni Institute of Macromolecular Chemistry, Romanian Academy, Iasi, Romania*
**ghiletchii.gheorghe@usm.md*

1. Introduction

Among the coordination compounds, the spin crossover compounds are one of the most representative examples of the molecular bistability. In this work, we present the synthesis of Fe(II) coordination materials which are able to switch between the paramagnetic (high spin S = 2) to diamagnetic (low spin S = 0) state and vice versa. This phenomenon implies significant magnetic, structural, electrical, optical and chromatic modifications. This opens up a plethora of potential applications in the fields of display, memory [1], nanoscience [2] as well as in the other areas.

Beside the fact that this phenomenon is known since 1931 [3] and hundreds of compounds were studied until now, just a little of them show bistability properties around room temperatures, property which is required for device applications [4]. Also, it was observed that, the transition temperature and cooperativity of a SCO systems are depending of intermolecular interactions in the crystal lattice and also by molecules themselves [5].

2. Experimental

Here, we study the interaction of $Fe(NCS)_2$ with tridentate ligands derived from 2-formylpyridine and 4-phenylsemicarbazide. In the process of synthesis, we employed direct synthesis and molecular assembly using different chemical techniques. The obtained products were separated by filtration, dried in vacuum and characterized by physico-chemical, elemental analysis, single crystal X-ray study and electrochemical investigations.

Cyclic voltammetric experiments with 0.5 mM solutions of studied compounds in 0.1 M n-Bu_4NPF_6 supporting electrolyte in acetonitrile were performed under argon atmosphere using a three-electrode arrangement with a platinum disk working electrode, platinum wire as a counter electrode, and silver wire as a pseudo reference electrode. All potentials in voltammetric studies were quoted vs ferricenium/ferrocene (Fc+/Fc) redox couple. A Heka PG310USB potentiostat with a PotMaster 2.73 software package served for the potential control in voltammetric studies.

In situ ultraviolet-visible-near-infrared (UV–Vis–NIR) spectroscopic and spectroelectrochemical measurements were performed on a spectrometer Avantes in 1 cm quartz cuvette or the spectroelectrochemical cell kit with the Pt-microstructured honeycomb working electrode. The cell was positioned in the CUV-UV Cuvette Holder connected to the diode-array UV–Vis–NIR spectrometer by optical fibres. UV–Vis spectra were processed using the AvaSoft software package.

3. Results and discussion

In this work, we present the synthesis, characterization and electrochemical investigation of a new series of materials, based on Fe(II) and semicarbazones organic ligands (SCZ) with the aim to obtain spin crossover system. These types of ligands were employed in different studies until now due to their remarkable biological, electrochemical and analytical properties [7].

We selected these types of ligands, based on the fact that: I) they are polydentate ligands and can coordinate to the metal center by NNO, N2 or N3 set of atoms in function of the nature of carbonyl used; II) also, we observed that in function of the ratio between metal, the nature of carbonyl and solvent employed during the syntheses, different architectures mono- or polynuclear can be obtained; III) the possibility of obtaining a wide range of new Fe(II) based materials with N-substituted semicarbazones ligands; IV) possibility to play with different carbonyl types ligands in order to influence the crystalline packing and intermolecular interactions of the materials with the aim of obtaining structure-properties interactions.

The Figure 1 shows the crystal structures of a two Fe(II) species: mononuclear **1** and binuclear **2**. Compound **1** are N4O2 coordination sphere: N2O from semicarbazide ligand, O – from methanol group and two thiocyanate groups. In the case of **2**, two mononuclear units N4O are dimerized via thiocyanate group. The iron center in **2** are N4OS coordinated. In all cases the iron center are in an octahedral geometry.

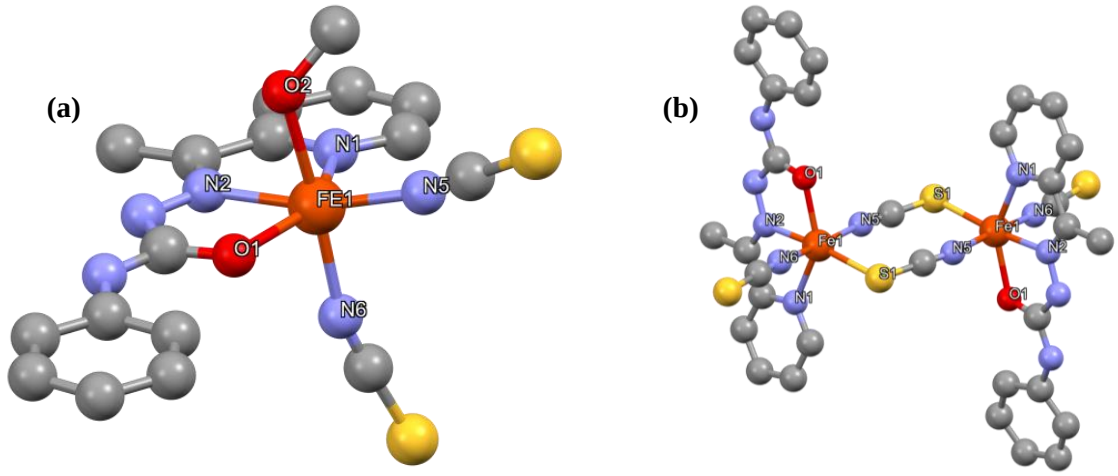

Figure 1. (a) Crystal structure of mononuclear compound (**1**) and (b) dinuclear assembly (**2**)

To investigate the redox behaviour of reported compounds in solutions, a detailed electrochemical studies were performed by cyclic voltammetry, as well as UV–Vis–spectroelectrochemistry in acetonitrile (MeCN). The potential separation between the first two oxidation peaks for dimeric forms of investigated Fe(II) complexes can be considered as a measure of the electron interaction in the corresponding oxidized dimeric forms in solution.

This was studied by the cyclic voltammetry of mononuclear and dinuclear complexes with identical

molar concentrations. The cyclic voltammograms of monomeric unit of **1** as well as its corresponding dimeric form **2** in MeCN/n-Bu_4NPF_6 at Pt working electrode (scan rate 100 mV s^{-1}) show in the anodic part at low oxidation potentials very similar almost reversible oxidation peak with anodic half-wave potential $E_{1/2}$ = +0.05 V vs Fc^+/Fc^0 (Figure 2a).

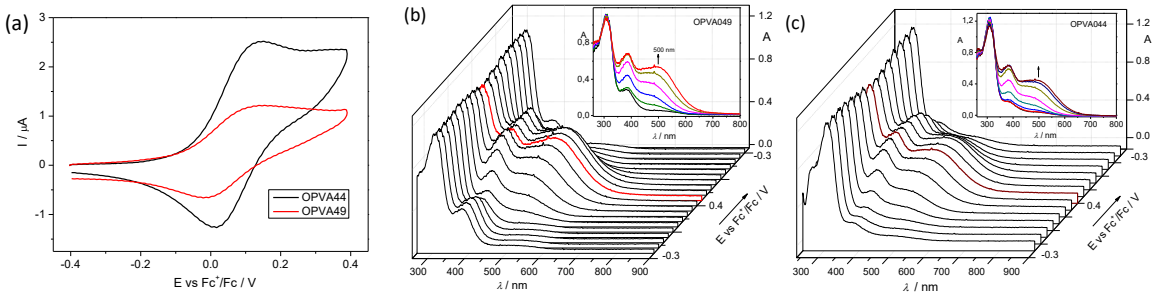

Figure 2. (a) Cyclic voltammetry of OPVA-49 (**1**) and OPVA-44 (**2**) in MeCN/n-Bu_4NPF_6 at Pt working electrode (scan rate 100 mV s^{-1}). (b) UV–Vis spectra detected simultaneously upon the cyclic voltammetric scan in the region of the first anodic peak of **1** (scan rate 10 mV s^{-1}, Pt-microstructured honeycomb working electrode) and of (c) **2** in MeCN/n-Bu_4NPF_6 (Insets: evolution of UV-Vis spectra in 2D projection in the forward scan).

4. Conclusions

In this work we present the synthesis, characterization and electrochemical investigation of new Fe(II) coordination compounds with polydentate organic ligands derived from semicarbazides. It was observed that in function of reaction conditions different mono or polinuclear materials can be obtained. For all obtained compounds were determinate the single X-ray structures and electrochemical investigations.

Acknowledgements

The authors of this study express their grateful thanks for the financial support to AUF - Soutien aux Equipes de Recherche en Europe Centrale et Orientale – SER-ECO project: Matériaux intelligents à transition de spin, synthèse, étude et caractérisation MatIntComp.

References

[1]. Kahn O, Martinez CJ. Spin-transition polymers: From molecular materials toward memory devices. *Science*. 279, 44-48, 1998
[2]. Molnar G, Salmon L, Nicolazzi W, Terki F, Bousseksou A. Emerging properties and applications of spin crossover nanomaterials. *J. Mater. Chem. C*. 2, 1360-1366, 2014
[3]. Cambi L, Gagnasso A. Iron dithiocarbamates and nitrosodithiocarbamates. *Atti. Accad Naz. Lincei.* 13, 809, 1931
[4]. Salitros I, Madhu NT, Boca R, Pavlik R, Ruben M. Room-temperature spin-transition iron compounds. *Monatsh. Chem.* 140, 695-733, 2009
[5]. Halcrow M. Structure:function relationships in molecular spin-crossover complexes. *Chem. Soc. Rev.*, 40, 4119-4142, 2011
[6]. Shepherd HJ, Palamarciuc T, Rosa P, Guionneau P, Molnar G, Letard JF, Bousseksou A. Antagonism between extreme negative linear compression and spin crossover in [Fe(dpp) 2(NCS) 2]·py. *Angew. Chem., Int. Ed.* 124, 3976-3980, 2012
[7]. Patel RN, Shukla KK, Singh A, Choudhary M, Chauhan UK, Dwivedi S. Copper(II) complexes as superoxide dismutase mimics: Synthesis, characterization, crystal structure and bioactivity of copper(II) complexes. *Inorg. Chim. Acta.* 362, 4891-4898, 2009

VERSATILE MAGNETIC FILMS INSPIRED BY NATURAL SOURCES

Ioana A. Duceac,* Raluca Ioana Baron, Gabriela Biliuta,
Maria Valentina Dinu, Sergiu Coseri
Petru Poni Institute of Macromolecular Chemistry, Romanian Academy, Iasi, Romania
**duceac.ioana@icmpp.ro*

1. Introduction

In the activities that make up our daily lives, polymers and polymer composites have gradually demonstrated their importance. High-performance cellulose (hydroxypropyl cellulose, HPC) is a derivative with remarkable properties such as biocompatibility [1], biodegradability [2], and even edibility [3]. As a result, this water-soluble polymer can now be used for a variety of industrial purposes, such as a thickening and stabilizing food, and as a bulking agent and drug release agent in pharmaceuticals [4]. Gelatin is a tasteless, colorless, water-soluble protein derived from the partial or complete hydrolysis of collagen and is a low-cost, readily available product. Gelatin's high availability and biocompatibility make it suitable for applications in food packaging and other industries [5]. It is often used as a polymer owing to its capacity to generate thermo-reversible gels and exhibit gelling ability. This trait, along with its melting point at body temperature, renders it very significant in many applications within the realms of food and pharmaceuticals [6]. Moreover, there has been a recent increased interest for bioadhesive materials, both polymeric and composite. Bioadhesion is a complex interfacial phenomenon, encompassing both the polymer behavior and available moieties, and the surface to which the material is put in contact with. In this context, the aim of this work was to prepare and characterize some new magnetic nanocomposite films based on HPC, gelatin, and magnetic nanoparticles.

2. Experimental

Materials: Gelatin (bovine, type B), HPC (average Mw ~ 80.000, average Mn ~ 10.000), TEMPO, NaBr, 15% NaClO, $NaIO_4$ and other chemicals and solvents were of pure grade (Sigma Aldrich), and were used as received. The water-based Fe_3O_4/OA.OA ferrofluid (Ms = 160 Gs, ρ = 1.1323 g/cm^3 at 26.3°C) was prepared at the Romanian Academy-Timisoara Branch according to the procedure described in detail in [7].

Oxidation of the HPC in the presence of $NaIO_4$ (*HPCoxP*): HPC (2 g) was dissolved in 200 ml of distilled water with vigorous stirring, and then $NaIO_4$ (5 mmol/g of HPC) was added. The reaction was carried out at R.T. in the dark for 24 hours. Throughout the reaction, the pH of the suspension was about 4. After 5 hours, the periodate excess was removed with ethylene glycol.

Oxidation of the HPC in the presence of TEMPO (*HPCoxT*): HPC (1 g) was dissolved in 400 ml distilled water under vigorous stirring. TEMPO (0.1 mmol/g HPC) and NaBr (10 mmol/g HPC) were added to the reaction mixture. A 15% NaClO solution (20 mmol/g HPC) was then added to the reaction. The pH was carefully maintained at about 10 by adding a 2M NaOH solution. The reaction was carried out for 2 hours at R.T. and then quenched by adding a few drops of ethanol.

Fabrication of the HPCox/GEL/MFs films: 0.15 g of oxidized HPC was dissolved in 15 ml Millipore water. GEL (0.4 g) was also dissolving in 20 ml Millipore water by magnetic stirring at temperature. The MFs was dispersed by sonication for 15 min before use. The solutions obtained in

this way were mixed in a ratio 1:1:2, and the obtained films were named as HPCoxP/GEL/MFs, and HPCoxT/GEL/MFs. Also, films were prepared without MFs, called HPCoxP/GEL and HPCoxT/GEL/MFs. The reaction mixture was transferred to a Petri dish and dried at room temperature until complete evaporation of the water, when flexible and homogeneous nanocomposite films were obtained.

Characterization: The FTIR spectra were recorded using a Bruker Vertex 70 spectrometer (Bruker) with 4000 ÷ 400 cm^{-1} scanning range. SEM and EDX analyses were obtained on an QUANTA200 scanning electron microscope coupled with an energy-dispersive X-ray spectroscope (FEI Company, 20 kV, low vacuum mode, LFD detector). Bioadhesion measurements were performed using a TA.XT texture analyzer; the samples were kept in contact with a cellulose membrane for 30 s. The force and work of adhesion were determined using the dedicated software of the instrument.

3. Results and discussion

In a first step, the secondary hydroxyl groups of the oligo(hydroxypropyl) chains are selectively oxidized to aldehyde groups in the presence of sodium periodate, with simultaneous cleavage of the C2-C3 linkage, and the primary available hydroxyl groups of HPC chains are selectively oxidized to carboxyl groups in the presence of TEMPO, sodium bromide, and sodium hypochlorite. In a second step, the oxidized HPC derivatives are mixed with GEL and MFs. The chemical structures of the polymers and magnetic nanocomposite films were characterized by FTIR, and the obtained spectra are shown in Figure 1a.

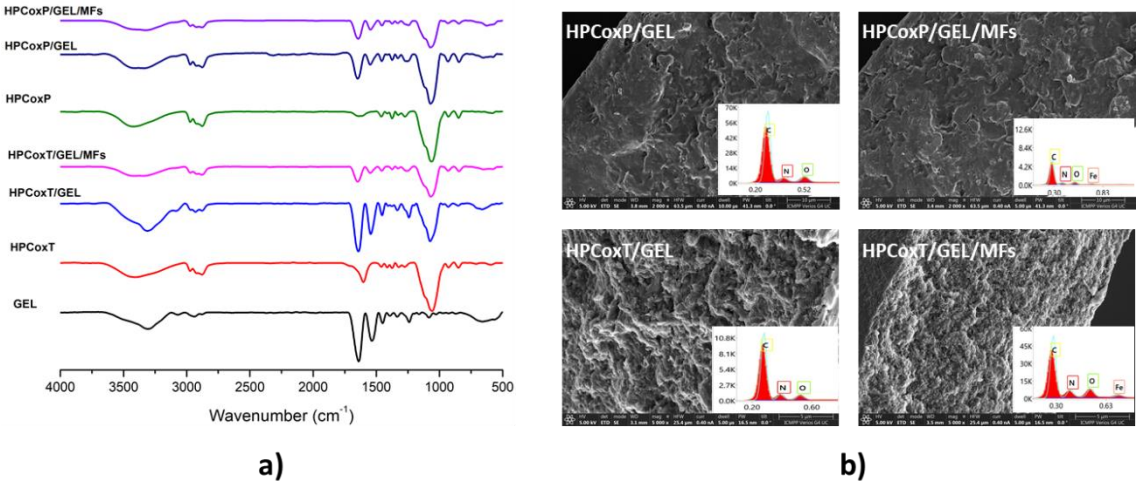

Figure 1. (a) Fourier transform infrared (FTIR) spectra and
(b) Energy-dispersive X-ray (EDX) spectra of HPC films.

The spectrum of GEL shows the characteristic bands at 3230 cm^{-1} (amide A), 1632 cm^{-1} (amide I), 1544 cm^{-1} (amide II), and 1237cm^{-1} (amide III). The film spectra retained these peaks, but at lower intensities. The films also exhibited the characteristic bands of HPC at 3445 cm^{-1} and 1085 cm^{-1} and shoulders at 2972 cm^{-1} and 2880 cm^{-1}. Complementary information on the chemical composition of the films was obtained by energy dispersive X-ray spectroscopy (EDX) on randomly selected areas of the films. In the EDX pattern of the HPCoxP/GEL and HPCoxT/GEL polymer blend films shown in Figure 1b, the main elements observed were carbon and oxygen, while the spectra of the nanocomposite films containing functionalized MFs (HPCoxP/GEL/MFs and HPCoxT/GEL/MFs) additionally showed signals specific for Fe, confirming that the MFs had been successfully loaded into the oxidized HPC/GEL polymer matrix.

Table 1. Bioadhesion properties of the nanocomposite films

Sample no.	1	2	3	4	5
Force (N)	0.06	2.95	2.68	2.83	2.94
Work (N*s)	0.20	1.84	5.13	1.34	3.14

The new magnetic nanostructured functionalized cellulose/gelatin-based composite films were tested in terms of bioadhesion. The results are in Table 1 and the samples are as follows: (1) cellulose membrane control; (2) HPCoxP/GEL/MFs nanocomposite; (3) HPCoxP/GEL polymer blend; (4) HPCoxT/GEL/MFs nanocomposite; (5) HPCoxT/GEL/MFs blend. As it can be observed, the materials have significantly improved bioadhesive properties as compared to the control. Moreover, the impact of the oxidation protocol can be clearly noticed – the samples with periodate-oxidized HPC led to higher values of the adhesion work. In addition, the presence of MFs in the nanocomposites significantly changed the internal organization of the network, since the adhesiveness compared to the corresponding blends is reduced. Being given these results, the structure-bioadhesion relationship is still an aspect that requires further research.

4. Conclusions

In this paper, we present an effective technique for producing nanostructured magnetic composite films made of selectively oxidized HPC, gelatin and MFs. This method is straightforward and economical, resulting in films with a variety of potential applications in the biotechnology and biomedical industries. Most importantly, two naturally occurring polymers were functionalized and used to successfully create new polymer networks and composite materials with or without magnetic nanoparticles, as confirmed by the FTIR and EDX spectra. The data regarding the bioadhesion properties of the studied films is promising and further investigations is required to establish the phenomena involved at the interface between the film and the cellulose membrane, as well as inside the nanocomposite architecture.

Acknowledgements

This work was supported by a grant of the Ministry of Research, Innovation 464 and Digitization, CNCS/CCCDI – UEFISCDI, project number PN-III-P1-1.1-PD-2021-0462, within 465 PNCDI III.

References

[1]. Espinha A, Dore C, Matricardi C, Alonso MI, Goñi AR, Mihi A. Hydroxypropyl cellulose photonic architectures by soft nanoimprinting lithography. *Nat Photonics*. 12, 343, 2018
[2]. Seddiqi H, Oliaei E, Honarkar H, Jin J, Geonzon LC, Bacabac RG, Klein-Nulend J. Cellulose and its derivatives: towards biomedical applications. *Cellulose.* 28, 1893, 2021
[3]. Barty-King CH, Chan CLC, Parker RM, Bay MM, Vadrucci R, de Volder M, Vignolini S. Mechanochromic, Structurally colored, and edible hydrogels prepared from hydroxypropyl cellulose and gelatin. *Adv. Mater.* 33, 2102112, 2021
[4]. Ming S, Zhang X, Chan CLC, Wang Z, Bay MM, Parker RM, Vignolini S. Exploiting the Thermotropic Behavior of Hydroxypropyl Cellulose to Produce Edible Photonic Pigments. *Adv. Sustain. Syst.* 7, 2200469, 2023
[5]. Ciannamea EM, Castillo LA, Barbosa SE, Angelis MGD. Barrier properties and mechanical strength of bio-renewable, heat-sealable films based on gelatin, glycerol and soybean oil for sustainable food packaging. *React. Funct. Polym.* 125, 29-36, 2018
[6]. Achet D, He XW. Determination of the renaturation level in gelatin films. *Polymer.* 36, 787-791, 1995
[7]. Bica D, Vékás L, Avdeev MV, Marinica O, Socoliuc V, Balasoiu M, Garamus VM. Sterically stabilized water based magnetic fluids: Synthesis, structure and properties. *J. Magn. Magn. Mater. 311*, 17-21 2007

DEVELOPMENT OF SUSTAINABLE MATERIALS WITH POTENTIAL APPLICATION IN CIRCULAR ECONOMY

Claudiu-Augustin Ghiorghita,* Maria Marinela Lazar, Madalina-Mihaela Barzu, Ioana-Victoria Platon, Irina-Elena Raschip, Maria Valentina Dinu
Petru Poni Institute of Macromolecular Chemistry, Romanian Academy, Iasi, Romania
**claudiu.ghiorghita@icmpp.ro*

1. Introduction

The concept of *one material – multiple uses* is increasingly explored in the design of innovative strategies aiming to contribute to the development of a sustainable "*circular economy*".

Over the years, many materials obtained from different polysaccharides (chitin/chitosan (CS), alginate, cellulose, starch etc.) have been investigated as sorbents for the removal of heavy metal ions from contaminated waters with different performance depending on their synthetic parameters (constituent polymers, type of chelating functional group, cross-linker amount, etc.) and characteristics of tested wastewater [1]. The most important disadvantage of using sorbents for wastewater treatment is their limited sorption capacity due to a finite number of interaction sites.

The current approach of increasing their economic value consists in the desorption of retained pollutants in a small elution volume, followed by regeneration of functional groups and subsequent reuse for a certain number of cycles, with a different degree of recoverability. However, this results in the accumulation of concentrated residual wastes, whose disposal creates additional environmental and economic problems.

Hydrogels are 3D structured physically or chemically cross-linked networks composed of natural and/or synthetic polymers that possess high water absorption capacity. Among the many hydrogels prepared so far, the macroporous ones, usually obtained by cryogelation (i.e. denoted as *cryogels*) [2], are the most interesting because they exhibit a ultrafast swelling rate, an also elastic and sponge-like features. Consequently, they support a fast transport of solute species from the external medium to the internal phase, which makes them very promising for wastewater treatment applications.

So far, little attention has been paid to the identification of new potential valorization strategies of spent cryogels after sorption of heavy metal ions.

In this respect, this work presents: (i) the preparation of new macroporous cryogels comprised of CS with/without thiourea (TU) as sulphur bearing ligand using formaldehyde (FA) as cross-linker [3]; (ii) their subsequent use in the sorption of Ag(I) and Cu(II) ions in simulated static conditions; (iii) the generation of new organic/inorganic composites by *in situ* chemical reduction the sorbed metal ions to metal nanoparticles; (iv) identification of new water purification pathways in which the wastes (e.g. used sorbents and formation of concentrated waste residues) are minimized.

The general layout of the proposed experimental pathway is illustrated in Figure 1.

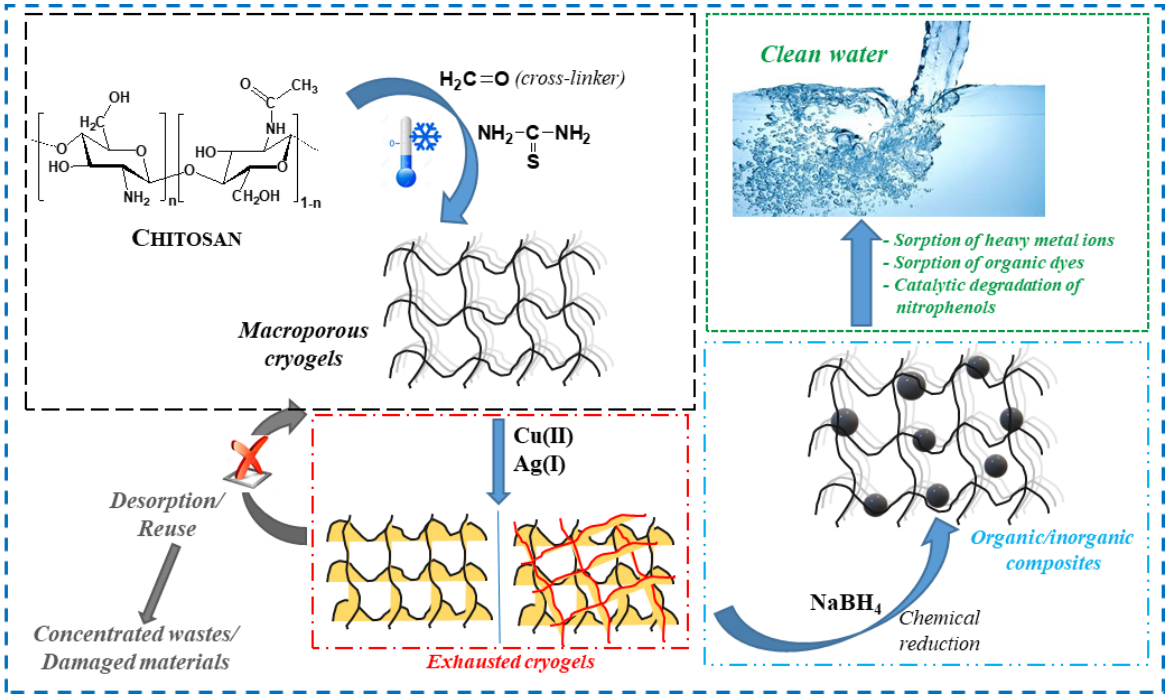

Figure 1. Graphical layout with the general strategy of valorizing the prepared cryogels.

2. Experimental

The CS and CS-TU cryogels were synthesized as monoliths by FA mediated cross-linking starting from 1 % and 2 % (*w*/*v*) CS solutions (prepared in 2 % CH_3COOH aqueous solution). CS cryogels were obtained as follows: (i) CS solution was first cooled on ice bath, then specific volumes of 37 % FA solution were added, under strong magnetic stirring; (ii) after 15 min the mixtures were drawn in syringes and kept at − 20 ºC for 24 h in a cryostat; (iii) the syringes containing the cryogels were thawed at room temperature for 30 min, then they were pushed out and cut in pieces of approximately 0.5 cm; (iv) they were then frozen in liquid nitrogen (− 196 ºC) and stored in the freezer (− 18 ºC) for minimum 24 h; (v) the cryogels were thawed again at room temperature, washed with distilled water to remove all residual reactants, frozen again in liquid nitrogen (− 196 ºC) and freeze-dried for 48 h.

The above steps were replicated in the synthesis of CS-TU cryogels, the only modification consisting in the solubilization of TU in the starting CS solution before adding the FA [3].

The sorption of Ag(I) and Cu(II) ions was investigated with respect to initial pH, contact time and equilibrium concentration by batch experiments. The influence of initial solution pH was followed in the pH range of 2 to 7. The effect of contact time on HMIs sorption capacity was studied at optimum pH at incremental time intervals from 15 to 480 min. The sorption equilibrium investigations were carried out at optimum pH in concentration range 50–1000 mg/L Ag(I) and Cu(II) [3].

3. Results and discussion

The prepared cryogels exhibited a macroporous structure with honeycomb interconnected pores, remarkable low densities (0.0021–0.0103 g/cm^3) and very high specific surface areas (416.641–447.267 m^2/g), influenced by the molar ratio between components.

A remarkable elasticity and toughness with no significant recovery loss was recorded for the CS cryogels prepared at an NH_2/FA molar ratio of 1:10.

The optimum initial pH for the sorption of Cu(II) and Ag(I) ions was 5 and 6, respectively, while the contact time required to attain the sorption equilibrium was 240 minutes, irrespective of cryogels composition. The maximum experimental sorption capacity of the CS cryogels prepared at NH_2/FA molar ratio of 1:10 for the Ag(I) and Cu(II) ions was 102.87 mg/g and 98.93 mg/g, respectively, while for the CS-TU cryogels prepared at the same NH_2/FA molar ratio was 119.76 mg/g and 110.55 mg/g respectively. Cryogels/metallic nanoparticles have been successfully prepared by in situ reduction of the sorbed Ag(I) and Cu(II) ions with $NaBH_4$.

Preliminary experiments revealed that the obtained composite frameworks exhibited excellent catalytic properties for reduction of 4-nitrophenol to 4-aminophenol, and good sorption capacity for Congo Red dye and Cu(II) ions modulated by the type of metallic nanoparticle. Besides this, the Ag(I) ions-loaded CS-TU cryogels also showed excellent antimicrobial properties against bacterial pathogens.

Overall, the obtained results indicate the strong multitasking potential of the new designed cryogels in complementary and/or cascade-based applications, which could offer new perspectives in the development of a sustainable "*circular economy*".

Acknowledgements

This work was supported by a grant of the Ministry of Research, Innovation and Digitization, CNCS/CCCDI – UEFISCDI, project number PN-III-P1-1.1-TE-2021-0771 (TE3/2022).

References

[1]. Ghiorghita CA, Dinu MV, Lazar, MM, Dragan ES. Polysaccharide-based composite hydrogels as sustainable materials for removal of pollutants from wastewater. *Molecules* 27, 8574, 2022
[2]. Lozinsky VI. Cryostructuring of Polymeric Systems. 55. Retrospective view on the more than 40 years of studies performed in the A.N. Nesmeyanov Institute of Organoelement Compounds with respect of the cryostructuring processes in polymeric systems. *Gels* 6, 29, 2020
[3]. Ghiorghita CA, Lazar MM, Platon IV, Humelnicu D, Doroftei F, Dinu MV. Feather-weight cryostructured thiourea-chitosan aerogels for highly efficient removal of heavy metal ions and bacterial pathogens. *Int. J. Biol. Macromol.* 235, 123910, 2023

SOME COORDINATION POLYMERS WITH PYRIDINE-BASED LIGANDS: SYNTHESIS AND STRUCTURAL CHARACTERIZATION

Alexandru-Constantin Stoica,* Mihaela Dascalu, Madalin Damoc, Maria Cazacu,
Department of Inorganic Polymers,
Petru Poni Institute of Macromolecular Chemistry, Romanian Academy, Iasi, Romania
**stoica.alexandru@icmpp.ro*

1. Introduction

Coordination polymers (CPs) are assemblies of metal ions or clusters of metals and organic ligands connected by coordination bonds in highly ordered structures extending infinitely in 1, 2 or 3 dimensions [1] that combine the characteristics of the two components. Low dimensionality (1D, 2D) coordination structures can form higher structures (2D and 3D, respectively) through supramolecular interactions (π - π-stacking, hydrogen bonds, van der Waals forces). This class of compounds enjoys particular interest due to the wide range of properties (porosity, chirality, optical, electrical, magnetic properties) and applications such as: catalysis, magnetism, gas storage and/or separation, optoelectronics [2-4].

The extremely large number of organic ligands available or that can be obtained and the possibilities of combining them with metal ions allows obtaining a wide range of synthetically tunable properties depending on the requirements. The variations of the reaction conditions constitute additional ways of regulating the structure and implicitly the properties. N-Heterocycles are widely used as ligands in coordination chemistry. Due to the sp^2-hybridized nitrogen atoms, pyridyl-based ligands are excellent for metal coordination and a multitude of complexes with such compounds as ligands or co-ligands are reported [5]. Three new coordination polymers based on ligands derived from pyridine and Ni(II) and Co(II) as metal ions are reported here.

2. Experimental

*Synthesis of $\{[BiPyNi(DMSO)_4]\cdot 2ClO_4\}_n$ (**1**) and $\{[AzoPyCo(DMSO)_4]\cdot 2ClO_4\}_n$ (**2**)*

1 mmol 4,4'-bipyridyl (BiPy) (0.1561 g) or 1 mmol 4,4'-azopyridine (AzoPy) (0.1842 g), dissolved in 5 mL methanol, and 1 mmol $Ni(ClO_4)_2x6H_2O$ (0.365 g) or 1 mmol $Co(ClO_4)_2x6H_2O$ (0.365 g), respectively, dissolved in 2 mL distilled water have loaded in a round-bottomed flask. Then, 1 mL of dimethylsulfoxide (DMSO) was added, and the mixture was heated at 60 °C for 1 h, after which this was cooled at room temperature, filtered and allowed to crystallize.

*Synthesis of $\{[AzoPyCo(H_2O)_2]\cdot 2ClO_4\}_n$ (**3**)*

In a round-bottomed flask were loaded 1 mmol AzoPy (0.1842 g), dissolved in 5 mL methanol, 2 mmol $Co(ClO_4)_2x6H_2O$ (0.730 g), dissolved in 5 mL distilled water. The mixture was heated at 60 °C for 1 h, after which this was cooled, filtered and allowed to crystallize.

3. Results and discussion

4,4'-Bipyridyl and 4,4'-azopyridine were used as unique ligands for the complexation of Ni(II) and Co(II) ions from perchlorates as sources. The reactions were conducted in a mixture of polar solvents, H_2O/MeOH/DMSO or H_2O/MeOH by heating to 60 °C, the reactions proceeding according to Scheme 1.

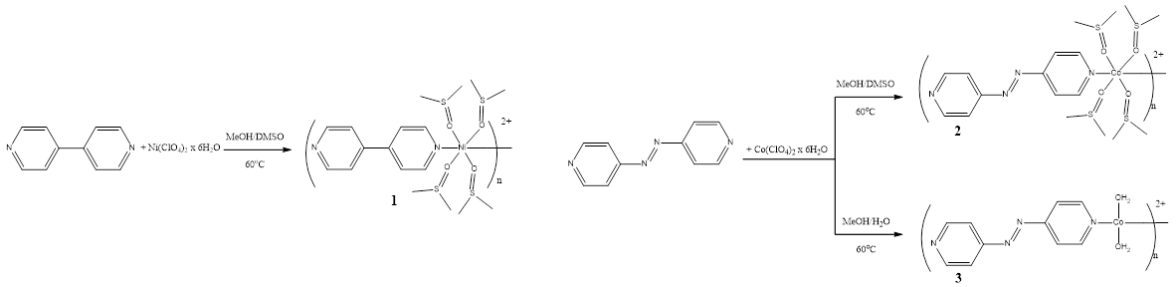

Scheme 1. Reaction leading to the compounds: **1**-{[BiPyNi(DMSO)$_4$]·2ClO$_4$}$_n$;
2 -{[AzoPyCo(DMSO)$_4$]·2ClO$_4$}$_n$; **3** - {[AzoPyCo(H$_2$O)$_2$]·2ClO$_4$}$_n$.

In all three cases, the reaction products were isolated as crystals (Figure 1) suitable for single crystal X-ray diffraction analysis. For compound **1**, this evidenced the formation of a 1D coordination polymer. The asymmetric unit comprises one Ni^{2+} atom occupying a special position on the inversion center, half of BiPy acting as bidentate-bridging ligand, two coordinated DMSO molecules and one ClO_4^- anion in the ionization sphere (Figure 2). Chemical composition of the crystal **1** is an agreement with the formula {[BiPyNi(DMSO)$_4$]·2ClO$_4$}$_n$.

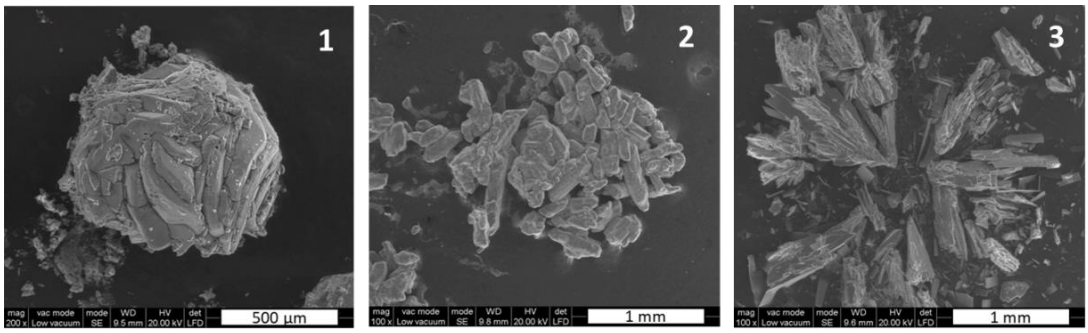

Figure 1. SEM images of the isolated crystalline mass for compound **1**, **2** and **3**.

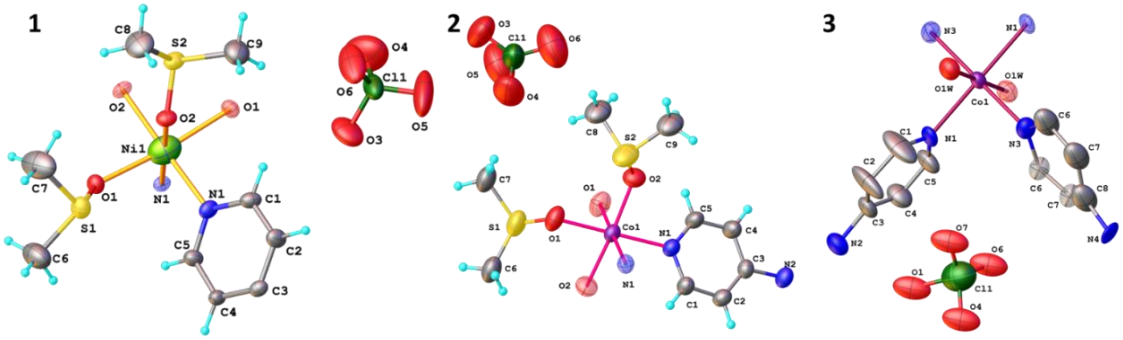

Figure 2. View of the asymmetric unit with thermal ellipsoids at 50% level and atom labeling showing the coordination of the metal atom. The atoms generated by elemental symmetry are drawn with faded color. Symmetry code for **1**: 1 – *y* + *x*, 2 – *y*, 4/3 – z; Symmetry code for **2**: 1 – *x*, + *y*, 3/2 – *z;* Symmetry code for **3**: O1*w*, N1, C6, C7: 1 – *x*, + *y*, 1 – z, N3: 1 – *x*, 2 –*y*, 1 – *z*.

In the case of compound **2**, single crystal X-ray diffraction analysis also highlights the formation of a 1D coordination polymer. The Co atom shows the same type of coordination as Ni in compound **1**, the bridge role being played by AzoPy (Figure 2). Chemical composition is an agreement with the formula {[AzoPyCo(DMSO)$_4$]·2ClO$_4$}$_n$. Instead, for compound **3,** single crystal X-ray diffraction analysis highlights the formation of a 2D coordination polymer, with chemical formula

$\{[AzoPy_2Co(H_2O)_2]\cdot 2ClO_4\}_n$. The asymmetric unit comprises one Co^{2+} atom occupying a special position on the inversion center, half of two AzoPy molecules acting as bidentate-bridging ligand, one coordinated water molecule and one ClO_4^- anion out of coordination sphere (Figure 2).

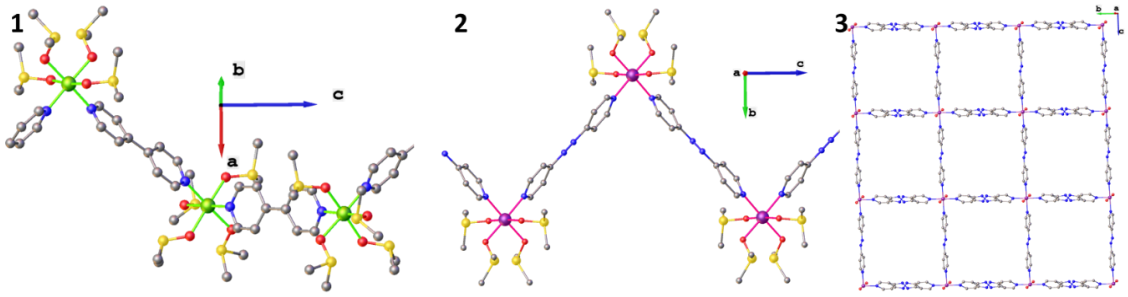

Figure 3. A view of one-dimensional coordination polymer **1** in the form of a spiral along 0 0 1 axis, polymer **2** and two-dimensional coordination polymer **3.**

The structures identified by SC-XRD were supported by the results of the FTIR analysis, which mainly reveals shifts of the absorption bands characteristic of the bonds of the pyridinic nitrogen atoms (C_{ar} = N) involved in the coordination with the metal ions.

4. Conclusions

Three new coordination polymers were synthesized and structurally characterized. Under identical reaction conditions, both BiPy with nickel perchlorate and AzoPy with cobalt perchlorate led to 1D structure, while changing the ratio between the reactants and the reaction medium in the second case a 2D structure was obtained. Compound **1** is a high purity coordination porous polymer that crystallizes into a chiral form.

Acknowledgments: This work was supported by a grant of Ministery of Research, Innovation and Digitization, CNCS - UEFISCDI, project number PN-III-P4-ID-PCE-2020-2000 (2D-PerMONSil), within PNCDI III, Contract 207/2021.

References

[1]. Engel E, Scott JL., Advances in the green chemistry of coordination polymer materials, *Green Chemistry*, 22, 3693-3715, 2022
[2]. Kepert CJ, Prior TJ, Rosseinsky MJ. A versatile family of interconvertible microporous chiral molecular frameworks: The first example of ligand control of network chirality, *J. Am. Chem. Soc.*, 22, 5158-5168, 2000
[3]. Singh NP, Kumar A, Metal Organic Framework and Its Application : A review, *Comput. Biol. Chem.*, 1, 10-18, 2016
[4]. Ohtani R, Yoneda K, Firikawa S, Horike N, Kitagawa S, Gaspar AB, Munoz MC, Real JA, Ohba M. Precise control and consecutive modulation of spin transition temperature using chemical migration in porous coordination polymers, *J. Am. Chem. Soc.*, 133, 8600-8605, 2011
[5]. Al-Anber M, Vatsadze S, Holze R, Lang H, Thiel WR., π-Conjugated N-heterocyclic compounds: correlation of computational and electrochemical data, *Dalton Trans.*, 22, 3632, 2005

ELECTRONIC EXCITATIONS AND TRANSIENT SPECIES IN THE ISOMERIZATION PROCESS OF THE AZOBENZENE MOLECULAR SYSTEM

Dragos Lucian Isac,* Carmen Gherasim, Anton Airinei, Emilian Rosca, Radu Tigoianu, Aatto Laaksonen
Petru Poni Institute of Macromolecular Chemistry, Romanian Academy, Iasi, Romania
**isac.dragos@icmpp.ro*

1. Introduction

Light-activated molecules have attracted attention in past decades because they can be used in order to produce energy from light [1]. Azobenzene is an organic compound that has in chemical structure two aromatic rings linked by a double -N=N- bond. The presence of phenyls units in the azobenzene structure permits this molecular system to be switchable. The property to be switchable of azobenzene is given by freedom degree of the molecular coordinates. In this case, the dynamics is determined by the free motion of phenyls rings along the single C-N bond. Even if the double bond is present in the azobenzene structure, this in turn can undergo a conversion by breaking the π-type bond.

Of course, under these conditions, a large enough energy is needed to break this double bond. In this case, UV light can be used, which favors this breaking process. Following the irradiation process an isomerization reaction can be occur. Trans and cis isomers are two antagonism isomers of azobenzene. Trans is a coplanar conformer where the dihedral angle formed by the Csp^2-N=N-Csp^2 sequence has a value closer to 180°. On the other hand, the cis isomer is twisted conformer because the Csp^2-N=N-Csp^2 angle has a value under 60°. Trans azobenzene is more stable from the energetic point of view, while cis is metastable due to sterically repulsion between phenyls rings. Another aspect worth emphasizing is that the trans isomer has an approximate dipole moment of 0 D, while the cis has over of 3 D [2]. Therefore, trans conformers have affinity for non-polar and cis isomers for polar solvents.

Along the irradiation with UV light, some electronic transitions can appear. In trans isomers, the π → π * transitions are dominant and contrary in cis the n → π* ones. The π → π* transition occurs along the $S_0 \rightarrow S_2$ excitation and n → π* belong to $S_0 \rightarrow S_1$ state [3]. The conversion from trans to cis isomers occurs with intersystem changing of energy levels and namely the intensity of π → π* transition decreases followed by the increase of n → π* excitation. Once the stationary photo state is reached through the formation of the cis isomer, it can return to its initial form, i.e. to the most stable form (coplanarity). In this case the intensity of n → π* transition decrease and now π → π* character increases [3]. The return can take place through a thermal way as well as by using external sources such as light from the visible range of the electromagnetic spectrum. For each isomerization reaction, namely from trans to cis and *vice versa*, there may be several stages or reaction mechanisms of chemical processes.

Regarding the mechanism of the isomerization reaction, four pathways were proposed. Rotation involves the twisting of the dihedral angle Csp^2-N=N-Csp^2 sequence, whilst the valence angle remains fixed at 120°. In this way, a rupture of the π-bond in the double bond -N=N- can happen which permits the free motion along the -N-N- length. In the inversion, N=N-Csp^2 valence angle can enhance up to 180°, and in this step of the reaction the Csp^2-N=N-Csp^2 angle remains

unchangeable at 0°, resulting a semiliniar structure. In the inversion mechanism small but significant variations were observed in dihedral and valence angles as well as in the -N=N- bond. In the reaction mechanism that takes place by inversion assisted by rotation both dihedral and valence angles are changed, but a more significant modification appears in torsional sequence Csp^2-N=N-Csp^2. Like in the inversion pathway, in inversion assisted by rotation, a semilinear transition state appears, one of the phenyl units has a twisted orientation as compared to the other one. In the elementary step of the isomerization reaction which takes place by the concert inversion, the Csp^2-N=N and N=N-Csp^2 angles increase until 180° resulting in a coliniar transition state without of dipole moment. Recently for isomerization reaction another transition state was accepted which includes a variation of central torsional Csp^2-N=N-Csp^2 angle, where the phenyl rings remain roughly stationary [4]. This version of the mechanism is knowns as the "pedal motion" or hula-twist" process [4]. All these proposed mechanisms can occur after the excitation $S_0 \rightarrow S_1$ or $S_0 \rightarrow S_2$ as well as along the decay $S_2/S_1/S_0$. Even if it seems that the mechanism has been summarized, a unanimous point of view is not still accepted in the literature, as compared to the case of stilbene molecule where the isomerization takes place through the rotational pathway.

Hence, in this study we performed an analysis of experimental data relating to the azobenzene molecule based on the UV-Vis absorption spectra and transient absorption spectroscopy. Also, a probing of new processes of excitations such as $S_1 \rightarrow S_2$ and $S_2/S_1/S_0$ was realized. Our data reveal the possibility of multiple excitation process such as ground state bleach and induced absorption, respectively occur. Along these excitations, three transient species were found at 450, and 512 nm. These experimental data was correlated with theoretical results based on TD-DFT methods.

2. Experimental details

UV-Vis absorption spectra were measured on a SPECORD 210 PLUS Analytik Jena, whereas the transient absorption spectra were recorded with the Edinburgh LP980 transient absorption spectrometer. All measurements were realized in the dichloromethane.

3. Computational details

The theoretical results were obtained with DFT-CAM-B3LYP/cc-pVTZ and TD-DFT-CAM-B3LYP/cc-pVTZ methods. Gaussian version 16 was employed as motor for theoretical calculations.

4. Results and discussion

The UV Vis spectra of azobenzene reordered in dichloromethane show two bands at 320 and 448 nm. The band from 320 nm corresponds to $\pi \rightarrow \pi^*$ transitions, and at 448 nm for $n \rightarrow \pi^*$ excitation, being typically for azobenzene. In the spectra obtained from transient measurements the $\pi \rightarrow \pi^*$ transitions correspond to ground state beach, which follow the $S_0 \rightarrow S_2$ excitations. This result was obtained after irradiation with 355 nm incident laser. After irradiation process, a signal at 450 nm was obtained which correspond formation of cis isomer and another with a very small intensity at 512 nm. The signal obtained at 450 nm present a $n \rightarrow \pi^*$ character.

Figure 1 reveals that during the irradiation with the incident laser at 355 nm the band at 320 nm corresponding to the ground state bleach transition decreases, while the signal from 450 nm increases, which confirm the trans → cis conversion. Also, the data from Figure 1 show multiple possible ways of excitations and the presence of different transient species. These signals correspond to possible vertical transitions from S_1 to S_n. The induced absorption bands were

localized from 200 to 300 nm. Regarding the species localized at 512 nm, we used the theoretical method (DFT-CAM-B3LYP/cc-pVTZ and TD-DFT-CAM-B3LYP/cc-pVTZ methods) for interpretation. Our results confirming the presence of „pedal motion" isomer along the trans → cis conversion. Moreover, based on the same methods above mentioned, we localized different transient species which can appear into S_2 and S_3 energies levels, confirming the possibility of $S_1 \rightarrow S_2$ and $S_1 \rightarrow S_3$ processes of excitations. In present study the reverse conversion from cis → trans was monitored. In this case an incident laser at 410 nm was used and reverse isomerization was confirmed.

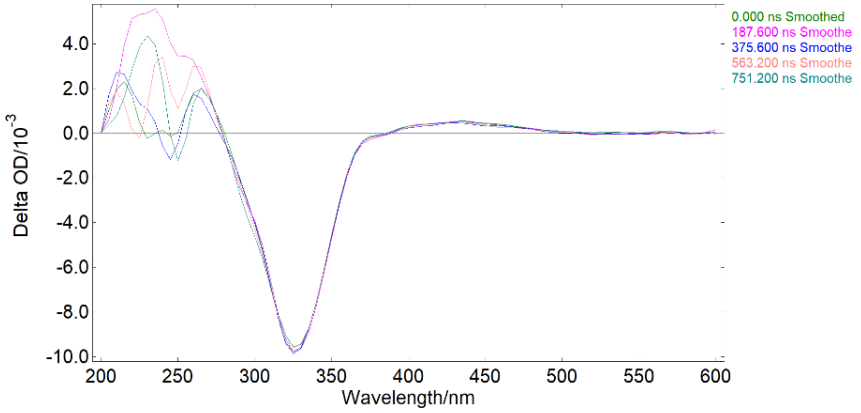

Figure 1. Transient spectra of trans and cis azobenzene in dichloromethane upon 355 nm irradiation. Ground state bleach excitation is negative and excited-state absorption is positive.

4. Conclusions

In the present work we have been monitored the trans → cis and the reverse process of isomerization reaction. Our experimental and theoretical results indicated the presence of π → π * and n → π * transitions as well as some transient species. The transient species were localized at 512 nm during the irradiation with the incident laser of 355 nm. Using the same incident laser the cis isomer was localized at 450 nm.

Acknowledgements

This work was supported by a grant of the Ministry of Research, Innovation and Digitization, CNCS - UEFISCDI, project number PN-III-P1-1.1-PD-2021-0060 (FingerprintAZO), within PNCDI III. This work also was supported by the research infrastructure developed through the European Social Fund for Regional Development, Competitiveness Operational Programme 2014–2020, Axis 1, Action: 1.1.3, Project "Infra SupraChem Lab-Center for Advanced Research in Supramolecular Chemistry" (Contract 339/390015/25.02.2021, cod MySMIS: 108983).

References

[1]. Kolpak AM, Grossman JC. Visible-light-photomeltable azobenzenes as solar thermal fuels. *ACS Appl. Opt. Mater.* 1, 633-639634, 2023
[2]. Oscurato SL, Salvatore M, Maddalena P, Ambrosio A. From nanoscopic to macroscopic photo-driven motion in azobenzene-containing materials. *Nanophotonics* 7, 1387-1422, 2018
[3]. Isac DL, Airinei A, Maftei D, Humelnicu I, Mocci F, Laaksonen A, Pinteala M. On the charge-transfer excitations in azobenzene maleimide compounds: A theoretical study. *J. Phys. Chem. A* 123, 5525-5536, 2021
[4]. Merrrit ICD, Jacquemin D, Vacher M. Cis → trans photoisomerisation of azobenzene: a fresh theoretical look. *Phys. Chem. Chem. Phys.* 23, 19155-19165, 2023

THEORETICAL INVESTIGATION OF DISSOCIATION REACTIONS IN THE CASE OF UROCANIC ACID AFTER UV IRRADIATION PROCESS

Dragos Lucian Isac,[1]* Adina Coroaba,[2] Mihaela Silion,[2] Razvan Puf,[2] Narcis Cibotariu,[2] Andrei Neamtu,[2] Teodora Rusu,[2] Mariana Pinteala,[2] Aatto Laaksonen[2]

[1]*Physical Chemistry of Polymers Department,*
Petru Poni Institute of Macromolecular Chemistry, Romanian Academy, Iasi, Romania
[2]*Centre of Advanced Research in Bionanoconjugates and Biopolymers,*
Petru Poni Institute of Macromolecular Chemistry, Romanian Academy, Iasi, Romania
**isac.dragos@icmpp.ro*

1. Introduction

E isomer of urocanic acid [(2E)-3-(1H-imidazol-4-yl)prop-2-enoic acid] represents a molecular system recognized for photoimmunosuppression [1]. This molecule is localized as a filter for human skin (into the *stratum corneum* of the epidermis) in the case of UV light action [1,2].

Recently, more studies confirmed that E isomer of urocanic acid under UV light action is converted into Z isomer by its intramolecular conversion, which can interact with the DNA system, producing damage into the human body [3-5]. The conversion of E isomer under UV radiation can absorb the electromagnetic energy and pass it to the Z-urocanic isomer. Figure 1 reveals that this process is reversible and the back conversion can be realized with the same external source of irradiation.

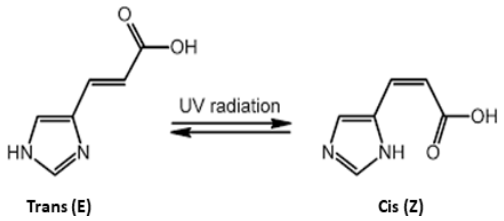

Figure 1. Description of the isomerization reaction of urocanic acid from the isomer E to Z under UV light irradiation.

In particular, the structure of urocanic acid has been for a long time scrutinized, and different tautomers and conformers were evinced by experimental and theoretical studies [5-7]. Moreover, the urocanic acid can be sensitive to the pH variation due to the presence of -COOH moiety [8].

Several works based on TD-DFT and post ab initio methods indicate the presence of excited states ($\pi\pi^*$ and $n\pi^*$) for each form of urocanic neutral/zwitterionic acid structure [9,10]. Also, different mechanisms of isomerization and the decay's reaction for the E to Z conversion have been proposed along the $\pi\pi^*$ and $n\pi^*$ excitation. Into the excited states, the energy levels can be also populated with different conformers, when intramolecular coordinate modification leads to planar structures, N−H stretching and the ring-puckering mechanisms inherently to the imidazole moiety.

This may therefore be most relevant to the study of urocanic acid from a biological and chemical point of view. Concerning the role of urocanic acid in the skin to protect or to immunosuppression the biological systems, some scientific papers reveal that this process can be realized after the interaction of urocanic acid with reactive oxygen species [3,11]. The results indicated that trans urocanic acid can act as a radical scavenger while cis isomer can generate free radicals [3,11].

Our aim is to reveal how radical's species can be obtained from the interaction of cis urocanic acid with a peroxide molecular system after the UV radiation in order to explain a possible situation for the formation of cancer skin.

The present work involves a theoretical investigation which later was correlated with some experimental data provided in our labs (High-performance liquid chromatography [HPLC] and UV-Vis absorption spectra).

2. Results and discussion

Our research is based to use DFT method namely UMN12SX/cc-pvtz level of theory. The first step of this research was to localize the lowest rotamer and tautomer of cis isomer. Then, based on the isodesmic reaction pathways, to explain how radicals can be obtained from urocanic acid molecular system.

Figure 2 reveals that in the reaction of the urocanic acid and hydrogen peroxide, the H· radicals can appear. The H· species can be obtained from both urocanic acid and hydrogen peroxide molecular systems. Other radical species was hydroperoxyl radical which becomes highly reactive when it reacts with another molecule in order to complete the vacant orbital or unpaired electron.

Also, the hydroperoxyl radical can interact with the peroxide molecular system resulting molecular oxygen (O_2), water (H_2O) and HO· radicals (reaction (r1)). Moreover, the radical hydroperoxyl radical can also lead to supplementary reactions (r2 and r3).

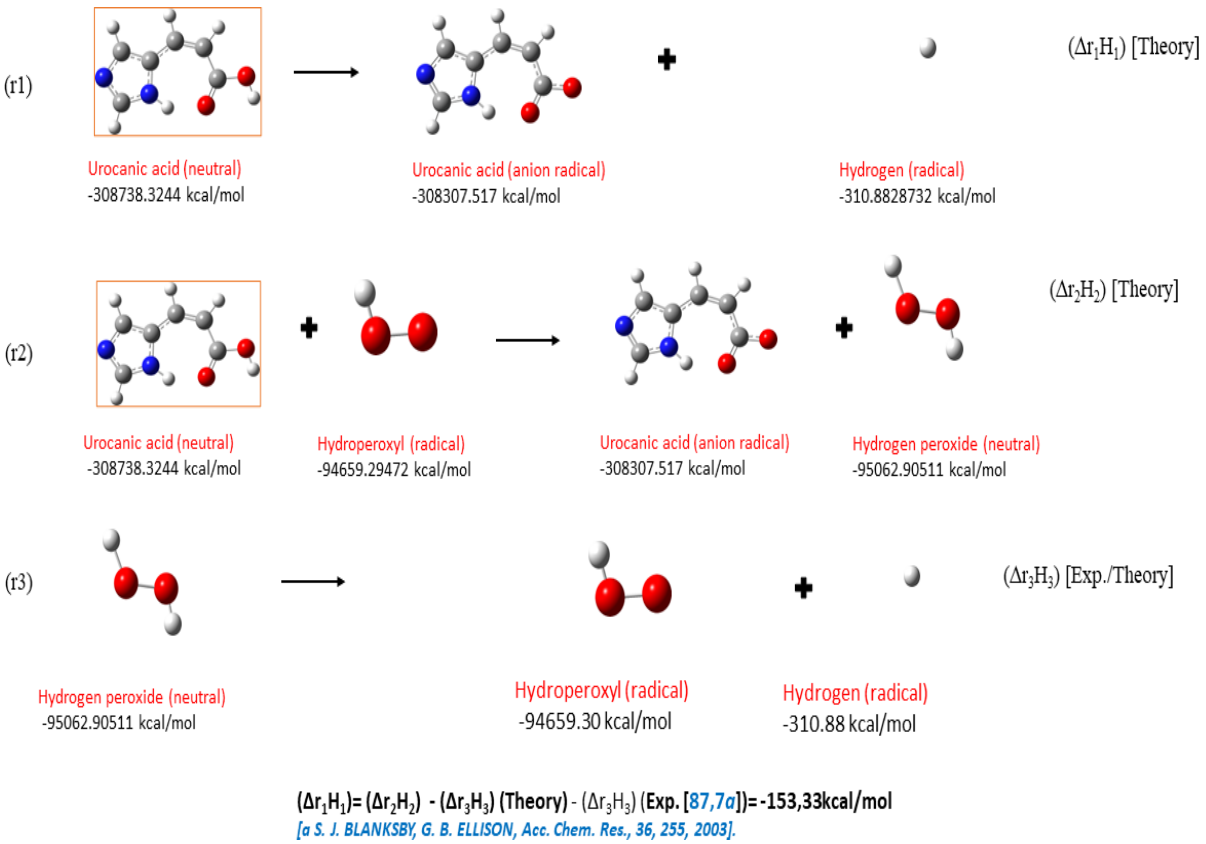

Figure 2. The proposed reaction between urocanic acid and hydrogen peroxide and how the radical species can be obtained from the interplay of these molecular systems. The enthalpy of the reaction in the case of hydrogen dissociation from urocanic acid was calculated.

$$HOO\cdot + H_2O_2 \rightarrow O_2 + H_2O + HO\cdot \quad (r1)$$

$$HOO\cdot \leftrightarrow 2O\cdot\ H^+ \quad (r2)$$

$$2O\cdot + H_2O_2 \rightarrow O_2 + HO^- + HO\cdot \quad (r3)$$

Unless specified, the enthalpy of reaction (r1) which occurs with the formation of H· species from urocanic acid was around -153.33 kcal/mol being an exothermic process. Other pathways of hydrogen dissociation will be probed.

4. Conclusions

In this study we have been proved the interaction of urocanic acid molecular system with the hydrogen peroxide reagent. The formation of radicals' species such as H·, HOO·, HO·, O· was observed. These radicals can be responsible for DNA damage in a possible interaction.

Acknowledgements

This was supported by European Union's Horizon Europe research and innovation programme under grant agreement No. 101086667, project BioMat4CAST (BioMat4CAST-''Petru Poni" Institute of Macromolecular Chemistry Multi-Scale In Silico Laboratory for Complex and Smart Biomaterials). This work also was supported by the research infrastructure developed through the European Social Fund for Regional Development, Competitiveness Operational Programme 2014–2020, Axis 1, Action: 1.1.3, Project "Infra SupraChem Lab-Center for Advanced Research in Supramolecular Chemistry" (Contract 339/390015/25.02.2021, cod MySMIS: 108983).

References

[1]. Kumar N, Thomas S, Rao R, Maiti N. Surface-enhanced Raman scattering based sensing of trans-urocanic acid, an epidermal photoreceptor using silver nanoparticles aided by density functional theoretical calculations. *J. Raman Spectrosc.* 50, 837-846, 2019
[2]. Tuna D, Sporkel L, Barbatti M, Thiel W. Nonadiabatic dynamics simulations of photoexcited urocanic acid. *Chem. Phys.* 515, 521-534, 2018
[3]. Shen L, Ji HF. Theoretical investigation of the photosensitization mechanisms of urocanic acid. *J. Photochem. Photobiol., B.* 91, 96-98, 2008
[4]. Schwarz T. Mechanisms of UV-induced immunosuppression. *Keio J. Medicine* 54, 165-171, 2005
[5]. Barbatti M. The role of tautomers in the UV absorption of urocanic acid. *Phys. Chem. Chem. Phys.* 13, 4686-4692, 2011
[6]. Cooper GA, Medcraft C, Gougoula E, Walker NR. Conformational isomers of trans-urocanic acid observed by rotational spectroscopy. *Phys .Chem. Chem. Phys.* 21, 9495-9503, 2019
[7]. Sharifian A, Abyar F, Behjatmanesh-Ardakani R. Electronic structure and characterization of the spectra of trans/cis tautomers of urocanic acid isomers: A diagnostic tool. *J. J. Photochem. Photobiol., A.* 400, 112652, 2020
[8]. Brookman J, Chacón JN, Sinclair RS. Some photophysical studies of cis- and trans-urocanic acid. *Photochem. Photobiol. Sci.* 1, 327-332, 2002
[9]. Danielsson J, Ulicny J, Laaksonen A., A TD-DFT Study of the photochemistry of urocanic acid in biologically relevant Ionic, rotameric, and protomeric forms. *J. Am. Chem. Soc.* 123, 9817-9821, 2001
[10]. Dmitrenko O, Reischl W, Bach RD, Spanget-Larsen J. TD-DFT Computational Insight into the origin of wavelength-dependent E/Z photoisomerization of urocanic acid. *J. Phys. Chem. A* 108, 5662-5669, 2004
[11]. Tiwari S, Mishra PC. Urocanic acid as an efficient hydroxyl radical scavenger: a quantum theoretical study. *J. Mol. Model* 17, 89-72, 2011

CONSTRUCTING CONJUGATED POROUS POLYMERS CONTAINING TRIPHENYLAMINE MOIETIES FOR DETECTION OF NITROAROMATIC DERIVATIVES

Andra-Elena Bejan,* Loredana Vacareanu
Petru Poni Institute of Macromolecular Chemistry, Romanian Academy, Iasi, Romania
**bejan.andra@icmpp.ro*

1. Introduction

Conjugated porous polymers (CPPs) belong to a category of amorphous polymer networks intentionally designed with complete cross-linking and full π-conjugation. The cross-linked nature of CPPs ensures a permanent intrinsic micro/nanoscale porosity, setting them apart from other porous polymeric materials due to their combination of full π-conjugation and structural porosity. Besides to the general characteristic of porosity, each class itself presents unique aspects in synthesis methods, physicochemical stability, degree of conjugation, and origin of porosity, which can closely affect the final properties and applications of the material. Among all porous materials, CPPs stand out through their unique and convenient combination of high surface area/permanent porosity and an extended π-conjugated electronic system throughout the interconnected polymer network [1]. Such powerful combination is especially favorable to various key in many applications including gas separation and storage, opto-electronics and energy storage, chemical sensors, and photocatalysis [2]. These porous structures induce many opportunities for electron and ion transmission based-applications, a distinguishing property that separates CPPs from other linear polymers. Recently, one of the most important uses of CPPs is the identification/detection of various organic contaminants from environment which received an enormous international attention. Among multiple organic micropollutants, nitroaromatics-containing wastes are widely documented to possess severe detrimental impacts on mankind because of their toxicity, mutagenicity, and carcinogenic behavior. Detection based on fluorescence quenching methods have been identified as the most advantageous and promising techniques for sensing of nitroaromatic compounds due to their high efficiencies, quick response times, simplicity of implementation at low cost, and environmental friendliness. For example, 2,4,6-trinitrophenol (TNP, picric acid), a nonbiodegradable environmental micropollutant, damages red blood cells and is the main cause of skin damage. Hence, there is an urgent need for the efficient and reliable detection and removal of TNP which is receiving growing attention at present [3]. CPPs used for detection of different harmful species have frequently been obtained using common C–C coupling, but chemical oxidative polymerization proved to be one of the simplest and straightforward method [4]. It occurs by the oxidation of monomers with an oxidizing agent, such as ferric chloride ($FeCl_3$), to generate radical cations, and later the coupling between the radicals to generate the final polymer. In addition, emulsion polymerization using the single-phase oxidative system is a way to obtain well-ordered macromolecular architectures. This synthesis method uses a surfactant to manipulate the shape and size of the particles [5]. Triphenylamine (TPA) is an appealing candidate for construction of a three-dimensional skeleton as it possesses several advantageous characteristics: it has three reactive sites located at the para-position on the phenyl arms (i.e. C3 tecton type) which can be easily functionalized; it possess fluorescent properties which opens the way for the design of solid state sensors based on fluorescence quenching. For these reasons, it is widely used as a building block in the construction of (hyper)branched, star and dendrimer conjugated architectures

for a wide range of applications. Considering all these, TPA group has been already used for the synthesis of conjugated microporous polymers. For example, Xiao et al. have synthesized TPA-based CPPs for hydrogen evolution from water. Recently, have been reported TPA-based CPPs in heterogeneous photocatalysis because of their excellent photo-redox property [3]. While CPPs containing TPA units are suitable for various applications, there are no such reports where TPA based-polymers have been obtained by monophasic oxidation reaction using appropriate surfactant, and especially, comparatively studied with those obtained by classical oxidative reaction. In this study, we report the synthesis of four CPPs containing TPA units successfully prepared by chemical oxidative polymerization with ferric chloride ($FeCl_3$) as the oxidizing agent, with and without surfactant, and the investigation of the influences of these two methods on photo-physical properties, with a great concern on their morphological aspects and detection capability.

2. Experimental

Four TPA-based polymers with π-conjugated structure were synthesized by chemical oxidative polymerization in $CHCl_3$ with $FeCl_3$ as oxidizing agent; for two of them sodium dodecyl sulfate (SDS) was used as surfactant. The purification protocol of the obtained polymers included fractionation stage where the insoluble/soluble fractions were separated by using chloroform. The general reaction conditions, yields and the obtained fractions percentage are presented in Table 1.

Table 1. The general reaction conditions.

Polymer	Reaction temperature (°C)	Reaction time (h)	Feed ratio: $FeCl_3$: star-shaped oligomer	Reaction yield (η, %)		
				Total	Insoluble	Soluble
Pox1	45	24	4/1	76.2	70.1	6.2
Pem1	45	48	4/1	86.9	74.5	12.5
Pox2	45	24	4/1	85.6	62.1	23.5
Pem2	45	48	4/1	78.1	46.1	32.0

3. Results and discussion

Structural identification of TPA-based polymers was accomplished by FTIR and NMR spectroscopies in comparison with those of the starting monomers (Figure 1). Generally, the most important proton signals/characteristic bands were identified in polymers at slightly shifted values relative to those of the corresponding monomer.

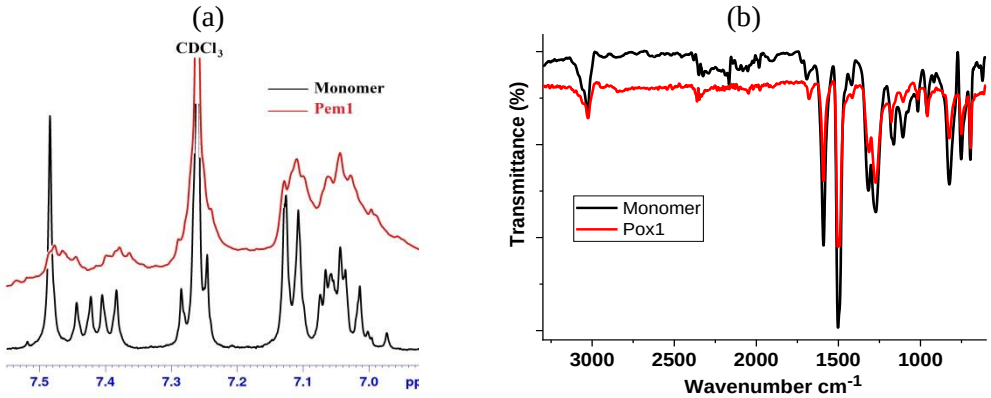

Figure 1. (a) The ^{1}H-NMR spectra of Pem1 and the monomer; (b) The FTIR spectra of Pox1 and the monomer.

The morphology of the polymers was analyzed by SEM technique which revealed porous structures in case of all polymers, the porosity measurements reveal promising results. The sensing potential of the polymers was tested for picric acid in solution with a fully quenched emission in response to the analyte. For example, the PL spectra of Pem1 before and after TNP contact are presented in Figure 2. The mechanism behind this efficient detection could be the formation of a complex between the protonated sensor and the picrate anion.

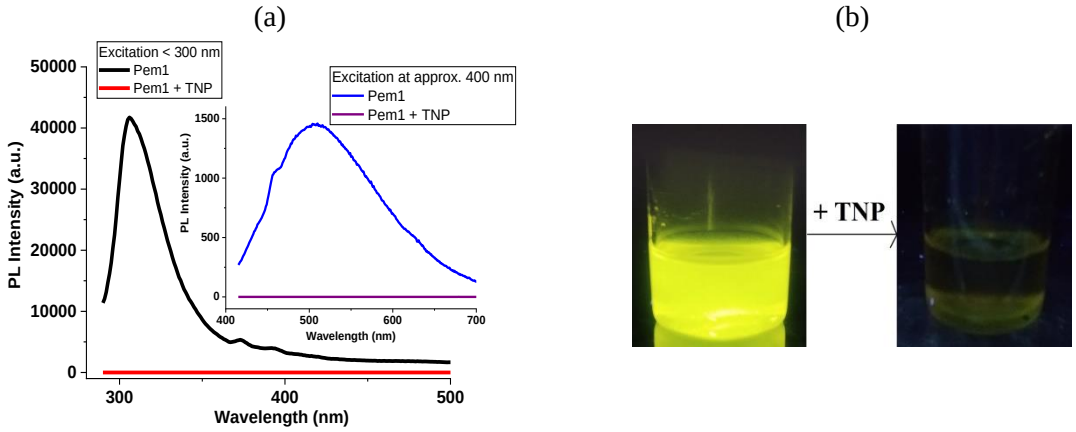

Figure 2. (a) The PL spectra of Pem1 before and after picric acid adding;
(b) The corresponding photos (under UV lamp, 365 nm) for detection process

4. Conclusions

In conclusion, in this work we present a systematic investigation of the synthesis process, structural characterization, and properties of triphenylamine-based CPPs. By elucidating the relationship between polymerization conditions and resulting material properties, we aim to contribute to the fundamental understanding of CPPs and their potential applications. The obtained conjugated polymers exhibit porous microstructure and they have good potential in the field of nitroaromatic harmful derivatives detection.

Acknowledgements

This work was supported by a grant of the Ministry of Research, Innovation and Digitization, CNCS - UEFISCDI, project number PN-III-P1-1.1-TE-2021-1068, within PNCDI III.

References

[1]. Dawson R, Cooper AI, Adams DJ. Nanoporous organic polymer networks, *Prog. Polym. Sci*., 37, 530-563, 2012
[2]. Taylor D, Dalgarno SJ, Xu Z, Vilela F. Conjugated porous polymers: incredibly versatile materials with far-reaching applications, *Chem. Soc. Rev*., 49, 3981, 2020
[3]. Sau S, Banerjee F, Samanta SK. Triphenylamine–anthracene-based conjugated microporous polymers for the detection and photocatalytic degradation of organic micropollutants. *ACS Appl. Nano Mater.* 6, 11679-11688, 2023
[4]. Samy MM, Mohamed MG, Sharma SU, Chaganti SV, Mansoure TH, Lee JT, Chen T, Kuo SW. Constructing conjugated microporous polymers containing triphenylamine moieties for high-performance capacitive energy storage. *Polymer*, 264, 125541, 2023
[5]. Kesornsit S, Direksilp C, Phasuksom K, Thummarungsan N, Sakunpongpitiporn P, Rotjanasuworapong K, Sirivat A, Niamlang S. Synthesis of highly conductive poly(3-hexylthiophene) by chemical oxidative polymerization using surfactant templates. *Polymers*, 14, 3860, 2022


MACRO Iași 2023

BioMat4CAST
MULTI-SCALE IN SILICO LABORATORY FOR COMPLEX AND SMART BIOMATERIALS

Teodora Rusu,* Mariana Pinteala, Aatto Laaksonen, Tudor Vasiliu
Petru Poni Institute of Macromolecular Chemistry, Romanian Academy, Iasi, Romania
**teodora.rusu@bionanotech.ro*

1. Introduction

The Multi-Scale In Silico Laboratory for Complex and Smart Biomaterials, BioMat4CAST, is a European research project focused on developing computational models to design and test biomaterials for various biomedical applications. The project uses advanced computational simulations to model different factors such as the material's structure, properties, and interactions with biological systems.

The strategic objective of the BioMat4CAST project is to implement a structural change within in the scientific management paradigm of "Petru Poni" Institute of Macromolecular Chemistry (ICMPP), Iasi, Romania, by setting up a competitive research group in the field of computational chemistry under the supervision of an outstanding researcher manager in the field of computational chemistry, Prof Aatto Laaksonen (Arrhenius Laboratory, Stockholm University, Sweden).

The BioMat4CAST project addresses the design and development process for smart biomaterials applications in fields ranging from drug delivery systems, implantable devices, and tissue engineering to regenerative medicine and personalized medicine. The technology developed in the project has the potential to accelerate the discovery and development of new biomaterials for biomedical applications.

2. Computational Chemistry

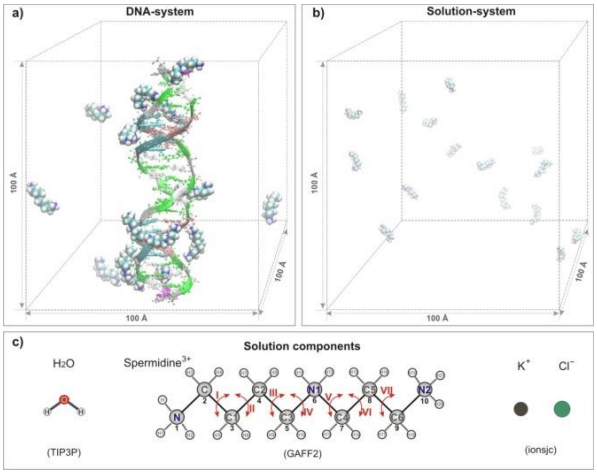

The computational chemistry has revolutionized the way we approach research in the field of chemistry, providing a powerful tool for investigating the structures, properties, and interactions of molecules and materials without the need for extensive laboratory experimentation. As a result, many researchers believe that computational chemistry is the laboratory of the future, offering numerous advantages that traditional laboratory methods cannot provide. An example of a situation where computational chemistry has a clear advantage over traditional laboratory methods is in elucidating the interaction between different compounds, as depicted in the figure to the right, where two simulations were performed to compare how spermidine, a natural polyamine that plays an important role in DNA condensation, behaves when

alone in solution or when interacting with the DNA molecule. Understanding these types of interactions between DNA and natural molecules, i.e. how spermidine changes is conformational space, is important to better design new and improved non-viral carriers for DNA [1].

One of the significant benefits of computational chemistry is the speed and efficiency in simulating experiments. It is possible to perform extensive simulations of chemical and biological systems quickly and accurately, making it easier to identify chemical reactions and molecular interactions that might not be observable under laboratory conditions. Another significant advantage of computational chemistry is the ability to access molecular structures in unprecedented detail. By using molecular modelling and simulation techniques, researchers can observe the behaviour of molecules at the atomic level, which can provide valuable insights into the chemical and physical properties of materials and substances.

The design of polymers with imposed properties involves tailoring the chemical structure of the polymer to achieve specific properties, such as mechanical strength, thermal stability, or biodegradability. This process can be achieved through various methods, including monomer selection, polymerization conditions, and post-polymerization modifications. Polymerization conditions can also be adjusted to influence the properties of the final polymer. For example, the type of initiator, solvent, and temperature used in the polymerization process can affect the molecular weight, reaction rate, and morphology of the polymer. By properly controlling these parameters, it is possible to tailor the polymer's properties to meet specific requirements.

Post-polymerization modifications can also be used to adjust the properties of a polymer. These modifications can include chemical reactions, physical treatments, or the addition of other substances to alter the polymer's properties. For example, surface modification techniques can be used to improve the biocompatibility of a polymer for medical applications.

In summary, the design of polymers with imposed properties involves a combination of monomer selection, polymerization conditions, and post-polymerization modifications. By carefully tailoring these factors, it is possible to create polymers with precisely targeted properties to meet specific needs.

3. The Safe and Sustainable by Design (SSbD) European Strategy

The SSbD framework is an approach to guide the innovation process for chemicals and materials, that *"aims to:*

- *steer the innovation process towards the green and sustainable industrial transition*
- *substitute or minimise the production and use of substances of concern, in line with, and beyond existing and upcoming regulatory obligations*
- *minimise the impact on health, climate and the environment during sourcing, production, use and end-of-life of chemicals, materials and products*

The framework is composed of a ***(re-)design phase*** *and an* ***assessment phase*** *that are applied iteratively as data becomes available"* [2].

The central objective of the safe and sustainable by design strategy is to minimize the environmental and health impact of products and materials throughout their entire lifecycle, from the manufacturing stage to the end of the product's useful life. There are several key principles of this strategy:

- Use non-toxic and sustainable raw materials for the production of products and materials wherever possible.
- Strive to minimize or eliminate hazardous substances and chemicals that can pose a threat to human health and the environment.
- Minimize waste and pollution by designing products and materials that can be easily recycled and reused.
- Design for durability and longevity to reduce the need for frequent replacement and disposal of products and materials.
- Promote sustainability throughout the entire supply chain, including responsible sourcing of raw materials, responsible manufacturing practices, and safe and sustainable disposal and recycling practices.
- Consider the entire lifecycle of the product in the design process, including the energy required to produce the material, the energy consumed during use, and the impact on the environment and human health after disposal.

By incorporating these principles into the design process, the safe and sustainable by design strategy aims to create products and materials that are safe for human health and the environment, durable, and conducive to sustainability. Thus, the BioMat4CAST project will support the ICMPP research to comply with the sustainable by design chemicals and materials principles by focusing on the aim to minimize the use of non-renewable resources, reduce waste and pollution, and promote a circular economy.

4. Conclusions

In conclusion, computational chemistry has the power to change the future of laboratory-oriented chemistry, providing researchers with powerful tools to predict, design, and develop new molecules and materials, while also reducing the cost and environmental impact of laboratory experimentation. The BioMat4CAST project is bringing the future of chemistry in ICMPP.

Acknowledgements

This paper is supported by European Union's Horizon Europe research and innovation programme under grant agreement No 101086667, project BioMat4CAST (BioMat4CAST - Multi-Scale In Silico Laboratory for Complex and Smart Biomaterials).

References

[1]. Perepelytsya S, Vasiliu T, Laaksonen A, Engelbrecht LDV, Brancato G, Mocci F. Conformational flexibility of spermidine3+ interacting with DNA double helix. *J. Mol. Liq.* 389, 122828, 2023

[2]. See documents defining the SSbD framework on: https://ec.europa.eu/info/research-and-innovation/research-area/industrial-research-and-innovation/key-enabling-technologies/advanced-materials-and-chemicals_en

UNIUNEA EUROPEANĂ
Instrumente Structurale 2014-2020

INFRA SUPRACHEM LAB - CENTER FOR ADVANCED RESEARCH IN SUPRAMOLECULAR CHEMISTRY

Marcela Mihai, Narcisa-Laura Marangoci
Petru Poni Institute of Macromolecular Chemistry, Romanian Academy, Iasi, Romania
**nmarangoci@icmpp.ro*

1. General information

- *Beneficiary*: Petru Poni Institute of Macromolecular Chemistry Iasi (Institutul de Chimie Macromoleculara Petru Poni, ICMPP)
- Project co-financed by European Regional Development Fund under the Competitiveness Operational Program 2014-2020
- *Priority Axis 1* – Research, Technological Development and Innovation to Support Economic Competitiveness and Business Development
- *Investment priority 1a* – Improving research and innovation infrastructures and capacities to develop excellence in RDI and promoting centers of expertise, especially those of European interest
- *Action 1.1.3* Creating synergies with the RDI actions of the European Union's HORIZON 2020 framework program and other international RDI programs
- *Period*: 25.02.2021 – 24.06.2023.
- *MySMIS*: 108983

2. General objective

The overall objective of the Infra SupraChem Lab project is to create an advanced infrastructure that deserves the supramolecular chemistry working group SupraChem Lab, a group created within the Horizon 2020 Project WIDESPREAD 2-2014: ERA Chairs (667387) - SupraChem Lab Laboratory of Supramolecular Chemistry for Adaptive Delivery Systems ERA Chair initiative.

3. Specific objectives / Expected results

O1. Realization of the design component for the Infra SupraChem Lab project - objective already in implementation
O2. Realization of the infrastructure of the SupraChem Lab center
O3. Equipping and launching the SupraChem Lab center
O4. Dissemination and publicity
O5. Project management

The implementation of the **Infra SupraChem Lab project** represents the creation of an adequate structure for the activity of the **SupraChem Lab group**, a group formed through a Horizon 2020 ERA CHAIR project (Horizon 2020 WIDESPREAD 2-2014: ERA Chairs Project no 667387).

The SupraChem Lab project started in 2015 and with the support of EC investment of 2.5 MEuro, the foundation of a young team of researchers was laid, focused on the principles of supramolecular chemistry knowledge. The team's research areas range from the creation of dynamic systems for targeted biomedical applications to the dynamic molecular modeling of the interaction of complex supramolecular systems. The group human resource represents a secure core for the training of new generations of specialists, able to continue and develop new fields with great applicative impact.

Over the last ten years, ICMPP's research directions have clearly evolved into interdisciplinary fields and have been adapted to global research trends, while also presenting their own original directions, based on knowledge and experience gained over time.

The implementation of the Infra SupraChem Lab project would contribute to the improvement of the existing research within ICMPP and SupraChem Lab team and to the development besides the fundamental research directions and of some applied research directions for new top products.

An important part in the development of new directions is based on a modern infrastructure, aimed at interdisciplinary research. An infrastructure based on the synthesis and complete characterization of new materials represents a real support for the development of application fields. The Infra SupraChem Lab infrastructure is a step forward to create the premises for application of the results of fundamental research obtained by the newly created group.

Infra SupraChem Lab will be set up in spaces owned by the ICMPP - in buildings currently unused, under conservation. The new center will also benefit from the arrangement of auxiliary spaces, for the storage of chemicals, glassware and laboratory materials as well as the related access ways to facilitate the access to the research infrastructure.

The structure of Infra SupraChem Lab will include the following departments:

A. **Operating department** consisting of:

A1. Chemical and biochemical synthesis laboratory
A2. Laboratory for the study of special properties and possible applications
A3. Physical and chemical characterization laboratory

The laboratories are be provided with chemical ventilation niche and specific laboratory equipment for chemical syntheses (eg: magnetic stirrers, inert gas purification installations, vacuum pumps, electric ovens, etc.), study of properties and material characterization (e.g. X-ray diffractometer for wide angles, Photo-DSC, Automatic confocal imaging system for scanning, characterization and data analysis in cell biology, Semi-automatic inverted fluorescence microscope, Diffractometer with dual X-ray source for single crystals, Motorized stereomicroscope with fluorescence with the possibility of in-depth analysis, and many others).

B. **Data processing department**

Within this department, the data will be processed and structural optimization studies will be performed.

C. **Department of projects and technology transfer**

All departments are provided with computers connected to the Internet and implicitly to the internal network of the center.

The project has as **direct beneficiaries** the SupraChem Lab team, the project being addressed also to other interest groups as follows:

- graduates of the universities of Iasi and not only who could join the SupraChem Lab team or could benefit from training within the newly created Center
- teachers from universities in Iasi and not only, who will be able to carry out educational activities within the center
- researchers from ICMPP or other collaborating research institutions, who will be able to perform tests or determinations on the equipment within the center
- different SMEs that will be able to benefit from technology transfer facilities of the patented results that will be obtained within the center.

PETRU PONI INSTITUTE OF MACROMOLECULAR CHEMISTRY

Infra SupraChem Lab

Center for Advanced Research in Supramolecular Chemistry

THE RM ROADMAP PROJECT AND THE AMBASSADORS NETWORK

Raluca-Oana Andone*
Petru Poni Institute of Macromolecular Chemistry, Romanian Academy, Iasi, Romania
RM Roadmap Ambassador for Romania
**raluca_andone@icmpp.ro*

1. Introduction

The project entitled "Creating Framework Conditions for Research Management to Strengthen the European Research Area" (RM ROADMAP), financed by the European Commission under the call HORIZON-WIDERA-2021-ERA-01, has a duration of 36 months, between 1 September 2022 and 31 August 2025. It is implemented by a consortium, coordinated by the European Association of Research Managers and Administrators (EARMA) - Belgium, and is composed of HETFA Research Institute - Hungary, Nova University Lisbon - Portugal, Association of European Science & Technology Transfer Professionals - Netherlands, Crowdhelix Limited - Ireland, Cyprus Institute - Cyprus and associated partners Janssen & Janssen and Una Europa - Belgium. It has the objectives of "connecting new and existing networks on a community platform, in order to create a bottom-up consensus about the future of research managers and to inform about the existing training, networking, funding and mobility opportunities, clarifying the role and potential for research managers to support the European research area (ERA) and the research and innovation (R&I) system" [1].

2. Current situation of RMA's (Research Managers and Administrators)

There is a growing need for the "professionalization of science management at research performing and funding organizations, in order to improve their ability to participate in ERA-wide collaboration networks", which determined the European Commission to launch a pilot action for a Europe-wide networking program for science managers [2]. The ERA Action 17 - "Enhance the strategic capacity of Europe's public research performing and funding organizations" call aims to improve the European R&I system across the entire ERA; the expected outcome seen by the Council Conclusions is that "by the end of 2024, there will be an involvement of at least 100 participating public research performing and funding organizations and their research management staff in the training and networking programs" [3]. As an implementation of the ERA Action 17 call, the Research Management Initiative focuses on the following actions: "- recognition (contribution to professionalization); - networking (supporting best-practice exchange); - upskilling (improving training and skills of research management staff); - capacity building (supporting less R&I intense regions and organization)" [4].

3. The RM Roadmap project and the Ambassadors network

The RM Roadmap project is expected to deliver "a community perspective from across Europe, terms and definition of RM, preliminary data about each interested country, thought leadership on the role and value proposition of research managers, overview of training, networking, mobility, funding opportunities and a roadmap to help enable a game changer in RM to the benefit of researchers, R&I system and ERA" [5]. Policy makers, researchers, research managers (RM), research funding organizations (RFO), research performing organizations (RPO), ministries, stakeholders are the actors involved in this action, who can contribute to answering the following

questions: „- what is a research manager/administrator (RMA)?; - what are the types of research managers?; - what research managers do and what are the different types of support? ; - what is the value of research managers for the R&I system?; - what is the plan to improve the R&I system through RM (ROADMAP)" [2]?

Within the RM Roadmap project, in March-April 2023 around 110 ambassadors were recruited from 40 countries, in April 2023 the Helix platform was launched at the EARMA Conference, in May 2023 the first ambassadors meeting and Action 17 Workshop took place in Budapest. It is planned that in September 2023 there will be the onboarding of the Knowledge & Community Platform (KCP) and in October 2023 the first on-line session will take place on the KCP. It is estimated that the RM Roadmap project will map the landscape of national networks and associations until October 2023, define who are reseach managers and who are their skills and competences until March 2024, establish training, netwoking and professional development opportunities by June 2024, establish a career development framework in November 2024 and finally make a value proposition in March 2025 [2]. In March 2024 it is estimated to take place the second ambassadors meeting in Lisbon and in November 2024 the third ambassadors meeting in Brussels [5]. The RM Ambassador network is „bringing together community builders and leaders from countries accross Europe to co-create the future of research management in Europe through the RM ROADMAP project", and was recruited for the following roles: „ - engage communities to participate in RM ROADMAP to design the future of research management; - gather input from national and local Research Management (RM) community; - function as on-line moderators to inform the co-creation of the future of research management in Europe" [5]. The RM ROADMAP Ambassadors Network will contribute to the creation and functioning of the digital Knowledge and Community Platform (KCP).

4. RMA community in Romania and the RO RM ROADMAP Ambassadors Team

The RMA community in Romania, though estimated to consist of over 200 individuals, "lacks organization and a cohesive structure. There is currently no active effort to establish a national RM network, and researchers typically engage in RM without dedicated administrative support for their projects, as this responsibility usually falls on institutional departments. The absence of any references to RM *per se* in Romanian legislation further complicates the situation. While some institutions have project support offices, their effectiveness is limited" [6]. Within the Structural Funds 2014-2023, 13 Project Support Centers have been created, including the *BioNanoTech Centre* from PPIMC, but their funding is ending in June/December 2023, with no provisions for future financial support. It is hoped that support for establishing the Romanian RM network will come from the RO HEU NCP and the RO EEN.

The Romanian RM Roadmap Ambassadors Team was recruited by the RM Roadmap project and is composed of the following members: - Dr. Raluca-Oana Andone is a senior legal adviser at the "Petru Poni" Institute of Macromolecular Chemistry under the Romanian Academy, and member of the management team of several structural and European research projects; she is also the Vice President of the National Council for Ethics of Scientific Research, Technological Development and Innovation of the Ministry of Research, Innovation and Digitalization; she was a member and the legal responsible of the BioNanoTech Project Support Center within PPIMC, a consultancy and support center for European and international research projects; - Dr. Ulpia-Elena Botezatu is a researcher at the National Institute for Research & Development in Informatics from Bucharest and a space policy officer at the Romanian Space Agency; she is Romania's National Contact Point for Civil Security for Society and a national delegate to the United Nations Committee for the Peaceful

Uses of Outer Space Affairs, ESA-Program Board on Space Situational Awareness, the European Commission and Space Surveillance and Tracking Partnership, International Academy of Astronautics, and NATO STO on space related issues; - Dr. Corina Georgeta Barna is an assistant professor and head of international students office at University of Life Sciences "King Michael I" from Timisoara; she is also the National Contact Point for Marie Skłodowska-Curie Actions and a member of the MSCA-NET project, which facilitates the transnational cooperation between National Contact Points for the MSCA; she is a governmental expert for the EURAXESS service center for the mobility of researchers and a human resources strategy for researchers (HSR4R) assessor. "The RO team will use its contact database to disseminate the RM Roadmap project objectives within the Romanian RM community. The contact database regards Romanian RM from public and private research institutions. The RO team will search for financial support for the organization of these events (e.g. within projects from the National Innovation and Research Plan or other financial resources) and can organize, host or participate in joint events with other RM Ambassadors, in order to benefit from other countries experience. Different dissemination and networking activities will be used by the RO team to create and organize the Romanian RM network such as: on-line/on-site/hybrid conferences, workshops, meetings, and seminars etc., following the EARMA RM Roadmap project principles and objectives" [2].

3. Conclusions

EARMA is delivering an important project that will support the strengthening of an inclusive research management community in Europe. RM Roadmap will chart a course for the future of research management (RM) in Europe and a community to support its delivery [5]. The RO RM Roadmap Ambassadors team will use its networks to create a bridge between the EARMA RM Roadmap project and the Romanian RM community.

Acknowledgements

We would like to thank to the project "*Creating Framework Conditions for Research Management to Strengthen the European Research Area*" (RM ROADMAP), Grant no. 101058475, financed by the European Union under the call HORIZON-WIDERA-2021-ERA-01 and coordinated by the EARMA - Belgium.

References

[1]. Claesen N. RM Roadmap project. Presentation. 1st RM Roadmap Ambassador Meeting. 9 May 2023. Budapest.
[2]. Claesen N. RM Roadmap vision and objectives. Presentation. 1st RM Roadmap Ambassador Meeting. 9 May 2023. Budapest.
[3]. Council of the European Union. Council conclusions on the new ERA. 1 December 2020. https://data.consilium.europa.eu/doc/document/ST-13567-2020-INIT/en/pdf. Accessed 16 Aug. 2023.
[4]. Delauré S. The new European Research Area - ERA Action 17: Research Management Initiative presentation. 1st RM Roadmap Ambassador Meeting. 9 May 2023. Budapest.
[5]. https://www.rmroadmap.eu/. Accessed 16 Aug. 2023.
[6]. Andone R. RM Roadmap Romanian Ambassadors and national network set up. Presentation. BioNanoTech Project Final Conference. 8 June 2023. Iasi.

MACRO Iași 2023

APEL LASER – 20 YEARS OF EXCELLENCE IN LASER SYSTEMS AND INSTRUMENTS FOR SCIENCE

APEL LASER SRL, Mogosoaia, Romania
**www.apellaser.ro; +40 21 31 70 910*

1. Introduction

20 Years of Excellence: APEL LASER has proudly served as a leading supplier and integrator of laser systems and instruments for both the scientific and industrial communities. Over two decades, we have committed ourselves to delivering innovative solutions and exceptional services, establishing ourselves as a trusted partner in Romania and South-Eastern Europe.

@About APEL LASER: Proven Ambition and Professionalism: APEL LASER has risen to prominence as one of the primary distributors of lasers, laser systems, industrial equipment, and scientific instruments in the region. Our commitment to ambition and professionalism has propelled us into partnerships with the world's most renowned companies.

2. Our Partners. We are honored to be associated with industry giants who share our dedication to excellence:

COHERENT: A world leader in laser technology, offering innovative solutions across diverse applications.
HORIBA: A Japanese company known for manufacturing measurement and analysis equipment for industrial and scientific applications.
TSI Incorporated: An American engineering and technology company, providing measurement and analysis solutions for industrial, environmental, and health applications.
Cellink: An innovative biotechnology company specialized in 3D bioprinting and cell biology solutions.
Thorlabs: A global supplier of optical equipment and laser systems, supporting research, development, and industrial applications.
Nanosurf: A provider of advanced instruments for microscopy and other technologies, used across materials science, biology, medicine, and technology.

3. Comprehensive Services. Our product range is complemented by a suite of services including:

- **Specialized Consulting:** Tailored guidance to meet your unique needs.
- **Installation**: Seamless integration of our equipment into your operations.
- **Technical Assistance**: Ongoing support to ensure optimal performance.
- **Industrial Process Automation**: Innovative solutions for improved efficiency.

4. Our Values. At APEL LASER, our values are the bedrock of our success:

- **Innovation**: We embrace change and progress to stay at the forefront of technology.
- **Quality**: Our commitment to excellence is reflected in every product and service we provide.
- **Professionalism**: We conduct ourselves with the highest level of integrity and expertise.
- **Respect**: We value our clients, partners, employees, and the environment.

5. Our Mission. Our core mission is unwavering:

- **Adaptation**: We continuously evolve to align with market and technological changes.
- **Success**: Your success is our success; we approach every project with dedication.
- **Proactivity**: Our proactive approach ensures we meet your needs effectively.

6. Achievements. Our track record speaks for itself:

- **30 Completed Projects**: Demonstrating our capabilities and experience.
- **1 ongoing Horizon Europe Project:** Commitment to cutting-edge research.
- **11 Projects Submitted**: A pipeline of innovation.
- **100+ Scientific Articles Published**: Our dedication to research and development.
- **10 Patents Obtained:** A testament to our innovative spirit.

7. Quality Management. We adhere to the highest standards:

ISO Certified: APEL LASER is ISO 9001:2015 certified.
Fairness and Integrity: We maintain our integrity while raising our standards.

8. Key Benefits. Why choose APEL LASER?

- **Diverse Range of Equipment**: We offer the latest in technological standards for various industries.
- **Experienced Team**: Our experts specialize in multiple fields to provide tailored solutions.
- **Customer-Centric Approach**: We prioritize understanding your specific needs.
- **Complete Solutions**: Our offerings include equipment, services, and technical support.
- **Global Products**: We partner with the world's leading companies to provide the best.
- **Product Customization**: Tailored solutions for unique requirements.
- **Free Consultation:** Access our experts for advice and assistance.
- **R&D Collaboration**: We actively engage in research and development projects.
- **Technical Support**: Count on our expert team for comprehensive assistance.

APEL LASER - Diverse Product Range for Your Needs:

Scientific Cameras
- High-performance scientific cameras for research and analysis.
- Cutting-edge imaging technology for precise data capture.

Optics and Optical Instruments
- High-quality optical components and mechanisms.
- Essential components for optical systems and lasers applications.

Analytical Instruments
- Comprehensive tools for advanced analysis and research.
- Reliable instruments to support data-driven decision-making.

Climatic monitoring systems
- Cutting-edge systems for accurate climate monitoring.
- Data-driven solutions for environmental and industrial needs.

Cold Forming of Sheet Metal and Profiles Machines
- State-of-the-art machinery for precision sheet metal forming.
- Customized solutions for various industrial applications.

Custom Solutions
- Tailored solutions to meet your unique requirements.
- Collaborative approach to address specialized challenges.

Lasers
- A wide range of lasers for diverse applications.
- Advanced laser technology for industrial and scientific use.

Microscopy and Accessories
- Microscopes and accessories for detailed analysis.
- Tools to explore the micro world with precision.

3D Printing
- Innovative 3D printing solutions for various industries.
- Customizable and precise printing for your projects.

Spectrometers
- High-performance spectrometers for precise spectral analysis.
- Essential tools for scientific research and quality control.

Laboratory Equipment
- A comprehensive range of laboratory equipment.
- Supporting research and development across industries.

Deburring Sheet Metal & Sheet Metal Parts Machines
- Precision machines for deburring and straightening.
- Streamlining manufacturing processes for efficiency.

Advanced Scientific Materials
- Cutting-edge materials for scientific experiments.
- Enabling breakthroughs in research and development.

Laser Systems
- Comprehensive laser systems for various applications.
- Providing complete solutions for your laser needs**.**

Light Sources
- Advanced light sources for diverse applications.
- Illuminating possibilities across industries.

Our Vision
- **Successful Partnerships**: We aim for success through collaboration with industry and research specialists.
- **Innovation Through Experience**: Passion for our work drives us to achieve outstanding results.

Contact Information

Website: www.apellaser.ro
Phone: +40 21 31 70 910
Email: office@apellaser.ro | sales@apellaser.ro | service@apellaser.ro

Thank you for considering APEL LASER as your partner. We look forward to collaborating and driving innovation together.

ELEVATING SCIENTIFIC RESEARCH WITH RIGAKU'S CUTTING-EDGE EQUIPMENT PORTFOLIO

AMS 2000 TRADING IMPEX SRL, Bucharest, Romania
**claudia.gavrilescu@ams.ro; www.ams.ro; 0730 711 952*

1. Introduction

AMS 2000, member of BATM Group, is one of the most reliable, experienced and well-known companies in analytical and medical solutions in Romania.

The company started operating back in 1997 as an accredited distributor for several renowned international suppliers and currently operates with three departments: Analytical Department, Medical Department, Food Industry and Environment Department.

Since 2010, the year when the Analytical Department was established within AMS 2000, the company aimed to develop as a market leader in the X-ray equipment supply segment in both academia and industry. Under the aegis of the prestigious Japanese company, Rigaku Corporation, present on the international market for more than seven decades, AMS 2000 have brought to the Romanian market scientific and industrial instruments based on X-ray technologies, as well as Raman spectroscopy technology.

Today, with hundreds of major innovations to their credit, the Rigaku group of companies are world leaders in the fields of general X-ray diffraction, thin film analysis, X-ray fluorescence spectrometry, small angle X-ray scattering, protein and small molecule X-ray crystallography, Raman spectroscopy, X-ray optics, semiconductor metrology, X-ray sources, computed tomography, nondestructive testing and thermal analysis.

The Rigaku equipment into the AMS 2000 portfolio:

X-ray technology equipment

- X-ray diffractometers (XRD) for powders and thin films
- Single crystal X-ray diffractometers for small molecules 3D structure analysis and proteins
- Wavelength dispersive X-ray fluorescence spectrometers
- X-ray microscopy systems
- X-ray residual stress measurement systems
- Micro CT (computed tomography) systems

Raman technology equipment

- Raman portable spectrometers

„At AMS 2000 Trading Impex, we are proud of our reputation built in the 13 years of collaboration with researchers in Romania, which positions us as a reliable and reliable partner in this high-level scientific community. we understood from the very beginning the challenges facing the

research field and we are committed to providing the best equipment to researchers, sometimes unique at the national and global level, at the highest level of service, with on-going technical and scientific support from the manufacturer Rigaku Corporation." mentions Claudia Gavrilescu, Sales Manager within the Analytical Department.

Supermini200
High-power benchtop sequential WDXRF spectrometer

Elemental analysis of solids, liquids, powders, alloys and thin films

As a high-power benchtop sequential wavelength dispersive X-ray fluorescence (WDXRF) spectrometer, for elemental analysis of oxygen (O) through uranium (U) in almost any material, the Supermini200 uniquely delivers low cost-of-ownership (COO) with high resolution and lower limits-of-detection (LLD).

Analyzing complex matrix materials with a wide range of light and heavy elements, from trace to high concentration levels, is this instrument's core competency. With its high powered (200 W) X-ray tube, Rigaku Supermini200 delivers high XRF sensitivity for light elements with superior spectral resolution for resolving line overlaps in complex matrices without the need for complicated mathematical peak deconvolution. Analyzing low concentration levels of light elements (F, Na, Mg, Ca, Si, Al, and P) is easy.

SmartLab 9kW
Automated multipurpose X-ray diffractometer

SmartLab 9kW: Whether you are working with thin films, nanomaterials, powders, or liquids the SmartLab will give you the XRD functionality to make the measurements you want to make when you want to make them. Coupling a computer-controlled alignment system with a fully automated optical system, and the User Guidance functionality within the SmartLab Studio II software, makes it easy to switch between hardware modes, ensuring that your hardware complexity is never holding back your research.

Rigaku

XtaLAB Synergy-ED
Fully integrated electron diffractometer

XtaLAB Synergy-ED: XtaLAB Synergy-ED is a new and fully integrated electron diffractometer, creating a seamless workflow from data collection to structure determination of three-dimensional molecular structures. The XtaLAB Synergy-ED combines core technologies from the two companies: Rigaku's high-speed, high-sensitivity detector (HyPix-ED), and instrument control and single crystal analysis software platform (CrysAlisPro ED), and JEOL's expertise in generation and control of stable electron beams.

XtaLAB Synergy-S
Combining the ultrabright microfocus PhotonJet X-ray source technologies and innovative HyPix detectors

XtaLAB Synergy-S: Using a combination of leading-edge components and user-inspired software tied together through a highly parallelized architecture, the XtaLAB Synergy-S produces fast, accurate data in an intelligent fashion. In the latest generation of Rigaku's XtaLAB Synergy systems, the combination of the latest ultrabright microfocus PhotonJet X-ray source technologies and innovative HyPix detectors allows us to lower the barrier for absolute structure determination.

CT Lab HX
Compact X-ray microtomography

CT Lab HX: Rigaku CT Lab HX is a benchtop micro CT (computed tomography) scanner. The adjustable SOD (source-to-object distance) and SDD (source-to-detector distance) make this benchtop micro CT scanner flexible. It covers from 2.1 um voxel resolution in the high-resolution mode and 200 mm FOV (field of view) in the large FOV mode. The CT Lab HX is equipped with a 130 kV - 39 W high power X-ray source. The X-ray source settings and X-ray filters are adjustable to optimize the X-ray energy to various sample materials and sizes.

If you would like to find out more about the projects implemented using Rigaku equipment distributed by AMS 2000 Trading Impex, please reach out to us.

AMS 2000

Scan to have a brief story of Rigaku

DECORIAS SRL

DECORIAS SRL, Rediu, Romania
**office@decorias.ro; www.decorias.ro; www.reactivi.ro*

1. Introducere

Furnizor pe plan national de aparatura si echipamente de laborator, consumabile, reactivi pentru analiza si cercetare in chimie, biochimie, microbiologie, standarde si materiale de referinta, scheme de intercomparare.

Suntem ingineri chimisti, experti, pasionati de chimie, cu aproximativ 20 de ani vechime in dotarea laboratoarelor din universitati, institutii de cercetare si laboratoare de analiza chimica, fizica si microbilogica din industria alimentara, a mediului, farmaceutica, petrochimica, feroase, neferoase etc.

Oferim toata gama de produse necesare in desfasurarea activitatii de laborator de la consumabile, sticlarie si reactivi, la echipamente dedicate aplicatiilor.

Produsele furnizate de noi sunt de inalta calitate, respecta standardele internationale ISO 9001, ISO/IEC 17025, ISO 17034 si ISO 1043, produse de firmele de top din domeniu.

Compania noastra este Certificata ISO 9001:2015 si detine autorizatii speciale de comercializare emise de organismele statului roman.

2. Ne plac provocarile!

Daca nu reusiti sa identificati un furnizor sau producator de reactivi necesari in desfasurarea proiectului dumneavoastra, contactati-ne pentru a ne transmite lista dumneavoastra. Avem reputatia de a-i ”*scoate si din piatra seaca*”.

In parteneriat cu producatori mondiali, oferim reactivi chimici de laborator cu utilizare speciala, reactivi chimici custom made, de puritate inalta, pentru diferite aplicatii de laborator. Reactivii sunt insotiti la livrare de Certificate de Analiza, Fise de Securitate si MSDS-uri.

Detinem autorizatii de comercializare emise de institutiile statului roman, pentru comercializarea reactivilor controlati sau cu regim special.

Furnizam reactivi chimici de laborator, de puritate inalta, puritate analitica sau tehnica folositi in industria chimica sau in laboratoarele de cercetare si analiza. In gama noastra se regasesc solventi, reactivi pentru cromatografie, reactivi HPLC, standarde analitice, materiale de referinta, etc. Oferim produse de nisa si reactivi controlati, utilizati in laboratoare de analize specifice in toxicologie si criminalistica. Reactivi acreditati ISO/IEC.

3. Control extern

Furnizam scheme de intercomparare/control extern organizate de parteneri internationali acreditati ISO 17043. Matrici: apa potabila, apa reziduala, produse lactate, produse alimentare, furaje, analize clinice, aer, contaminare sol, bauturi alcoolice si sucuri, bere, cosmetice, jucarii, medicamente de abuz, toxicologie, radiochimie, lubrifianti, textile, tesut animal, etc.

In portofoliul nostru gasiti o gama larga de materiale de referinta si standarde analitice, cum ar fi:

- tulpini de referinta pentru microbiologie;
- standarde analitice si materiale de referinta obtinute prin sinteza si purificarea substantelor naturale;
- standarde si materiale de referinta pentru analiza chimica a alimentelor si a mediului;
- standarde pentru pesticide;
- standarde pentru industria farmaceutica;
- standarde ICP/ICP-MS, AA, IC, HLPC;
- reziduuri veterinare etc.

Valorile noastre fundamentale se reflecta in tot ceea ce facem. Fiecare ne aminteste sa ramanem fideli cu noi insine, sa modelam caracterul echipei noastre in timp ce oferim cele mai bune solutii pentru clientii nostri.

Invatam unii de la altii, ne aliniem, impartasim cunostinte, oferim si primim feedback obiectiv. Comunicarea ne ajuta sa crestem ca echipa si stabileste baza pentru a lucra impreuna in mod constructiv si respectuos, pentru a obtine solutii inovatoare si pentru a indeplini solicitarile clientilor nostri.

4. Suntem prezenti si in Sistemul Electronic de Achizitii Publice (S.E.A.P)

Produsele ofertate, pot fi achizitionate prin intermediul catalogului nostru din SEAP. Departamentul de achizitii al institutiilor publice, poate solicita publicarea anumitor produse ofertate sau pot achizitiona direct produse deja publicate in catalog.

ROMANIAN CHEMICAL SOCIETY
SOCIETATEA DE CHIMIE DIN ROMANIA, SChR

"Chemistry is not everything, but anything is nothing without chemistry"

SChR Objective: "*Attracting young people towards chemistry as study field and profession* "

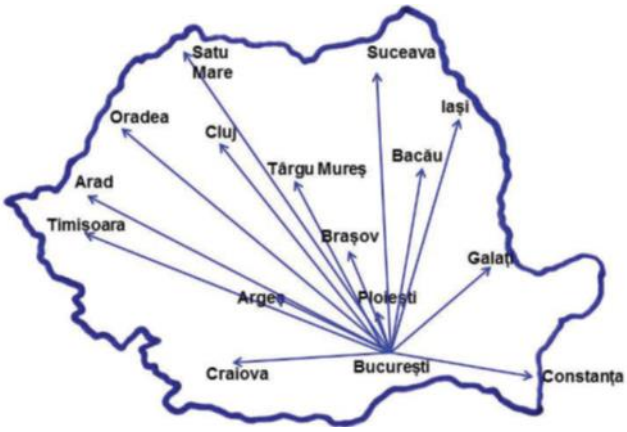

Sections and Local Branches

21 Local branches

7 Sections

3000 Members
(including honorary and affiliated members – students and pupils)

The activity of organizing scientific meetings is continued and developed:

- *ICOSECS, The International Conference of the Chemical Societies of the South Eastern European Countries* is organized by regional cooperation with the chemical societies from Albania, Bulgaria, Cyprus, Greece, Macedonia, Montenegro and Serbia
- *COFrRoCA, The Franco-Romanian Colloquia of Applied Chemistry* is organized in cooperation with the universities of Bacau (Romania) and Orleans (France)
- Periodically international conferences of a high scientific level are organized in cooperation with the University Politechnica Bucharest, Ovidius University Constanta, Petru Poni Institute of Macromolecular Chemistry Iasi.

The present publications of SChR include the ***Bulletin of the Romanian Chemical Society*** (an information journal on the activity in chemistry in Romania), ***Revista de Chimie*** (a scientific journal publishing original results, with a constantly rising ISI impact factor), ***Chimia*** (a publication for undergraduates), as well as a series of publications of the local sections of SChR: *ProChimia*, *Universul Chimiei*, *ChimMax*.

The ***Bulletin of the Romanian Chemical Society*** founded in 1919, since the very beginning of SChR, aims to periodically present the life and activity of SChR, the actions of the Society for the promotion of chemistry and its position on the chemistry policy.

Among the modern numbers is the one from 2009 where one can find detailed information about the SChR history as well as about some outstanding personalities of the Romanian chemistry.

For high school students, the journal ***Chimia*** was launched in the early 2000s. It included comprehensive articles on the topics of contemporary chemistry (sometimes written by eminent students), exciting problems and experiments, curiosities and biographical notes of the great Romanian or universal chemists.

"SChR grants medals, prizes and awards as recognition of scientific and/or professional activities of the chemists, located in the country or abroad" – SChR Rules

Petru Poni – first SChR medal

...in Pre-university Education

....in Inorganic Chemistry

... in Organic Chemistry

... in Chemical Engineering

Many important figures of the chemical world are honorary members of SChR and visited Romania on various occasions. SChR signed bilateral agreement papers with several societies within Europe.

SChR - Member of EUChemS

EuChemS, the European Chemical Society, is an umbrella organisation representing national Chemical Societies and other chemistry-related organisations in Europe. EuChemS aims to nurture a platform for scientific discussion and to provide a single, unbiased European voice on key policy issues in chemistry and related fields. Contact: www.euchems.org

EuChemS
European Chemical Society

The local sections of SChR together with the universities have as an important activity to attract young people in the study of chemistry. The constant orientation to increase weight of the experimental activity is not aleatory, nor is it isolated. It comes from the tendency to fill, even partially, the gaps in experimental instruction of the undergraduate studies and it follows the recommendations of SChR. Many of the activities promoted by the local sections and the sections of the society belong to this line of action.

STC – "Sectia Tinerilor Chimisti" - the Youth Division of SChR is an active and dynamic group.

The STC SChR members were part of the initiative group that sign the formation of EYCN in 2007 in Berlin. Since then, members of STC were part of the EYCN board and in 2011-2013 chaired EYCN/

Contact: Romanian Chemical Society, Str. Gheorghe POLIZU, nr. 1-3, sector 1, BUCURESTI, ROMANIA, Phone: +4 021 402 3962; +4 021 402 3912, Email: secretargenschr@icmpp.ro